Modelling of a Sediment Bank along the King River, Western Tasmania

Kate Polglase

UNIVERSITY OF TASMANIA

A research thesis submitted in partial fulfillment of the requirements of the Degree of Bachelor of Science/Law with Honours

CODES SRC

School of Earth Sciences, University of Tasmania

November 2000

CONTENTS

Chapter 3

Chapter 4

Chapter 5

Chapter 6

LIST OF FIGURES

LIST OF TABLES

LIST OF PLATES

LISTS OF EQUATIONS

Acknowledgements

A thesis requires a great deal of work, not solely from the author. Many thanks need be directed towards my co supervisors, James Reid and Jianwen Yang. James for the patience in teaching geophysics to a novice and Jianwen for the enlightening discussions about MODFLOW.

Appreciation is extended to my field trip colleagues: Jane, Shane, Nickki, Noel, Dad and Roachie and the 3rd year geophysics class.

People who have helped with this project in some way or another, the list is endless: Bear McPhail, Helen Locher, Hydro Tasmania, Peter Cornish, Gary Davidson. Special thanks to Rachael Manson, from surveying, for devoting so much time to datum points that fluctuate.

I'm very grateful to June Pongratz, who bribed Darren Turner with chocolate in exchange for computer memory for MODFLOW operation.

Special people to thank are the great people around the department who go out of their way to help, your time and your laughs were very much appreciated and needed. Andrew Fitzpatrick, Kevin, Rowdy, Catherine, Cathryn, Ali, Rob, Andrew Rae, Kellie, Cynthia, Mary and all the poppets.

Thanks to all my friends (if I've got any left now).

Special thanks to the stimulant companies such as Nodoz and Redbull. Your supported was greatly appreciated.

Lastly I would like to thank my family for the tremendous support they have all been over the last several months, and for leaving the house unlocked at wee hours of the morning. The question "so how is the modelling going?" will haunt me forever.

This thesis is dedicated to my sister Alice.

Chapter 1: Introduction

1.1 Introduction

In the late 1880s, Mt Lyell Copper Mine was established at Queenstown. Between 1916 and 1994 the ore pre-concentration process adopted by the mine discharged an estimated 97 million tonnes of mine tailings, 45 million tonnes of smelter slag and 10 million tonnes of topsoil into the Queen River (Locher, 1997).

The input into the river system has resulted in channel infilling, a 250-hectare delta at the mouth of the King River and the formation of 21 prominent sediment banks along the King River. This study is focussed on one well-exposed bank along the river, which Locher (1997) has alphabetically labeled bank H. The bank is approximately 55 m wide and 500 m long.

1.2 King River setting

The King River catchment has an area of 809km^2 and is located approximately 2km east of Strahn in Western Tasmania. The Mt Lyell mine lease is drained by Haulage Creek, a tributary of King River, before draining into Maquarie Harbour (Figure 1.1). Hence mine tailings, slag and contaminated water that were pumped into Haulage Creek were subsequently transported approximately 15km to the King River, with the majority of material being transported a further 20km out into Macquarie Harbour.

The climate of the region is temperate with an average temperature of 8^{o}C to 22^{o}C in summer and 2^{o}C to 13^{o}C in winter. The annual rainfall range is between 1800mm and 2600mm. Precipitation occurs as a result of westerly winds, carrying moisture from the Indian Ocean, meeting the mountains of the West Coast Range of Tasmania.

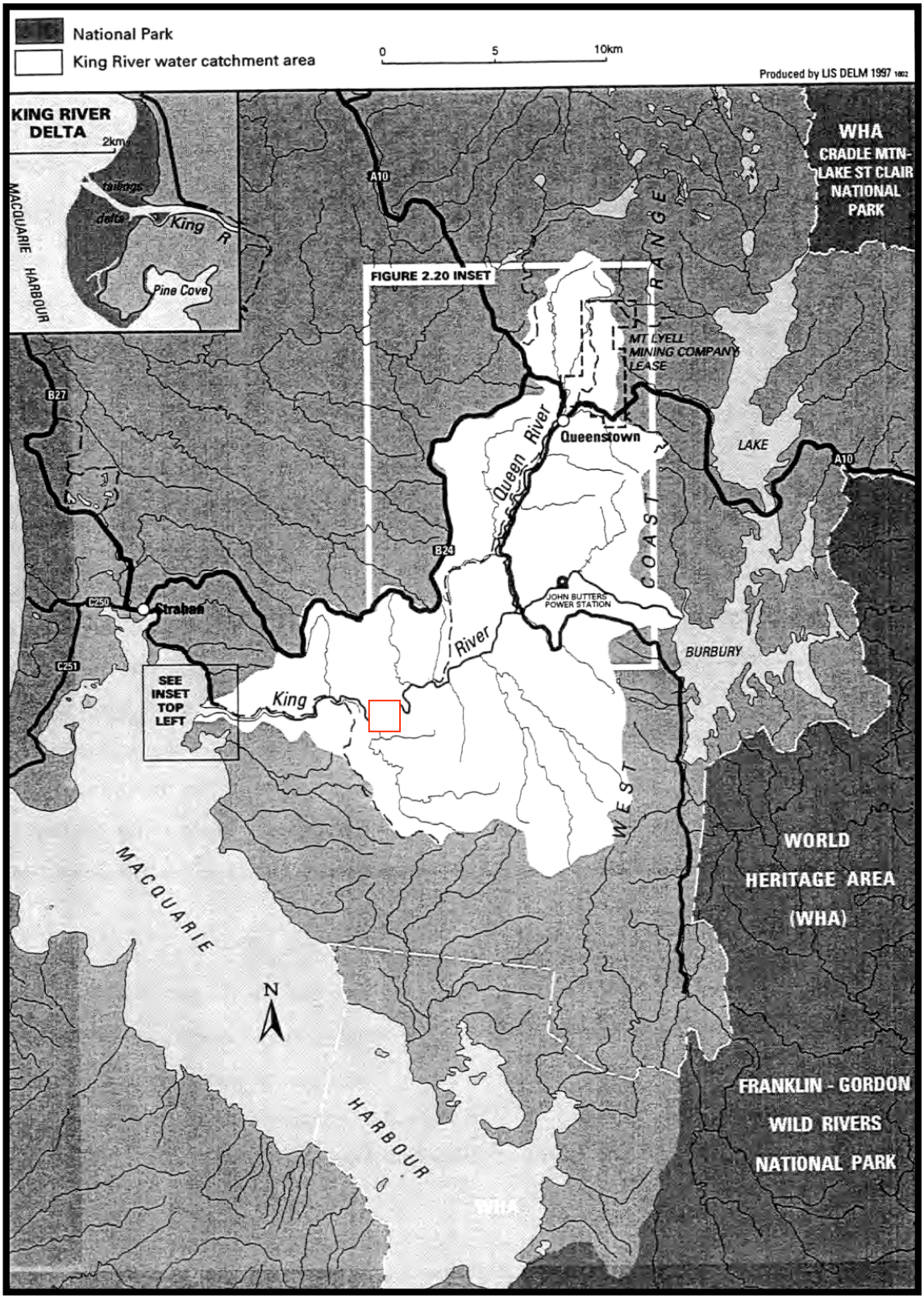

Figure 1.1. Location map of the King River, showing the location of the study area (red square).

1.3 Formation of sediment banks

Locher (1997) suggested that the original sediment banks were in a levee configuration. Original pre-mining sediment is characterised by a brown-black colour, due to a higher organic content. In contrast, redeposited mine tailings sediment is a vivid orange colour. The study found that the mine tailings had been deposited over the original levee structure during successive flood events. Plate 1.1 illustrates the individual stratigraphic units defined by colour changes from brown to orange to white.

Plate 1.1. Sediment stratigraphy exposed in bank M showing levee structure of original sediment bank prior to tailings deposition. From Locher (1997).

Locher (1997) utilised other methods to aid in determining the pre and post mining sediment boundary. One such analysis involved testing samples of the bank for Caesium-137, a radioactive isotope produced from Mt Lyell mining practices known to adsorb onto fine sediment. Locher intended to further define the pre and post mining boundary by assuming that the pre mining sediments would contain no trace of this isotope. However, positive results for Caesium-137 in all but two samples were deemed unreliable due to evidence that Caesium may leach down a profile to contaminate original bank sediment.

In addition, Locher used sediment copper concentrations to further define the pre and post mining boundary, with the assumption that copper concentrations would be far greater in those sediments considered to be mine derived. Generally copper concentrations were greater in the assumed mine sediments, however, relatively high concentrations also at greater depth in the natural bank suggested that copper is leaching through to the 'natural' sediments.

Despite leaching problems, Locher found some consistent characteristics. Relatively coarse orange sand or sand clay near the surface is considered mine-derived sediment, while at depth, yellow brown, brown or black, finer grained sediment (>20% silt and clay) with a loam component is indicative of a natural sediment bank. Based on these determining characteristics, Locher's findings for sediment bank H show mine derived sediment covering original sediment bank at a thickness ranging between 0.5 and 2m (Appendix 1).

1.4 Environmental Concern

Taylor et al (1996) suggested that the sulphide mineral content of the tailings is 2-3%. Green (1997) suggested that the overall mass loading of acid and metals from the groundwater and sediment in all riverbanks plus the delta, represents less than 1-5wt% of the total loading from the Mt Lyell minesite.

The largest environmental problem resulting from the tailings banks is oxidation of pyrite as when the oxidised tailings interact with water sulphuric acid is produced. Increased acidity can in turn facilitate adsorption of a range of soluble metals illustrated by the following reactions:

$$FeS_2 + 3O_2 + H_2O = Fe^{2+} + 2SO_4^{2-} + 2H^+ \quad (1)$$

$$Fe^{2+} + 2.5H_2O + 0.25\ O_2 = Fe(OH)_3 + 2H^+ \quad (2)$$

$$Fe^{2+} + 0.25O_2 + H^+ = Fe^{3+} + 0.5H_2O \quad (3)$$

$$FeS_2 + 14Fe^{3+} + 8H_2O = 15Fe^{2+} + 2SO_4^{-2} + 16H^+ \quad (4)$$

Reaction 1 proceeds directly from contact of pyrite with air and/or water. Once this has occurred, reaction 2 and 3 are self-perpetuating and result in precipitation of hydroxides and Fe^{3+} respectively. The presence of sulphur-oxidising bacteria in reaction 3 acts as a catalyst

for the reactions (Bird, 1995; Kelly, 1988). In addition, indirect oxidation is possible with trivalent ferric iron serving to oxidize pyrite. Hence production of Fe^{3+} from reaction 3 allows for the oxidation of pyrite in reaction 4. This reaction produces substantially more acidity than air/water oxidation (Smith, 1998).

The production of acid from these reactions can then serve to mobilise heavy metal ions such as Al, Fe, Mn and Cu at toxic levels into the groundwater and river systems. Indeed this has been the case in the King River, which is now essentially devoid of aquatic life (Koehnken, 1997).

1.5 Thesis aims and objectives

The overall aim of the study reported in this thesis is to determine the discharge of groundwater from bank H into the King River with consideration of climatic effects. Two approaches are taken to achieve this goal: a) analytical methods and b) numerical modelling methods. To achieve the study aim, the following objectives were set which necessitated both a hydrological and a geophysical investigation.

ANALYTICAL METHODS

- Determine the groundwater flow paths using hydraulic head measurements from installed piezometers
- Determine the sediment hydraulic properties from recovery tests

NUMERICAL METHODS

In addition to the hydraulic data required for the analytical method, the banks internal structure was sought by means of a geophysical investigation. A meticulous topographic survey was conducted on the 1st and 2nd of March for numerical modeling purposes and to determine topographic relationships with hydraulic and electromagnetic responses (Figure 1.2).

The final aim of this project is to compare the results from this study to that of bank D (Hooper 1997) and a less detailed investigation of bank H completed by Taylor et al (1996).

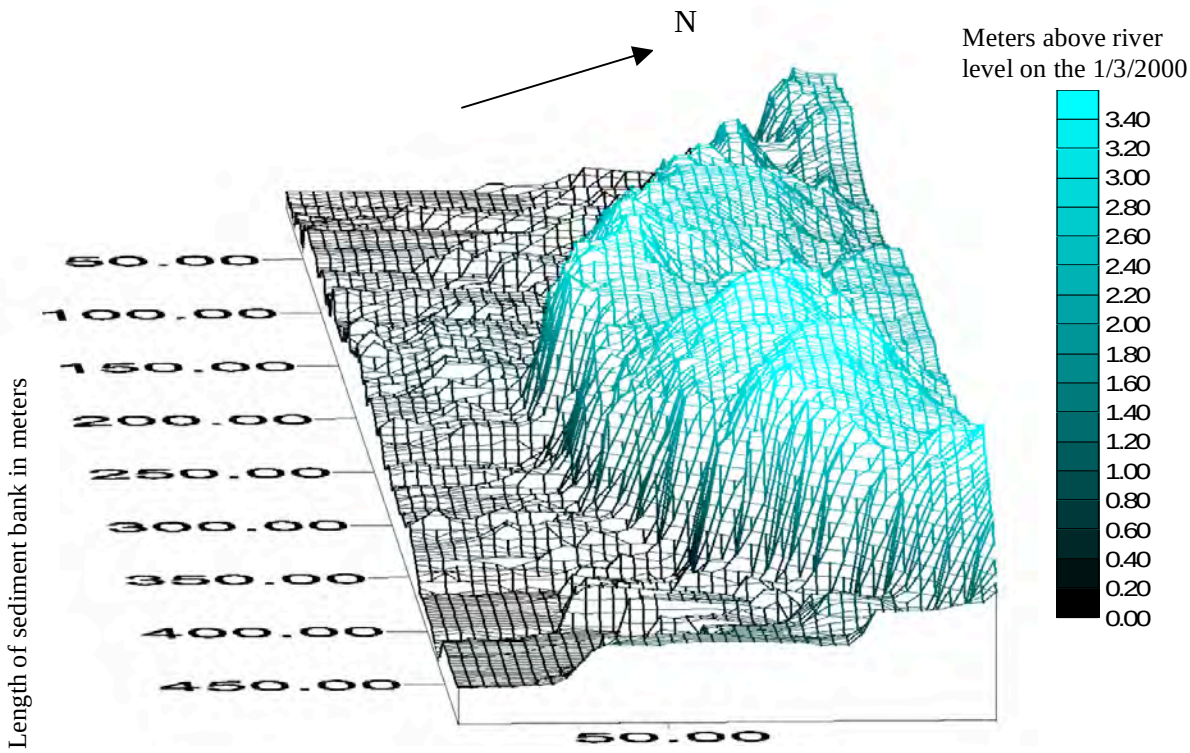

Figure 1.2. Topographic surface contour image.

1.5 Previous work

There is substantial literature related to the King River and associated environmental issues. This includes Locher (1997), Taylor et al (1996), Green, (1997), Hooper (1997) and 16 separate projects emanating from the 'Mt Lyell remediation research and demonstration program' funded by the Department of Environment and Land Management, Tasmania and the Office of the Supervising Scientist, Commonwealth of Australia.

Chapter 2: Design and Methods of Hydrogeological Investigation

2.1 Introduction

An invasive groundwater investigation involved the installation of monitoring wells (piezometers) into the sediment bank. This enabled the hydraulic head and hydraulic conductivity of the sediment to be determined. The data has been used to suggest flow paths, including the distribution of recharge and discharge areas and the rate of groundwater movement (chapter 3). In addition, the piezometers enabled groundwater samples to be collected at varying depths for electrical conductivity (EC) measurements (chapter 5).

2.2 Monitoring network

2.2.1 Placement of Piezometers

The design of the monitoring network was based on Hooper's (1997) finding that the dominant flow direction through bank D is perpendicular to the river. Consideration was also given to provide adequate coverage of the aquifer. This was achieved by running a base line at 95^{o} E along the length of the bank and installing piezometers approximately evenly spaced along traverses extending at 90^{o} to the base line (Figure 2.1). Hence, the network not only facilitated cross-sectional analysis perpendicular to the river but also laterally along the bank.

The emplacement depth of the piezometers was dependent on the feasibility of hand augering and the degree of saturation of the sediment. Whilst the network was aimed at establishing a uniform depth of emplacement, the desired depth was not always achieved. At several locations, deeper piezometers were installed adjacent to shallow piezometers (piezometer nests) to determine whether a component of vertical groundwater movement exists. To minimise the disruption of sediment at these locations, piezometers were inserted with a 1 metre lateral separation. Table 2.1 lists the penetration depth of individual piezometers. Hooper (1997) and Green (1997) established that at bank D, recharge is greatest close to the road and flow predominantly discharges into the river. Subsequently, piezometer nests were inserted along a traverse in the middle of the bank (240mW), providing information on the variation of vertical groundwater movement in a potential recharge zone (240mE, 3.9mS), discharge region (240mE, 45.8mS) and transmission zones (240mE, 32.3mS). Nests were also sited at 140mE, 10mS and 300mE, 21mS to provide a spatial comparison.

A topographic depression downstream (west) of the bank forms a discharging creek. This area was monitored by piezometers 1, 3-9 (Figure 2.2), to determine whether this surface feature is a prominent subsurface groundwater path.

Piezometer	Easting	Southing	depth below surface (m)
1	70	18	1.888
2	80	6.3	0.908
3	80	19.3	1.054
4	120	2	0.456
5	120	12	1.014
6	120	30.7	1.423
7	140	10	0.8
8	141	10	1.28
9	180	10	0.463
10	180	30	2.322
11	180	44	1.916
12	240	3.9	0.5
13	241	3.9	0.7
14	240	12.3	0.548
15	240	32.3	1.35
16	241	32.3	1.998
17	240	45.8	2.556
18	241	45.8	1.71
19	300	2	0.802
20	299	21	2.4
21	300	21	1.87
22	301	21	1.346
23	300	36	1.019
24	360	2	0.53
25	360	11	1.008
26	360	32	1.366
27	450	5	1.598
28	450	10	1.91

Table 2.1 Number and location of piezometers and their corresponding depth. Depths are taken from the elevation topography at the location of the piezometer. Depths of less than 1.4 metres were considered shallow, and greater than 1.4 metres (highlighted) considered deep.

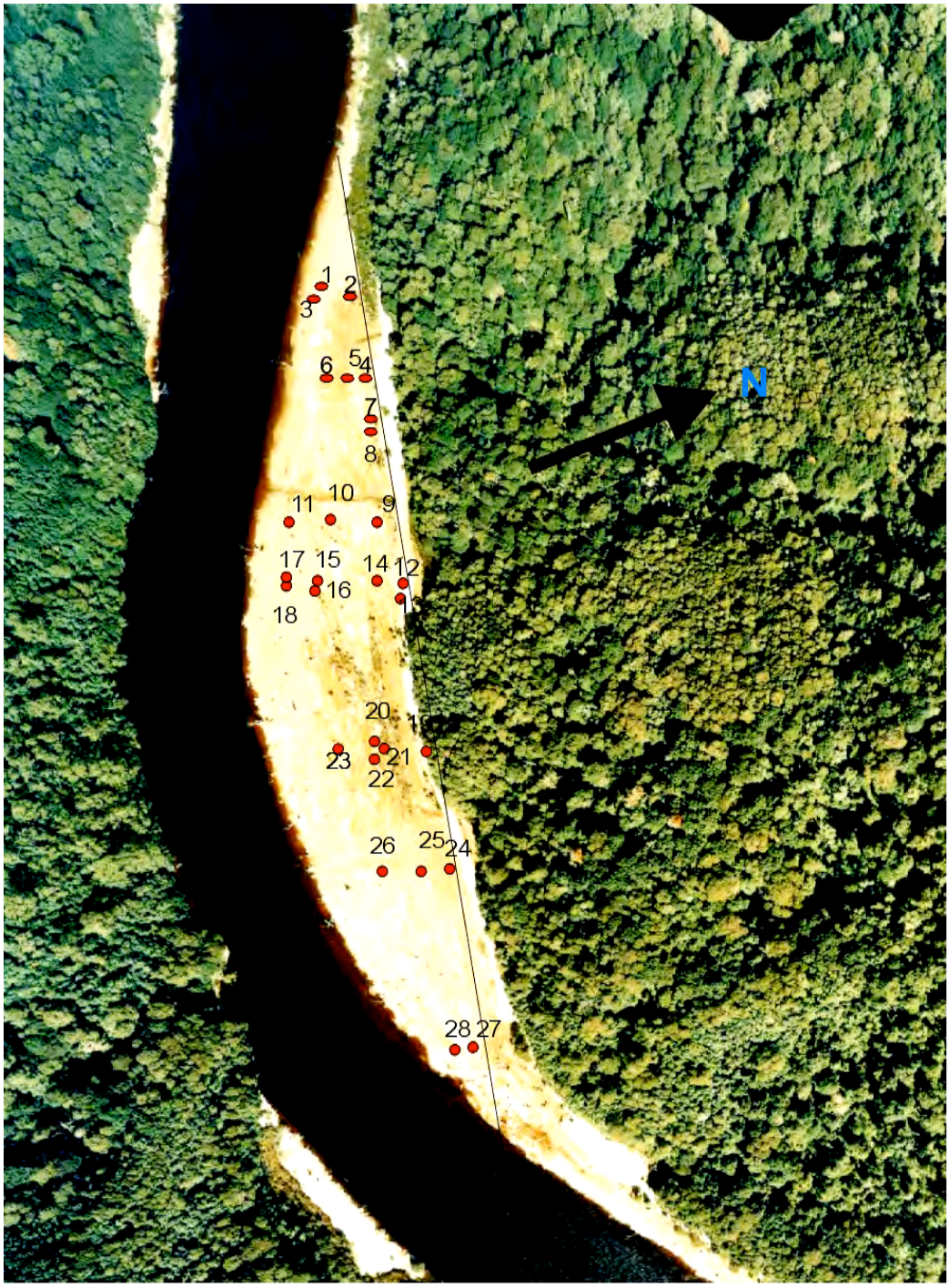

Figure 2.1. Piezometer location map.

2.2.2 Design and Construction of Piezometers

Twenty-eight piezometers were manufactured based on a design by Taylor et al., (1996). An angle grinder or a hand saw was used to cut 3mm thick slots into opposite sides at one end of 50mm ID PVC pipes. All slotted intervals were 40cm and covered with a 125 m mesh attached with epoxy resin. A PVC plug was fastened to the slotted end with plumbing glue (Plate 2.1)

2.2.3 Emplacement of piezometers

A 70mm barrel hand auger was used to core out sediment, with additional 1 metre extensions added for greater penetration depths. An initial hole was drilled until the water content became so great that it was not possible for the auger to extract the sediment. A 75mm diameter plastic casing was then forced into the sediment. Working quickly to overcome recovery rates, water was bailed from the casing and augering continued until the sediment again proved too saturated for use of the auger. This process was repeated until the desired depth was reached or progress ceased. The auger was then driven as far into the tailings as possible to suspend the sediment and allow insertion of the piezometer.

To insert the deeper piezometers, a shallow ditch was dug before augering to combat suction of the casing which prevented its removal. To disturb the sediment as little as possible, care was taken not to exceed ditch depths of 50cm.

Once the piezometers were in place, the annulus between the outer edge of the auger holes and piezometers was back filled with the excavated sediment. As the sediment is unconsolidated, it collapses around the base of the piezometer preventing any packing and sealing of the screened intervals (McPhail, 2000).

Small scale possibly confining clay seams were observed in several trenches (Plate 2.2). Lenses were discontinuous (lateral extent <30cm and thickness <10cm) and thus, believed unlikely to represent confining layers.

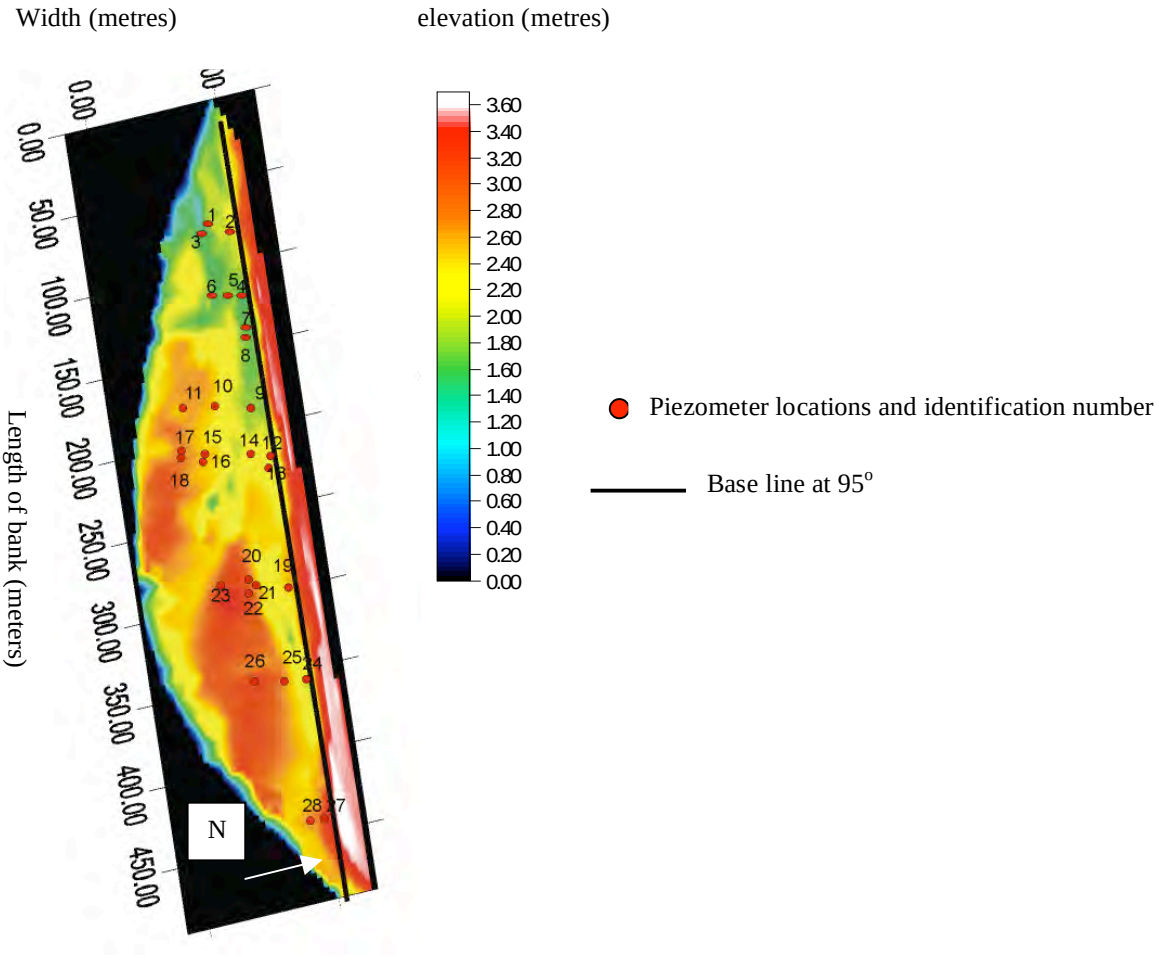

Figure 2.2. Location of piezometers in relation to topography (measurements have not been adjusted to the Australian Height Datum).

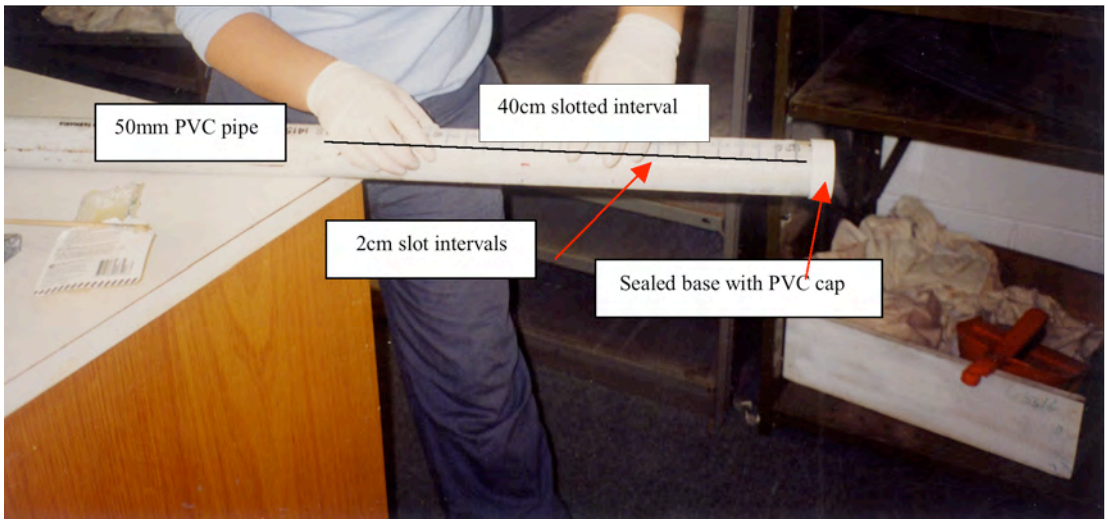

Plate 2.1. The construction of a piezometer

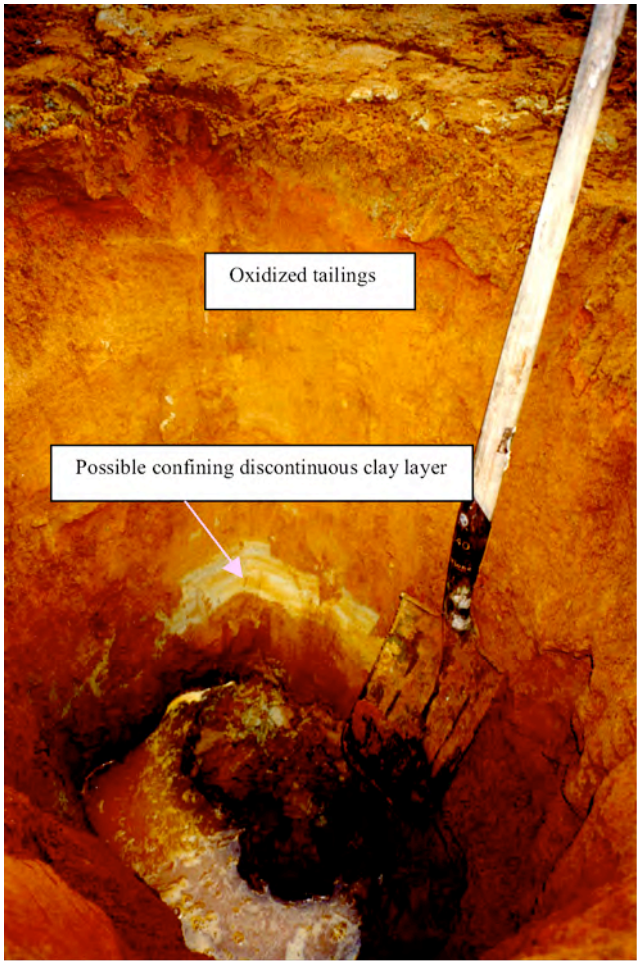

Plate 2.2. A discontinuous possible confining clay lens (~10 x 30 cm) was noted when digging an initial trench and again in core samples from deeper augering. Location of piezometer is 240mE, 48.8mS.

2.2.4 Preparation for monitoring

As hydraulic head within the piezometers may have become unsettled during well installation, wells were purged and left to recover for a minimum of three weeks before hydraulic head measurements were taken. The piezometers were capped with a PVC plug to prevent rain and aerial sediment from entering the well.

Before the hydraulic data could be processed, it was necessary to relate the piezometers to each other and a fixed datum. Accordingly, piezometer lengths were measured prior to installation and height of protrusion above the bank surface (stick up) were measured post installation. A topographic survey using a dumpy level and staff was conducted to determine the elevation of the piezometers in relation to the river level (as at 1st of March, 2000). On the 2nd of March, the river level rose by ~16 cm before falling back to the previous day's level in the afternoon. It is thought that this river level fluctuation was related to the operation of the John Butters power station. However, the bank is far enough downstream to be influenced by the tides (Taylor et al, 1996; Locher, 1997). The topographic levels were adjusted to be consistent with the first day's river level (Appendix 2).

The river level for 1st March was obtained from Hydro Tasmania which has a monitoring site below Cutten Creek, approximately 800 m upstream from bank H. The zero of their gaugeboard is at 0.22 m AHD. This enabled all levels to be adjusted to AHD.

Average river levels at the time of hydraulic measurements (16th April, 24th July and 24th August) were also obtained from Hydro Tasmania and adjusted to AHD (Appendix 3).

The topographic survey was repeated on 16th April to verify the survey heights of the piezometers.

2.2.5 Monitoring groundwater levels

Effectively, hydraulic head is the height of the water level within a piezometer relative to a datum point. It is directly proportional to the hydraulic pressure of the fluids intercepted by the piezometer screen. In an unconfined aquifer, hydraulic head represents the water table whereas in a confined aquifer, it represents a potentiometric surface.

An electric water-sensitive tape was used to measure depth to water in each piezometer. Combined with the surveyed data, hydraulic head measurements can be calculated by either of two simple methods;

1. survey height + "stick up" – depth to water = hydraulic head (Figure 2.3), or
2. elevation head (Eh) + pressure head (Ph) = hydraulic head (Figure 2.3), where Eh is the survey height plus stick up, minus the length of the piezometer and Ph is the length of the piezometer minus depth to water. Note that survey height is to the ground / piezometer intersection.

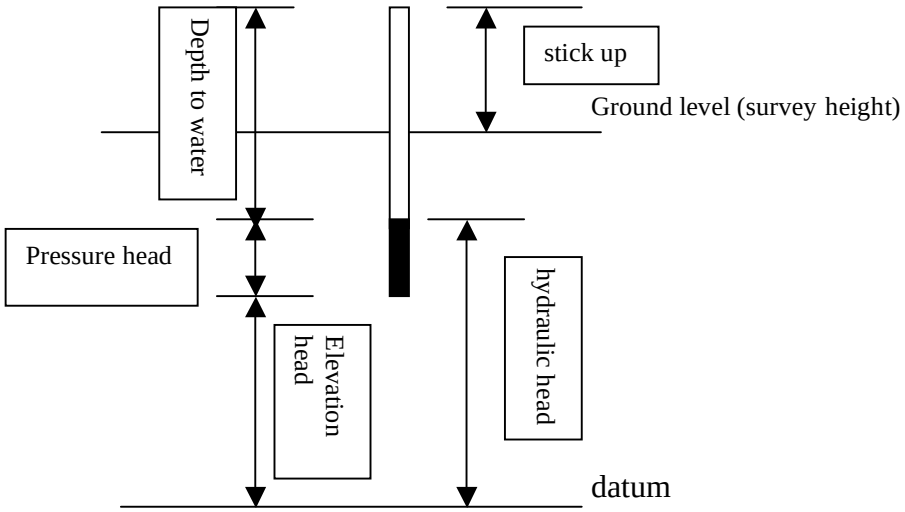

Figure 2.3 Two methods for calculating hydraulic head from survey and field data.

2.3 Monitoring hydraulic properties

The hydraulic conductivity (K) of the sediment was determined by performing rising head using the Hvlorslev technique, which assumes the aquifer to be homogenous and isotropic (Hvlorslev, 1951, in Freeze and Cherry, 1979).

The Hvlorslev method involves bailing a unit of water from a piezometer and recording the depreciated depth at time 0 seconds. Price (1996) suggests that the well must be lowered by at least 10 – 50cm. The rising water levels (recoveries) are recorded with their corresponding times until the level has fully recovered or reached at least 40% of the initial head value (Figure 2.4 a). The proportional rises in head (h/Ho) are then plotted against time on a semi logarithmic graph (Figure 2.4 b). The Hvlorslev analytical method and how it relates to this particular study is discussed in chapter 4.

A limitation of the slug test is that it is heavily dependent on how well the piezometers are designed. If the screen becomes clogged with sediment or corroded, hydraulic conductivity values will be poorly representative of the material (Freeze and Cherry, 1979). However, the general consensus is that in situ field measurements are preferential to grain size and porosity analysis and use of a constant head permeameter test because samples for laboratory work can be disturbed during sampling and transporting (Robertson, 1994; Taylor, 1995; Hooper, 1997; McPhail, 2000; Brassington, 1998).

Brassington (1998), suggested that the single well test provides an accurate determination of aquifer transmissivity (average K x the saturated thickness of the unconfined aquifer).

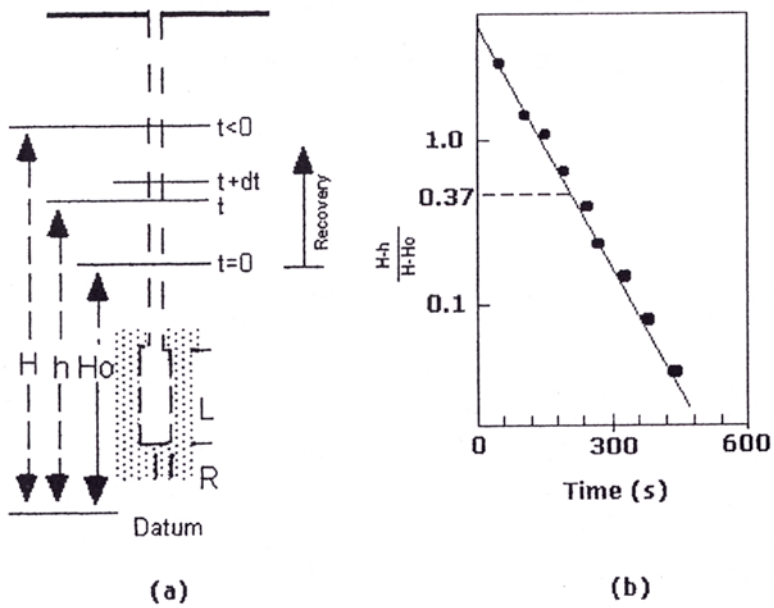

Figure 2.4. The geometry of the Hvlorslev rising head test (a) and (b) the method of analysis (Freeze and Cherry, 1979).

Chapter 3: Hydrogeology of sediment bank H

3.1 Introduction

To understand an aquifer system, a preliminary knowledge of the features that influence groundwater flow paths and velocities is essential. A hydrogeological investigation is critical in assessing the hydraulic and storage properties of the aquifer system within the sediment bank. By combining hydrogeological and geophysical studies, classification of the groundwater storage unit and boundary conditions of the flow system is possible.

3.2 Hydrological Analysis Methods

3.2.1 Hydraulic data

Piezometer hydraulic head values and ponded surface water elevations were calculated on three separate occasions (field trips, 16th April; 24th July; 24th August). Hydraulic head calculations are shown in Appendix 4. River levels for each time interval were provided by Hydro Tasmania, and were averaged and adjusted to relate to the Australian Height Datum (AHD), (Appendix 3). This was possible as the elevation of the King River base was known (0.22m above sea level), along with the average river level at the time of the topographic survey. River levels for subsequent field days were also obtained from Hydro Tasmania. As the river's edge was used as a reference plane for topographic elevations, hydraulic head measurements were also adjusted to relate to AHD.

Hydraulic head contours were calculated using the above hydraulic data for each field day and interpolating between data points applying a kriging method in the computer program *Surfer*. Because piezometer elevations are related to AHD and 3 hourly river levels were known for each field day, the respective river level provided a constant head boundary condition at the river's edge.

To determine horizontal flow, values from the shallow piezometers (depth less then 1.5 metres) were used. To represent vertical flow, hydraulic differences between the upper and lower piezometers were contoured.

3.3.2 Hydraulic Conductivity

Recovery tests (section 2.3) were performed using the Hvorslev method on two separate occasions (16th April; 24th July) to ensure a valid recovery response. Based on these field results, the water level in the well (the ratio of the measured head difference over the original head difference, h/Ho) is plotted against time on a log scale. The time the piezometers took to recharge to 37% of their original level (T_o) could be read off the graph, or calculated from the equation of the line for the few instances when the well did not recover to 37%. Results from the latter method were treated with care as the initial recovery curve was incomplete. By applying the resulting T_o values to a variation of the Hvorslev equation, in conjunction with specific dimensions of the piezometers, the hydraulic conductivity (K) can be estimated (equation 3.1). The Hvorslev equation used requires that the length of the screen interval to be more than 8 times the radius of the well for all tested piezometers (Brassington, 1998).

$$K = \frac{r^2 \, Ln(L_e / R)}{2 L_e T_0} \qquad (3.1)$$

where :

K= hydraulic conductivity (m/s)
r = piezometer radius (m)
L_e = length of the screen interval of the piezometer (m)
R = radius of the well screen (r = R for this experiment)
T_o = time taken for the water level to rise to 37% of the original change.

For an accurate interpretation of T_o and hydraulic conductivity (K), the Hvorslev semi-log graphs used to extrapolate T_o, were analysed. A plot of field recovery data should show an exponential decrease in recovery rate with time. Therefore, when data is plotted on a semi-logarithmic scale, a straight- line plot results (Bouwer, 1974). The majority of graphs conform to the plot requirements (Appendix 5). Those that did not may reflect well construction errors.

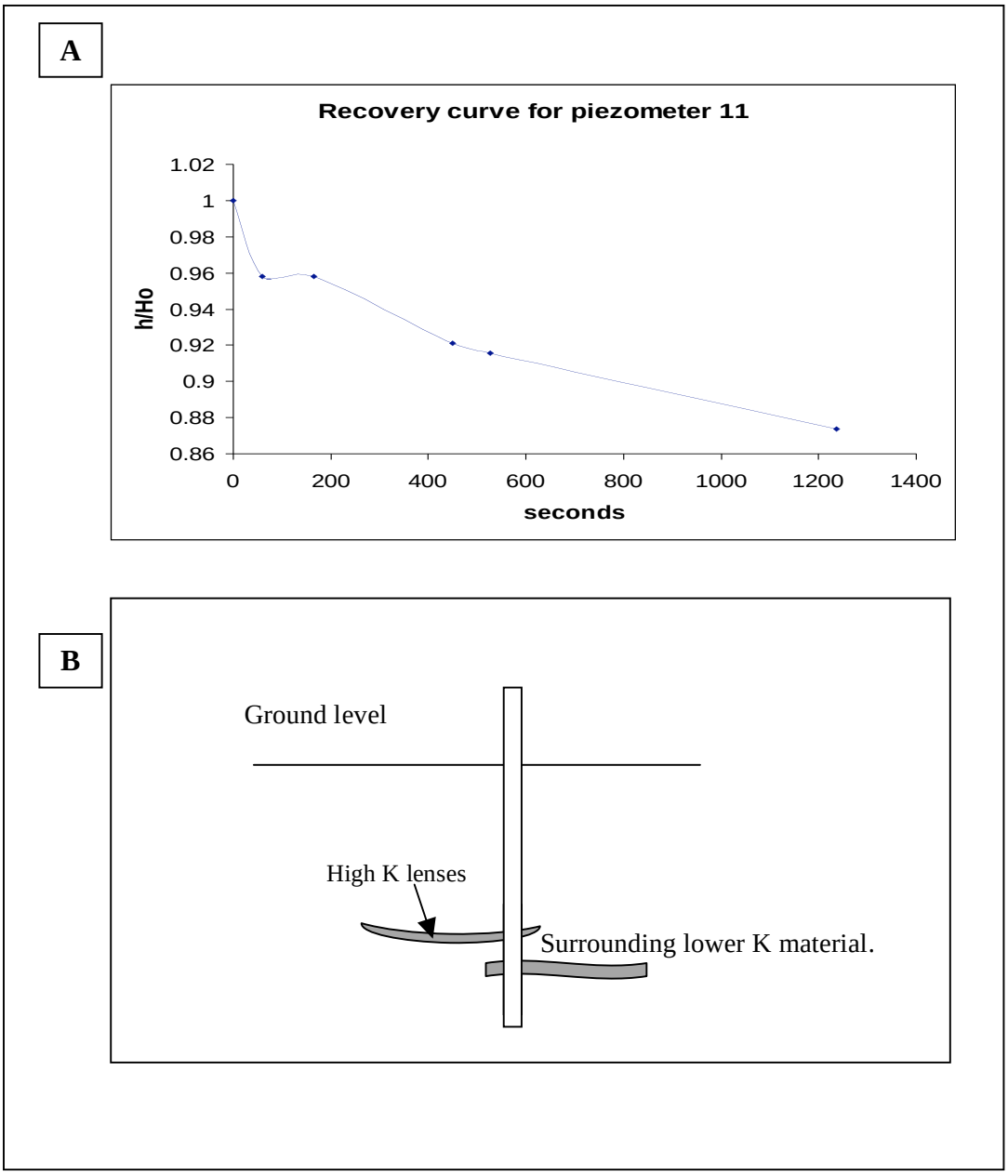

Figure 3.1.A, Recovery response for piezometer 11, showing an initial increase in recovery. After one minute, no increase is noted for a further 100 seconds followed by a slower recovery rate.

Figure 3.1 B, Schematic representation of a possible scenario for such a response. Lenses of higher K material that produces an initial relatively large increase in recovery intersect the screen interval. Once these lenses are drained the surrounding material responds to the reduced head. As this material has a lower K, the response rate is relatively slower.

On both the 16th April and 24th July, the recovery response of piezometer 11 emulates an initial increase in recovery. However, after one minute, no increase is noted for a further 100

seconds, followed by a slower recovery rate (Figure 3.1.A). A possible explanation for such a scenario is that a lens (or lenses) of higher K material intercept the screen interval (Figure 3.1.B). The response could also be explained by well error. For example, augering may have resulted in the annulus (the gap between the piezometer and the augered hole) refill sediment having a higher K value then the surrounding material explaining the sudden initial influx of water. However, this is unlikely for two reasons, a) the unconsolidated sediment is believed to collapse around the piezometer base directly after insertion and b) the difference between the casing and piezometer diameter is 10mm. Thus, it can be assumed that the refill has minimal effect on the recovery characteristics because of the small volume of refill.

Piezometer 1 mimicked a slow initial recovery rate on both field trips (Figure 3.2). It is possible that the force of driving the piezometers into the ground caused compaction of the surrounding sediment, resulting in a slower initial recovery.

An average T_o for each piezometer was taken when values were similar (within a 25% difference of each other). For inconsistent values, the most probable response curve was favoured (Table 3.1).

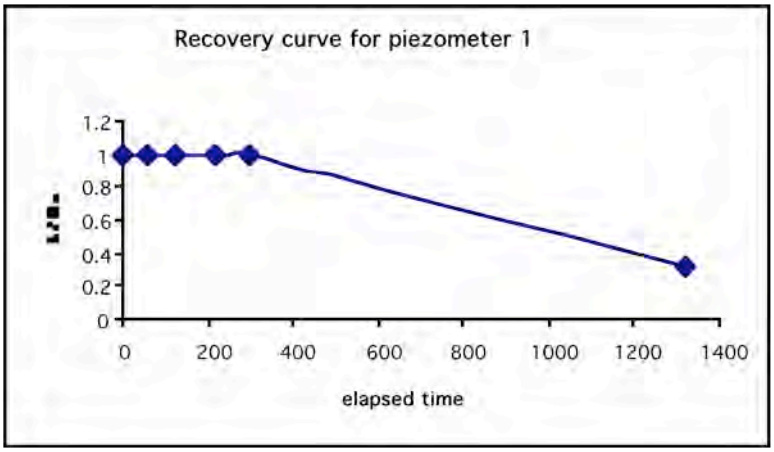

Figure 3.2 Retarded initial response of recovery for piezometer 1 on the 16/4/2000. The second field 24/7/2000) shows a similar response as shown in appendix 5.

Piezometer number	Justification of response curve used from the 16/4 and 24/7
3	The final stage of recovery on the 24/7 suggested a blockage formed due to sediment clogging the screen.
7 , 26, 16, 20	Ideal response curves were produced from the four wells on the 16/4. On the 24/7, the wells were almost fully recovered after 30 seconds. The only explanation for this is piezometer corrosion.
8	Response curve for 16/4 can not be explained. If the slow decrease in recovery is ignored (last 4 values), the T_o values for the two graphs vary by only 5%. Blockage is unlikely, as response of the 24/7 is normal.
27	On the 24/7, there is evidence of consistent blocking from the beginning of the test indicated by a linear recovery curve and high calculated T_o values in comparison to faster recovery rates and ideal recovery curve on the 16/4.

Table 3.1 Possible reasons for why recovery tests between the two field trips yielded inconsistent T_o values (time taken to recover 37% of initial head decrease). Refer to the recovery graphs in Appendix 5.

3.3 Groundwater flow direction

Groundwater flow direction at bank H is dependent on both precipitation (and possibly evapotranspiration) and river levels.

Hydraulic head values were on average 20 cm higher on the 24th July, 2000 than on the 16th April, 2000. Respective total rainfall for both months were 79mm and 203mm. With the exception of several higher head values close to the river on the 16th April, 2000, measurements are similar to those on the 24th August, 2000. As rainfall is slightly lower in August (63 mm/month), higher evaporation in April (Appendix 6) may play a role in lowering hydraulic head.

Hydraulic head contours were constructed to infer horizontal flow direction (Figure 3.3). Hydraulic head values were consistently higher in the bank compared with respective river levels at the time of measurement and were of the highest elevation in the middle northern section of the bank for the three field trips.

This pattern suggests that flow radiates from this area at approximately right angles to the river. Contour levels decrease towards the river, indicating that flow is progressing from the banks towards the river. This is in agreement with studies of bank D (Hooper, 1997) and banks N, H, R (Taylor et al., 1996). However, on the 16th April, 2000, relatively high

hydraulic head values exist proximal to the river, with lower head values on the same traverse in the centre of the bank (Figure 3.3a). This indicates a reverse hydraulic gradient. This scenario could be justified if the river level was higher than water levels within particular piezometers close to the river. This could occur in periods of a) low rainfall or b) high river levels, or a combination of the two. If the reversal is true, it can be suggested that river levels were higher prior to field measurements on the 16th April and that the bank had not yet stabilised to the hydrological stresses at the time of measurement. Alternatively, the hydraulic head values of piezometers 20-22 (centre of traverse) could be in error, or indicate a perched water table. The latter is unlikely as measurements from the other two field trips contradict this explanation (section 3.3.1).

Hooper (1997) calculated localised reverse hydraulic gradients upstream at bank D during summer. McPhail (2000) suggested that reverse gradients could affect the sediment and water compositions of the bank. As the river is likely to be more oxygenated, increasing the dissolved oxygen levels in the bank may increase oxidisation of the sediment, and thus, the potential for increased acid production and dissolution and precipitation of minerals. For example, dissolution of sulphides results in the precipitation of iron oxyhydroxides minerals. In addition, element concentration of the contaminated groundwater would be elevated due to the higher metal concentrations in the river (Green, 1997).

The surface creek downstream of bank H (~140 m E), is shown to represent a subsurface conduit, especially in high rainfall (Figure 3.3b). This is indicated by the interaction between the conduit flow path and hydraulic contours observed by contour “kinks” peaking towards the river. Similar contour “kinks” peaking towards the river are identified at 240m E, 300m E and 360m E on all three images (Figure 3.3). Although surface drainage channels were not observed in the field, it can be suggested that they represent preferential subsurface paths (Figure 3.3).

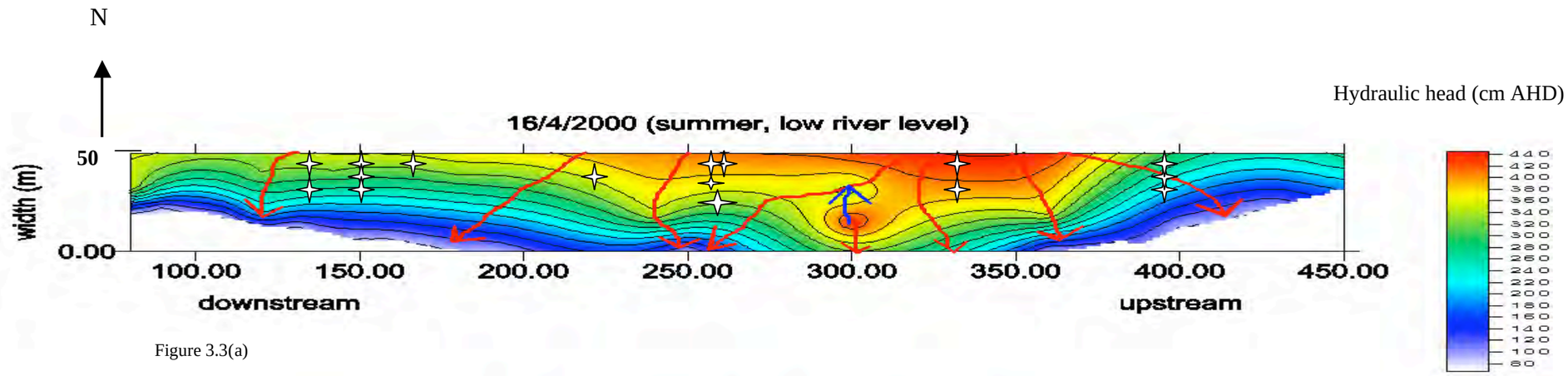

Figure 3.3(a)

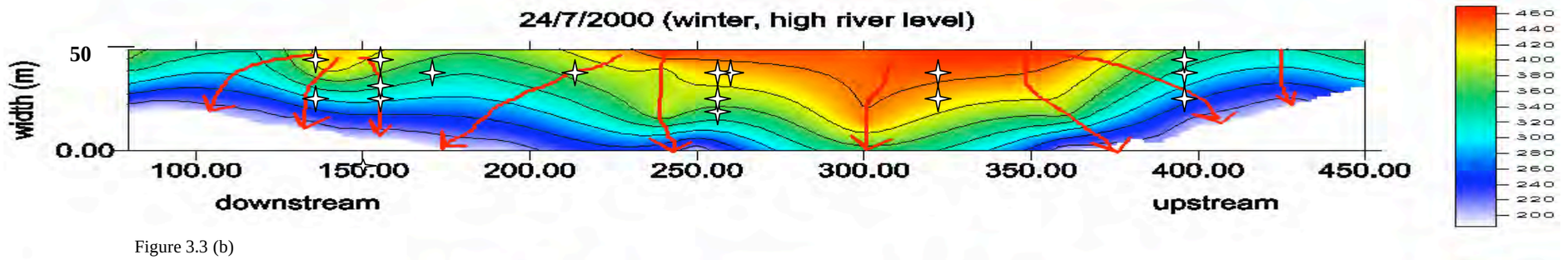

Figure 3.3 (b)

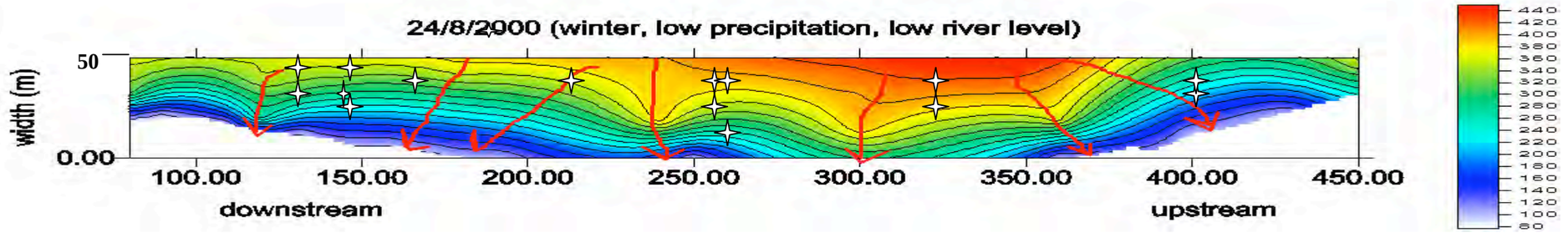

Figure 3.3 (c)

Figure 3.3 Hydraulic contours were constructed from hydraulic head data from shallow piezometers (location indicated by stars), surface water elevations and average river levels at the time of measurement. Images for all three field trips illustrate a general trend of ground water flow towards the river. Possible remnants of reverse hydraulic gradient were observed on the 16/4 (figure 3.3a) indicated by the blue arrow. Groundwater velocities increase proximal to the river indicated by closely spaced contours. Velocities on the 24/7 are slower despite higher rainfall due to a higher river level resulting in a decrease in the hydraulic gradient.

3.3.1. Vertical recharge zones

By contouring the vertical hydraulic difference between shallow and deep piezometers, areas of possible vertical recharge can be inferred. Limited piezometer nests severely retarded this component of the hydrogeological investigation. However, some important observations were made.

Piezometer	Easting (m)	Southing (m)	16/4/'00 (cm)	27/7/'00 (cm)	27/8/'00 (cm)
7 to 8	141	10	3.7	0	4
12 to 13	241	3.9	0	0	0
15 to 16	241	32.3	3	2.7	5.2
18 to 17	241	45.8	-84	-68.6	-63.8
20 to 21	300	31	-20.7	-6.9	-21.7
21 to 22	301	31	10.1	0.3	1.9

Table 3.2 The hydraulic head difference between deep and shallow piezometers at certain nest locations. A negative difference indicates a downward component of flow (recharge) and positive values infer an upward component of flow (discharge) or perched water tables.

Table 3.2 lists the hydraulic head difference between shallow and deep piezometers for particular times of measurement and Figure 3.4 illustrates spatial distribution of differences for the 24th July, 2000. As illustrated in Table 3.2, hydraulic head difference images for the 16th April and 24th August are spatially identical to Figure 3.4.

Groundwater has the greatest potential for recharge in the middle of the bank proximal (approximately 5m) to the river and the least potential to the north of the bank closest to the road. Hooper (1997), discovered the opposite (vertical recharge greatest closest to the northern boundary decreasing towards the river). A possible explanation for the contradicting results between the two banks is the occurrence of clay horizons in either the saturated or unsaturated zone at bank H. If these hypothesised horizons inhibit percolation, a localised perched water table is probable. On the 24/7, piezometers 19 and 24 had higher piezometric heads than surface topography (Figure 3.5). Piezometric heads were closer to the surface on the 16/8 and just below the surface on the 28/7. It is possible that increased hydraulic loading during the higher rain period supported higher pressure levels in piezometers that intersecting a confining layer. This theory is suggested for other locations where the pressure head is higher than the inferred water table (Figure 3.5).

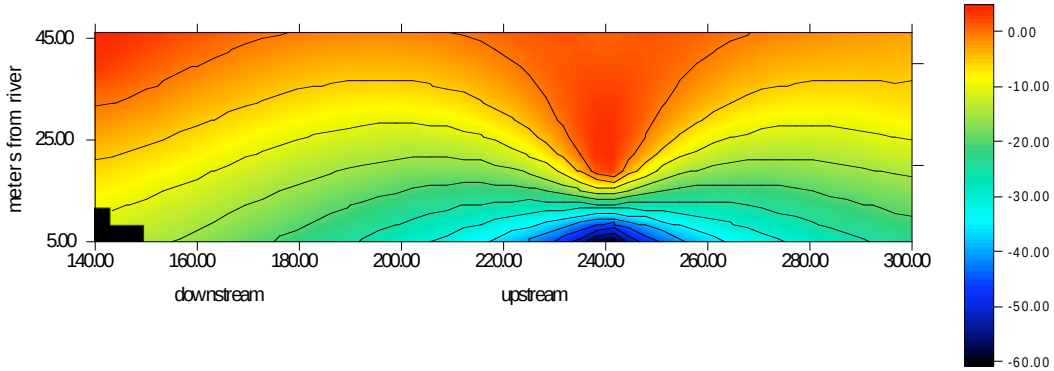

Figure 3.4. Vertical hydraulic differences in pressure between upper and lower piezometer values, indicating regions of likely downward movement and possible perched water tables at bank H.

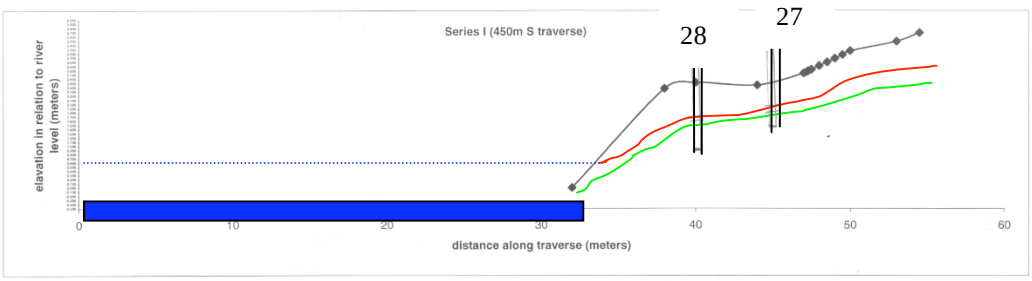

King river level on the 24/8/2000

King River level on the 24/7/2000

Water table for the 24/8/2000, potentiometric head

Water table for the 24/7/2000 potentiometric head

Figure 3.5. Cross sections of piezometer traverses illustrating hydraulic gradients, hydraulic head and possible potentiometric heads in hypothesised confined scenarios. Cross sections continued on following pages.

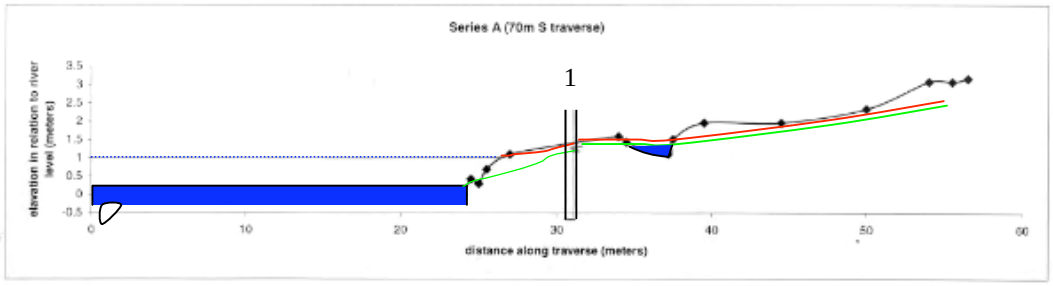

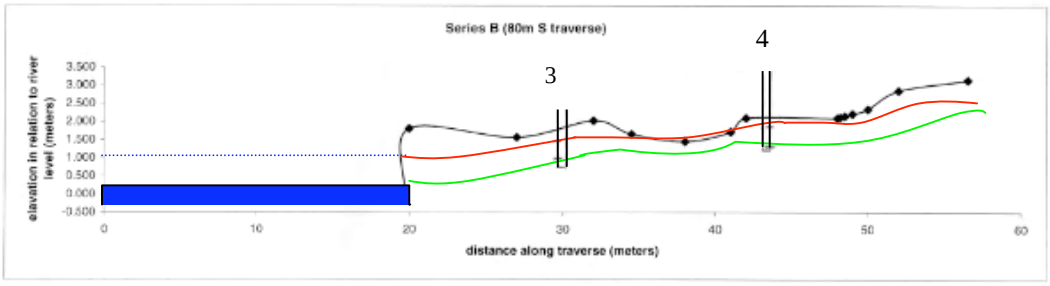

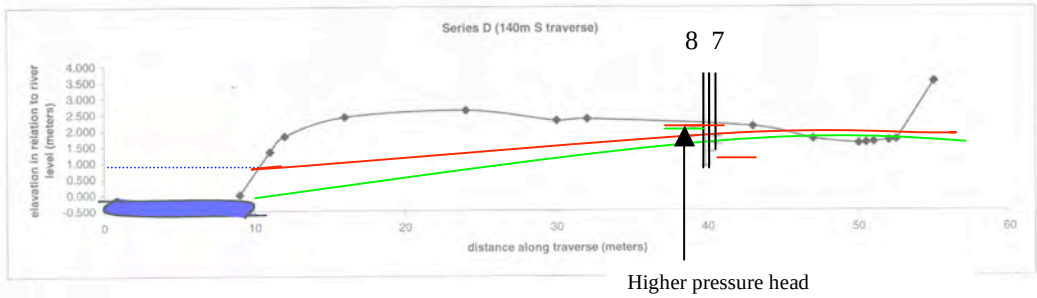

King river level on the 24/8/2000

King River level on the 24/7/2000

Water table for the 24/8/2000, potentiometric head

Water table for the 24/7/2000 potentiometric head

Figure 3.5. Cross sections of piezometer traverses illustrating hydraulic gradients, hydraulic head and possible potentiometric heads in hypothesised confined scenarios. Cross sections continued on following page.

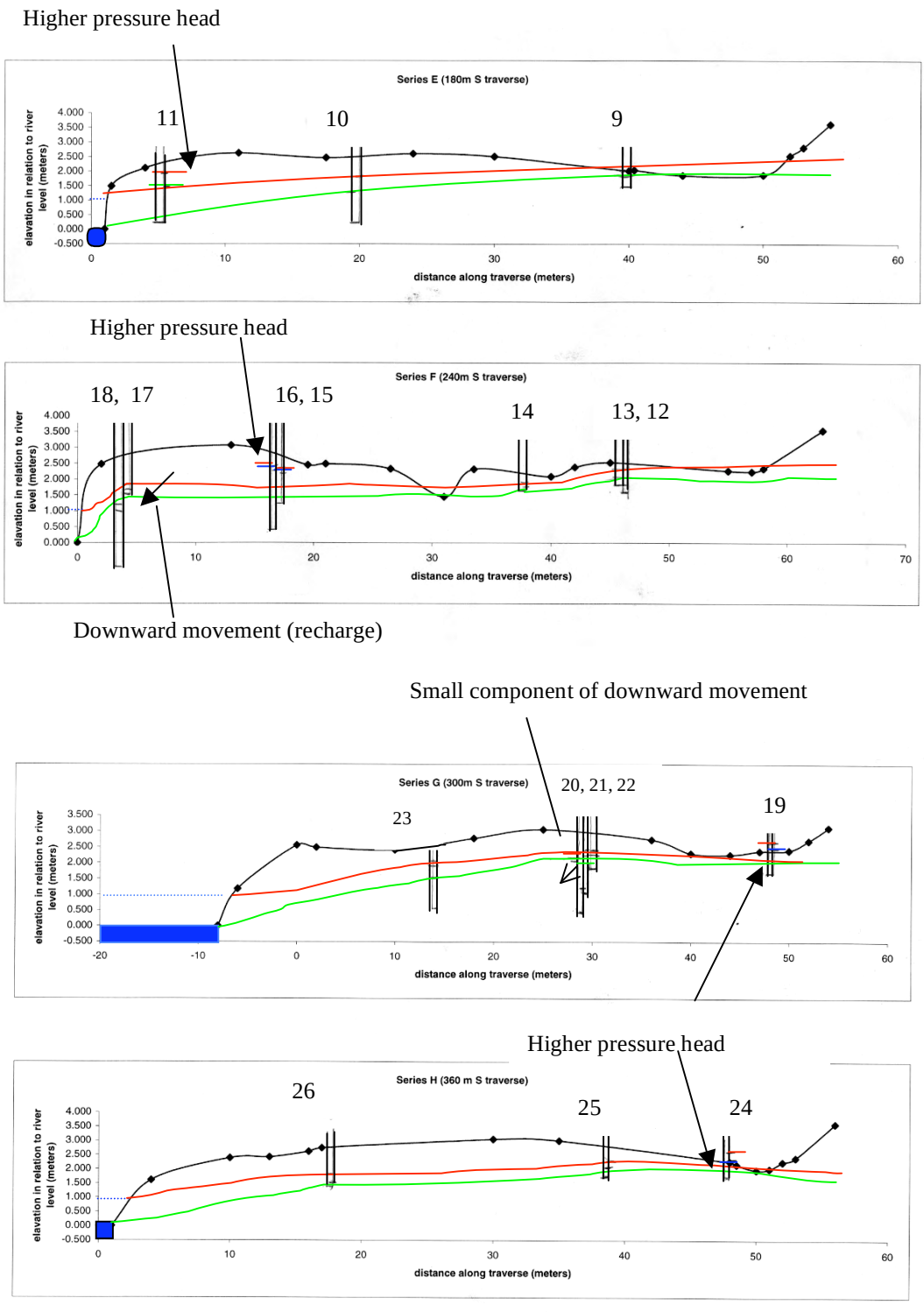

Figure 3.5 continued. Cross sections of piezometer traverses illustrating hydraulic gradients, hydraulic head and possible potentiometric heads in hypothesised confined scenarios.

The hypothesised confining horizon(s) could either result from a) clay lenses as suggested by several piezometer recovery responses, or b) from the formation of hardpans at depth. Hardpan layers can form above the water table due to cementation of secondary precipitants forming a crust, and behave as an aquitard (Robertson, 1994**)**. Such a feature may have formed subsurface at bank H during a depositional flooding event (chapter 1). As a result, hardpans that form subsurface may produce perched water tables (Chermak et al., 1996; Taylor, 1998). Sparse, thin (mm), surficial hardpan layers are evident at bank H (Plate 3.1), which may suggest repetition subsurface. Evidence for hardpan occurrence is the ponding of infiltrating water. Although stagnant water pools may be seen at several locations along the bank, it is possible that they represent the water table. In addition, no confining hardpan layers were observed when augering.

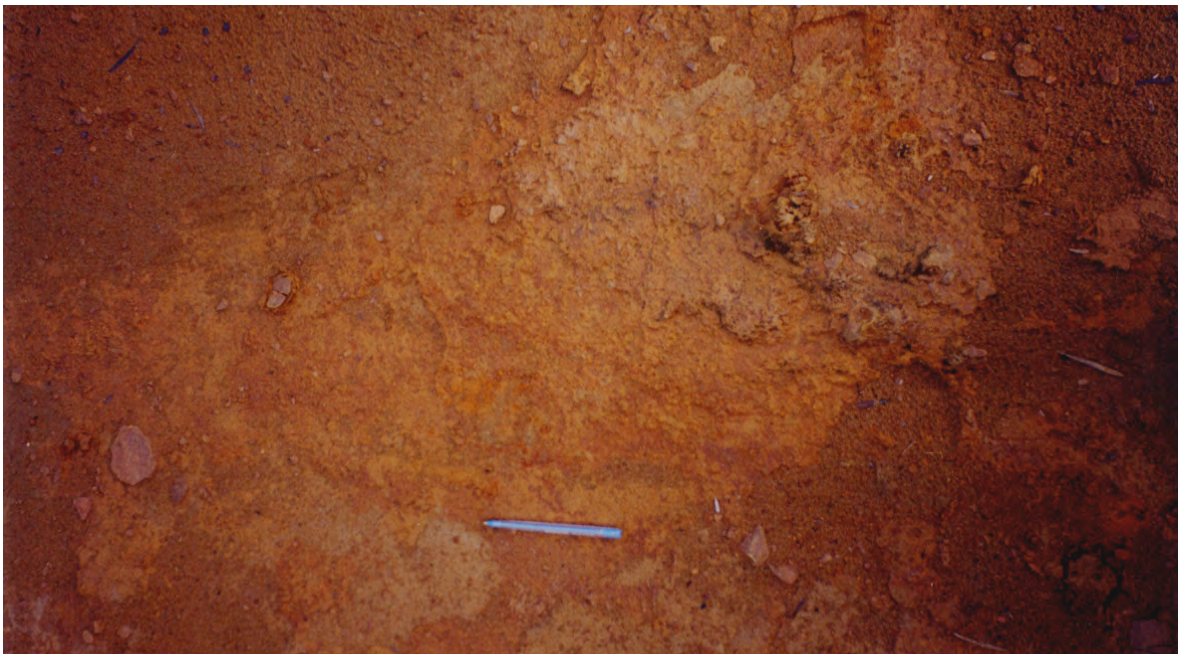

Plate 3.1. Surficial hardpans may suggest occurrence subsurface.

Additional evidence to suggest the presence of at least confining/semi confining unit (units) at shallow depths include auger hole results along a traverse through the centre of bank H, analysed by Locher (1997). Locher (1997) classified the sediment between 1 and 3 metres as natural bank sediment with small particle size (diameter 50<1mm) of sandy clay loam nature. Depending on the clay content, this unit may characterise a low hydraulic conductivity.

3.4 Groundwater flow rates

Groundwater flow rates can be calculated by applying Darcy's law in the following form,

$$v = \frac{Q}{A} = - K \frac{dh}{dl} \qquad (3.2)$$

where v is Darcy's velocity (apparent velocity), Q is the amount of flow (total discharge), A is the cross sectional area of the aquifer (A). As v is equal the hydraulic conductivity (K) multiplied by the hydraulic gradient (*dh/dl*), Q can be determined (Figure 3.6). This equation assumes that the groundwater flows across the entire cross-sectional area of the aquifer. As flow is restricted to the pore spaces, the actual velocity (Va) is much greater than Darcy's velocity and can be calculated as follows :

$$Va = \frac{Q}{aA} \qquad (3.3)$$

where a is the effective porosity of the aquifer (Brassington, 1988; Fetter, 1994). By multiplying the actual velocity by the discharge area (equation 3.2), total discharge flux can be calculated.

To develop an understanding of the flow rate through the bank, the bank was divided into 7 sectors based on the piezometer traverses (Figure 3.7).

3.4.1 Hydraulic Conductivity

Hydraulic conductivity of the sediment ranges between 6.5 E -8 to 7.4 E -5 (Table 3.3), which is generally consistent with values for fine unconsolidated sand (Brassington, 1998). K values lower than 2 E -7 have been suggested by Brassingston (1998) to represent silt, clay and mixture of sand, silt and clay. Sediment samples that yield these low conductivities are generally from the deepest depths. An average value of K for shallow piezometers (less then 1.5 m) is 4.3 E -5. Based on Locher's (1997) finding that tailings are at a maximum thickness of 1.5 metres at bank H (chapter 1), it can be suggested that the lower K values are related to tailings and higher K values associated with the underlying natural fluvial sediment. Hooper (1997), noted that hydraulic conductivities were higher towards the western (downstream) end of the bank. An absence of any lateral trends in K was noted at bank H.

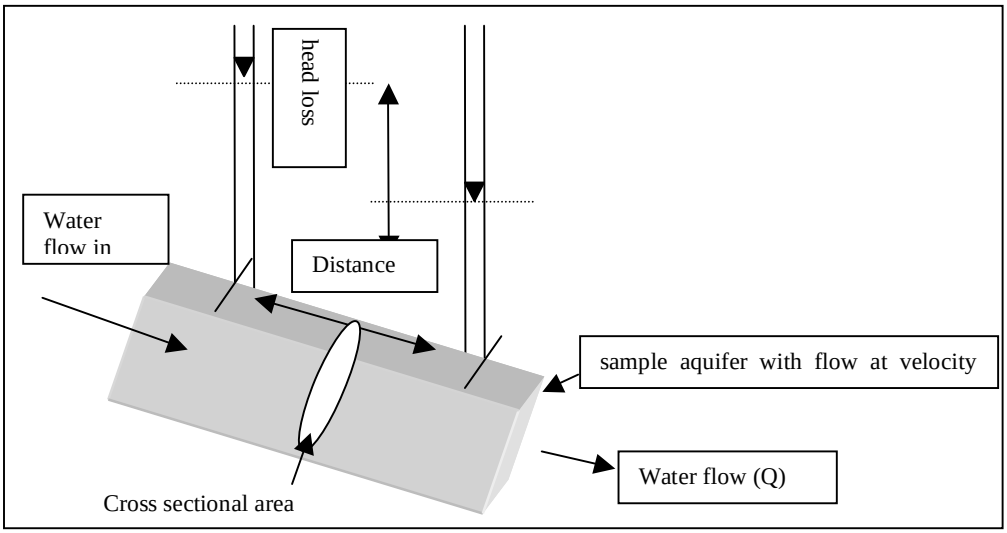

Figure 3.6: Schematic representation of how Darcy's law can be used to calculate apparent velocity. Darcy's velocity (v) is equal to hydraulic gradient (dh/dl) multiplied by hydraulic conductivity (K). The velocity (v) and the cross sectional area of the aquifer (A) determine Q.

Piezometer	depth of piezometer (m)	To (seconds)	r (meter)	R (meters)	Le (meters)	r2ln(Le/R)	2Le*To	K (m/s)	K (m/d)
1	1.888	1146	0.025	0.026	0.4	0.001708	916.8	1.86339E-06	0.160997
2	0.908	68	0.025	0.026	0.4	0.001708	54.4	3.14036E-05	2.71327
3	1.054	370.5	0.025	0.026	0.4	0.001708	296.4	5.76368E-06	0.497982
4	0.456	63	0.025	0.026	0.4	0.001708	50.4	3.38959E-05	2.928609
5	1.014	164	0.025	0.026	0.4	0.001708	131.2	1.3021E-05	1.125014
6	1.423	1025	0.025	0.026	0.4	0.001708	820	2.08336E-06	0.180002
7	0.8	266	0.025	0.026	0.4	0.001708	212.8	8.02798E-06	0.693618
8	1.28	952	0.025	0.026	0.4	0.001708	761.6	2.24311E-06	0.193805
9	0.463	50	0.025	0.026	0.4	0.001708	40	4.27089E-05	3.690047
10	2.322	1426	0.025	0.026	0.4	0.001708	1140.8	1.49751E-06	0.129385
11	1.916	5581	0.025	0.026	0.4	0.001708	4464.8	3.82627E-07	0.033059
12	0.5	29	0.025	0.026	0.4	0.001708	23.2	7.3636E-05	6.36215
13	0.7	115	0.025	0.026	0.4	0.001708	92	1.85691E-05	1.604368
14	0.548	18.5	0.025	0.026	0.4	0.001708	14.8	7.11815E-05	6.150078
15	1.35	7380	0.025	0.026	0.4	0.001708	5904	2.54826E-07	0.022017
16	1.998	32749	0.025	0.026	0.4	0.001708	26199.2	6.52064E-08	0.005634
17	2.556	1685	0.025	0.026	0.4	0.001708	1348	1.26733E-06	0.109497
18	1.71	557	0.025	0.026	0.4	0.001708	445.6	3.83383E-06	0.331243
19	0.802	59	0.025	0.026	0.4	0.001708	47.2	3.6194E-05	3.127158
20	2.4	2426	0.025	0.026	0.4	0.001708	1940.8	8.80232E-07	0.076052
21	1.87	685	0.025	0.026	0.4	0.001708	548	3.11744E-06	0.269346
22	1.346	2858	0.025	0.026	0.4	0.001708	2286.4	7.47181E-07	0.064556
23	1.019	250	0.025	0.026	0.4	0.001708	200	8.54178E-06	0.738009
24	0.53	73.5	0.025	0.026	0.4	0.001708	58.8	2.90537E-05	2.510236
25	1.008	99.5	0.025	0.026	0.4	0.001708	79.6	2.14617E-05	1.854295
26	1.366	334	0.025	0.026	0.4	0.001708	267.2	6.39354E-06	0.552402
27	1.598	10254	0.025	0.026	0.4	0.001708	8203.2	2.08255E-07	0.017993
28	1.91	3472	0.025	0.026	0.4	0.001708	2777.6	8.54178E-08	0.00738
average								1.49422E-05	1.291007

Table 3.3. Estimates of Hydraulic Conductivity from rising head tests.

3.4.2 Calculated hydraulic gradients

In addition to suggesting flow direction, hydraulic gradients are important for determining groundwater flow velocities as illustrated in equation 3.2. Horizontal hydraulic gradients were calculated both perpendicular and subparallel to the river for both high and low precipitation periods. Because summer results suggested the possibility that bank H was not in hydraulic equilibrium at the time of measurement (e.g. localised reverse hydraulic gradient, low river level), data from the 24th July and 24th August was utilised to suggest the effects of increased rainfall.

Approximate horizontal gradients perpendicular to the river were estimated along traverses between the piezometer closest to the northern boundary and the river level (Table 3.4). Hydraulic gradients vary from 0.06 – 0.16 towards the river in the lower precipitation month (24th August) and were shallower (0.42 – 0.16), in the highest precipitation month (24th July). The river level was 1 m higher on the 24th July than on the 24th August. Based on Hooper's (1997) calculations of hydraulic gradients at bank D (where a constant average river level was used over the study period), it is expected that the hydraulic gradients would be steeper in winter. As illustrated in Table 3.4, hydraulic gradients for both times of measurement were steeper in series 1 and 7 (far upstream and far downstream) of the bank.

Series	from piezo	head 24/7	head 24/8	distance	gradient 24/7	gradient 24/8
1	2	3.939	3.609	28	0.069	0.093
2	4	3.734	3.644	35	0.049	0.075
3	9	3.777	3.647	39	0.045	0.068
4	12	4.66	3.97	51	0.052	0.058
5	19	4.363	4.298	56	0.042	0.059
6	24	4.43	4.31	47	0.051	0.07
7	27	3.832	3.592	18	0.1	0.143

Table 3.4. Hydraulic gradients from the furthest northern piezometer, to the river's edge. All measurements are in metres.

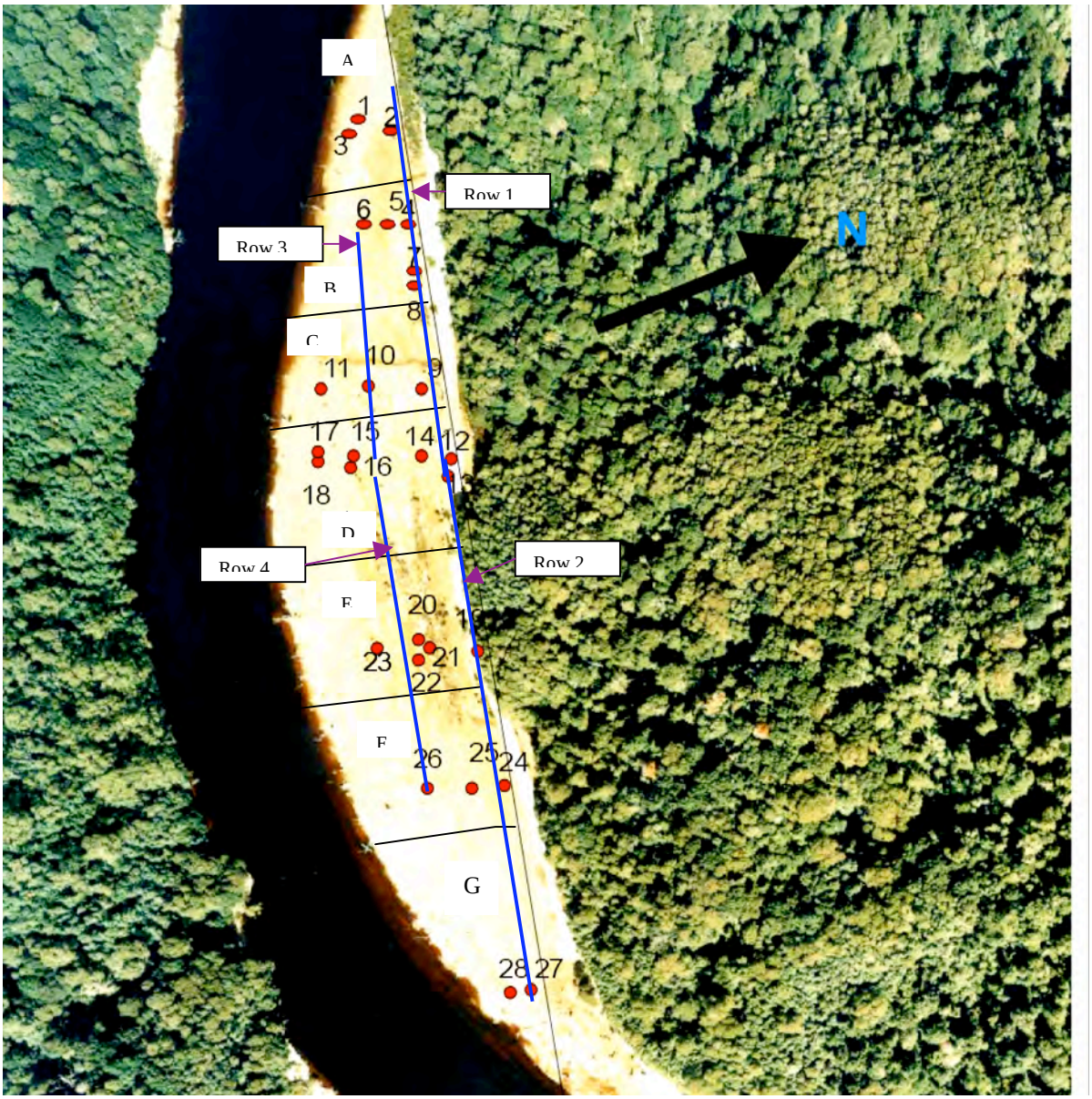

Figure 3.7 For calculation of groundwater discharge, the bank was divided into alphabetical sectors. Blue lines indicate parallel gradient traverses referred to as row numbers.

The topography of the bank is relatively uniform until a rapid decline in elevation to the river over less than 1 metre (Figure 3.8). As a result, the hydraulic gradients were hypothesised to be steeper between piezometers closest to the river and the river's edge, in comparison with gradients through the bank prior to the rapid elevation decline. The contour images also suggest this, evidenced by closer spacing of contours towards the river (Figure 3.3). Calculations suggested that the gradients were approximately 13 times greater closer to the river (Table 3.5 and Table 3.6).

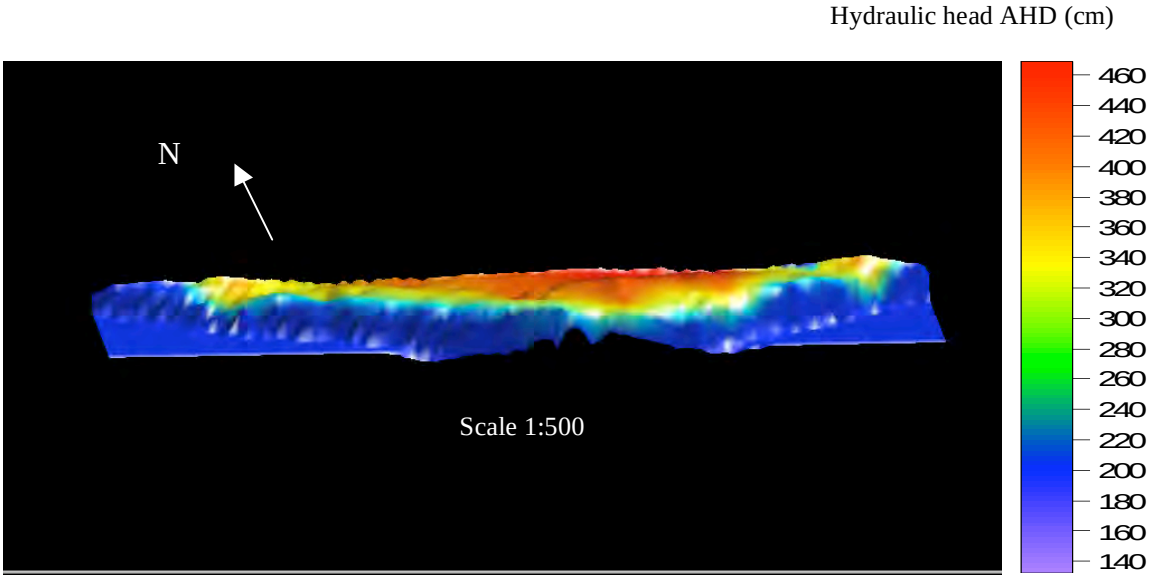

Figure 3.8. 3-Dimensional image of hydraulic head values from shallow piezometers on the 24/7 overlaying topography. Image indicates that the hydraulic head mimics topography. The most rapid decline in hydraulic head values is approximately 1 metre from the edge of the bank.

Series	from piezo	to piezo	24/7 (h1-h2)	24/8 (h1-h2)	distance (m)	24/7gradient	24/8 gradient
1	2	3	0.443	0.313	13	0.034	0.024
2	4	6	0.6	0.72	28.7	0.02	0.025
3	9	10	0.109	0.389	20	0.005	0.019
4	12	17	1.529	0.789	42	0.036	0.019
5	19	23	0.051	0.336	34	0.001	0.009
6	24	26	0.405	0.625	30	0.01	0.02
7	27	28	0.102	0.062	5	0.02	0.012

Table 3.5. Hydraulic gradients between piezometers closest to the northern boundary and piezometers closest to the river before decrease in topography. All measurements are in metres.

Series	from piezo	24/7 (h1-h2)	24/8 (h1-h2)	distance	24/7gradient	24/8 gradient
1	3	1.486	2.286	8	0.185	0.28
2	6	1.124	1.914	7	0.16	0.27
3	10	1.658	2.248	19	0.087	0.11
4	18	1.807	2.809	9	0.2	0.31
5	23	2.302	2.952	12	0.19	0.246
6	26	2.015	2.675	17	0.12	0.16
7	28	1.72	2.52	8	0.215	0.315

Table 3.6. Hydraulic gradients between piezometers closest to the river and the river's edge. All measurements are in metres.

Hydraulic gradients parallel to the river were calculated between hydraulic head values in the middle of the bank (300mE) and piezometers at a similar south location upstream. The same was done for piezometers downstream (Figure 3.6). Hydraulic gradients parallel with the river are between 5 and 160 times smaller than gradients perpendicular with the river. Minimal variation is evident between the two times of measurements (0.0004-0.007 on the 24th July and 0.0008-0.007 on the 24th August), however on both trips, gradients were slightly higher upstream compared with gradients towards the downstream.

row	from piezo	to piezo	24/7 (h1-h2)	24/8 (h1-h2)	distance	24/7gradient	24/8 gradient	
1	12	2	0.721	0.361	160	0.00450625	0.00225625	upstream
2	12	27	0.828	0.378	210	0.003942857	0.0018	downstream
middle of bank								
3	15	6	0.941	0.866	120	0.007841667	0.007216667	upstream
4	15	26	0.05	0.105	120	0.000416667	0.000875	downstream

Table 3.7. Hydraulic gradient parallel to the river. Measurements are in metres.

3.4.3. Discharge calculations

When determining groundwater discharge by the method explained in equations 3.2 and 3.3, flow was assumed to be horizontal only (Dupuit-Forchheimer theory). To determine actual velocity, a porosity value of 47% was used based on the average porosity of bank D (Hooper, 1997). Hydraulic gradients used to determine velocity were between the most northern piezometer (closest to the road) and the river's edge and between the piezometers along the traverse parallel with the river. Hydraulic conductivities were determined by averaging all the values in each sector and the depth of the cross-sectional area of flow was assumed to be 2.80 m for the 24/7 and 1.20 m for the 24/8. The depth estimation was calculated knowing the river channel depth in relation to AHD and the river level at the time of measurement in relation the AHD (Figure 3.9).

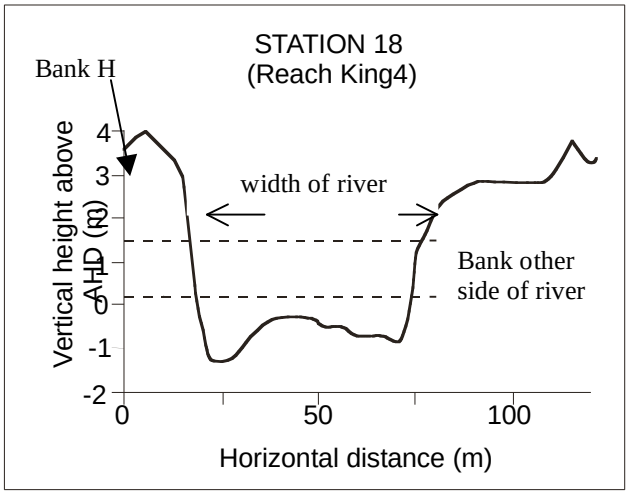

Figure 3.9. Height profile of Bank H and the King River base elevation in relation to AHD (measured by Locher in 1997). Dashed lines represent the depth of the cross sectional area applied to this study based on river levels at the time of measurement. Upper line - 24th July; lower line - 24th August. Profile adapted from Locher, 1997.

Calculated velocities for each sector are displayed in Figure 3.10. As piezometers rarely exceed depths of 2 metres, the averaged K is not a likely representation of the hydraulic conductivity of the deeper sediment, especially considering the trend for lower K with increasing depth. In addition, some sectors relied heavily on a limited number of piezometers for K estimations. Again, this may not assign an accurate representation of the overall K in the sector. For example, although sector 7 had the highest hydraulic gradients on both days of measurement, only two piezometers were in the sector, both yielding low K values. As a result, sector 7 has the lowest velocity. As hydraulic gradients are calculated between piezometers, they may also only represent an approximate horizontal component of the overall hydraulic gradients for the entire bank (McPhail, 2000).

Actual velocities range from 0.0028 – 0.27m/day on the 24/7 and 0.004 – 0.3 m/day on the 24/8. These velocities are approximately 80 times higher than bank D in 1997 (Hooper, 1997). It is probable that the difference is mostly due to this study having both a) higher hydraulic conductivities and b) higher hydraulic gradients (Table 3.8).

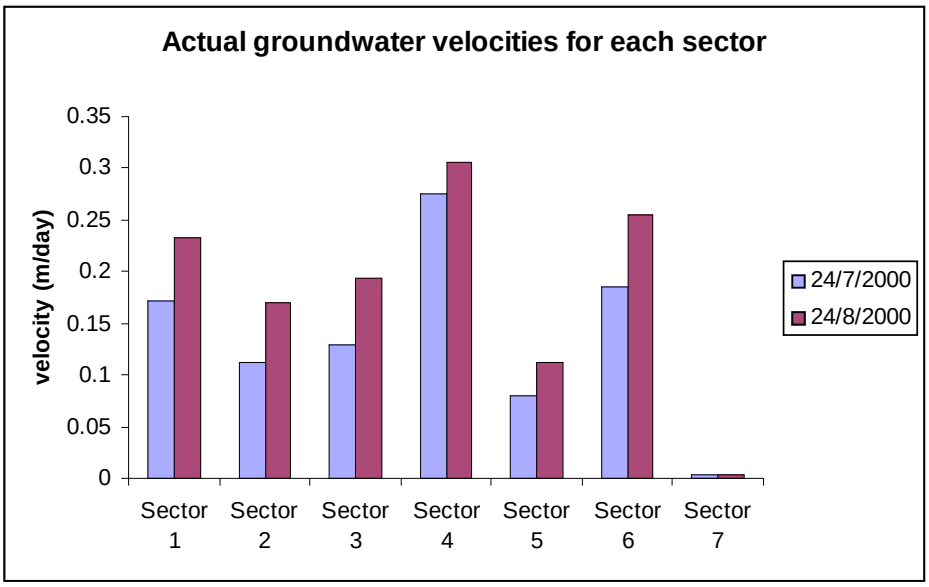

Figure 3.10. Actual velocities for each sector of bank H on the 24/7 and the 24/8.

	this study	Hooper, 1997
Average hydraulic conductivity (m/s)	1.40E-05	2.90E-06
Hydraulic gradient range	0.042 - 0.14	0.007 - 0.060

Table 3.8. Comparison of hydraulic conductivity and hydraulic gradient at this study site (bank H) and bank D (Hooper, 1997). Difference in hydraulic gradient probably due to differences in elevation between the two banks.

Knowing the actual velocity of the groundwater through the bank and the length of the flow paths (width of bank), the residence time of the groundwater within the bank was estimated (Table 3.9). For the fastest velocities and/or the narrowest paths, residence times are as low as 4 months. For the slower velocities and /or longer horizontal flow paths, residence was up to 17.5 years.

	actual velocity (m/y)			Residence time (years)	
Sector	24/7	24/8	length, m	24/7	24/8
1	62.91117	84.79332	28	0.45	0.33
2	40.70664	62.30608	35	0.86	0.56
3	46.87197	70.82875	39	0.8	0.55
4	100.1985	111.7599	51	0.5	0.46
5	29.12784	40.91767	56	2	1.4
6	67.79904	93.05751	47	0.7	0.5
7	1.029028	1.47151	18	17.5	12.3

Table 3.9. Residence times of groundwater dependent on actual velocity. Residence can be explained as the time it takes for groundwater to flow from the northern boundary and discharge into the King River.

Flow rates for each sector of the bank are displayed in Figure 3.11. In comparison to flow perpendicular to the bank, velocities and discharges are both minimal parallel to the bank (Table 3.10).

Total discharge of groundwater into the river at bank H on the 24th July (high rainfall, high river level) was calculated as 187 m^3/day. On the 24th August (low rainfall, low river level), total discharge equated to 108 m^3/day. Despite increased velocities on the 24th August, an increase of 1.6 metres in the river level (determined discharge depth) lowered the hydraulic gradient, resulting in a lower discharge rate than on the 24th July.

Hooper (1997) suggested that the total groundwater flow discharge at bank D was only 8 m^3/day and 19 m^3/day in summer and winter respectively. Taylor et al., (1996) calculated a maximum discharge of 27 m^3/day for bank H. The variation in discharge rates between those studies and this project, is presumably due to increased velocities in bank H (discussed above) as approximately similar discharge depths were used. Further, Taylor et al. (1996) based their investigation on only three piezometers installed in bank H, and as a result their hydraulic gradients and K values may not be an accurate representation of the bank.

The average daily flow of the King River flow was 42 m^3/sec on the 24th July, 2000, and 50.3 m^3/sec on the 24th August, 2000. Accordingly, groundwater discharge from bank H represents only 0.005 % of the river flow on the 24th July and 0.002 % on the 24th August.

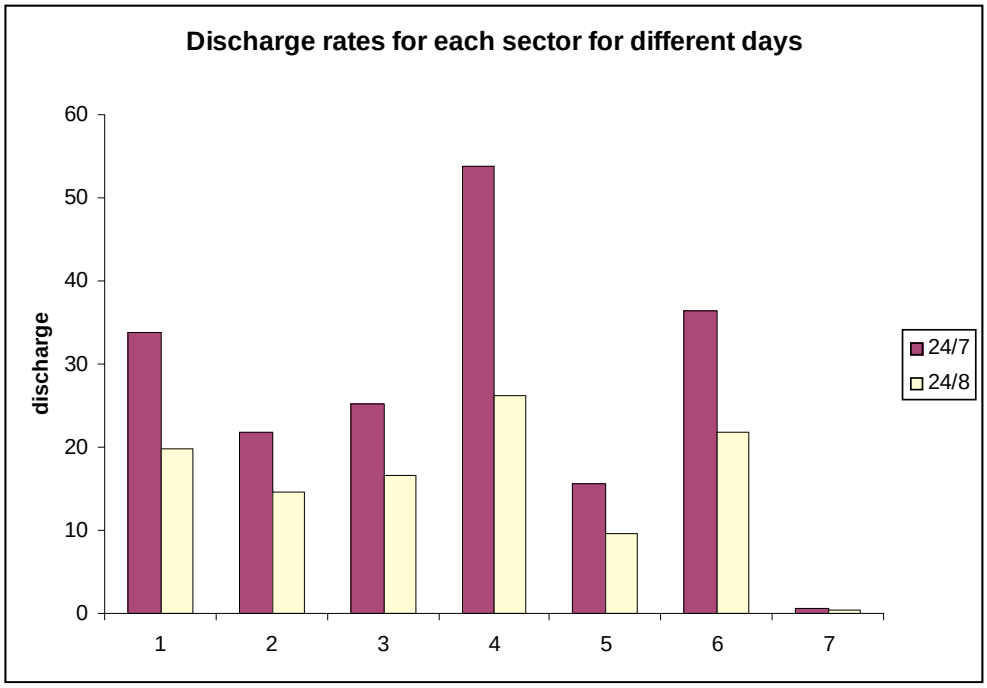

Figure 3.11 Total discharge rates for each sector at bank H on the 24th July and the 24th August.

24/7/2000		
row	actual vel m/day	discharge (m3/day)
1 (upstream)	0.013	0.9
1 (downstream)	0.011	0.8
2 (upstream)	0.022	1.57
2 (downstream)	0.001	0.08
24/8/2000		
1 (upstream)	0.006	0.19
1 (downstream)	0.005	0.16
2 (upstream)	0.02	0.6
2 (downstream)	0.002	0.08

Table 3.10. Actual velocity (m/day) and discharge (m^3/day) for horizontal flow parallel to the river on the 24th July and 24th August.

3.5 Limitations of analytical method

Limited data has prevented a sound understanding of the flow paths in the hydrological system. Therefore, both velocity and discharge calculations represent only an approximate horizontal component.

A geophysical investigation inferred that the groundwater system (aquifer) might extend to 12 metres (chapter 4). For water to enter the river, if groundwater flow is predominantly horizontal, flow paths would need to migrate near vertically upwards underneath the river.

Nested piezometers would need to be installed in the river to confirm this. If the aquifer has a large vertical component adjacent to the river, there is the potential for flow to migrate downwards through the bank. The lack of piezometer nests severely limited this component of the study.

Even if the discharge depth was assumed to be 12 metres (e.g. all groundwater contributing to the river), the analytical method does not consider velocity variations with depth. Numerical modelling can build on the analytical method by simulating the three-dimensional flow system. Visual MODFLOW, which uses the finite-difference method was utilised for this task.

3.6 Conclusion

Groundwater flow direction at bank H is dependent on both precipitation and river levels. At all measurement times, groundwater is flowing from the bank and discharging approximately perpendicularly into the King River. Hydraulic gradients from the 16th April, 2000, suggest the possibility of flow from the river back into the bank at particular locations during times of low rainfall and /or high river levels (reverse hydraulic gradients).

Vertical hydraulic gradients suggest the possibility of a confining or partially confining layer at depth at approximately 200 mE to 360 mE, and extending approximately 40 m towards the river. This is suggested by higher potentiometric pressure heads from several deeper piezometers than the inferred water table.

Actual velocities perpendicular to the river were calculated as between 0.0028 – 0.27 m/day on the 24th July and 0.004 – 0.3 m/day on the 24th August. These are approximately 80 times higher than Hooper's (1997) study at bank D. The difference is most likely due to higher hydraulic conductivities and increased hydraulic gradients in this study compared with Hooper (1997). Velocities parallel with the river were comparatively minimal when compared to perpendicular velocities, in both studies.

The total discharge at bank H was calculated as 187 m^3/day on the 24/7 (high rainfall, high river level) and 108 m^3/day on the 24/8 (low rainfall, low river level). Discharge calculations at bank D in 1997, were only 8 m^3/day and 19 m^3/day in summer and winter respectively.

Despite the variation in discharge results between the two studies, both studies suggest that groundwater discharge from each bank represent only a small percentage of the King River flow. Maximum percentage calculated at bank H was 0.005% and 0.002% from the study on bank D.

Chapter 4: Geophysical investigation

4.1 Introduction

A geophysical investigation was applied to bank H to further an understanding of the internal geological structures and water distribution of the bank. Boundaries that it was hoped could be discriminated included the unsaturated/ saturated boundary, tailings/ natural sediment (conductivity variation) and the basal contact (porosity contrasts). Although geophysical measurements are unable to measure the physical properties involved in hydrogeological studies, the same intrinsic features of a medium usually affect both the hydraulic and physical properties that govern several geophysical responses (Endres, 1998). Intrinsic features include the pore structure, lithology, and pore fluid species. On this basis, EM 31, DC resistivity, time domain EM (PROTEM) and seismic refraction were employed.

This chapter discusses the purpose, method and results of each survey.

4.2 Purpose of geophysical methods

As most rocks are insulators, electrical current flows are by electrolytic conduction within the pore fluid. Subsequently, the measured resistivity is primarily a function of the following parameters (McNeill, 1990):

1. Increasing effective porosity values results in a greater potential for hosting water, which in turn, decreases resistivity.
2. The main reason clays have low resistivity is that they are highly actively charged, thus they increase the number of ions in the saturating electrolyte (Milsom, 1996). In addition, clays are highly porous.
3. Pure water is only ionized to a small extent, thus properties of the fluid (such as salts and total dissolved metals) have a substantial impact on conductivity. An increase of 1ppm of TDS results in a conductivity increase of 0.22 mS/m (Telford *et al.*, 1990).
4. The mobility of ions in solutions has a dependency on temperature, with higher temperatures corresponding with lower resistivities. The temperature variability of Bank H is minor (8.5-11.2 ^{o}C), thus, it was assumed that temperature would have little effect on resistivity indescrepencies. However, temperature variability is unknown for depths exceeding 3 meters.

5. Despite the ionization of pure water being small (Milsom, 1996), the presence of groundwater acts as an electrolyte, hence, the greater the water saturation, the lower the resistivity (Lowrie, 1997).

4.2.1. Electrical and electromagnetic methods

The transition zone between the saturated and vadose zones in unconfined aquifers, usually results in a significant geophysical response. This is due to large physical property changes that occur with water content variations (van Overmeeren et al, 1994). Combined with the fact that acidic mine waters generally contain elevated total dissolved metal concentrations, higher conductivities were expected in the saturation zone. King and Pesowski (1993) found a good correlation between sulphate concentrations in groundwater and apparent resistivity measured by using an EM-16R instrument.

Endres (1999), suggested that large changes would occur in electrical properties of the subsurface with varying chemical states. This creates the possibility of mapping chemical zonations of highly oxidized versus unaltered tailings or natural sediment.

Resistivity begins to rapidly decrease in material as the weight percentage of contaminated sulphides increases (Figure 4.1). It was hoped that a resistive boundary would be defined relating the pyritic tailings and natural sediment interface.

4.2.2. Seismic

Seismic refraction was chosen to characterise layers by their velocities. Physical properties that affect velocity include porosity, water saturation and density. Depending of rock properties, seismic surveys usually have excellent penetration depths. Subsequently, seismic provided the possibility of deciphering deeper boundaries, such as basement rock.

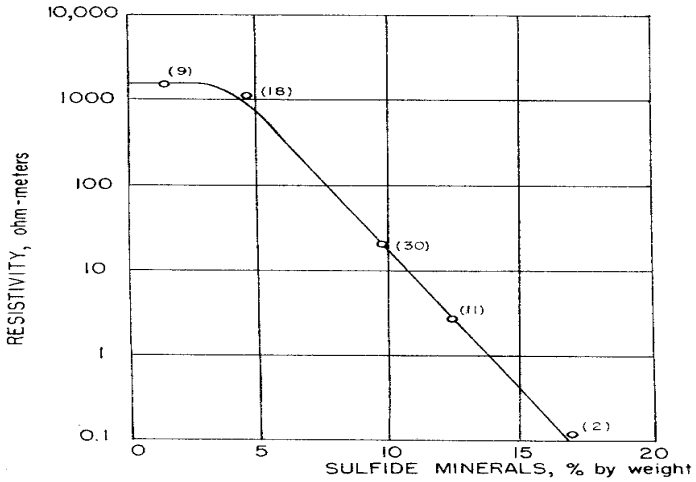

Figure 4.1. Resistivity vs. wt% of sulphides. More than 3 wt% of sulphides are needed to reduce the resistivity of a sample. From Keller and Frischknecht, 1966.

Figure 4.2. Location of seismic, EM31, Protem and DC resistivity traverses.

4.3 DC resistivity

4.3.1 Method

A Wenner array was used to conduct a vertical electrical sounding orientated E-W profile of the bank (Figure 4.2). The Wenner configuration is one of the most applicable to hydrogeological investigations (Milsom, 1996). A description of this method is explained in Appendix 7. As the bank is flat, and laterally relatively homogeneous, sounding is applicable (Greenhouse and Gudjuris, 1994).

Electrode spacing ranged from 10 cm to 100 meters on a log scale and electrodes were expanded around a fixed point. For spacing less than 1 meter, metal potential electrodes were used, and ceramic porous pots containing a Cu electrode soaked in $CuSO_4$ solution were emplaced for spacing of greater than 1 meter. A vertical profile of the earth's resistivity was produced using RINVERT. This computer program assumes a maximum of a 3 layered earth.

4.3.2. Results

Three layers of differing resistivity were depicted in the RINVERT model (Figure 4.3). The top layer has a thickness of 0.23 meters with a corresponding true resistivity of 227.4 ohm.m. The second layer has a low resistivity of 15.7 ohm.m. It is reasonable to suggest that the boundary between the two layers defines the water table. This can be considered probable for two reasons. Firstly, the second layer is below the water table and thus, fully saturated. Appendix 7.1 illustrates the effect of increased water content on certain rocks. In addition, the groundwater also contains additional dissolved ions released as a result of acidification. Secondly, a site investigation suggests that 30cm is a reasonable average depth to the water table.

A second resistivity boundary is evident between the wet unconsolidated sediment and a third layer. The true resistivity of layer three is 35,980 ohm.m and it has an infinite thickness. The high resistivity suggests fresh crystalline bedrock (Appendix 7.1).

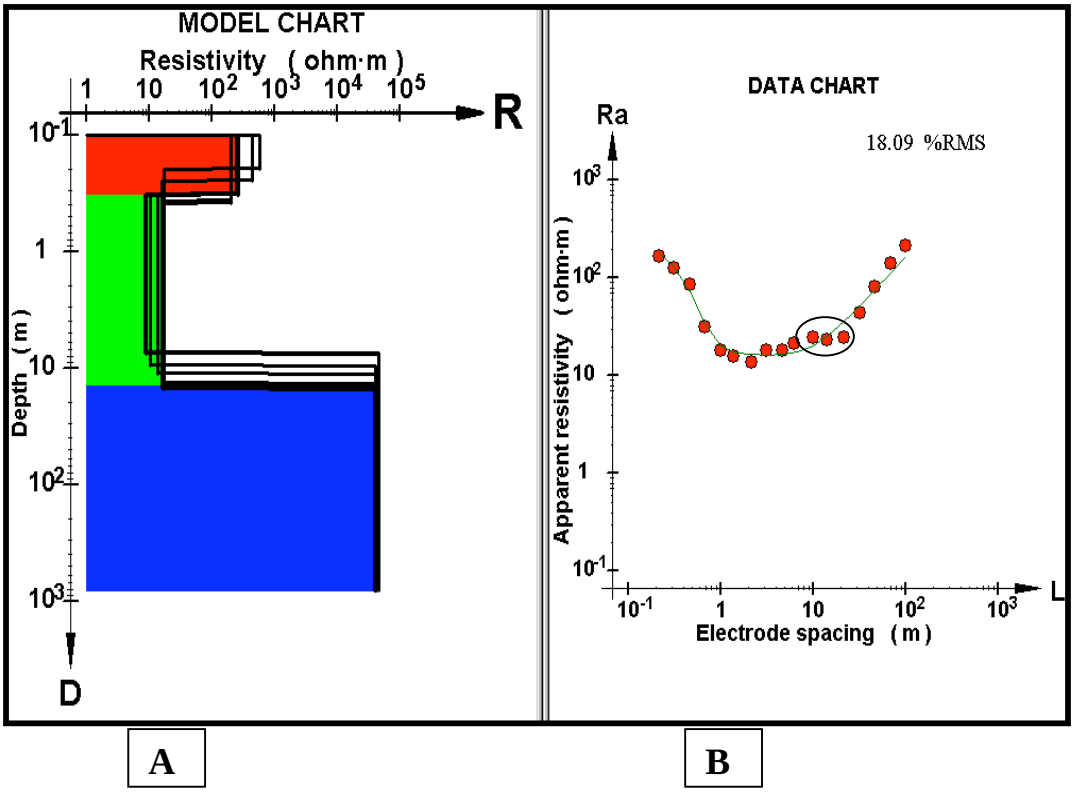

Figure 4.3. DC resistivity RINVERT model at bank H. Panel A also shows an equivalence analysis of the inverted model. Black lines show a number of different three layer models which fit the data equally well. Panel B shows field data measurements (red dots) and the green line is the response of the three layered model. Circle indicates possible additional layer if a 4 layered earth model was utilised.

Layer	Depth (m)	Resistivity (ohm.m)	Resistivity range from other models (ohm.m)	Layer thickness (m)	Layer thickness from other models (m)
1	0	227.4	220-580	0.228	0.2-.56
2	0.228	15.68	9.5-19	13.77	0.5-15.68
3	13.978	35980	35980	Infinite	Infinite

Table 4.1 Resistivity and corresponding depth estimates for each layer from the Rinvert program. The accuracy of predicted values distinguished by equivalence analysis is displayed in the range columns. The lower the range, the higher the accuracy.

4.3.3 Reliability of the model

Equivalence analysis is the process of finding a number of alternative earth models that replicate the field data within a root mean square (RMS) error two times that of the original model. The black lines in figure 4.3(a) are the results from these mathematical models. As the interpretations of the models are close to the original, it be can concluded that the current model is relatively reliable (table 4.1).

A limitation of the RINVERT model is that is assumes a maximum three-layer earth. If a four- layer program were to be run, there is a possibility that a third boundary could be detected. Figure 4.3(b) alludes to the deeper section of the second layer having a higher resistivity than the upper layer. Locher (1997), suggested that the tailings are on average 1.5 meters thick. Thus, this hypothesized boundary may represent a tailings/ natural sediment interface, weathered base rock/unconsolidated sediment boundary, or a number of other possibilities. However, even if a four-layer model were to be utilized, there is no certainty that the model would have a better fit then a RMS error of 18.09%.

A second limitation of the RINVERT program is that it assumes each layer to be isotropic and homogeneous. There may be large horizontal variations within the layers themselves, that through modelling are averaged out. Field evidence for this is the existence of thin vertical discontinuous clay lenses that were not distinguished by the model. In addition, the program assumes each layer to be horizontally infinite and have a uniform thickness. Protem interpretations suggest that each layer is roughly uniform in thickness, however, in reality, the bank does not have an infinite horizontal extent.

4.4 Electromagnetics

Two active source electromagnetic methods were utilized, EM31 which operates in the frequency domain (FEM) and PROTEM which operates in the time domain (TEM). An apparent resistivity can be calculated from EM data by determining the half-space model which fits the data at each time or frequency and transmitter/receiver geometry. The general principle of the electromagnetic method is explained in Appendix 8.

For the purpose of comparing EM31 and PROTEM TEM data with the DC resistivity results, apparent conductivity was converted to the reciprocal, resistivity.

4.4.1 EM31

The Geonics EM31 was designed to operate at low induction numbers where the quadrature (out of phase) secondary magnetic field is linearly proportional to terrain conductivity. At low induction numbers, the response is within the resistive limit, and there is little EM interaction between induced currents. Accordingly, the instrument automatically converts the measured quadrature response to an apparent conductivity (mS/m). In addition, the instrument operates at low frequencies. As the in-phase (ppt of primary field) measurements were less than 10ppm (low ground conductivites), the in-phase response is proportionally related to quadrature (Figure 4.4), and thus, measurements were corrected to apparent conductivity using a program by Reid (2000, pers.comm.)

The EM31 operates in the frequency domain and consist of two coplanar coils (receiver and transmitter) mounted on a mobile boom with a constant 3.7meter separation. The instrument may be oriented in either the horizontal dipole (HD) mode or the vertical dipole mode (VD) (Figure 4.5). The quadrature response in these orientations have a site investigation depth of ~3 and ~6m respectively.

Recent work has suggested that the in-phase response may yield information from relatively shallower depths than the quadrature responses for both orientations.

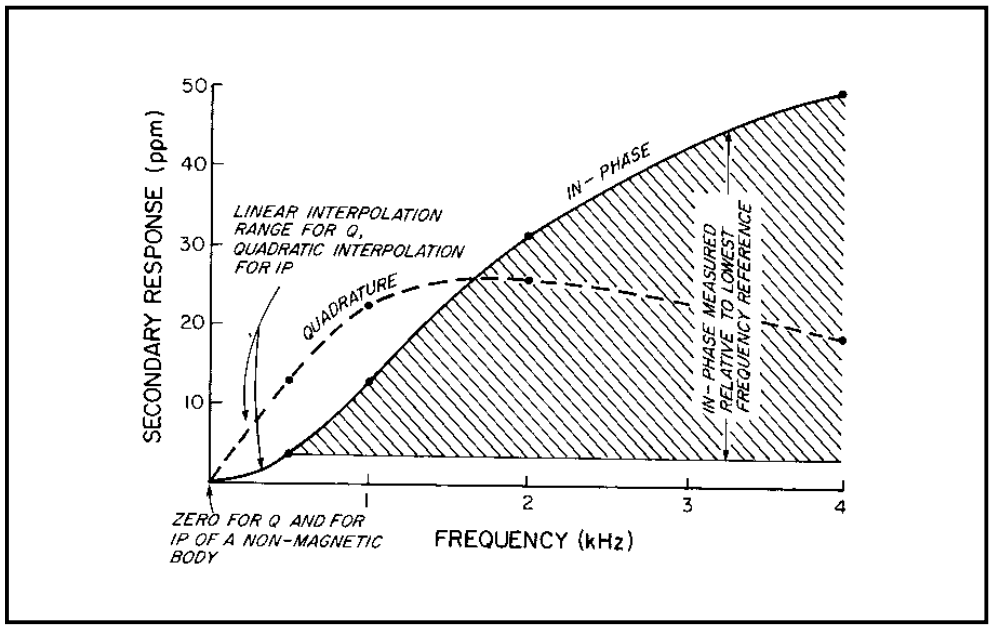

Figure 4.4. Schematic diagram of the inphase and quadrature components of secondary response. At low frequencies and secondary in-phase responses less than 25 ppt, both out-of phase and in-phase are linearly related. From Palacky and West, 1991.

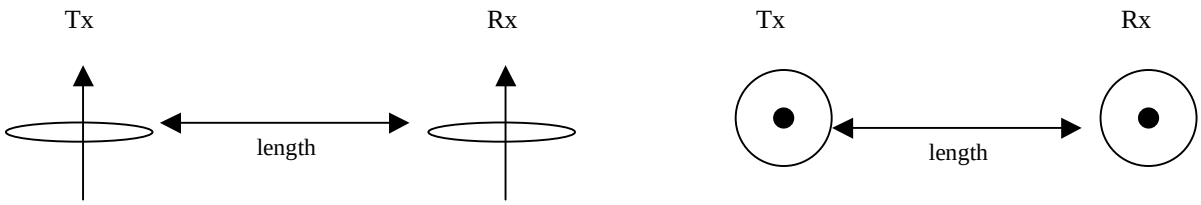

Figure 4.5 a) Coils of wire in the horizontal coplanar orientation (vertical dipole mode; VD) and b) coils of wire in the vertical coplanar orientation (horizontal dipole mode; HD).

4.4.2. Method

EM31 readings were carried out along each traverse (10mW to 480mE) at approximately 10-meter spacings (figure 4.2). As the signals in slingram surveys are referenced to primary field strength, the 100% level should be confirmed at the start of each day (Milsom, 1996). The level difference between the two days had no real effect of conductivity readings as the VD and the HD only varied by 0.2 and 0.8 mS/m respectively. In contrast, the inphase measurements were 1.79 and 1.98 mS/m out for the VD and HD respectively. Latter, day two results were adjusted to comply with day one.

Before measurements were taken, the instrument was calibrated on the supposedly non-anomalous road. Both the in-phase and out-of phase meters were zeroed.

The results were gridded in *Surfer* and then displayed overlaying the topography using *ER Mapper*.

4.4.3. Results

The VD mode in-phase resistivity response varies from 8 to 16 ohm.m (figure 4.6b). This resistivity range is analogous to the second layer of the DC resistivity model (15 ohm.m). As the second layer of the DC resistivity has been interpreted as responding to fully saturated sediment, the assumption has been made that the site investigation depth of the VD mode is below or close to the water table. Figure 4.6 c and d suggest that the HD quadrature meter (3 m) yields a slightly higher resistivity response (~30 ohm.m) compared with the VD mode quadrature (6m) response (~ 25 ohm.m). This suggests increasing conductivities with depth.

Both quadrature images (Figure 4.6 c and d) illustrate high resistivity values to the far east of the bank. The confined feature extends linearly to the northern boundary (bank/ road interface). Hence, it is a possibility that the trend is the result of resistive road fill material. Despite the images having been inferred to relate to the properties and the degree of saturation of the sediment, low resistivity in both the HD and VD quadrature responses (between 300 and 350 east), may relate to discontinuous thick clay horizons exceeding a depth of 3 meters.

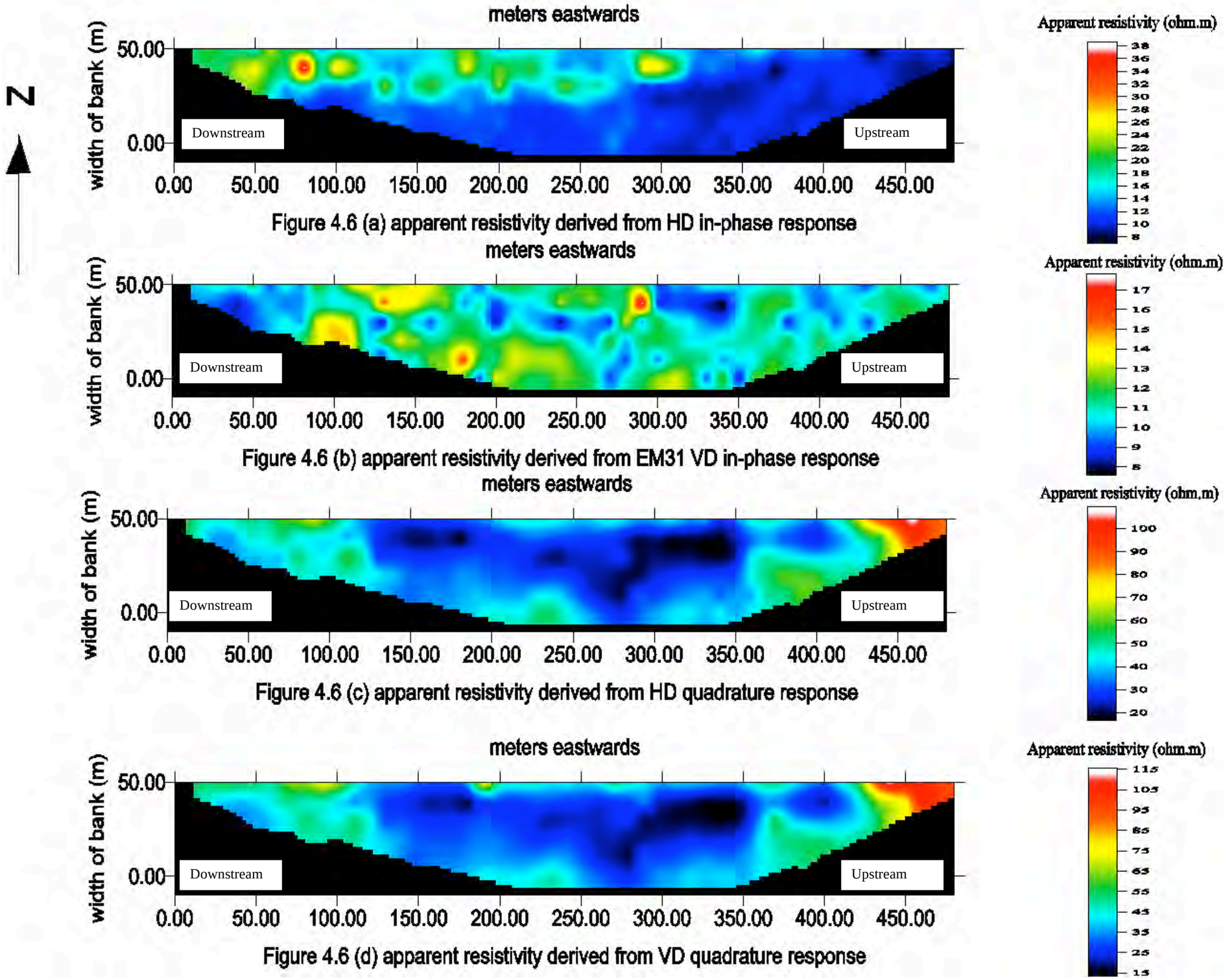

Figure 4.6. Quadrature and in-phase EM31 images for the vertical and horizonal coil orientation. Images arranged in order of increasing depth of investigation.

Topographic relationship

Gridded apparent resistivity data sets were imported into ER Mapper as raster files and overlayed on the topography algorithm. A linear pseudocolour scale of apparent resistivity was applied to both the horizontal and vertical coplanar.

The HD mode in-phase has the shallowest depth of investigation (less then 3m) and assigned an anomalous east –west trending linear feature approximately 5 meters from the road. The corresponding feature for the other three investigations, yielded relatively low resistivities. By draping the image over the topography (figure 4.7), the feature relates to topographic lows, representative of a drainage channel. As EM31 was operated in wet conditions, the anomalous reading for the shallowest slice (figure 4.7a) has been interpreted as corresponding to contaminated surface pools diluted by freshwater (rainfall). The channel was discharging quickly the day EM31 was conducted, thus, there would be minor opportunity for recharge of fresh water into the system. This theory is supported by the deeper site investigation (figure 4.7 b, c and d) exhibiting decreased resistivities in the channel. The VD mode in-phase is the second shallowest investigation and indicates the importance of the subsurface conduit. This is observed by higher conductive measurements along the channel and surface ponds (8 ohm.m), within surrounding resistive values (12-16 ohm.m).

Hydraulic relationship

Data sets of hydraulic head values were obtained the same day that the EM31 was conducted. As hypothesised, a linear relationship exists between increasing conductivities and hydraulic head calculations at measured piezometers (Figure 4.7 a and b). The EM images defines added structural detail of the subsurface hydraulic features, thus were used to estimate water table elevation. As the shallow piezometers were interpreted as representing the water table elevation, the VD in-phase meter (which excludes less conductive surface pools and views to the second shallowest investigation depth), was used as a guide to estimate water table elevations between the fixed piezometers (Figure 4.8 a).

Both the VD and HD quadrature responses show increased conductivities between ~150 m E and ~400 m E (Figure 4.6 c and d). As the deeper investigations include the shallower features in their responses, the high conductivity area may be suggesting a locally higher water table (perched). The VD quadrature response shows slightly less structure than the shallower HD quadrature response (Figure 4.6 c and d). Because of the greater distance between the shallower feature and the VD investigation depth, this response may not be

picking up the shallower feature to the same extent as the HD quadrature meter (shallower depth of investigation). In addition, the higher conductivity area defined by the quadrature meters was similar to areas where deeper piezometers had higher potentiometric heads (Figure 4.8 b). As an increase in pressure head can be related to piezometers intersecting a confining layer, there is a possibility that the hypothesised perched water table could be the result of the confining layer(s). It is also possible that the higher conductivity is due to increased dissolved ions at depth. Whilst both the EM31 investigation and electrical conductivity probe (EC) results suggest that conductivity increases with depth, the latter also suggest that conductivities are relatively uniform at depth (Appendix 9).

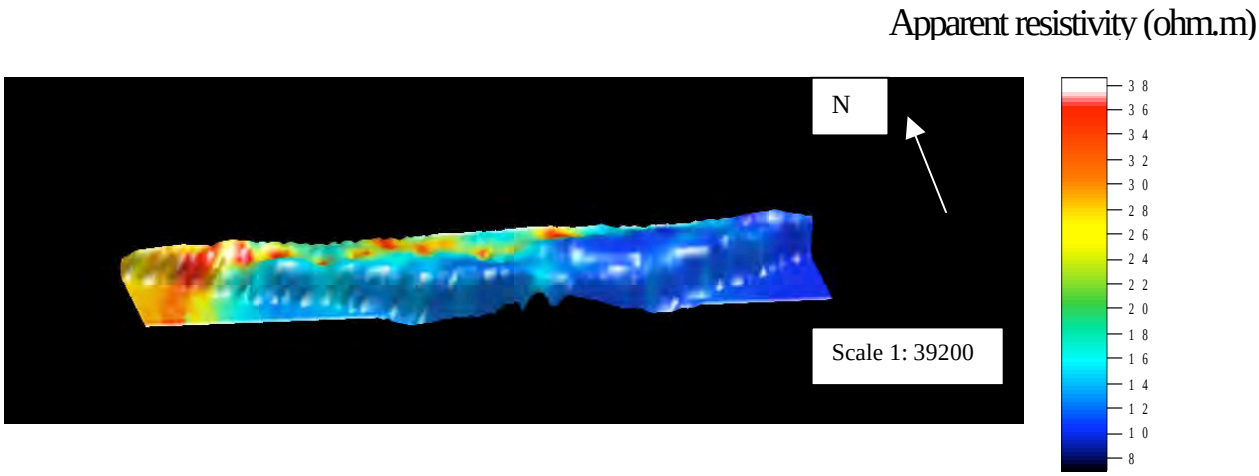

Figure 4.7 (a) Apparent resistivity derived from EM31 HD mode in-phase response.

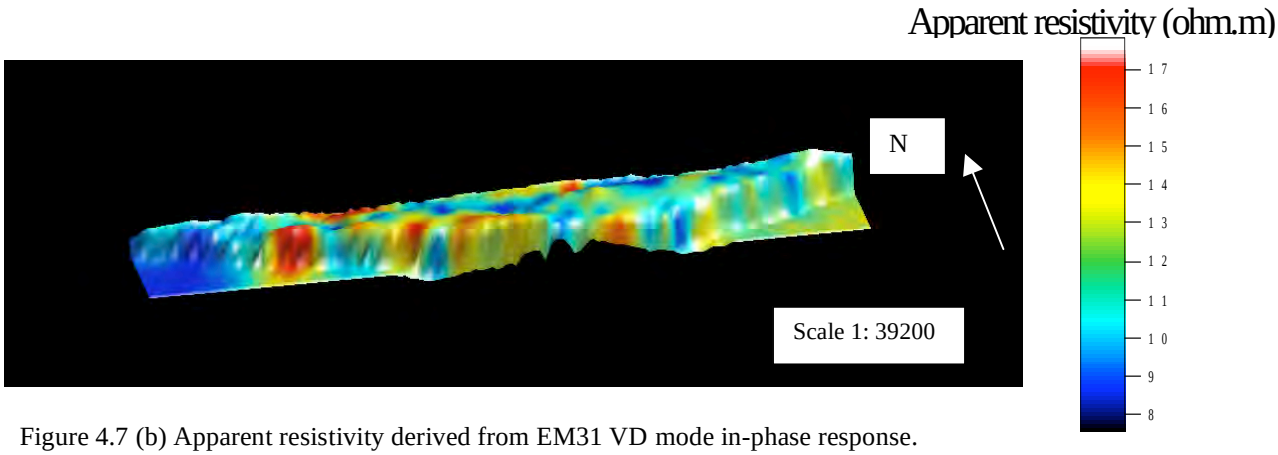

Figure 4.7 (b) Apparent resistivity derived from EM31 VD mode in-phase response.

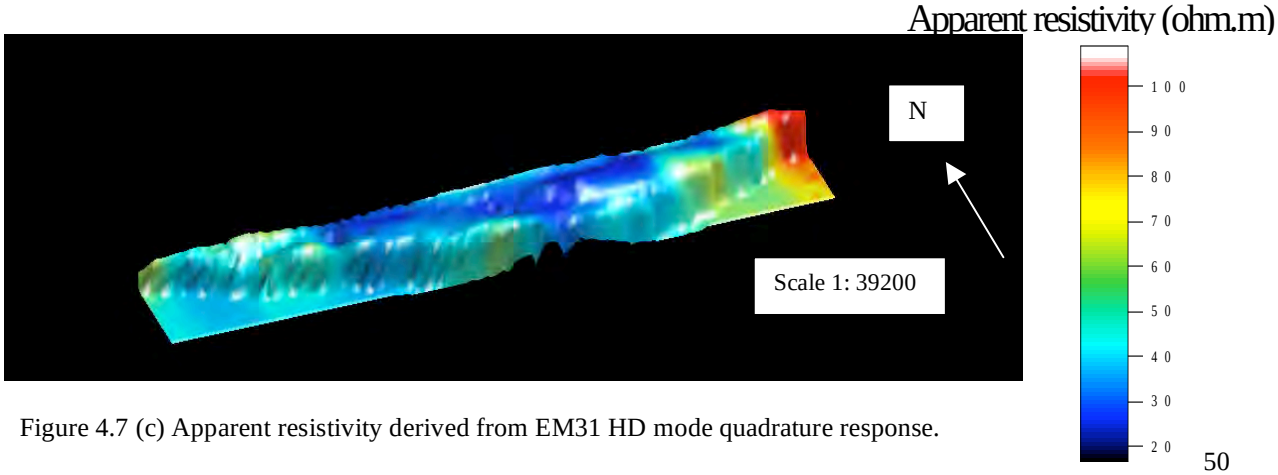

Figure 4.7 (c) Apparent resistivity derived from EM31 HD mode quadrature response.

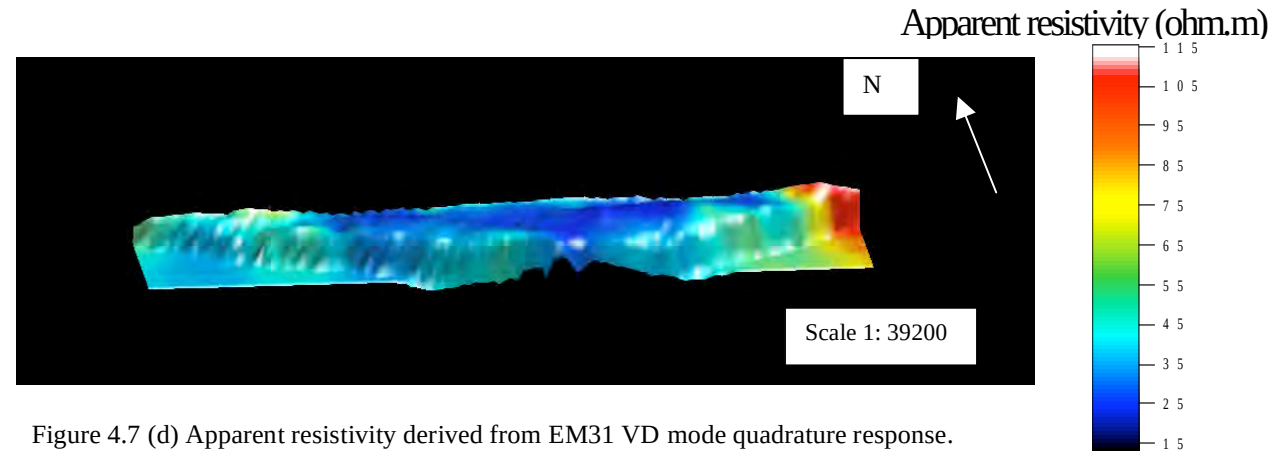

Figure 4.7 (d) Apparent resistivity derived from EM31 VD mode quadrature response.

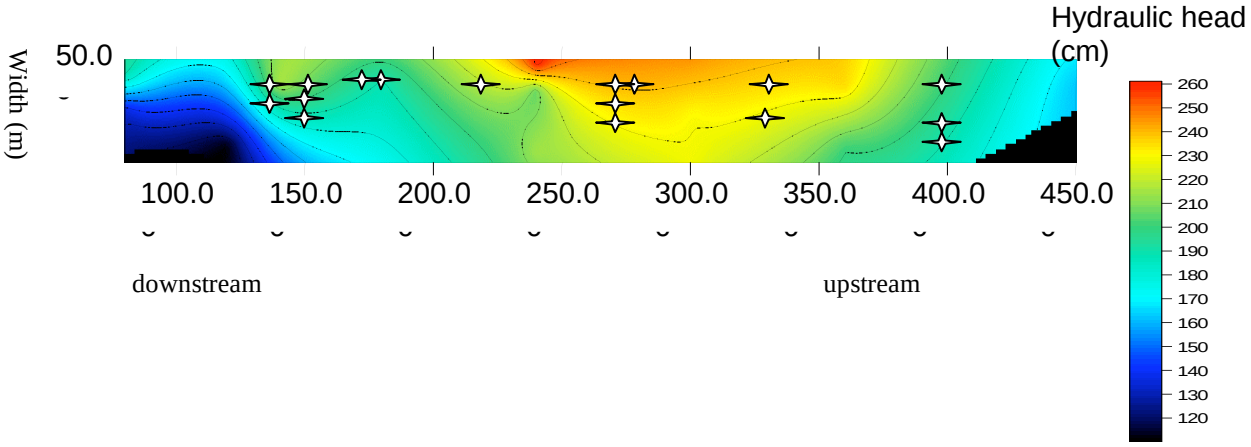

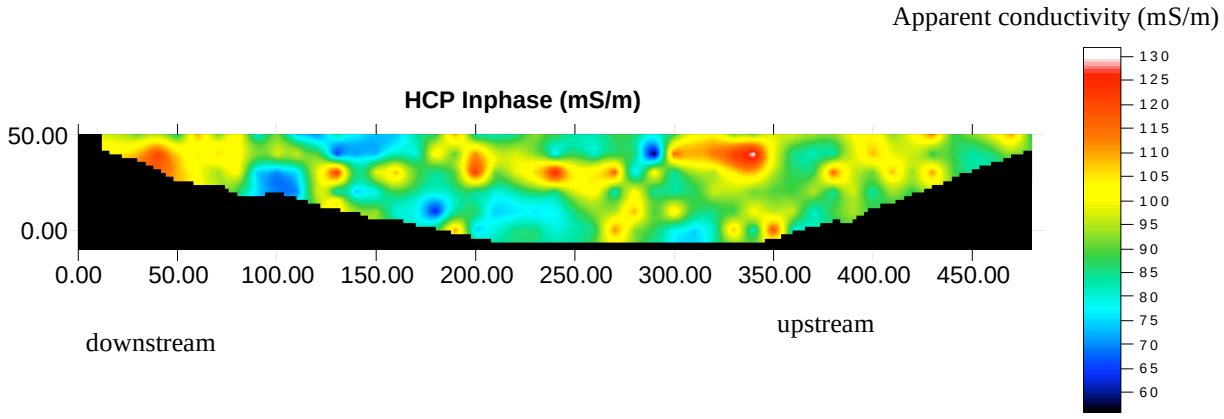

Figure 4.8 (a) Comparison of equipotential contours from shallow piezometer heads (insertion depths less then 1.5 meters) and VD mode in- phase response. The stars on the hydraulic head image are locations where direct measurements from piezometers were taken. High hydraulic head values equate to a shallow water table and relatively high conductivity values correspond with the high hydraulic head measurements.

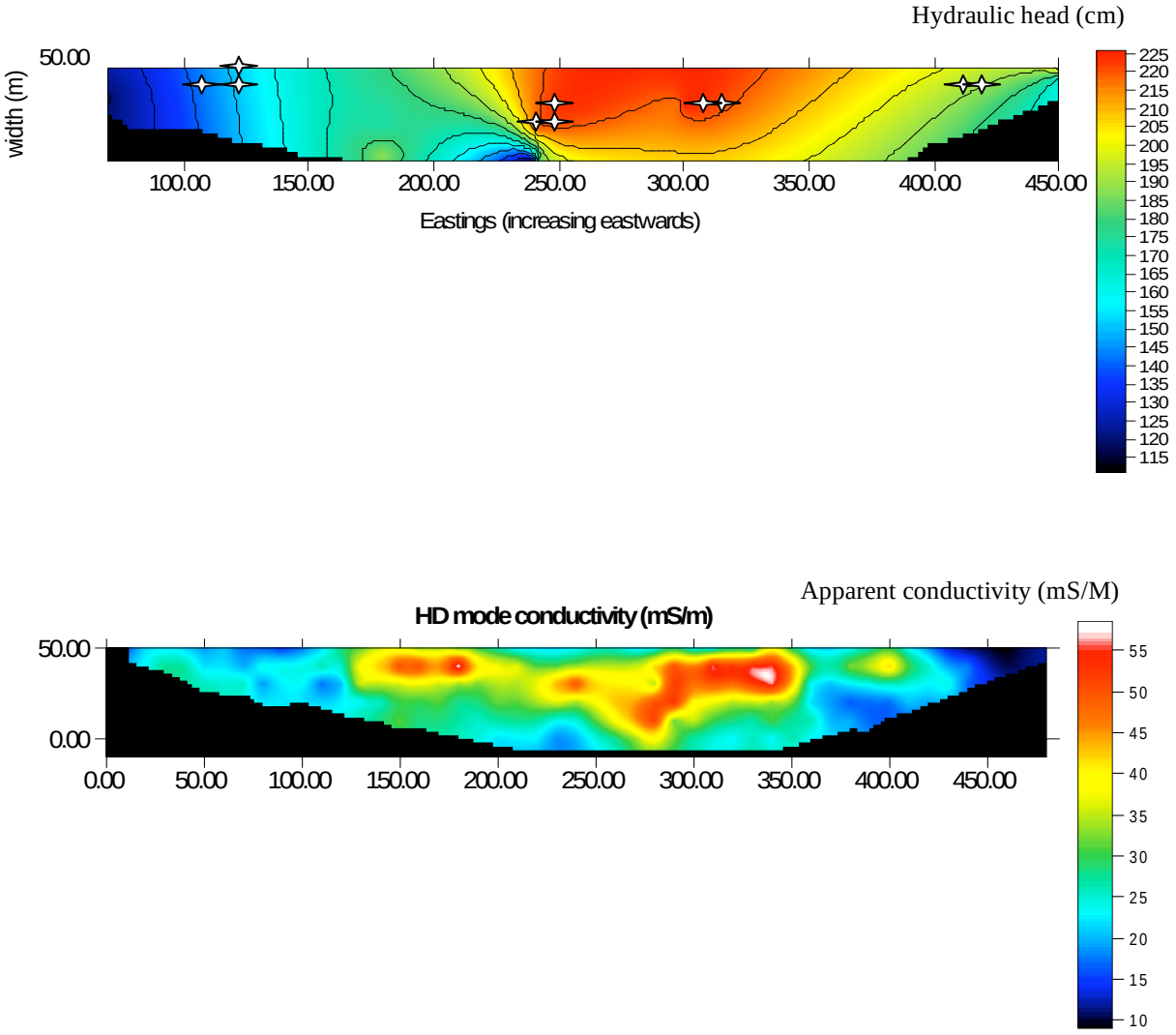

Figure 4.8 (b) Comparison of equipotential contours from deep piezometers (greater than 1.5 meters) and HD mode quadrature response. The stars on the hydraulic head image are locations where measurements from piezometers were taken. High hydraulic head values correspond with relatively high conductivity values.

4.5 EM47

The EM47 is often referred to as PROTEM after the name of the receiver type. Unlike the EM31, it in the time domain (transient) (TDEM). TDEM have the advantageous ability to penetrate to large depths in the presence of a conductive surface layer.

4.5.1 Method

Protem readings were carried out along a 240m profile (figure 4.2). A moving loop configuration was used with loop-coil slingram geometry. Square transmitter loops had 25m sides with the receiver (Rx) at a fixed distance outside the transmitter loop (Tx) (27.5m from the center of the Tx loop). The transmitter repetition rate was 262.5 Hz. Apparent conductivity values for the purpose of depth transformation were obtained by applying the method put forward by Reid and Fullagar (1998). Readings were plotted as apparent conductivity and were converted into resistivity for the construction of a depth pseudosection.

4.5.2 Results

The apparent conductivity-depth pseudosection resolved two layers of contrasting resistivity (figure 4.9). The less resistive upper layer most probably represents unconsolidated sediment $^{+}_{-}$ pyrite. This interpretation places an absolute maximum thickness of 20 meters on the unit, however the true thickness is most probably substantially less (Appendix 10).

The unconsolidated sediment thickness is relatively uniform along the bank, with the exception of a slight thinning towards the far east of the profile. As this is upstream, it is possible that tailings were not deposited to the same extent as down stream due to the higher energy environment.

The profile also suggests shallow high conductivities at 220-280 meters west. A feasible explanation for this is the existence of locally higher quantities of pyrite in the tailings or due to locally increased TDS.

4.6 Seismic refraction

Seismic refraction was attempted on two separate occasions As the first breaks were difficult to pick, both proved relatively unsuccessful. This can be explained by bad coupling as the seismic waves failed to propagate through the unconsolidated sediment. Results were only recorded for the second trip with the 3rd year geophysics students.

4.6.1 Method

With spacing of 5 meters, a 12 geophone linear array was run parallel to the resistivity sounding (figure 4.2). Shots were fired from 6mE, 5mW and 50mE and W. The energy sources utilised were a hammer for closer shots and explosives for the +-50m shots (Figure 4.10). An outline of the seismic refraction method is illustrated in Appendix 11.

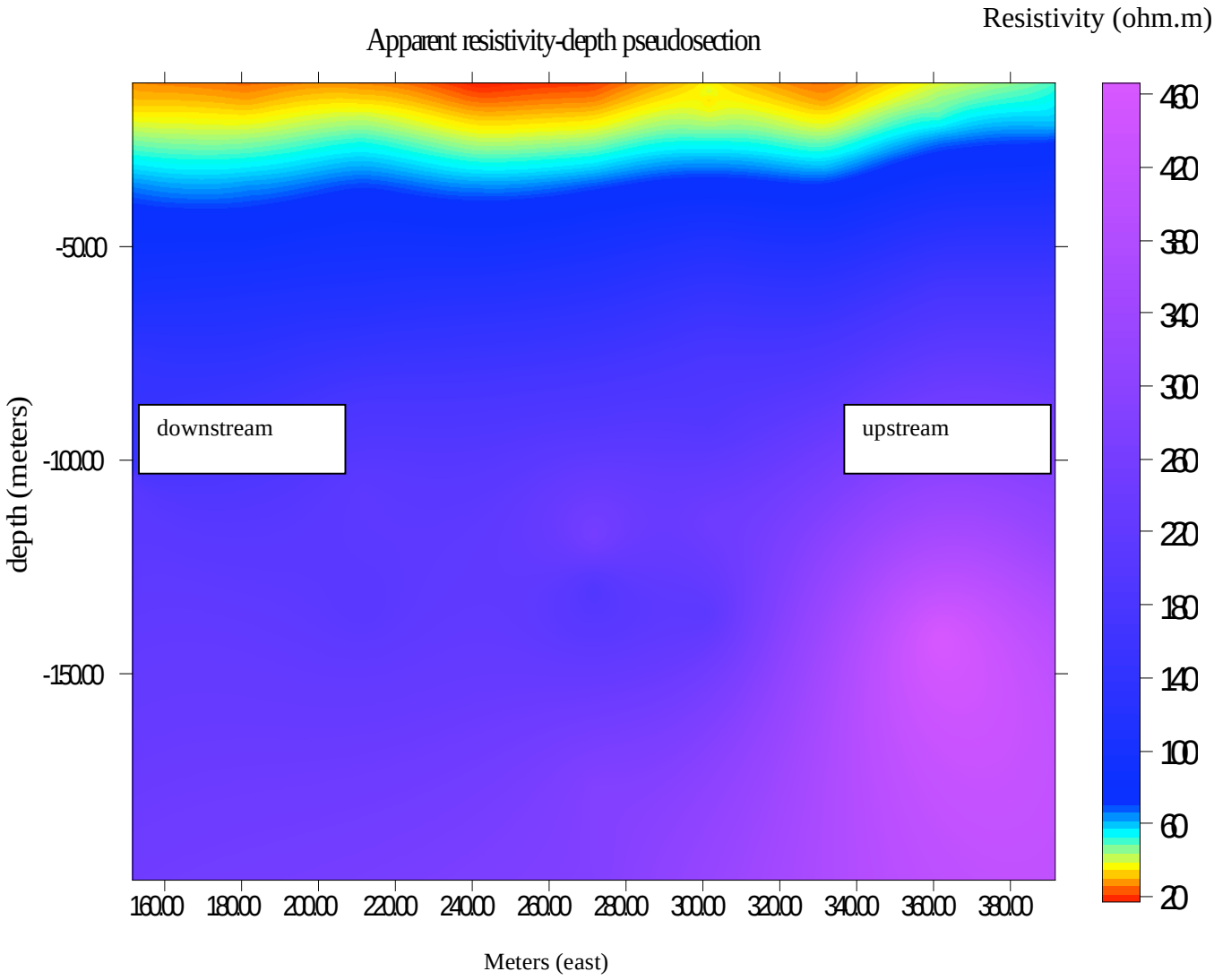

Figure 4.9 Apparent resistivity-depth pseudosection from EM47 defining two contrasting resistivity layers and structure within the upper layer. Colour scale has been stretched so the image appears identical to the apparent conductivity-depth pseudosection as $a = 1/a$.

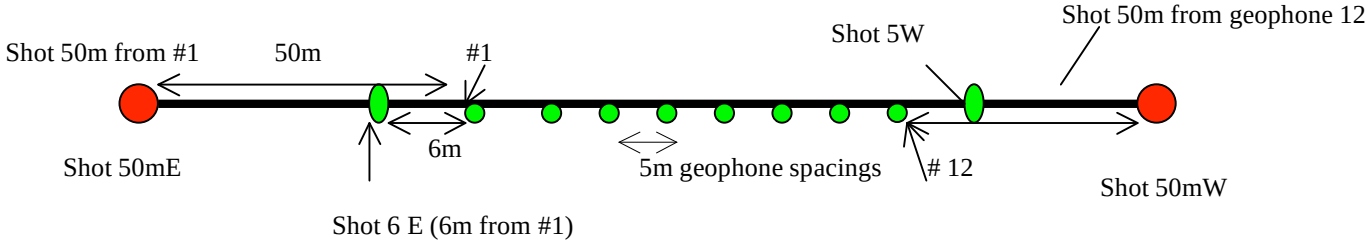

Figure 4.10 Schematic representation of seismic set up, note- diagram is not to scale.

First arrivals, (consistently P waves, Milsom, 1996), were picked (Appendix 11.1) and plotted against distance (Figure 4.11). Velocities for each inferred layer were derived from the gradient of the line and layer thickness and depth estimates were calculated by applying the reciprocal method where velocities of reciprocal shots cross over (Leaman, 1997).

4.6.2 Results

Overlaps of V2 were interpreted at geophone 4(15m) and 5 (20m) from the 5mW and 6E shots (Figure 4.11). An average velocity for layer 1 was calculated at 577m/s and 1421.6m/s for layer 2 (table 4.2). By applying these velocities to a depth conversion chart based on Snell's law, a velocity factor of 675 was determined. Using a method which converts the critical paths to depth, V2 was assigned a layer thickness of 11 meters at both geophone 4 and 5 (table 4.3).

Wet unconsolidated sediments generally have velocities slightly more then that of water (Milsom, 1996). As the velocity of water is approximately 1500m/s (Telford *et al.*,1990), it can be suggested that layer 1 represents dry sediment based on the velocity of air being 330 m/s (Milsom, 1996). The velocity of layer 2 may represent unconsolidated sediment or weathered base rock as 1420 m/s is too low for fresh rock (rarely under 2200ms^{-1}, Milsom, 1996).

A possible V4 overlap could be interpreted, however, the velocity of this layer is less than layer 3 and therefore it is assumed to be inaccurate.

Line	V1	V2
6mE	566.0377	1666.667
50mE		
5mW	588.2353	1176.471
50mW		
Average	577.1365	1421.569

Table 4.2. Velocity calculations of layer one and two in meters per second for each shot.

Overlap of v2	Time taken to reach geophone # (ms)						
	From 6mE	From 5mW	Shot-shot time (	V1	V2	Velocity factor	Layer Thickness (m)
Geophone 4 (15m)	49	48.5	65	577.1	1422	675	10.96875
Geophone 5 (20m)	52	46	65	577.1	1422	675	11.1375

Table 4.3. Calculated thickness for V2 using reciprocal method.

seismic

4.7 Conclusions

Water table interface.

The DC resistivity model resolved a boundary at 23cm between a thin resistive layer (227.4 ohm.m) and a more conductive layer (15.7 ohm.m). This boundary has been interpreted to represent the water table interface in an unconfined aquifer system.

EM47 failed to register the upper more resistive dry unconsolidated sediment. Accordingly, it can be assumed that the current traveled through the resistive layer at such speeds, that even at the earliest measured times, the current had already passed through the layer.

The EM31 has been interpreted as responding mainly to the degree of water saturation and perhaps also to pore water conductivity. There is also the possibility that the quadrature meters may have responded to a clay horizon at depth. Both the VD and HD quadrature response show higher conductivities spatially similar to the hydraulic heads in the deeper peizometers. This association may be related to a confining layer at depth. The higher piezometric heads may have resulted from piezometers penetrating the horizon/ horizons and the deeper EM responses maybe responding to a perched water table as a result of the confining layer. A spatial relationship is also seen with the VD inphase response and the hydraulic heads in the shallow piezometers. As the hydraulic head measurements in the shallow piezometers have been interpreted as representing the water table, the VD inphase image was used as a guide to indicate the water table elevation between piezometers.

Seismic failed to define the water table boundary because the seismic data was of poor quality and perhaps the geophone spacing was too large.

Natural sediment / tailings boundary

The resistivity of the tailings/unconsolidated sediment given by EM31 and EM47 range from 8 to 60 ohm.m. The sulphide content needed to yield these values would be between 7 and 20wt% (Figure 4.1). Taylor *et al.*, (1996) estimated that bank's tailings contained only 2-3wt% of disseminated pyrite. Accordingly, it appears that EM did not resolve the boundary between pyritic tailings and barren sediment.

Interface between unconsolidated sediment and fresh basement

The DC resistivity sounding defined a transition zone at 14 meters between a conductivity (15.7ohm.m) middle layer and a more resistive basement (35,980 ohm.m). The basement layer has been interpreted as fresh crystalline bedrock based on the layer's high resistivity.

The Protem apparent resistivity versus depth pseudosection provides information about variations of resistivity with depth and laterally along the profile. The pseudosection (which identified two layers) defines the basement at ~20 meters. However, the true depth is probably less as the depth transformation overestimates the thickness of surficial conductive layers. The sediment thickness is relatively uniform along the bank, with the exception of a slight thinning towards the far east of the profile.

Although waves were attenuated in the unconsolidated sediment, seismic refraction detected a second layer with a velocity of ~1400ms with an estimate of layer 1 thickness of 11 meters. This layer is more likely to represent unconsolidated sediment or weathered base rock as the calculated velocity is too low for fresh rock.

Chapter 5: Numerical Simulation

5.1 Introduction

Groundwater models provide a quantitative understanding of the mechanisms and controls of groundwater systems by considering the interactions between the essential features of the aquifer under changing conditions (Heijde, 1996). In this project, the framework of the hydrogeological system was varied in order to obtain the most reasonable simulation for the imported hydraulic data. This involved performing sensitivity analysis in concurrence with calibration of the model.

Zannetti (1995) suggested that modelling is the only available tool for "what if" analysis for exploring hypothetical scenarios. Thus, once the system was simulated satisfactorily, predictions were made about the aquifer behavior under alternative scenarios. Two hypothetical scenarios were run:

a) the possibility of the formation of an upper confining layer such as hardpans, and
b) fluctuating river levels.

Simulations were carried out utilising Visual MODFLOW. Developed by the United States Geological Survey, MODFLOW is the most popular numerical modelling package used by government agencies and consulting companies in the United States (Merrick, 1999).

5.2 Groundwater modelling

5.2.1. Data requirements

For a consistent and comprehensive conceptualisation of a groundwater system, available data can be integrated from numerous disciplines. The minimum requirement of data quality and quantity depends on the complexity of the aquifer system and surface water interactions (Merrick, 1999), and the cost and feasibility of obtaining data.

The data entered into the program can be broken down into two major components, the hydrogeological framework and hydrogeological stresses. The framework includes the conceptual and mathematical model (the main features of the aquifer system) and hydrogeological stresses are concerned with the simulation of temporal and spatial variability (Appendix 11) (Merrick, 1999; Domenico and Schwartrz, 1990). For this study the framework and stresses include data derived from hydrogeological, geophysical and meteorological results.

5.2.2. Scale

The validity of a model is limited to the spatial and temporal scale for which it is developed (Merrick, 1999; Frind and Molson, 1994). As this study is concerned with the flow through a small space, the model was designed to give detailed information on a local scale. Accordingly, the model was applied to a short-term response. This was done by running separate steady-state simulations for a monthly period (30 days) for each of the three field trips for when hydraulic head distributions were measured. As a result, each simulation assumes that the hydrogeological stresses remain constant throughout each of the monthly periods.

5.3. Groundwater modelling methodology

5.3.1 Conceptual Model

The first step of modelling is to formulate a conceptual model of the hydrogeological system based on hydrologic framework information (Kalf and Dungeon, 1999). The essential boundaries determined in the conceptual model form the basis for the solution of the mathematical model (Merrick, 1999). Thus, the model should include all the essential features that may influence groundwater flow paths and contamination transport. The requirement of the hydrogeological framework is to establish the systems geometry and the hydraulic and storage properties of the system. Figure 5.1 is a schematic representation of bank H in cross section, based on data from field investigations.

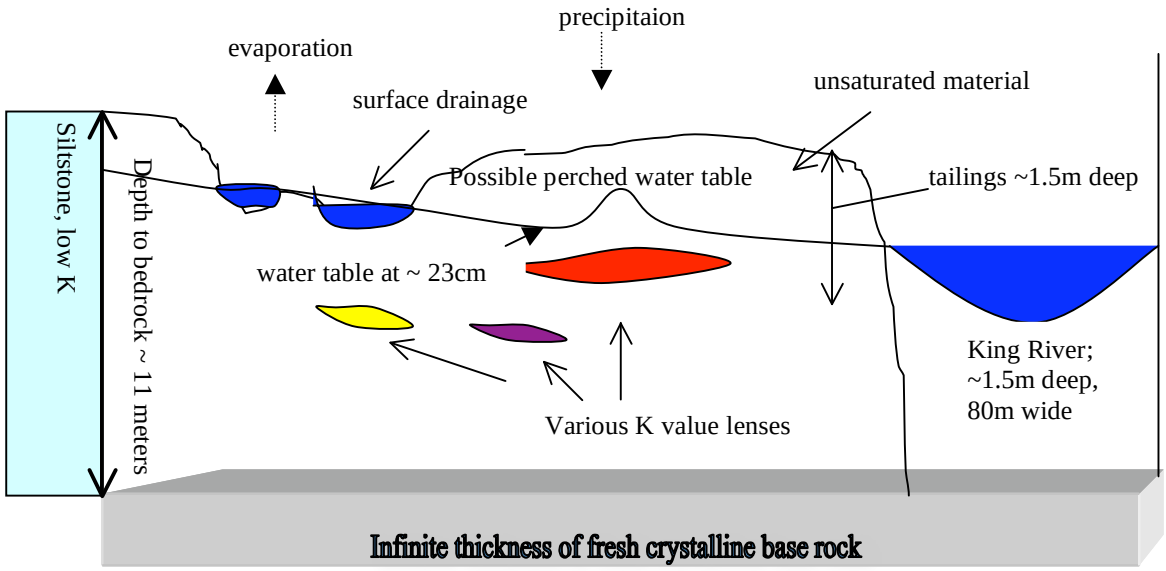

Figure 5.1 Schematic representation of the features of the groundwater system of bank H along the King River. Data was derived from hydrogeological, geophysical, meteorological and field observations. Illustration is not to scale.

5.3.2. Mathematical Model

MODFLOW solves the partial differential equation for the three-dimensional movement of groundwater of constant density (equation 5.1) (Merrick, 1999). Whilst the lack of density consideration is not a direct concern for groundwater movement, it can produce unrealistic simulations for solute transport.

$$\frac{\partial}{\partial x}\left(K_{xx}\frac{\partial h}{\partial x}\right)+\frac{\partial}{\partial y}\left(K_{yy}\frac{\partial h}{\partial y}\right)+\frac{\partial}{\partial z}\left(K_{zz}\frac{\partial h}{\partial z}\right)-W=S_s\frac{\partial h}{\partial t} \qquad 5.1$$

where,

K_{xx}, K_{yy}, and K_{zz} are the hydraulic conductivities in the x, y and z direction (LT^{-1})

h is the piezometric head (L)

W is a volumetric flux and represents sources and / or sinks of water (T^1)

S_s is the specific storage (L^{-1})

and t is time (T).

Combined with the boundaries and initial conditions, MODFLOW uses the finite difference method to obtain an approximate solution to the equation (Guiguer and Thomas, 1994).

Hydrogeological framework

From the second interface boundary defined by the DC resistivity model (RINVERT) and seismic refraction interpretations (chapter 4), a depth to bedrock was assigned at 11 metres. An estimation of the basement rock porosity was acquired by applying Archie's Law. This empirical equation relates the resistivity of a medium (r) to porosity (f) with consideration of the saturation (a), cementation (m) of the material, and the resistivity of the pore fluid (r_w) (equation 5.2). The latter was obtained in the field using an electrical conductivity probe meter. A pore water value was obtained by converting the average conductivity of the pore water to resistivity (17.5 ohm.m). The r value applied was again derived from the DC resistivity model (36,000 ohm.m). Typically, the empirical constants limits are $0.5 < a < 2.5$ and $1.3 < m < 2.5$ (Lowrie, 1997). The basement rock was assumed to be fully saturated (a =1), and the cementation was estimated at 2.

$$r = a r_w f^{-m} \qquad 5.2$$

Through the application of Archie's law, a porosity of 0.022 (2.2%) was obtained. Based on the low porosity, the basement was deactivated to represent a "no flow" boundary for all simulations.

For the purpose of modeling, the assumption was made that the entire unit above the base rock represents an unconfined aquifer with the majority of the simulations including laterally discontinuous potentially confining clay layers. The upper 1.5 metres of all models were assigned K values of 4.3e-5 m/s (figure 5.2). This figure was derived by averaging the K values from the shallow piezometers.

Archie's Law was again applied to estimate the average porosity of the unconfined aquifer based on the DC resistivity value of the unit. In this calculation, the resistivity of the medium was 15 ohm.m. The material was again assumed to be fully saturated (value of 1) and 1.2 was the cementation coefficient ascribed for m. A porosity of 115% was calculated by utilising Archie's law. There are two possible explanations for why Archie's law was not valid.

Firstly, the clay content may have a primary role in lowering the average resistivity of the bank. If this is the case, then there is a possibility that a thicker more continuous clay horizon or horizons occur at depth. Alternatively, as the water conductivities were taken on the 24/8 in a dry month and the DC resistivity conducted on a day during the wettest month of the year, the error could be due to climatic differences. This argument is based on Green (1997), who concluded that concentrations of both acid and metals were approximately 3 times higher in wet periods compared to dry conditions at bank D on the King River in 1997. So the in-situ value of K (3.9e-6 m/s) obtained from the deeper piezometers is adopted.

The northern boundary represents the road/sediment bank interface. The surrounding rock was observed in the field as a fine grained siltstone (sample 1) and documented by Baillie and Corbett (1985) as being the oldest part of the Cambrian succession. They classified the rock exposed along the King River as thinly interbedded laminated siltstones and slates and very fine grained sandstones and siltstones. Siltstone commonly has a low K value with an average value ~1e-7 m/s (Domenico and Schwartz, 1990; Morris and Johnson, 1967). Recovery tests estimated the average K of the sediment bank to be 1.6e-5 m/s. On the basis of the theorised magnitudinal difference between the two materials, the majority of the simulations were run with the impermeable northern boundary. Alternatively, simulations were also run applying a constant head boundary to the cells representing this interface. Depending on the elevation of the constant head boundary, groundwater will flow horizontally towards the river, from the bank into the siltstone (lower head in siltstone), or flow into the bank with a vertical component (higher head in the siltstone).

It is improbable that groundwater would flow from the bank into the siltstone due to the steep topographic decline towards the road. A constant head equal to the head values in pizometers closest to the road was preferred. As hydraulic head values are not uniform along the bank, the constant head nodes were singular adjusted along the column representing the boundary to conform to corresponding hydraulic head in the bank.

Simulations were run by assigning variable K lenses to certain cells based on the spatial and depth distribution of hydraulic conductivity. The lenses were suggested by comparing cross-sections in both the X and Y directions (Chapter 3). As K values were spatially constrained by piezometer spacing (10s of metres), lenses were extrapolated out in both the X and Y direction to several metres. An approximate thickness of 30 cm was assigned for each lens (figure 5.2). Field observations suggested that clay lenses range from 2 cm to 20 cm in thickness. A maximum lateral extent could not be known, as trenches dug were only $1m^3$. Minimum lengths of clay lenses were noted on a cm scale. A photo included in Locher's (1997) report on the King River suggest that possibly confining/semi-confining lenses may occur on at least a metre scale at bank M (chapter 1, plate 1.1).

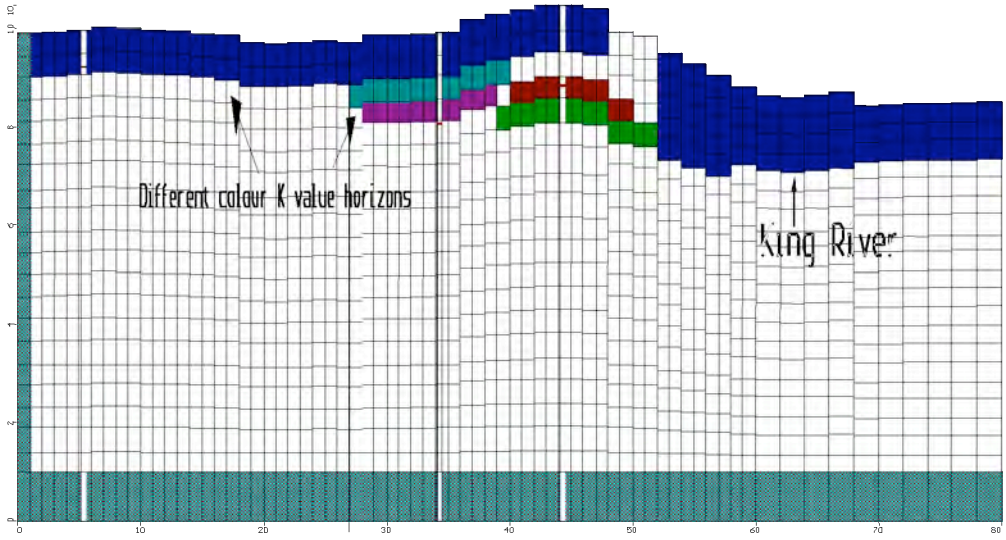

Figure 5.2. A cross-section illustrating an example of some of the imported hydrological framework requirements for the mathematical model. In this cross section, no flow boundary (green) and hydraulic conductivity variations (different colours) are included.

Models which incorporated the various clay lenses were simulated with the northern boundary deactivated and ascribing the rest of the cells in the solution domain with the default hydraulic conductivity (figure 5.2). This simulation was carried out for the three times of measurement. Due to the amount of memory required to run this simulation, the inferred clay lenses could not be included in subsequent simulations, as the model engines would terminate.

The quadrature responses of the EM31 suggested the possibility of a perched water table. There is no evidence to suggest whether the perched water table is the result of a confining layer (layers) which resulted in higher potentiometric pressure heads in the deeper piezometers, or whether there could be a confining / semi-confining layer at depth. The idea of a confining layer at depth was included in several simulations.

Hydrogeological stresses

The temporal and spatial data of hydrological stresses are provided, including a) river levels, b) rainfall, c) evaporation and d) hydraulic head distributions. Rainfall records were obtained from the Bureau of Meteorology from the base station at Strahan. The most proximal station for evaporation data was from 1967-1983 at Queenstown. It was assumed that Queenstown would have similar evaporation rates as Strahan in a given month with similar precipitation measurements (Appendix 6).

A combination of tidal effects and rate of discharge from the John Butters power station control river levels (Taylor et al., 1996; Locher, 1997). For each day of measurement, an average river level related to the Australian Height Datum was applied to the model. The EM31 images were used to infer the subsurface structure of the water table. Table 5.1 lists the values of the hydraulic stresses applied to simulations for each day of measurement.

Date	River level surface elevation (m)	river depth (m)	rainfall (mm/y)	evaporation (mm/y)
16/4/2000	0.71	1.7	930	448
24/7/2000	1.8	2.8	2500	250
24/8/2000	0.2	1.2	750	360

Table 5.1. Hydraulic stress values applied to models for each day of measurement. Locher (1997) measured the base of the river in relation to AHD, therefore the depth of the river could be calculated.

When using the recharge package in Visual MODFLOW, an option is available which requires either rainfall to be applied to the surface of the model or the highest activated cell in each column. A sensitivity analysis was performed by applying the first option to a simulation. The output image illustrated dry cells (land) for a depth exceeding 2 metres. Field observation and geophysical investigation suggested that the water table is near the surface, thus this was an unrealistic model. However, what it does suggest is that the majority of the

rainfall infiltrated through the tailings and surface run-off is minimal. This was observed in the field during wet periods.

Due to the shallow water table and unconsolidated nature of the tailings, an extinction depth of 1 metre was assigned to the evapotranspiration package.

One of the questions posed in this study was whether the surface drainage path to the west of the bank (discussed in chapter 3) is an essential feature of the hydrogeological system. The importance of the creek was established in chapter 3 by the hydraulic head contour images and in chapter 4 from the HCP Inphase (EM31) image. Accordingly, it was concluded that the pooled water at piezometers 7 and 8 represent the water table and that the connecting creek is removing water from the aquifer and draining directly into the King River. Thus, dependent on the water table elevation, the conduit may influence the proportion of discharge directly to the river, to the component of flow moving vertically through the bank (recharge).

MODFLOW'S river package (RIV) was adapted to include the creek as the drain package (DRN) required unobtainable detailed information for calculation of the drain conductance. The aquifer-to-drain leakage is assumed to follow Darcy's law (Merrick, 1999).

5.3.3. Calibration

Calibration can be carried out by adjusting the systems configuration and stresses until simulated results match observed data (Frind and Molson, 1994; Merrick, 1999). This was the method outlined in Visual MODFLOW and was used in conjunction with sensitivity analyses. Once the best possible fit of the data was obtained, the outputs were checked for validity based on observations made in the field and results from scientific investigations. The surface plan view of the models simulated with the northern boundary deactivated and inferred K lenses illustrated surface ponded water comparable to that observed in the field (Figure 5.3).

5.3.4. Zonations

Visual MODFLOW contains a zone budget package, which provides mass balance information to the entire model as well as specific mass balances for areas designated

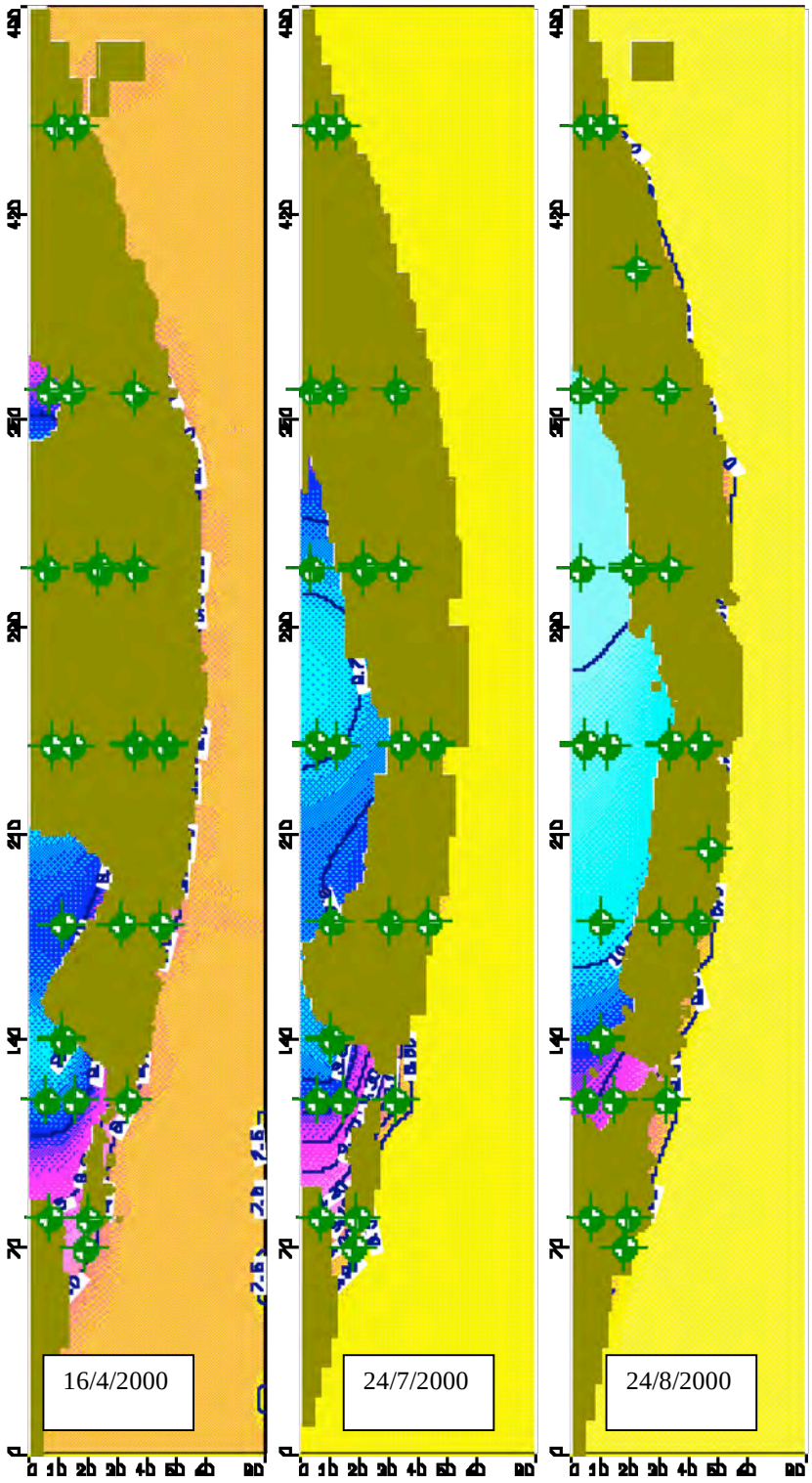

Figure 5.3. Plan view images of the surface layer of bank H illustrating areas of dry land (khaki), and areas of ponded water (coloured contours) for the 16/4, 24/7 and 24/8. Surface water areas were over estimated for the 24/7/2000.

by a zone budget. By default, zone 1 represents the entire solution domain. By assigning the sediment bank area extending the depth of the basement as zone 2, the bank is taken out of the entire solution domain, leaving zone 1 as only representing the area below the river (figure 5.4). One of the output modules details the flow rates (both in and out of each of the model domains) for each of the following:

-constant head

-rivers

-recharge

-evapotranspiration.

This package provides detail on the discharge into the river either directly from the sediment bank (predominantly horizontal flow) or the component of flow which discharges from zone 2 to 1. Flow moves with a strong upward vertical direction from zone 1 to the river. Thus, the total discharge from the bank to the river is the product of these two components. Figure 5.4 is used to illustrate the input and output component of discharge for each zone in the results section (5.5).

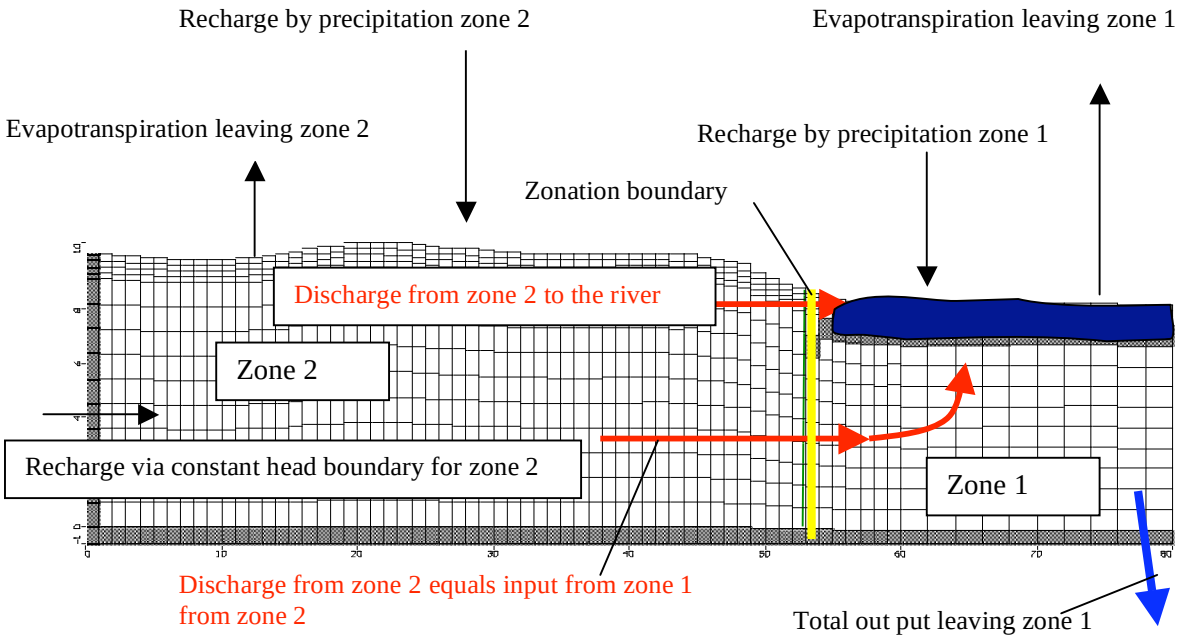

Figure 5.4. Schematic illustration of the mass balance calculations directly from the sediment bank (zone 2) – upper red arrow and discharge to the river from the sediment bank via zone 1 (below the river) – lower red arrows. Total discharge to the river from the bank is the product of discharge to the river from zone 2 and zone 1. Total output leaving zone 1 also considers rainfall recharge and evaporation outputs.

5.4 MODPATH

Essentially, groundwater movement controls the transport of solutes either by advection (dissolved constituents) or mass transport (particles e.g. colloids) (Merrick, 1999). This indicates the importance of the initial calibration of the groundwater flow to ensure that flow velocities and patterns are adequately simulated. Subsequently, the solute transport model (MODPATH) was run simultaneously with MODFLOW.

It was hoped that the MT3D model could produce contamination concentration contours. This would have lead to predicting the severity of the groundwater contamination discharge into the King River. Unfortunately, this engine was unable to operate successfully.

5.5. Numerical Modeling Results

Models were first simulated with a deactivated northern boundary and various K lenses. A simulation on the 24/7 resulted in a discharge of 22 m^3/day directly to the river and a discharge of 80 m^3 /day via zone 1 (Figure 5.5). It is observed that the discharge directly to the river is far less than the results from the analytical method. This is because high K values from the shallow piezometers severely increased the average hydraulic conductivity applied to the analytical method.

As figure 5.5 illustrates, groundwater moves preferentially through the upper most layer which has a higher hydraulic conductivity than the surrounding material. However, lower hydraulic conductivity lenses resulted in increased vertical velocities due to a comparatively higher hydraulic conductivity surrounding the lenses (Figure 5.6).

Under the same hydrogeological framework conditions, total discharge to the river on the 16/4 was calculated as 45.6 m^3/day; 8.6 m^3/day directly from the river and 37 m^3/day via zone 1 (Figure 5.5).

Despite higher evaporation rates on the 16/4 (table 5.1), evapotranspiration from the bank was higher on the 24/7, which was consistent with all other simulations. The most probable explanation is that increased surface areas of pooled water results in increased evapotranspiration.

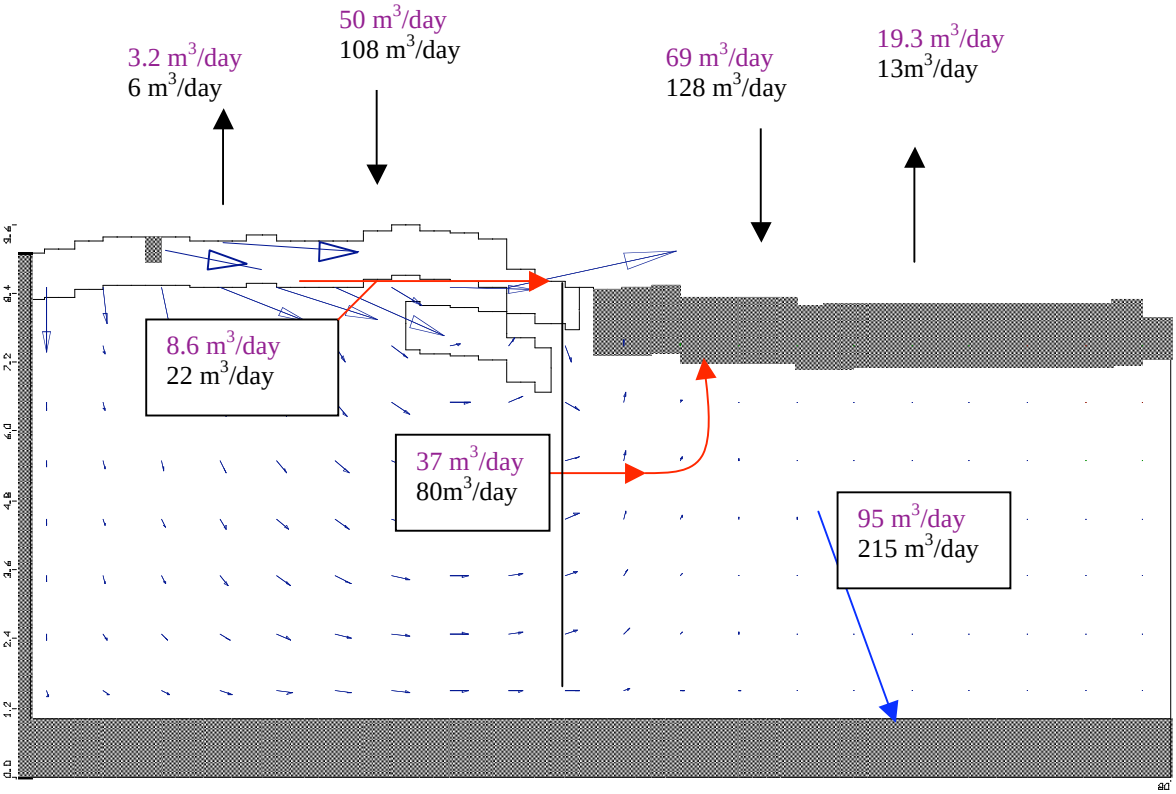

Figure 5.5. Groundwater discharge zone budget for the 16/4 (purple) and the 24/7 (black). The size of the MODFLOW arrows (blue) in the solution domain indicates the magnitude of the velocity vector. Note; surface river level elevations change for the two times of measurement.

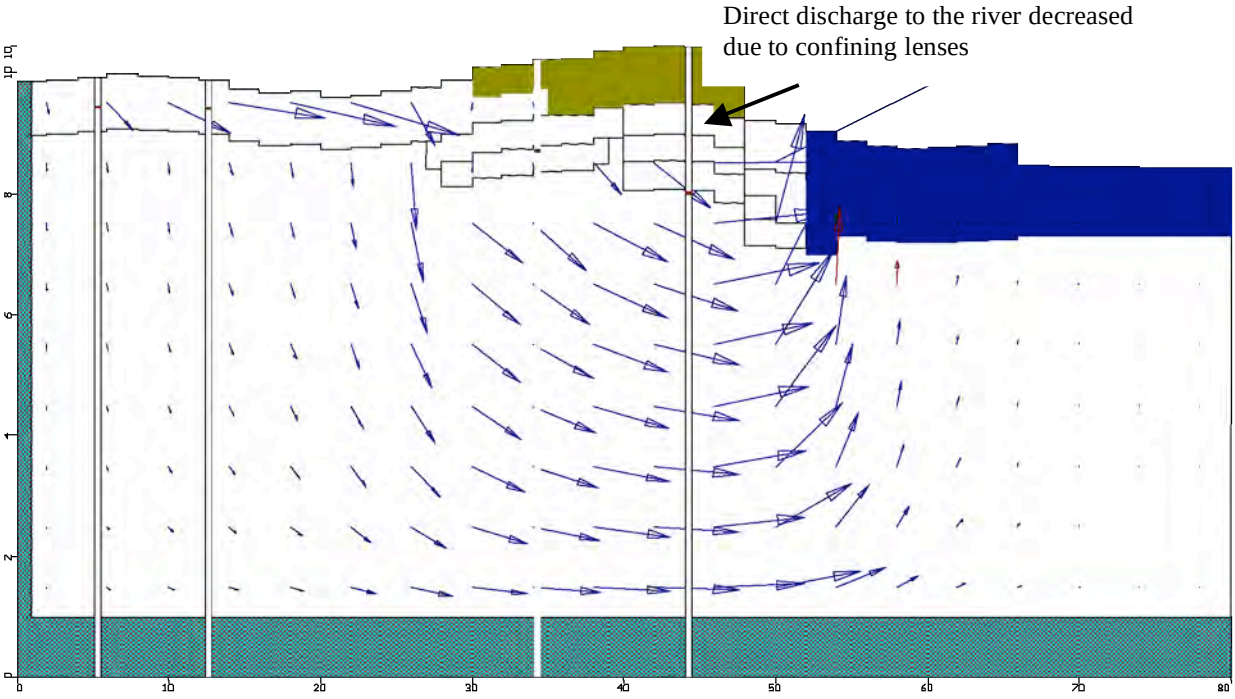

Figure 5.6. Low hydraulic conductivity lenses will result in increased velocities in the vertical component of flow.

A second model was simulated by replacing the K lenses with a low K unit (1e-7 m/s) at an approximate depth of 1 metre. The clay layer was assigned a thickness of 30cm and spatially extended to the area outlined by the EM31 quadrature responses as a possible perched water table. The low K layer had the effect of redistributing the discharge component for direct entry into the river or via zone 1. Discharge directly to the river increased by ~1.5 times the previous simulations that excluded the low K layer (Figure 5.7). This suggests that the hypothetical confining layer has an important role in horizontal flow.

When the upper most layers of the model were taken out of the simulations (high K, 4.3e-5), horizontal flow decreased dramatically (Figure 5.8). This infers that the unconsolidated high hydraulic conductivity tailing is the main determinant for flow directly discharging in to the river (mainly horizontal flow).

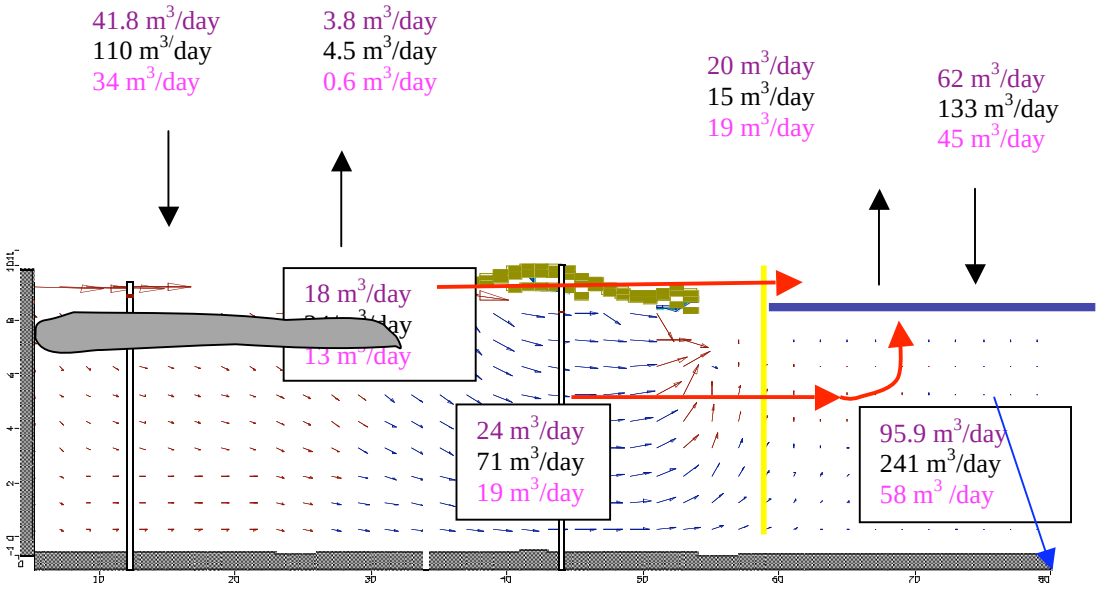

Figure 5.7. Groundwater discharge zone budget for the 16/4 (purple), 24/7 (black) and the 24/8 (pink). The size of the MODFLOW arrows (blue and purple) in the solution domain indicates the magnitude of the velocity vector. Upper red arrow indicates discharge directly from the bank (horizontal flow) and lower red arrow indicates discharge via zone 1 which is underneath the river. Note; elevation of the base of the river is shown and hydraulic conductivity was not an overlay in the models MODFLOW output. Instead the low K layer has been drawn in by hand (grey) estimating the depth.

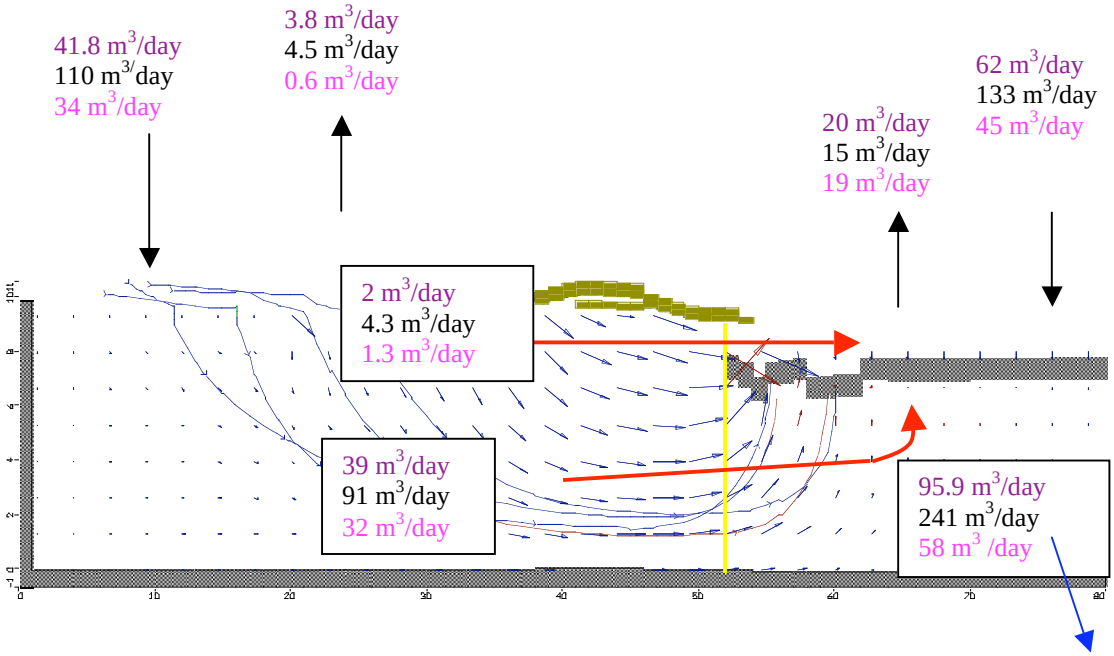

Figure 5.8. When the upper most high K layers are removed from the model, discharge rates directly to the river decrease substantially. Purple discharge rates are on the 16/4, black, 24/7 and pink, 24/8.

When constant head values were applied to the northern boundary, the calculated head values were consistently higher than the observed values (figure 5.9). This suggested that when flow was simulated through the northern boundary at the same rate as through the sediment bank (i.e. same K, no hydraulic gradient), the amount of water entering the system is too excessive to accurately represent the observed hydraulic heads.

Simulations that produced a better representation of the data were the models applying a constant head boundary in conjunction with low K material (1e –7m/s) along the northern boundary column. Figure 5.10 illustrates a comparison between the mass balance budget between the two scenarios on the 24/7. The total discharge to the King River when the northern boundary is represented by a constant head and flow inhibited by the siltstone (1e-7m/s) was 174 m^3/day. This discharge rate can be compared to 241 m^3/s in simulations when the northern boundary was treated as “no flow.”

In addition evapotranspiration is higher in zone 2 for the constant head simulations in comparison to simulations mentioned previously. This supports the theory of increased evaporation when pooled surface areas are more exposed.

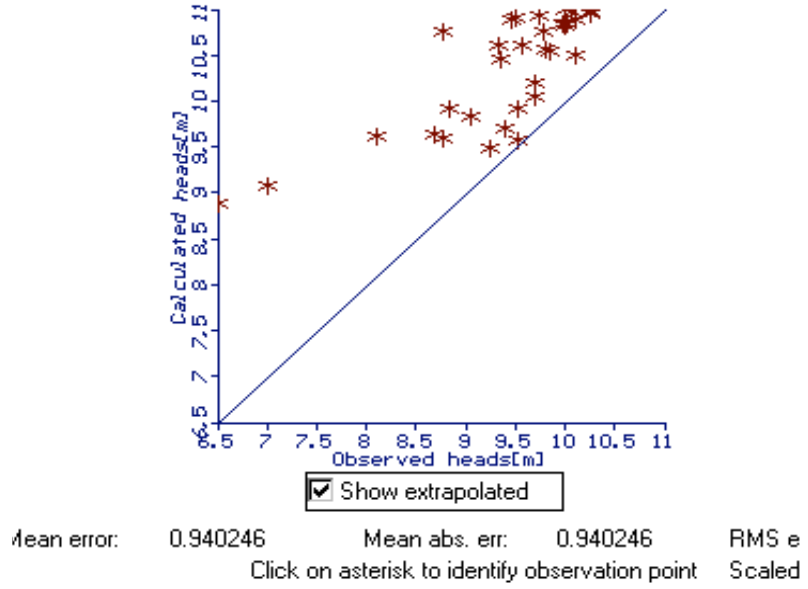

Figure 5.9. Calibration residual for calculated versus observed head for simulation of a model where the northern boundary is represented by a constant head boundary with the same value as the hydraulic head in the shallow piezometers closest to the road.

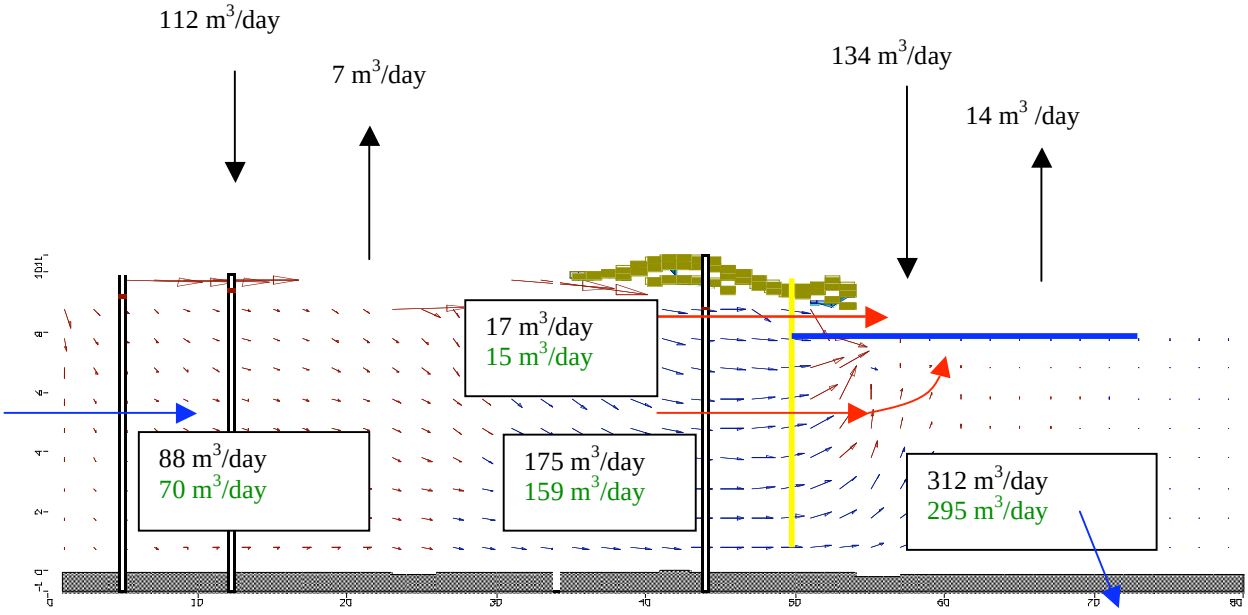

Figure 5.10. A comparison of the zone budgets on the 24/7, between a model with a constant head representing the northern boundary (black) and constant head and low K defining the northern boundary (green). Both simulations also include the low K layer at ~1 metre depth.

Models were also designed to determine the effects of a possible formation of hardpans on the surface over 80% of the bank. However, as MODFLOW only simulates flow in the zone of saturation, the impermeable layer was assigned below the water table. A hydraulic conductivity value of 4e-8 m/s was assigned to the layer based on the value found from a study on hematite crusts (Enviro Browser). As the hypothesised hardpan crust was essentially representing the same scenario as the confining clay, similar flow paths were simulated (Figure 5.11). However, due to a) hardpan crust covering the majority of the bank and b) considerable low K, there is minimal vertical flow and the majority of flow is discharged as predominantly horizontal flow within the upper most metre. It can be suggested that because the hardpan layer would in reality form on the surface, that under the same conditions, 59 m^3 /day would result in overland flow. This may greatly reduce subsurface acid drainage.

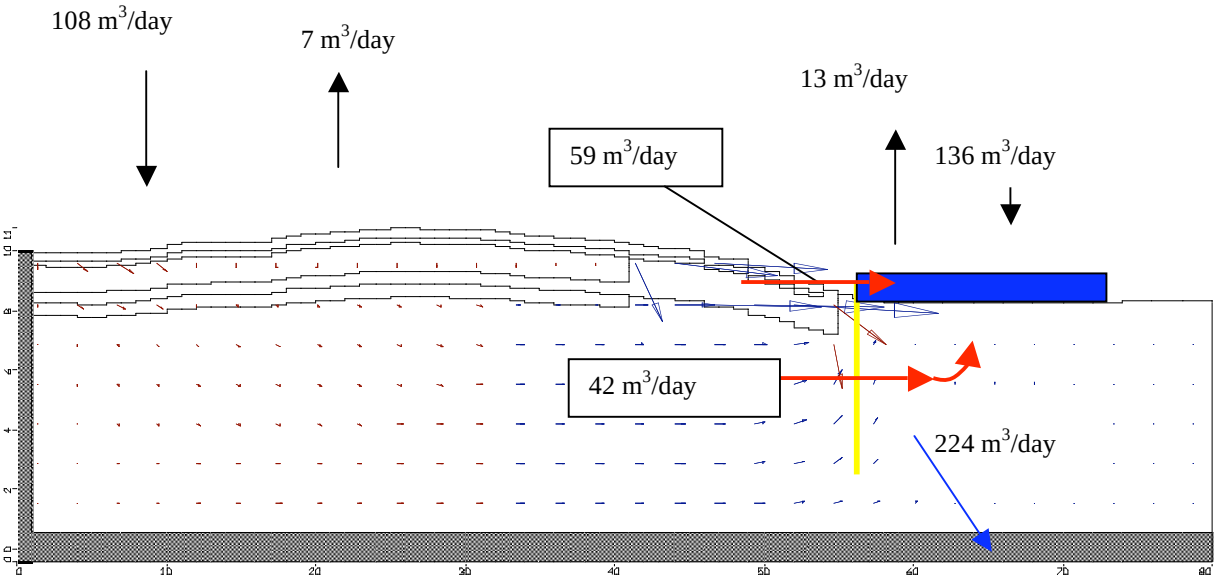

Figure 5.11. Simulation of a hypothetical development of a hardpan layer with an estimate K of 4e-8 m/s covering greater than 80 % of the bank.

Attempts to simulate an accurate response for models with a substantial rise in river levels proved relatively unsuccessful. However, models were more realistic when the river was only

raised by a small degree. For example, when the river was raised by ~ 50 cm in a simulation for the 16/4, 4.8 m^3/day was discharged back into the bank (Figure 5.12).

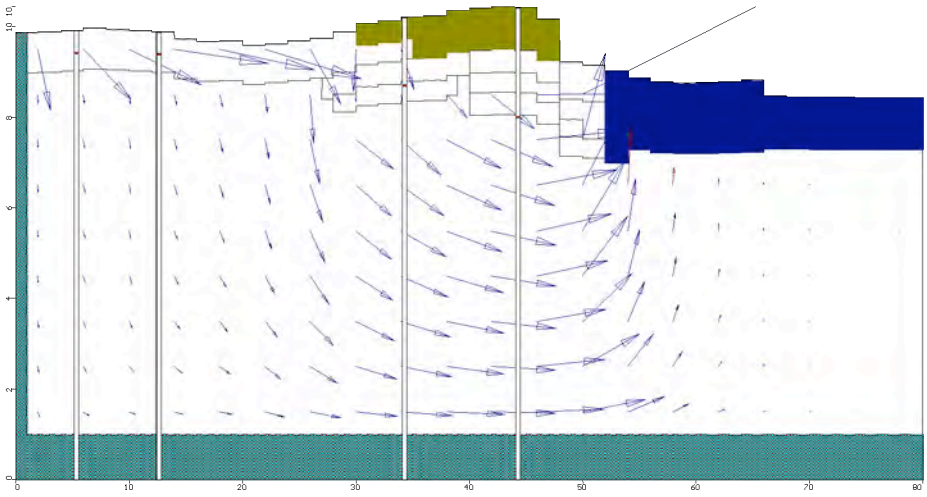

Figure 5.12. Simulation for a model with a no flow northern boundary and K lenses. River levels have been raised approximately 30 cm which resulted in a localised reverse hydraulic gradient back into the system.

Velocities for all simulations decreased with increasing depth and horizontal flow was on average an order of magnitude lower then flow perpendicular to the river. In the horizontal direction, groundwater velocities were consistently higher closest to the northern boundary, which supports the idea from the analytical contours.

The residence time is determined in Visual MODFLOW by how long it takes for a particle to move from a given place to the discharge zone. It proved difficult to compare residence between simulations due to the cluttering of particles and particle not being spatially consistent. Generally particle residence ranged from 5-25 years.

5.6 Limitations of Models

Confidence in the model prediction of aquifer behavior, under both the existing conditions and hypothetical scenarios, is based on the following:

- The knowledge about the reliability of the data and aquifer characteristics
- The accuracy of calibration and confidence in the validation of the model
- An understanding of the model's limitations (Merrick, 1999).

Because only 22 piezometers were installed in the bank, limited data can be input into MODFLOW to acquire simulations with a great degree of confidence. Areas of ambiguity arise from flow paths not being fully understood as well as the heterogeneous nature of the bank. Although higher piezometric heads in the nested deeper piezometers suggested the existence of confining layers, there is no evidence to suggest that confining layers occur at depth. There is also no evidence to suggest that the potentially perched water table inferred from the EM31 response is a result of a confining layer at depth or associated with lenses which affect the piezometers. As the majority of flow in all simulations was via zone 1 to the river, the discharge rate into the river is dependent on the hydraulic conductivity of the material. It is quite possible that an estimation of the average K from the deeper piezometers is not an accurate representation of the hydraulic conductivity below 2.5 metres.

5.7 Conclusions

The direction and velocity of groundwater movement through the bank are dependent on the characteristics of the solution domain. By adapting the boundaries and properties of the system, different proportions of groundwater will flow either horizontally to the river or down through the bank and discharge via zone 1 underneath the river.

The discharge to the river is on average 45 m^3 /day, 105 m^3 /day and 33 m^3 using hydraulic data from the 16/4, 24/7 and 24/8 respectively. These calculations were based on models with the northern boundary deactivated. The only boundary condition changed to alter the inputs into the system was assigning a constant head boundary to several simulations. This had the effect of increasing the hydraulic head values for the observed data and therefore, is probably not an accurate representation of the system. The only simulation for when discharge directly to the river was greater then discharge via zone 1 was a simulation which involved a hypothetical formation of hardpan confining unit over 80 % of the bank. This resulted in a discharge of 59 m^3/ day directly to the river compared with 42 m^3 /day via zone 1.

As all simulation were run at a steady state, there was no storage in the system and thus outputs always equal the inputs. What would be interesting for further research, would be to perform a transient simulation on the bank over a variable climatic period to determine the potential storage capacity of the bank.

Chapter 6: Conclusions

An understanding of the aquifer system of sediment bank H along King River has been attained through hydrogeological and geophysical investigations. Analytical and numerical methods were used to determine the groundwater discharge with consideration to climatic conditions and fluctuating river levels, which are primarily independent.

The study found groundwater flowing persistently from the bank and discharging perpendicularly into King River. Analytical methods calculated discharge to the river on the 24th of July to be 187 m^3/day during an abnormally high rainfall period with elevated river level. On the 24th of August, discharge was 108 m^3/day following a period of low rainfall and relatively low river level.

Hooper (1997) estimated discharge rates at bank D as 8 and 19 m^3/day in summer and winter respectively. The difference in rates between the current study and that of Hooper (1997) is due to actual groundwater velocities being 80 times higher in the current study. Velocities in this study were between 0.0028–0.27 m/day on the 24th of July and 0.004–0.3 m/day on the 24th of August. It is concluded that either: a) the sediment properties of the two banks are vastly different; b) there are marked difference in topographic-driven hydraulic gradients or; c) the datasets do not accurately reflect the aquifer system for either or both of the studies. Some exceptionally high hydraulic conductivities determined in this study may not provide a good representation of the overall bank properties. Despite the difference in discharge rates, both studies suggest that groundwater discharge from each bank represent only a small percentage of the King River flow. Maximum percentage calculated at bank H was 0.005%.

Vertical hydraulic gradients suggest the possibility of a confining or partially confining layer at depth. This is evidenced by higher potentiometric pressure heads from several deeper piezometers compared with the water table inferred by shallow piezometers. An EM 31 survey defined the same area as having a high electrical conductivity, which may be a response to a perched water table. It is also possible that the high conductivities from the quadrature responses could be reflecting a clay lens at depth.

EM 31 vertical dipole inphase measurements (second shallowest investigation depth) yielded higher conductivities in domains where higher hydraulic head values were calculated from the shallow piezometers. The hydraulic head measurements in the shallow piezometers have been interpreted as representing the water table. The VD inphase image correlates well with subsurface hydraulic structure and is therefore used as a guide to estimate water table elevations in between the piezometers.

The DC resistivity sounding defined a high resistivity (35 980 ohm.m) basement at 14m which has been interpreted as fresh rock. PROTEM defined the same boundary at ~20m, however, this is likely to be overestimated due to the thickness of surficial conductive layers. Seismic refraction detected the first layer response as having a thickness of 11m, however, a velocity of 1400m/s suggests this response is not fresh rock. Based on these geophysical responses, an estimation of the depth to the base of the aquifer was assigned to numerous models to simulate groundwater flow in three-dimensions.

Visual MODFLOW was used for numerical modeling, running simulations at a steady state. The residing boundaries and hydraulic properties applied to the solution domain will have an influence on flow direction and velocities. Therefore, boundaries and hydraulic properties have an effect on the percentage of flow discharged predominantly horizontally to the river (directly from zone 2) and flow that moves down through the bank and discharges to the river via a steep upwards gradient in zone 1 (underneath the river). In all simulations, discharge was greatest via zone 1 with the exception of a simulation which involved the hypothesised formation of a confining layer such as a hardcap over 80% of the bank. This resulted in a discharge of 59 m^3/day directly to the river compared with 42 m^3/day via zone 1.

Average discharge to the river is 45, 105 and 33 m^3/day using hydraulic data from the 16/4, 24/7 and 24/8 respectively, based on models with the northern boundary deactivated. This boundary condition was changed to alter inputs into the system by assigning a constant head boundary to several simulations. This led to an increase in hydraulic head values for the observed data and is thus probably not an accurate representation of the system.

References

Al, T.A., and Blowes, D.W., (1996). Storm-water hydrograph separation of run off from a mine tailings impoundment formed by thickened tailings discharge at Kidd Creek, Timmins, Ontario. *Journal of Hydrology*, 180, p55-78.

Al, T.A., and Blowes, D.W., (1999). The Hydrogeology of a tailings impoundment formed by central discharge of thickened tailings: implications for tailings management. *Journal of Contaminant Hydrology*, 38, p489-505.

Baillie, P.W., and Corbett, K.D., (1985). Geological Survey Explanatory Report. Tasmanian Department of Mines- Geological Atlas. 1:50,000 series, sheet 57 (7913N), Strahn.

Barbour, S.L., Wilson, G.W., and St-Arnaud, L.C., (1993). Evaluation of the saturated – unsaturated groundwater conditions of a thickened tailings deposit. *Canadian Geotechnical Journal*, vol 30. p935-945.

Bird, D.K., and Krauskopf, B. K., (1995). Introduction to Geochemistry. Third Edition. McGraw-Hill, Inc, U.S.A. p 647.

Blowes, D.W., and Gillham, R.W., (1988). The generation and quality of streamflow on inactive uranium tailings near Elliot Lake, Ontario. *Journal of Hydrology*, 97, p1-22.

Brassington, R., (1988). *Field Hydrogeology, 2nd Edition.* John Wiley and Sons Inc, England, p242.

Chermak, J.A., and Runnells, D.D., (1996). Self-sealing hardpan barriers to minimise infiltration of water into sulphide-bearing overburden, ore and tailings piles. *Tailings and Mine Waste'96.* P265-273.

Coggans, C.J., Blowes, D.W., and Robertson, W.D., (1992). Hydrogeology and Geochemistry of a nickel mine tailings impoundment, Copper Cliff, Ontario. *Proceedings Second International Conference Abatement Acidic Drainage*, 4, 1-26.

Donald, S., Welsch, D., Holl, N., and Landine, P., (1997). Recent hydrogeological developments in uranium mine tailings management in Canada: The Key Lake experience. *Engineering Geology and the Environment* p2371- 2377.

Domenico, P.A., and Schwartz, F.W., (1990). *Physical and Chemical Hydrogeology.* John Wiley and Sons, Inc, U.S.A.

Endres, T., (1999). Application of Geophysics to Minesite Problems: In Minesite Hydrology. Center for Groundwater studies, Sydney. p1 – 12.

Enviro Browser (1997). Waterloo Hydrogeologic software, consulting, training, v 2.1. Georef systems Ldt.

Freeze, A.R., (1983). Regional groundwater analysis in surface and subsurface hydrology. *Papers of the International Conference on Groundwater and Man,* Sydney. 1, 4.

Freeze, A.R., and Cherry,J.A.,(1979). *Groundwater*. Prentice-Hall, Inc, Ontario,United States.

Freeze, A.R., and Witherspoon, A.P., (1967). Theoretical Analysis of Regional Groundwater Flow. Effects of Water-Table Configuration and Subsurface Permeability Variation. *Water Resources Research.* 3, 2, p 623-634.

Frind, E.O., and Molson, J.W., (1994). The Physical Hydrology of Mill-tailings Impoundments. In: Jambor, J.L., and Blowes, D.W.,(eds) *Mineralogical Association of Canada Short Course handbook on Environmental Geochemistry of Sulfide Mine- Wastes.* Waterloo, Ontario.

Gillham, R.W.,(1984). The capillary fringe and its effect on water table response. *Journal of Hydrology,* 67, 307-324.

Green, D., (1997). *Geochemistry of a sediment bank along the King River, Tasmania.* Honours thesis, Department of Earth Science, Monash University, Melbourne, Australia.

Guiguer, N., and Thomas, F., (1994). Visual MODFLOW User's Manual. Waterloo hydrogeologic Inc., Waterloo, Ontario, Canada, p315.

Herbert, A.W., Jackson, C.P., and Lever, D.A., (1988). Coupled Groundwater and Solute Transport with Fluid Density Strongly Dependent Upon Concentration. *Water Resources Research.* 24, n°10, p1781-1795.

Hooper, C.W., (1997). *The Hydrogeology of a Sediment Bank on the King River, Tasmania.* Honours thesis, Department of Earth Science, Monash University, Melbourne, Australia.

Johnson, A.C, and Thornton, I. (1987). Hydrological and Chemical Factors Controlling the Concentration of Fe, Cu, Zn and As in a River System Contaminated by Acid Mine Drainage. *Water Resources Research.* 21, 3, p359-365.

Kalf, F.R.P., and Dungeon, C.R., (1999). Analysis of long term groundwawter dispersal of contaminants from proposed Jabiluka Mine tailings repositories. *Supervising Scientist Report,*143.

Keller, G. V., and Frischknecht, F. C., 1966, Electrical methods in Geophysical Prospecting: Pergamon Press.

Kelly, M., (1988). *Mining and the Freshwater Environment*. Elsevier and Applied Science, London, U.K, p134.

King, A., and Pesowski, M.S.,(1993). Environmental Applications of surface and airborne geophysics in mining. *CIM Bulletin*, v86,n.966, p58-67.

Leaman, D., (1997). Exploration Geophysics, Remote Sensing and GIS Master of Economic Geology Course Work Manual 13, Fourth Edition. Center of Ore Deposits Research, Tasmania.

Locher, H., (1997). Sediment storage and transport in the King River, Tasmania. P.h.D Department of Civil Engineering, Monash University, p523

Lowrie, W., (1997). *Fundamentals of Geophysics*. Cambridge University Press, United Kingdom. pp338.

McNeill, J.D., (1990). Use of electromagnetic methods for groundwater studies: In Ward SH (Ed). Geotecnical and Enviromental Geophysics. *Soc.Expl.Geoph.Spec.Pub.* No.5.vol. 1.p 191-218.

Merrick, N., (1999). Groundwater Modelling For Prediction. National Centre for Groundwater Management. Minesite Hydrology Conference, Sydney. 12-14/7/99.

Milsom,J., (1996). *Field Geophysics.* The Geological Field Guide Series. 2nd Edition, John Wiley and Sons, London.

Morris, D.A., and A.I. Johnson, (1967). Summary of hydrological and physical properties of rock and soil materials as analyzed by the hydrologic laboratory of the U.S. Geological Survey. *USGS Water Supply Paper* 1839-D.

Oelkers, E.H., (1996). Physical and Chemical Properties of Rocks and Fluids for Chemical Mass Transport Calculations. In: Lichtner, P.C., Steefel, C.I., Oelkers, E.H.,(eds) *Reactive Transport in Porous Media.* Reviews in Mineralogy vol 34.

Price, M., (1996). *Introducing groundwater.* The University and reading, UK and British Geological Survey. Chapman and Hall.

Palacky, G. J., and West G.F., (1991) Airborne Electromagnetic Methods. In Nabighian, M. N., (eds). Electromagnetic methods in applied geophysics. Vol 2, Application, part A and B. Society of Exploration Geophysicists, Oklahoma, p 811-879.

Reid, J.E., Fullagar, P.K.,(1998). Conductivity-depth transformation of slingram transient electromagnetic data. *Exploration Geophysics,* vol 29, p570-576.

Robertson,W.D.,(1994). The Physical Hydrology of Mill-tailings Impoundments. In: Jambor, J.L., and Blowes, D.W.,(eds) *Mineralogical Association of Canada Short Course handbook on Environmental Geochemistry of Sulfide Mine- Wastes.* Waterloo, Ontario.

Sevick, G.W., Paruvakat, N., Black, K.P., and Hockley, D. (1998). Engineered upland tailings management facility. *Tailings and mine waters'98.* Balkerma, Rotterdam, p93-102.

Taylor, J.R., Weaver, T.R., McPhail, D.C., and Murphy, N.C., (1996). *Mt Lyell Remediation.* Characterisation and impact assessment of mine tailings in the King River system and delta, Western Tasmania. Supervising Scientist.

Taylor, K.,(1998). *Acid Drainage from an Abandoned Smelter Site, Zeehan.* Honours Thesis, University of Tasmania.

Telford, W.M., Geldart, L.P., and Sheriff, R.E., (1990). *Applied Geophysics.* 2nd Edition, Cambridge University Press.

van der Heijde, P.K.M., (1996). Compilation of saturated and unsaturated zone modeling software. USEPA National Risk Management Research Laboratory, Ada, Oklahoma, EPA/600/SR-96/009.

Van Overmeeren, R.A., (1994). Georadar for Hydrogeology. *First Break*, v.12, pp401-408.

Woods, D.A., (1989). Concentrations of Radon and Radon Daughters During Semi-Dry Tailings Deposition at Nabarlek. *Supervising Scientist for Alligator River Region,* Technical memorandum, 29.

Woyshner, M.R., and Yanful, E.K., (1995). Modelling and field measurements of water percolation through an experimental soil cover on mine tailings. *Canadian Geotechnical Journal.* 32, 601-609.

Yang, J., Edwards, R.N., Molson, J.W., and Sudicky, E.A., (1996). Fracture-Induced Hydrothermal Convection in the Oceanic Crust and the Interpretation of Heat-flow. *Geophysical Research Letters,* 23, 9, 929-932.

Yang, J., Latychev, K., and Edwards, R.N., (1998). Numerical computation of hydrothermal fluid circulation in fractured Earth structures. *Geophysical Journal International.* 135, p627-640.

Zannetti, P., (1995). Environmental Modeling- Past, present and future. Proceedings of MODSIM 95 Conference, Newcastle, NSW Australia, 1-9.

Appendix 1

Auger holes drilled by Locher (1997) to determine pre and post mine tailings.

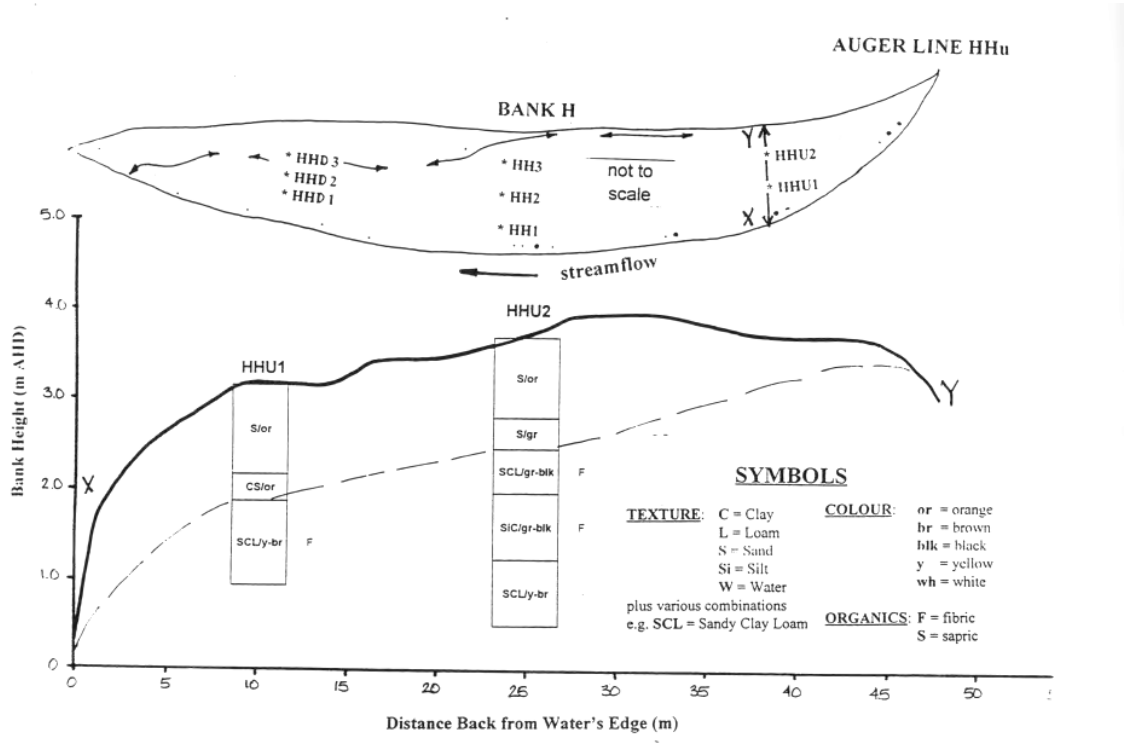

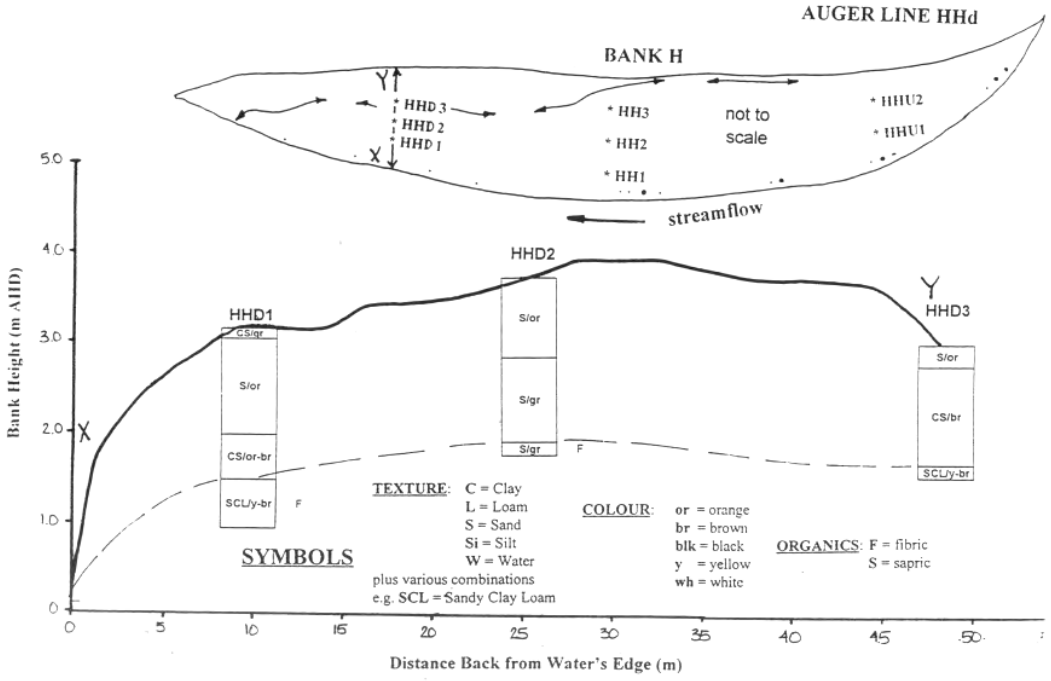

Appendix 2

Topography of the sediment bank using dumpy level and staff.

Back Sight	Inter Sight	Fore Sight	Rise	Fall	Reduced Level	Remarks	Final Level	Final level adjusted
3.656					0.000	sl, 4mS	0.000	0.000
	2.85		0.806		0.806	OmE. 1.5mS	0.806	0.806
	2.4		0.45		1.256	0mE.0m	1.256	1.256
	1.66		0.74		1.996	10mE,0m	1.996	1.996
	2.17			0.51	1.486	10mE,3mS	1.486	1.486
	2.67			0.5	0.986	10mE, 4mS	0.986	0.986
	3.66			0.99	-0.004	sl 10mE, ,7mS	0.000	0.000
	1.595		2.065		2.061	20mE,0m	2.061	2.061
	2.5			0.905	1.156	20mE, 7mS	1.156	1.156
	3.18			0.68	0.476	20mE,9mS	0.476	0.476
	3.66			0.48	-0.004	sl 20mE, ,10mS	0.000	0.000
	0.48		3.18		3.176	20mE, 8mN road edge	3.176	3.176
	1.575			1.095	2.081	30mE, 0m	2.081	2.081
	1.84			0.265	1.816	30mE,5mS	1.816	1.816
	1.71		0.13		1.946	30mE, 7mS	1.946	1.946
	1.7		0.01		1.956	30mE, 8mS	1.956	1.956
	2.95			1.25	0.706	30mE, 12mS	0.706	0.706
	3.6			0.65	0.056	sl 30mE, 13mS	0.000	0.000
	0.51		3.09		3.146	30mE, 6mN road edge	3.146	3.146
	1.405			0.895	2.251	40mE, 0m	2.251	2.251
	1.885			0.48	1.771	40mE, 5mS	1.771	1.771
	1.69		0.195		1.966	40mE, 9mS	1.966	1.966
	1.695			0.005	1.961	40mE, 11.1mS	1.961	1.961
	2.16			0.465	1.496	40mE, 13.S	1.496	1.496
	3.21			1.05	0.446	40mE, 15mS	0.446	0.446
	3.66			0.45	-0.004	sl 40mE, 15.5mS	0.000	0.000
	1.162		2.498		2.494	40mE, 4mN	2.494	2.494
	0.5		0.662		3.156	40mE, 8mN road edge	3.156	3.156
	1.57			1.07	2.086	50mE, 0m	2.086	2.086
	1.13		0.44		2.526	50mE, 4mN	2.526	2.526
	0.48		0.65		3.176	50mE, 7.5mN road edg	3.176	3.176
	1.65			1.17	2.006	50mE, 1mS	2.006	2.006
	2.02			0.37	1.636	50mE, 2mS	1.636	1.636
	1.835		0.185		1.821	50mE, 4mS	1.821	1.821
	1.605		0.23		2.051	50mE, 6mS	2.051	2.051
	1.6		0.005		2.056	50mE, 9mS	2.056	2.056
	1.605			0.005	2.051	50mE, 10mS	2.051	2.051
	2.19			0.585	1.466	50mE, 14mS	1.466	1.466
	2.79			0.6	0.866	50mE, 15.5mS	0.866	0.866
	3.65			0.86	0.006	sl 50mE, 22mS	0.000	0.000
	1.73		1.92		1.926	60mE, 0m	1.926	1.926
	1.555		0.175		2.101	60mE, 1mN	2.101	2.101
	0.795		0.76		2.861	60mE, 4mN	2.861	2.861
	0.55		0.245		3.106	60mE, 7.5mN road edg	3.106	3.106
	1.64			1.09	2.016	60mE, 3mS	2.016	2.016
	1.645			0.005	2.011	60mE, 9mS	2.011	2.011
	1.915			0.27	1.741	60mE, 10.7mS	1.741	1.741
	2.72			0.805	0.936	60mE, 12.7mS	0.936	0.936
	2.17		0.55		1.486	60mE, 15.5mS	1.486	1.486
	2.171			0.001	1.485	60mE, 20mS	1.485	1.485
	2.45			0.279	1.206	60mE. 21.2mS	1.206	1.206
	3.66			1.21	-0.004	sl 60mE, 24mS	0.000	0.000
	1.305		2.355		2.351	70mE, 0m	2.351	2.351
	1.685			0.38	1.971	70mE, 5.5mS	1.971	1.971
	1.68		0.005		1.976	70mE, 10.5mS	1.976	1.976
	2.13			0.45	1.526	70mE, 12.5mS	1.526	1.526
	2.54			0.41	1.116	70mE, 12.8mS	1.116	1.116
	2.22		0.32		1.436	70mE, 15.2 5mS	1.436	1.436
	2.06		0.16		1.596	70mE, 16mS	1.596	1.596
	2.065			0.005	1.591	70mE, 18mS	1.591	1.591

Appendix 2

Topography of the sediment bank using dumpy level and staff.

	2.54			0.475	1.116	70mE, 23mS	1.116	1.116
	2.95			0.41	0.706	70mE, 24.5mS	0.706	0.706
	2.955			0.005	0.701	70mE, 24.7mS	0.701	0.701
	3.35			0.395	0.306	70mE, 25mS	0.306	0.306
	3.22		0.13		0.436	70mE, 26mS	0.436	0.436
	3.63			0.41	0.026	sl 70mE, 26mS	0.000	0.000
	0.565		3.065		3.091	70mE, 4mN	3.091	3.091
	0.57			0.005	3.086	70m E, 5.5mN	3.086	3.086
	0.48		0.09		3.176	70mE, 6.5mN road edg	3.176	3.176
	1.315			0.835	2.341	80mE, 0m	2.341	2.341
	1.565			0.25	2.091	80mE, 2mS	2.091	2.091
	1.56		0.005		2.096	80mE, 8mS	2.096	2.096
	1.94			0.38	1.716	80mE, 9mS	1.716	1.716
	2.2			0.26	1.456	80mE, 12mS	1.456	1.456
	2		0.2		1.656	80mE, 15.5mS	1.656	1.656
	1.63		0.37		2.026	80mE, 18mS	2.026	2.026
	2.09			0.46	1.566	80mE, 23mS	1.566	1.566
	2.85			0.76	0.806	80mE, 30mS	1.806	1.806
	3.66			0.81	-0.004	sl 80mE, 30.3mS	0.000	0.000
	0.8		2.86		2.856	80mE, 2mN	2.856	2.856
	0.51		0.29		3.146	80mE, 6.5mN road edg	3.146	3.146
Day 1 ends and day 2 begins. Change in river level in the morning in comparison to day 1 afternoon.								
	1.56			1.05	2.096	90mE, 0m	2.096	1.936
	1.74			0.18	1.916	90mE, 5mS	1.916	1.756
	1.742			0.002	1.914	90mE, 8.5mS	1.914	1.754
	1.78			0.038	1.876	90mE, 9.8mS	1.876	1.716
	1.88			0.1	1.776	90mE, 10.8mS	1.776	1.616
	2.15			0.27	1.506	90mE, 11.5mS	1.506	1.346
	2.152			0.002	1.504	90mE, 14.2mS	1.504	1.344
	1.95		0.202		1.706	90mE, 14.6mS	1.706	1.546
	1.65		0.3		2.006	90mE, 15mS	2.006	1.846
	1.95			0.3	1.706	90mE, 16mS	1.706	1.546
	1.58		0.37		2.076	90mE, 16.7mS	2.076	1.916
	1.38		0.2		2.276	90mE, 20mS	2.276	2.116
	1.85			0.47	1.806	90mE, 26mS	1.806	1.646
	3.48			1.63	0.176	sl 90mE, 29.5mS	0.000	-0.16
	0.53		2.95		3.126	90mN, 5mN road edge	3.126	2.966
	1.59			1.06	2.066	100mE, 0m	2.066	1.906
	1.67			0.08	1.986	100mE, 3mS	1.986	1.826
	1.82			0.15	1.836	100mE, 6mS	1.836	1.676
	2.01			0.19	1.646	100mE, 6.5mS	1.646	1.486
	2.145			0.135	1.511	100mE, 10mS	1.511	1.351
	2.05		0.095		1.606	100mE, 13.5mS	1.606	1.446
	1.82		0.23		1.836	100mE, 13.7mS	1.836	1.676
	1.52		0.3		2.136	100mE, 16mS	2.136	1.976
	1.207		0.313		2.449	100mE, 19.8mS	2.449	2.289
	1.66			0.453	1.996	100mE, 27.3mS	1.996	1.836
	2.3			0.64	1.356	100mE, 30mS	1.356	1.196
	2.8			0.5	0.856	100mE, 30.6mS	0.856	0.696
	0.9		1.9		2.756	100mE, 4.5mN bank ed	2.756	2.596
	0.5		0.4		3.156	100mE, 5.2mN road ed	3.156	2.996
	3.5			3	0.156	sl 100mE, 30.7mS	0.000	-0.16
2		1.59	1.91		2.066	cp	2.066	1.906
	2.19			0.19	1.876	110mE, 0mS	1.876	1.716
	2.25			0.06	1.816	110mE, 4.8mS	1.816	1.656
	2.35			0.1	1.716	110mE, 5mS	1.716	1.556
	2.24		0.11		1.826	110mE, 6mS	1.826	1.666
	2.32			0.08	1.746	110mE, 6.7mS	1.746	1.586
	2.13		0.19		1.936	110mE, 7.5mS	1.936	1.776
	2.56			0.43	1.506	110mE, 8.5mS	1.506	1.346
	2.38		0.18		1.686	110mE, 12.5mS	1.686	1.526
	2.16		0.22		1.906	110mE, 13mS	1.906	1.746
	1.69		0.47		2.376	110mE, 20mS	2.376	2.216
	2.55			0.86	1.516	110mE, 32mS	1.516	1.356

Appendix 2

Topography of the sediment bank using dumpy level and staff.

	3.91			1.36	0.156	sl 110mE, 33.5mS	0.000	-0.16
	0.55		3.36		3.516	110mE, 5mN road edge	3.516	3.356
	2.46			1.91	1.606	120mE, 0m	1.606	1.446
	2.62			0.16	1.446	120mE, 1.5mS	1.446	1.286
	2.19		0.43		1.876	120mE, 2mS	1.876	1.716
	2.4			0.21	1.666	120mE, 4mS	1.666	1.506
	2.55			0.15	1.516	120mE, 10.5mS	1.516	1.356
	1.99		0.56		2.076	120mE, 12.5mS	2.076	1.916
	2.26			0.27	1.806	120mE, 14.7mS	1.806	1.646
	2		0.26		2.066	120mE, 17mS	2.066	1.906
	1.84		0.16		2.226	120mE, 19mS	2.226	2.066
	1.89			0.05	2.176	120mE, 31mS	2.176	2.016
	2.52			0.63	1.546	120mE, 35.5mS	1.546	1.386
	3.94			1.42	0.126	sl 120mE, 37.5mS	0.000	-0.16
	0.45		3.49		3.616	120mE, 5mN road edge	3.616	3.456
	2.42			1.97	1.646	130mE, 0m	1.646	1.486
	2.1		0.32		1.966	130mE,2mN	1.966	1.806
	1.09		1.01		2.976	130mE, 4mN	2.976	2.816
	0.42		0.67		3.646	130mE, 5.5mN road ed	3.646	3.486
	2.47			2.05	1.596	130mE, 4mS	1.596	1.436
	1.91		0.56		2.156	130mE, 7mS	2.156	1.996
	2.4			0.49	1.666	130mE, 15.5mS	1.666	1.506
	2.59			0.19	1.476	130mE, 19mS	1.476	1.316
	2.41		0.18		1.656	130mE, 20mS	1.656	1.496
	1.96		0.45		2.106	130mE, 33.5mS	2.106	1.946
	3.9			1.94	0.166	sl 130mE,37mS	0.000	-0.16
	2.49		1.41		1.576	140mE, 0m	1.576	1.416
	2.37		0.12		1.696	140mE, 2.5mN	1.696	1.536
	0.56		1.81		3.506	140mE, 5mN road edge	3.506	3.346
	2.35			1.79	1.716	140mE, 3mS	1.716	1.556
	1.96		0.39		2.106	140mE,7mS	2.106	1.946
	1.72		0.24		2.346	140mE,18ms	2.346	2.186
	1.77			0.05	2.296	140mE, 20mS	2.296	2.136
	1.45		0.32		2.616	140mE, 26mS	2.616	2.456
	1.655			0.205	2.411	140mE, 34mS	2.411	2.251
	2.25			0.595	1.816	140mE, 38mS	1.816	1.656
	2.73			0.48	1.336	140mE, 39mS	1.336	1.176
	3.91			1.18	0.156	sl 140mE, 41mS	0.000	-0.16
	2.44		1.47		1.626	150mE, 0m	1.626	1.466
	1.835		0.605		2.231	150mE, 9mS	2.231	2.071
	1.69		0.145		2.376	150mE, 19mS	2.376	2.216
	1.835			0.145	2.231	150mE,20mS	2.231	2.071
	2.025			0.19	2.041	150mE, 20.8mS	2.041	1.881
	1.84		0.185		2.226	150mE, 22mS	2.226	2.066
	1.59		0.25		2.476	150mE, 23mS	2.476	2.316
	1.45		0.14		2.616	150mE, 30mS	2.616	2.456
	2.09			0.64	1.976	150mE, 39.5mS	1.976	1.816
	2.97			0.88	1.096	150mE, 43mS	1.096	0.936
	3.95			0.98	0.116	sl 150mE, 43.3mS	0.000	-0.16
	0.55		3.4		3.516	150mE, 5mN road edge	3.516	3.356
	2.4			1.85	1.666	160mE, 0m	1.666	1.506
	2.26		0.14		1.806	160mE, 4.5mS	1.806	1.646
	1.9		0.36		2.166	160mE, 8mS	2.166	2.006
	1.46		0.44		2.606	160mE, 21mS	2.606	2.446
	1.465			0.005	2.601	160mE, 29mS	2.601	2.441
	1.74			0.275	2.326	160mE, 39mS	2.326	2.166
	1.91			0.17	2.156	160mE, 41mS	2.156	1.996
	2.55			0.64	1.516	160mE, 43mS	1.516	1.356
	3.9			1.35	0.166	sl 160mE, 44mS	0.000	-0.16
	1.91		1.99		2.156	160mE, 2mN	2.156	1.996
	1.73		0.18		2.336	160mE, 3mN	2.336	2.176
	1.36		0.37		2.706	160mE, 3.2mN	2.706	2.546
	0.51		0.85		3.556	160mE, 5mN road edge	3.556	3.396
	2.32			1.81	1.746	170mE,0m	1.746	1.586

Appendix 2

Topography of the sediment bank using dumpy level and staff.

	1.78		0.54		2.286	170mE, 2mN	2.286	2.126
	0.51		1.27		3.556	170mE, 5mN road edge	3.556	3.396
	2.32			1.81	1.746	170mE, 5.3mS	1.746	1.586
	1.96		0.36		2.106	170mE, 7.3mS	2.106	1.946
	1.81		0.15		2.256	170mE, 13mS	2.256	2.096
	1.54		0.27		2.526	170mE, 18mS	2.526	2.366
	1.45		0.09		2.616	170mE, 23mS	2.616	2.456
	1.43		0.02		2.636	170mE, 29mS	2.636	2.476
	1.48			0.05	2.586	170mE, 33mS	2.586	2.426
	1.7			0.22	2.366	170mE, 39mS	2.366	2.206
	1.91			0.21	2.156	170mE, 42mS	2.156	1.996
	2.5			0.59	1.566	170mE, 44mS	1.566	1.406
	3.02			0.52	1.046	170mE, 45mS	1.046	0.886
	3.92			0.9	0.146	sl 170mE, 46.6mS	0.000	-0.16
	2.2		1.72		1.866	180mE, 0m	1.866	1.706
	2.21			0.01	1.856	180mE, 6mS	1.856	1.696
	2.03		0.18		2.036	1880mE, 9.6mS	2.036	1.876
	2.05			0.02	2.016	180mE, 10mS	2.016	1.856
	1.56		0.49		2.506	180mE, 20mS	2.506	2.346
	1.46		0.1		2.606	180mE, 26mS	2.606	2.446
	1.6			0.14	2.466	180mE, 32.5mS	2.466	2.306
	1.46		0.14		2.606	181mE, 32.5mS	2.606	2.446
	1.6			0.14	2.466	179mE, 32.5mS	2.466	2.306
	1.44		0.16		2.626	180mE, 39mS	2.626	2.466
	1.61			0.17	2.456	180mE, 43mS	2.456	2.296
	1.95			0.34	2.116	180mE, 46mS	2.116	1.956
	2.58			0.63	1.486	180mE, 48.5	1.486	1.326
	3.91			1.33	0.156	sl 180mE, 49mS	0.000	-0.16
	1.54		2.37		2.526	180mE, 2mN	2.526	2.366
	1.25		0.29		2.816	180mE, 3mN	2.816	2.656
	0.45		0.8		3.616	180mE, 5mN road edge	3.616	3.456
	2.28			1.83	1.786	190mE, 0m	1.786	1.626
	2.27		0.01		1.796	190mE, 2mN	1.796	1.636
	0.64		1.63		3.426	190mE, 4mN	3.426	3.266
	2.28			1.64	1.786	190mE, 4.7 7mS	1.786	1.626
	0.48		1.8		3.586	190mE, 5.5m N road ed	3.586	3.426
	2.12			1.64	1.946	190mE, 4.8 8mS	1.946	1.786
	2.13			0.01	1.936	190mE, 8mS	1.936	1.776
	1.94		0.19		2.126	190mE, 9.7mS	2.126	1.966
	1.73		0.21		2.336	190mE, 18mS	2.336	2.176
	1.5		0.23		2.566	190mE, 25mS	2.566	2.406
	1.47		0.03		2.596	190mE, 29mS	2.596	2.436
	1.4		0.07		2.666	190mE, 30mS	2.666	2.506
	1.27		0.13		2.796	190mE, 36mS	2.796	2.636
	1.3			0.03	2.766	190mE, 38mS	2.766	2.606
	1.5			0.2	2.566	190mE, 43mS	2.566	2.406
	1.77			0.27	2.296	190mE, 47mS	2.296	2.136
	2.2			0.43	1.866	190mE, 49.3mS	1.866	1.706
	3.1			0.9	0.966	190mE, 50.5mS	0.966	0.806
	3.92			0.82	0.146	sl 190mE, 51mS	0.000	-0.16
	2.05		1.87		2.016	200mE, 0m	2.016	1.856
	1.98		0.07		2.086	200mE, 0.5mS	2.086	1.926
	1.98			0	2.086	200mE, 2.4mS	2.086	1.926
	2.08			0.1	1.986	200mE, 3.5mS	1.986	1.826
	2.2			0.12	1.866	200mE, 3.7mS	1.866	1.706
	2.15		0.05		1.916	200mE, 6.6mS	1.916	1.756
	2.1		0.05		1.966	200mE, 7.2mS	1.966	1.806
	1.92		0.18		2.146	200mE, 8mS	2.146	1.986
	1.84		0.08		2.226	200mE, 10mS	2.226	2.066
	1.93			0.09	2.136	200mE, 13mS	2.136	1.976
	1.86		0.07		2.206	200mE, 15.5mS	2.206	2.046
	1.78		0.08		2.286	200mE, 17.7mS	2.286	2.126
	1.82			0.04	2.246	200mE, 18.3mS	2.246	2.086
	1.81		0.01		2.256	200mE, 18.7mS	2.256	2.096

Appendix 2

Topography of the sediment bank using dumpy level and staff.

	1.67		0.14		2.396	200mE, 20mS	2.396	2.236
	1.49		0.18		2.576	200mE, 24mS	2.576	2.416
	1.52			0.03	2.546	200mE, 26mS	2.546	2.386
	1.36		0.16		2.706	200mE, 34mS	2.706	2.546
	1.68			0.32	2.386	200mE, 39mS	2.386	2.226
	1.68			0	2.386	200mE, 47mS	2.386	2.226
	1.94			0.26	2.126	200mE, 50mS	2.126	1.966
	3.9			1.96	0.166	sl 200mE, 52mS	0.000	-0.16
	2.2		1.7		1.866	200mE, 2mN	1.866	1.706
	0.75		1.45		3.316	200mE, 5.5mN	3.316	3.156
	0.45		0.3		3.616	200mE, 6mN road edge	3.616	3.456
	1.99			1.54	2.076	210mE, 0m	2.076	1.916
	1.78		0.21		2.286	210mE3mS	2.286	2.126
	1.84			0.06	2.226	210mE, 8mS	2.226	2.066
	2			0.16	2.066	210mE, 10mS	2.066	1.906
	2.1			0.1	1.966	210mE, 12mS	1.966	1.806
	2.02		0.08		2.046	210mE, 14mS	2.046	1.886
	1.67		0.35		2.396	210mE, 18mS	2.396	2.236
	1.54		0.13		2.526	210mE, 22mS	2.526	2.366
	1.55			0.01	2.516	210mE, 26mS	2.516	2.356
	1.28		0.27		2.786	210mE, 36mS	2.786	2.626
	1.3			0.02	2.766	210mE, 38mS	2.766	2.606
	1.29		0.01		2.776	210mE, 43mS	2.776	2.616
	1.72			0.43	2.346	210mE, 50mS	2.346	2.186
	2.16			0.44	1.906	210mE, 51.5mS	1.906	1.746
	3.9			1.74	0.166	sl 210mE, 54mS	0.000	-0.16
	2.05		1.85		2.016	210mE, 3mN	2.016	1.856
	1.56		0.49		2.506	210mE, 5mN	2.506	2.346
	0.44		1.12		3.626	210mE, 6.5mN on road	3.626	3.466
	1.84			1.4	2.226	220mE, 0m	2.226	2.066
	1.95			0.11	2.116	220mE, 2mN	2.116	1.956
	1.76		0.19		2.306	220mE, 4mN	2.306	2.146
	1.16		0.6		2.906	220mEm,5mN	2.906	2.746
	0.43		0.73		3.636	220mE, 7mN on road	3.636	3.476
	1.68			1.25	2.386	220mE, 5mS	2.386	2.226
	1.83			0.15	2.236	220mE, 13mS	2.236	2.076
	1.93			0.1	2.136	220mE, 13.1mS	2.136	1.976
	1.98			0.05	2.086	220mE, 15mS	2.086	1.926
	1.73		0.25		2.336	220mE, 17mS	2.336	2.176
	1.72		0.01		2.346	220mE, 19mS	2.346	2.186
	1.52		0.2		2.546	220mE, 31mS	2.546	2.386
	1.37		0.15		2.696	220mE, 33mS	2.696	2.536
	1.08		0.29		2.986	220mE, 42mS	2.986	2.826
	1.42			0.34	2.646	220mE, 50mS	2.646	2.486
	1.85			0.43	2.216	220mE, 51mS	2.216	2.056
	3.89			2.04	0.176	sl 220mE, 54mS	0.000	-0.16
	1.86		2.03		2.206	230mE, 0m	2.206	2.046
	1.69		0.17		2.376	230mE, 2mS	2.376	2.216
	1.66		0.03		2.406	230mE, 10mS	2.406	2.246
	1.97			0.31	2.096	230mE, 15mS	2.096	1.936
	2.24			0.27	1.826	230mE, 17mS	1.826	1.666
	2.07		0.17		1.996	230mE, 18mS	1.996	1.836
	1.84		0.23		2.226	230mE, 20mS	2.226	2.066
	1.72		0.12		2.346	230mE, 24mS	2.346	2.186
	1.54		0.18		2.526	230mE, 27mS	2.526	2.366
	1.65			0.11	2.416	230mE, 30mS	2.416	2.256
	1.335		0.315		2.731	230mE, 34.5mS	2.731	2.571
	1.33		0.005		2.736	230mE, 36mS	2.736	2.576
	1.15		0.18		2.916	230mE, 40mS	2.916	2.756
	1.45			0.3	2.616	230mE, 51mS	2.616	2.456
	2.45			1	1.616	230mE, 53.5mS	1.616	1.456
	3.9			1.45	0.166	sl 230mE, 54mS	0.000	-0.16
	1.9		2		2.166	230mE, 3.5mN	2.166	2.006
	1.25		0.65		2.816	230mE, 5mN	2.816	2.656

Appendix 2

Topography of the sediment bank using dumpy level and staff.

	0.5		0.75		3.566	230mE, 7m N on road	3.566	3.406
	1.8			1.3	2.266	240mE, 0m	2.266	2.106
	1.83			0.03	2.236	240mE, 2mN	2.236	2.076
	1.73		0.1		2.336	240mE, 3mN	2.336	2.176
	1.25		0.48		2.816	240mE, 5mN	2.816	2.656
	0.52		0.73		3.546	240mE, 8mN road edge	3.546	3.386
	1.54			1.02	2.526	240mE, 10mS	2.526	2.366
	1.68			0.14	2.386	240mE, 13mS	2.386	2.226
	1.98			0.3	2.086	240mE, 15mS	2.086	1.926
	1.88		0.1		2.186	240mE, 19.5mS	2.186	2.026
	1.75		0.13		2.316	240mE, 21.5mS	2.316	2.156
	2.16			0.41	1.906	240mE, 23mS	1.906	1.746
	2.62			0.46	1.446	240mE, 24mS	1.446	1.286
	2.14		0.48		1.926	240mE, 26mS	1.926	1.766
	1.74		0.4		2.326	240mE, 28.5mS	2.326	2.166
	1.78			0.04	2.286	240mEm 29mS	2.286	2.126
	1.6		0.18		2.466	240mE, 31mS	2.466	2.306
	1.58		0.02		2.486	240mE, 34mS	2.486	2.326
	1.67			0.09	2.396	240mE, 34.5mS	2.396	2.236
	1.62		0.05		2.446	240mE, 35.5mS	2.446	2.286
	1.47		0.15		2.596	240mE, 36mS	2.596	2.436
	1		0.47		3.066	240mE, 42mS	3.066	2.906
	1.59			0.59	2.476	240mE, 53mS	2.476	2.316
	3.89			2.3	0.176	sl 240mE, 55mS	0.000	-0.16
	1.82		2.07		2.246	250mE, 0m	2.246	2.086
	1.64		0.18		2.426	250mE, 3mS	2.426	2.266
	1.55		0.09		2.516	250mE, 12mS	2.516	2.356
	1.67			0.12	2.396	250mE, 16mS	2.396	2.236
	1.85			0.18	2.216	250mE, 17mS	2.216	2.056
	1.84		0.01		2.226	250mE, 20mS	2.226	2.066
	1.6		0.24		2.466	250mE, 23mS	2.446	2.286
	1.6			0	2.466	250mE, 25mS	2.466	2.306
	1.65			0.05	2.416	250mE, 28mS	2.416	2.256
	2.22			0.57	1.846	250mE, 30mS	1.846	1.686
	2		0.22		2.066	250mE, 31mS	2.066	1.906
	1.64		0.36		2.426	250mE, 32mS	2.426	2.266
	1.1		0.54		2.966	250mE, 43mS	2.966	2.806
	1.15			0.05	2.916	250mE, 51mS	2.916	2.756
	1.65			0.5	2.416	250mE, 54mS	2.416	2.256
	3.89			2.24	0.176	sl 250mE, 57mS	0.000	-0.16
	1.72		2.17		2.346	250mE, 4mN	2.346	2.186
	0.98		0.74		3.086	250mE, 6mN	3.086	2.926
	0.56		0.42		3.506	250mE, 8mN road edge	3.506	3.346
	1.78			1.22	2.286	260mE, 0m	2.286	2.126
	1.65		0.13		2.416	260mE, 4mS	2.416	2.256
	1.6		0.05		2.466	260mE, 10mS	2.466	2.306
	1.6			0	2.466	260mE, 11mS	2.466	2.306
	1.67			0.07	2.396	260mE, 12.5mS	2.396	2.236
	1.57		0.1		2.496	260mE, 13.7mS	2.496	2.336
	1.7			0.13	2.366	260mE, 14.4mS	2.366	2.206
	1.66		0.04		2.406	260mE, 15.3mS	2.406	2.246
	1.62		0.04		2.446	260mE, 16.2mS	2.446	2.286
	1.8			0.18	2.266	260mE, 18mS	2.266	2.106
	1.85			0.05	2.216	260mE, 19mS	2.216	2.056
	1.96			0.11	2.106	260mE, 19.5mS	2.106	1.946
	1.83		0.13		2.236	260mE, 20mS	2.236	2.076
	1.7		0.13		2.366	260mE, 22.5mS	2.366	2.206
	1.76			0.06	2.306	260mE, 24mS	2.306	2.146
	1.6		0.16		2.466	260mE, 26.5mS	2.466	2.306
	1.4		0.2		2.666	260mE, 28.5mS	2.666	2.506
	1.63			0.23	2.436	260mE, 31mS	2.436	2.276
	1.47		0.16		2.596	260mE, 39mS	2.596	2.436
	1.28		0.19		2.786	260mE, 42.3mS	2.786	2.626
	1.14		0.14		2.926	260mE, 46mS	2.926	2.766

Appendix 2

Topography of the sediment bank using dumpy level and staff.

	1.09		0.05		2.976	260mE, 50mS	2.976	2.816
	1.25			0.16	2.816	260mE, 52.3mS	2.816	2.656
	1.38			0.13	2.686	260mE, 53mS	2.686	2.526
	1.87			0.49	2.196	260mE, 55.3mS	2.196	2.036
	3.88			2.01	0.186	sl 260mE, 56mS	0.000	-0.16
	1.74		2.14		2.326	260mE, 2mN	2.326	2.166
	1.17		0.57		2.896	260mE, 4mN	2.896	2.736
	0.6		0.57		3.466	260mE, 6mN road edge	3.466	3.306
	1.65			1.05	2.416	270mE,0m	2.416	2.256
	1.72			0.07	2.346	270mE, 7mS	2.346	2.186
	1.6		0.12		2.466	270mE, 9mS	2.466	2.306
	1.72			0.12	2.346	270mE, 11mS	2.346	2.186
	1.57		0.15		2.496	270mE, 16mS	2.496	2.336
	1.2		0.37		2.866	270mE, 19.5mS	2.866	2.706
	1.25			0.05	2.816	270mE, 19.8mS	2.816	2.656
	1.2		0.05		2.866	270mE, 20mS	2.866	2.706
	1.57			0.37	2.496	270mE, 23mS	2.496	2.336
	1.67			0.1	2.396	270mE, 25mS	2.396	2.236
	1.6		0.07		2.466	270mE, 29mS	2.466	2.306
	1.57		0.03		2.496	270mE, 36mS	2.496	2.336
	1.53		0.04		2.536	270mE, 41mS	2.536	2.376
	1.38		0.15		2.686	270mE, 46mS	2.686	2.526
	1.65			0.27	2.416	270mE, 49.5mS	2.416	2.256
	1.6		0.05		2.466	270mE, 51.5mS	2.466	2.306
	1.4		0.2		2.666	270mE, 51.6mS	2.666	2.506
	1.2		0.2		2.866	270mE, 52.6mS	2.866	2.706
	1.4			0.2	2.666	270mE, 52.8mS	2.666	2.506
	1.45			0.05	2.616	270mE, 54.3mS	2.616	2.456
	1.73			0.28	2.336	270mE, 56mS	2.336	2.176
	2.27			0.54	1.796	270mE, 57mS	1.796	1.636
	2.75			0.48	1.316	270mE, 58mS	1.316	1.156
	3.89			1.14	0.176	sl 270mE, 58.6mS	0.000	-0.16
	1.57		2.32		2.496	270mE, 2mN	2.496	2.336
	0.612		0.958		3.454	270mE, 6mN road edge	3.454	3.294
	1.52			0.908	2.546	280mE, 0m	2.546	2.386
	1.6			0.08	2.466	280mE, 3mS	2.466	2.306
	1.82			0.22	2.246	280mE, 6mS	2.246	2.086
	1.7		0.12		2.366	280mE, 9.2mS	2.366	2.206
	1.85			0.15	2.216	280mE, 9.8mS	2.216	2.056
	1.75		0.1		2.316	280mE, 10.4mS	2.316	2.156
	1.88			0.13	2.186	280mE, 11mS	2.186	2.026
	1.77		0.11		2.296	280mE, 11.7mS	2.296	2.136
	1.32		0.45		2.746	280mE, 15.6mS	2.746	2.586
	1.05		0.27		3.016	280mE, 21mS	3.016	2.856
	1.48			0.43	2.586	280mE, 27mS	2.586	2.426
	1.65			0.17	2.416	280mE, 33mS	2.416	2.256
	1.58		0.07		2.486	280mE, 41mS	2.486	2.326
	1.53		0.05		2.536	280mE, 47mS	2.536	2.376
	3.91			2.38	0.156	sl 280mE, 57mS	0.000	-0.16
	1.48		2.43		2.586	280mE, 1mN	2.586	2.426
	1.3		0.18		2.766	280mE, 2mN	2.766	2.606
	1.2		0.1		2.866	280mE, 4mN	2.866	2.706
	0.63		0.57		3.436	280mE, 6mN road edge	3.436	3.276
1.85		1.52		0.32	2.546	cp2	2.546	2.386
	1.88			0.03	2.516	290mE, 0m	2.516	2.356
	2.06			0.18	2.336	290mE, 5mS	2.336	2.176
	2.16			0.1	2.236	290mE, 10mS	2.236	2.076
	1.4		0.76		2.996	290mE, 18mS	2.996	2.836
	1.37		0.03		3.026	290mE, 25mS	3.026	2.866
	1.77			0.4	2.626	290mE, 31mS	2.626	2.466
	2			0.23	2.396	290mE, 35mS	2.396	2.236
	1.93		0.07		2.466	290mE, 40mS	2.466	2.306
	2.58			0.65	1.816	290mE, 54.5mS	1.816	1.656
	3.22			0.64	1.176	290mE, 57mS	1.176	1.116

Appendix 2

Topography of the sediment bank using dumpy level and staff.

	4.25			1.03	0.146	sl 290mE, 58.5mS	0.000	-0.06
	1.52		2.73		2.876	290mE, 3mN	2.876	2.816
	1.29		0.23		3.106	290mE, 5mN	3.106	3.046
	0.65		0.64		3.746	290mE, 8mN road edge	3.746	3.686
	1.99			1.34	2.406	300mE, 0m	2.406	2.346
	2.13			0.14	2.266	300mE, 6mS	2.266	2.206
	2.09		0.04		2.306	300mE, 10mS	2.306	2.246
	1.66		0.43		2.736	300mE, 14mS	2.736	2.676
	1.34		0.32		3.056	300mE, 25mS	3.056	2.996
	1.62			0.28	2.776	300mE, 32mS	2.776	2.716
	1.98			0.36	2.416	300mE, 40mS	2.416	2.356
	1.91		0.07		2.486	300mE, 48mS	2.486	2.426
	1.84		0.07		2.556	300mE, 50mS	2.556	2.496
	3.22			1.38	1.176	300mE, 56mS	1.176	1.116
	4.25			1.03	0.146	sl 300mE, 58mS	0.000	-0.06
	1.69		2.56		2.706	300mE, 2mN	2.706	2.546
	1.28		0.41		3.116	300mE, 4mN	3.116	2.956
	0.65		0.63		3.746	300mE, 8.5mN road ed	3.746	3.586
	2.09			1.44	2.306	310mE, 0m	2.306	2.146
	1.84		0.25		2.556	310mE, 2mN	2.556	2.396
	1.4		0.44		2.996	310mE, 4mN	2.996	2.836
	0.7		0.7		3.696	310mE, 9mN road edge	3.696	3.536
	2.21			1.51	2.186	310mE, 8mS	2.186	2.026
	2.27			0.06	2.126	310mE, 10mS	2.126	1.966
	1.54		0.73		2.856	310mE, 15mS	2.856	2.696
	1.31		0.23		3.086	310mE, 27mS	3.086	2.926
	1.9			0.59	2.496	310mE, 40mS	2.496	2.336
	2.11			0.21	2.286	310mE, 47mS	2.286	2.126
	2.13			0.02	2.266	310mE, 50mS	2.266	2.106
	2.54			0.41	1.856	310mE, 53mS	1.856	1.696
	3.03			0.49	1.366	310mE, 54mS	1.366	1.206
	3.24			0.21	1.156	310mE, 55mS	1.156	0.996
	3.6			0.36	0.796	310mE, 56mS	0.796	0.636
	4.24			0.64	0.156	sl 310mE, 57mS	0.000	-0.16
	2.03		2.21		2.366	320mE, 0m	2.366	2.206
	1.72		0.31		2.676	320mE, 2mN	2.676	2.516
	1.85			0.13	2.546	320mE, 0.3mN	2.546	2.386
	1.38		0.47		3.016	320mE, 5mN	3.016	2.856
	0.75		0.63		3.646	320mE, 9mN road edge	3.646	3.486
	2.2			1.45	2.196	320mE, 2mS	2.196	2.036
	2.35			0.15	2.046	320mE, 4mS	2.046	1.886
	2.2		0.15		2.196	320mE, 7mS	2.196	2.036
	1.66		0.54		2.736	320mE, 12mS	2.736	2.576
	1.45		0.21		2.946	320mE, 21mS	2.946	2.786
	1.35		0.1		3.046	320mE, 30mS	3.046	2.886
	1.67			0.32	2.726	320mE, 38mS	2.726	2.566
	2.12			0.45	2.276	320mE, 46mS	2.276	2.116
	2.45			0.33	1.946	320mE, 52mS	1.946	1.786
	3.42			0.97	0.976	320mE, 55mS	0.976	0.816
	4.4			0.98	-0.004	sl 320mE, 56mS	0.000	-0.03
	1.72		2.68		2.676	330mE, 0m	2.676	2.646
	1.89			0.17	2.506	330mE, 0.5mS	2.506	2.476
	2.17			0.28	2.226	330mE, 1mS	2.226	2.196
	2.54			0.37	1.856	330mE, 2mS	1.856	1.826
	2.59			0.05	1.806	330mE, 3mS	1.806	1.776
	2.34		0.25		2.056	330mE, 4mS	2.056	2.026
	2.17		0.17		2.226	330mE, 6mS	2.226	2.196
	1.95		0.22		2.446	330mE, 8mS	2.446	2.416
	1.6		0.35		2.796	330mE, 12mS	2.796	2.766
	1.49		0.11		2.906	330mE, 15mS	2.906	2.876
	1.41		0.08		2.986	330mE, 30mS	2.986	2.956
	1.55			0.14	2.846	330mE, 36mS	2.846	2.816
	1.67			0.12	2.726	330mE, 37mS	2.726	2.696
	1.8			0.13	2.596	330mE, 40mS	2.596	2.566

Appendix 2

Topography of the sediment bank using dumpy level and staff.

	2.23			0.43	2.166	330mE, 48mS	2.166	2.136
	3.27			1.04	1.126	330mE, 53mS	1.126	1.096
	4.44			1.17	-0.044	sl 330mE, 55mS	0.000	-0.03
	1.79		2.65		2.606	330mE, 1mN	2.606	2.576
	1.99			0.2	2.406	330mE, 2mN	2.406	2.376
	1.96		0.03		2.436	330mE, 2.5mN	2.436	2.406
	1.82		0.14		2.576	330mE, 3mN	2.576	2.546
	1.82		0		2.576	330mE, 4mN	2.576	2.546
	0.789		1.031		3.607	330mE, 9mN road edge	3.607	3.577
	2.3			1.511	2.096	340mE, 0m	2.096	2.066
	2.12		0.18		2.276	340mE, 4mS	2.276	2.246
	1.67		0.45		2.726	340mE, 10mS	2.726	2.696
	1.8			0.13	2.596	340mE, 13mS	2.596	2.566
	1.57		0.23		2.826	340mE, 34mS	2.826	2.796
	1.49		0.08		2.906	340mE, 36mS	2.906	2.876
	2.05			0.56	2.346	340mE, 40mS	2.346	2.316
	2.26			0.21	2.136	340mE, 46mS	2.136	2.106
	2.34			0.08	2.056	340mE, 50mS	2.056	2.026
	4.42			2.08	-0.024	sl 340mE, 55mS	0.000	-0.03
	1.85		2.57		2.546	340mE, 3mN	2.546	2.516
	1.05		0.8		3.346	340mE, 4mN	3.346	3.316
	0.8		0.25		3.596	340mE, 7mN road edge	3.596	3.566
	2.23			1.43	2.166	350mE, 0m	2.166	2.136
	2.17		0.06		2.226	350mE, 2mS	2.226	2.196
	1.98		0.19		2.416	350mE, 5mS	2.416	2.386
	1.71		0.27		2.686	350mE, 8mS	2.686	2.656
	1.37		0.34		3.026	350mE, 16mS	3.026	2.996
	1.47			0.1	2.926	350mE, 30mS	2.926	2.896
	1.79			0.32	2.606	350mE, 40.5mS	2.606	2.576
	2.19			0.4	2.206	350mE, 45.5mS	2.206	2.176
	2.8			0.61	1.596	350mE, 48.5mS	1.596	1.566
	3.29			0.49	1.106	350mE, 49.5mS	1.106	1.076
	4.42			1.13	-0.024	sl 350mE, 51mS	0.000	-0.03
	2.12		2.3		2.276	350mE, 2mN	2.276	2.246
	1.97		0.15		2.426	350mE, 4mN	2.426	2.396
	0.8		1.17		3.596	350mE, 6mN road edge	3.596	3.566
	2.42			1.62	1.976	360mE, 0m	1.976	1.946
	2.23		0.19		2.166	360mE, 1.5mS	2.166	2.136
	2.13		0.1		2.266	360mE, 2mS	2.266	2.236
	1.39		0.74		3.006	360mE, 15mS	3.006	2.976
	1.34		0.05		3.056	360mE, 20mS	3.056	3.026
	1.44			0.1	2.956	360mE, 25mS	2.956	2.926
	1.65			0.21	2.746	360mE, 33mS	2.746	2.716
	1.78			0.13	2.616	360mE, 34mS	2.616	2.586
	1.98			0.2	2.416	360mE, 37mS	2.416	2.386
	2.01			0.03	2.386	360mE, 40mS	2.386	2.356
	2.79			0.78	1.606	360mE, 46mS	1.606	1.576
	4.44			1.65	-0.044	sl 360mE, 49mS	0.000	-0.03
	2.38		2.06		2.016	360mE, 1mN	2.016	1.986
	2.14		0.24		2.256	360mE, 2mN	2.256	2.226
	1.99		0.15		2.406	360mE, 3mN	2.406	2.376
	0.79		1.2		3.606	360mE, 6mN road edge	3.606	3.576
	2.2			1.41	2.196	370mE, 0m	2.196	2.166
	2.46			0.26	1.936	370mE, 2mN	1.936	1.906
	2.17		0.29		2.226	370mE, 3mN	2.226	2.196
	1.6		0.57		2.796	370mE, 4mN	2.796	2.766
	0.77		0.83		3.626	370mE, 6.5m N road ed	3.626	3.596
	2.01			1.24	2.386	370mE, 1mS	2.386	2.356
	2.06			0.05	2.336	370mE, 2mS	2.336	2.306
	1.72		0.34		2.676	370mE, 10mS	2.676	2.646
	1.34		0.38		3.056	370mE, 24mS	3.056	3.026
	1.65			0.31	2.746	370mE, 30mS	2.746	2.716
	2.1			0.45	2.296	370mE, 34mS	2.296	2.266
	2.16			0.06	2.236	370mE, 38mS	2.236	2.206

Appendix 2

Topography of the sediment bank using dumpy level and staff.

	1.84		0.32		2.556	370mE, 40mS	2.556	2.526
	4.43			2.59	-0.034	sl 370mE, 47mS	0.000	-0.03
	2.16		2.27		2.236	380mE, 0m	2.236	2.206
	1.69		0.47		2.706	380mE, 12mS	2.706	2.676
	1.43		0.26		2.966	380mE, 20mS	2.966	2.936
	1.43		0		2.966	380mE, 24mS	2.966	2.936
	1.38		0.05		3.016	380mE, 26mS	3.016	2.986
	1.55			0.17	2.846	380mE, 30mS	2.846	2.816
	2.16			0.61	2.236	380mE, 36mS	2.236	2.206
	3.76			1.6	0.636	380mE, 43mS	0.636	0.606
	4.41			0.65	-0.014	sl 380mE, 44mS	0.000	-0.03
	2.24		2.17		2.156	380mE, 2mN	2.156	2.126
	2.1		0.14		2.296	380mE, 3mN	2.296	2.266
	1.57		0.53		2.826	380mE, 4mN	2.826	2.796
	0.8		0.77		3.596	380mE, 6mN road edge	3.596	3.566
	2.16			1.36	2.236	390mE, 0m	2.236	2.206
	1.69		0.47		2.706	390mE, 12mS	2.706	2.676
	1.43		0.26		2.966	390mE, 20mS	2.966	2.936
	1.43		0		2.966	390mE, 24mS	2.966	2.936
	1.38		0.05		3.016	390mE, 26mS	3.016	2.986
	1.55			0.17	2.846	390mE, 30mS	2.846	2.816
	2.16			0.61	2.236	390mE, 36mS	2.236	2.206
	3.76			1.6	0.636	390mE, 43mS	0.636	0.606
	4.41			0.65	-0.014	sl 390mE, 44mS	0.000	-0.03
	2.24		2.17		2.156	390mE, 2mN	2.156	2.126
	2.1		0.14		2.296	390mE, 3mN	2.296	2.266
	1.57		0.53		2.826	390mE, 4mN	2.826	2.796
	0.8		0.77		3.596	390mE, 6mN road edge	3.596	3.566
	2.01			1.21	2.386	400mE, 0m	2.386	2.356
	1.64		0.37		2.756	400mE, 18mS	2.756	2.726
	1.57		0.07		2.826	400mE, 24mS	2.826	2.796
	1.23		0.34		3.166	400mE, 28mS	3.166	3.136
	1.88			0.65	2.516	400mE, 33mS	2.516	2.486
	3.84			1.96	0.556	400mE, 36mS	0.556	0.526
	4.42			0.58	-0.024	sl 400mE, 37mS	0.000	-0.03
	1.8		2.62		2.596	400mE, 1.5mN	2.596	2.566
	0.99		0.81		3.406	400mE, 3.5mN	3.406	3.376
	0.79		0.2		3.606	400mE, 5mN road edge	3.606	3.576
	1.96			1.17	2.436	410mE, 0m	2.436	2.406
	1.9		0.06		2.496	410mE, 1.5mS	2.496	2.466
	2.04			0.14	2.356	410mE, 5mS	2.356	2.326
	1.57		0.47		2.826	410mE, 25mS	2.826	2.796
	4.4			2.83	-0.004	sl 410mE, 34mS	0.000	-0.03
	0.74		3.66		3.656	410mE, 5mN road edge	3.656	3.626
	1.94			1.2	2.456	420mE, 0m	2.456	2.426
	1.85		0.09		2.546	420mE, 3mS	2.546	2.516
	1.99			0.14	2.406	420mE, 5mS	2.406	2.376
	1.86		0.13		2.536	420mE, 16mS	2.536	2.506
	1.6		0.26		2.796	420mE, 17mS	2.796	2.766
	1.47		0.13		2.926	420mE, 24mS	2.926	2.896
	4.42			2.95	-0.024	sl 420mE, 31mS	0.000	-0.03
	1.89		2.53		2.506	420mE, 1mN	2.506	2.476
	1.16		0.73		3.236	420mE, 3mN	3.236	3.206
	0.69		0.47		3.706	420mE, 5mN road edge	3.706	3.676
	1.32			0.63	3.076	430mE, 0m	3.076	3.046
	0.9		0.42		3.496	430mE, 3mN	3.496	3.466
	0.73		0.17		3.666	430mE, 3.5mN road ed	3.666	3.636
	1.62			0.89	2.776	430mE, 0.5mS	2.776	2.746
	1.88			0.26	2.516	430mE, 2mS	2.516	2.486
	1.97			0.09	2.426	430mE, 10mS	2.426	2.396
	1.96		0.01		2.436	430mE, 15mS	2.436	2.406
	1.55		0.41		2.846	430mE, 19mS	2.846	2.816
	1.88			0.33	2.516	430mE, 22mS	2.516	2.486
	4.42			2.54	-0.024	sl 430mE, 27mS	0.000	-0.03

Appendix 2

Topography of the sediment bank using dumpy level and staff.

	1.3		3.12		3.096	440mE 0m	3.096	3.066
	1.62			0.32	2.776	440mE, 2mS	2.776	2.746
	1.98			0.36	2.416	440mE, 15mS	2.416	2.386
	4.42			2.44	-0.024	sl 440mE, 23mS	0.000	-0.03
	0.9		3.52		3.496	440mE, 3mN	3.496	3.466
	0.7		0.2		3.696	440mE, 3.8mN road ed	3.696	3.666
	1.13			0.43	3.266	450mE, 0m	3.266	3.236
	1.66			0.53	2.736	450mE, 3mS	2.736	2.706
	1.94			0.28	2.456	450mE, 6mS	2.456	2.426
	1.88		0.06		2.516	450mE, 10mS	2.516	2.486
	2.02			0.14	2.376	450mE, 12mS	2.376	2.346
	4.42			2.4	-0.024	sl 450mE, 18mS	0.000	-0.03
	0.9		3.52		3.496	450mE, 3mN	3.496	3.466
	0.7		0.2		3.696	450mE, 4.5mN road ed	3.696	3.666
	1.5			0.8	2.896	460mE, 0m	2.896	2.866
	1.97			0.47	2.426	460mE, 4mS	2.426	2.396
	1.93		0.04		2.466	460mE, 8mS	2.466	2.436
	2			0.07	2.396	460mE, 10mS	2.396	2.366
	2.01			0.01	2.386	460mE, 11mS	2.386	2.356
	4.43			2.42	-0.034	sl 460mE, 13mS	0.000	-0.03
	0.8		3.63		3.596	460mE, 5mN road edge	3.596	3.566
	1.87			1.07	2.526	470mE, 0m	2.526	2.496
	1.38		0.49		3.016	470mE, 3mN	3.016	2.986
	0.8		0.58		3.596	470mE, 7mN road edge	3.596	3.566
	1.85			1.05	2.546	470mE, 7mS	2.546	2.516
	4.41			2.56	-0.014	sl 470mE, 10m	0.000	-0.03
	1.9		2.51		2.496	480mE, 0m	2.496	2.466
	1.87		0.03		2.526	480mE, 4mN	2.526	2.496
	1.83		0.04		2.566	480mE, 5mN	2.566	2.536
	0.85		0.98		3.546	480mE, 10mN road edg	3.546	3.516
	1.8			0.95	2.596	480mE, 2.5mS	2.596	2.566
	4.43			2.63	-0.034	sl 480mE, 6mS	0.000	-0.03
	2		2.43		2.396	490mE, 0m	2.396	2.366
	2.4			0.4	1.996	490mE, 5mN	1.996	1.966
	1.8		0.6		2.596	490mE, 10mN	2.596	2.566
	0.87		0.93		3.526	490mE, 15mN road edg	3.526	3.496
	2			1.13	2.396	490mE, 0.4mS	2.396	2.366
	4.4			2.4	-0.004	sl 490mE, 1mS	0.000	-0.03

Appendix 3

King River levels taken from Cutters Creek for the period of the topographic survey and times of hydraulic measurements. Cutters Creek is approximately 500m upstream of bank H and at similar elevation. Levels have not been adjusted to AHD.

Date and time	level (meters)	Remark
1/03/00 6:00	0.663249969	Topography levelling, day 1
1/03/00 9:00	0.673958302	
1/03/00 12:00	0.759958327	
1/03/00 15:00	0.79400003	
1/03/00 18:00	0.796166658	
1/03/00 21:00	0.799833357	
2/03/00 0:00	0.803458333	
2/03/00 3:00	0.819291651	
2/03/00 6:00	0.703916669	Topography levelling, day 2
2/03/00 9:00	0.90245831	
2/03/00 12:00	0.951083362	
2/03/00 15:00	0.953291655	
2/03/00 18:00	0.764874995	
2/03/00 21:00	0.749041677	
16/04/00 0:15	0.556999981	Hydraulic head trip 1
16/04/00 0:30	0.583999991	
16/04/00 0:45	0.619000018	
16/04/00 1:00	0.643000007	
16/04/00 1:15	0.657000005	
16/04/00 1:30	0.685000002	
16/04/00 1:45	0.708999991	
16/04/00 2:00	0.727999985	
16/04/00 2:15	0.755999982	
16/04/00 2:30	0.773000002	
16/04/00 2:45	0.779999971	
16/04/00 3:00	0.797999978	
16/04/00 3:30	0.808000028	
16/04/00 3:45	0.823000014	
16/04/00 4:00	0.842999995	
16/04/00 4:30	0.847000003	
16/04/00 4:45	0.842000008	
16/04/00 5:00	0.836000025	
16/04/00 5:15	0.824999988	
16/04/00 5:30	0.815999985	
16/04/00 5:45	0.805999994	
16/04/00 6:00	0.795000017	
16/04/00 6:15	0.787	
16/04/00 6:30	0.777999997	
16/04/00 6:45	0.771000028	
16/04/00 7:00	0.768000007	
16/04/00 7:15	0.768999994	
16/04/00 7:30	0.771000028	
16/04/00 7:45	0.769999981	
16/04/00 8:00	0.769999981	
16/04/00 8:15	0.772000015	
16/04/00 8:30	0.774999976	
16/04/00 9:00	0.776000023	
16/04/00 9:15	0.771000028	

16/04/00 9:30	0.76700002
16/04/00 9:45	0.754999995
16/04/00 10:00	0.754999995
16/04/00 10:15	0.745999992
16/04/00 10:30	0.74000001
16/04/00 10:45	0.720000029
16/04/00 11:00	0.70599997
16/04/00 11:15	0.688000023
16/04/00 11:30	0.674000025
16/04/00 11:45	0.663999975
16/04/00 12:00	0.644999981
16/04/00 12:15	0.633000016
16/04/00 12:30	0.614000022
16/04/00 12:45	0.601000011
16/04/00 13:00	0.592999995
16/04/00 13:15	0.583999991
16/04/00 13:30	0.574000001
16/04/00 13:45	0.566999972
16/04/00 14:00	0.566999972
16/04/00 14:15	0.56099999
16/04/00 14:30	0.550999999
16/04/00 14:45	0.546000004
16/04/00 15:00	0.542999983
16/04/00 15:15	0.535000026
16/04/00 15:30	0.532999992
16/04/00 15:45	0.523999989
16/04/00 16:00	0.521000028
16/04/00 16:15	0.514999986
16/04/00 16:30	0.518999994
16/04/00 16:45	0.521000028
16/04/00 17:00	0.500999987
16/04/00 17:15	0.48300001
16/04/00 17:30	0.479999989
16/04/00 17:45	0.470999986
16/04/00 18:00	0.460999995
16/04/00 18:15	0.453000009
16/04/00 18:30	0.449000001
16/04/00 18:45	0.43599999
16/04/00 19:00	0.426999986
16/04/00 19:15	0.421000004
16/04/00 19:30	0.412
16/04/00 19:45	0.407000005
16/04/00 20:00	0.400999993
16/04/00 20:15	0.388000011
16/04/00 20:30	0.384000003
16/04/00 20:45	0.379000008
16/04/00 21:00	0.372000009
16/04/00 21:15	0.365999997
16/04/00 21:30	0.358999997
16/04/00 21:45	0.356000006
16/04/00 22:00	0.344999999
16/04/00 22:15	0.340999991
16/04/00 22:30	0.338999987
16/04/00 22:45	0.335000008
16/04/00 23:00	0.323000014
16/04/00 23:15	0.323000014
16/04/00 23:30	0.323000014
16/04/00 23:45	0.323000014
24/07/00 0:00	1.338510156
24/07/00 3:00	1.813766718
24/07/00 6:00	1.770773172

24/07/00 9:00	1.594987988	
24/07/00 12:00	2.009619474	
24/07/00 15:00	1.855209231	Hydraulic head trip 2
24/07/00 18:00	1.607965708	
24/07/00 21:00	1.535513878	
24/08/00 0:00	0.914	
24/08/00 3:00	0.528	
24/08/00 6:00	0.111	
24/08/00 9:00	0.147	Hydraulic head trip 3
24/08/00 12:00	0.180	
24/08/00 15:00	0.352	
24/08/00 18:00	0.562	
24/08/00 21:00	0.792	

Appendix 4

Hydraulic head can be calculated as the sum total of elevation head plus pressure head. Elevation head is the survey height plus the "stick up" minus the depth to water in the piezometer. Pressure head is length of the piezometer minus depth to water. Measurements have been adjusted to relate to AHD.

Date **16/4/2000**

Piezometer	Easting	Southing	Piezometer length (cm)	Stick up (cm)	Survey height (cm)	Elevation head (cm)	Depth to water (cm)	Pressure head (cm)	Total Head (cm)
1	70	18	201	12.2	361	172.2	57	144	316.2
2	80	6.3	200	109.2	412.7	321.9	142	58	379.9
3	80	19.3	200	94.6	407	301.6	128	72	373.6
4	120	2	153	107.4	380	334.4	120	33	367.4
5	120	12	199	97.6	392	290.6	128	71	361.6
6	120	30.7	185	42.7	404.7	262.4	157.5	27.5	289.9
7	140	10	200	120	412	332	169.5	30.5	362.5
8	141	10	200	72	412	284	117.8	82.2	366.2
9	180	10	150	103.7	387	340.7	117.8	32.2	372.9
10	180	30	301	68.8	442	209.8	163	138	347.8
11	180	44	351	159.4	431	239.4	227	124	363.4
12	240	3.9	131	81	432	382	99	32	414
13	241	3.9	199	129	432	362	147	52	414
14	240	12.3	139	84.2	430	375.2	109	30	405.2
15	240	32.3	197	62	432	297	115	82	379
16	241	32.3	300	100	432	232	150	150	382
17	240	45.8	300	43	484.7	227.7	252	48	275.7
18	241	45.8	182	11	484.7	313.7	136	46	359.7
19	300	2	141	60.8	432	351.8	59	82	433.8
20	299	21	298	66.4	482.6	251	151	147	398
21	300	21	300	113.3	483.6	296.9	178.2	121.8	418.7
22	301	21	201	58	482.6	339.6	132	69	408.6
23	300	36	198	96.1	466.1	364.2	121.2	76.8	441
24	360	2	200	147	432	379	141.3	58.7	437.7
25	360	11	199	98.2	469	368.2	148.2	50.8	419
26	360	32	201	64.4	476.1	339.5	156	45	384.5
27	450	5	167	7.2	452	292.2	138	29	321.2
28	450	10	200	9	460	269	88	112	381

Date **24/07/2000**

Piezometer	Easting	Southing	Piezometer length (cm)	Stick up (cm)	Survey height (cm)	Elevation head (cm)	Depth to water (cm)	Pressure head (cm)	Total head (cm)
1	70	18	201	12.2	361	172.2	64.5	136.5	308.7
2	80	6.3	200	109.2	412.7	321.9	128	72	393.9
3	80	19.3	200	94.6	407	301.6	152	48	349.6
4	120	2	153	107.4	380	334.4	114	39	373.4
5	120	12	199	97.6	392	290.6	123	76	366.6
6	120	30.7	185	42.7	404.7	262.4	134	51	313.4
7	140	10	200	120	412	332	161	39	371
8	141	10	200	72	412	284	109	91	375
9	180	10	150	103.7	387	340.7	113	37	377.7
10	180	30	301	68.8	442	209.8	144	157	366.8
11	180	44	351	159.4	431	239.4	207	144	383.4
12	240	3.9	131	81	432	382	80	51	433
13	241	3.9	199	129	432	362	128	71	433
14	240	12.3	139	84.2	430	375.2	107	32	407.2
15	240	32.3	197	62	432	297	86.5	110.5	407.5
16	241	32.3	300	100.2	432	232.2	122	178	410.2
17	240	45.8	300	44.4	484.7	229.1	216	84	313.1
18	241	45.8	182	11	484.7	313.7	114	68	381.7
19	300	2	141	60.8	432	351.8	56.5	84.5	436.3
20	299	21	298	66.4	482.6	251	121	177	428
21	300	21	300	113.3	483.6	296.9	162	138	434.9
22	301	21	201	58	482.6	339.6	106	95	434.6
23	300	36	198	96.1	466.1	364.2	131	67	431.2
24	360	2	200	147	432	379	136	64	443
25	360	11	199	98.2	469	368.2	140.5	58.5	426.7
26	360	32	201	64.4	476.1	339.5	138	63	402.5
27	450	5	167	7.2	452	292.2	76	91	383.2
28	450	10	200	9	460	269	96	104	373

Date **24/08/2000**

Piezometer	Easting	Southing	Piezometer length (cm)	Stick up (cm)	Survey height (cm)	Elevation head (cm)	Depth to water (cm)	Pressure head (cm)	Total Head (cm)
1	70	18	201	12.2	361	172.2	118	83	255.2
2	80	6.3	200	109.2	412.7	321.9	161	39	360.9
3	80	19.3	200	94.6	407	301.6	172	28	329.6
4	120	2	153	107.4	380	334.4	123	30	364.4
5	120	12	199	97.6	392	290.6	129	70	360.6
6	120	30.7	185	42.7	404.7	262.4	155	30	292.4
7	140	10	200	120	412	332	184	16	348
8	141	10	200	72	412	284	132	68	352
9	180	10	150	103.7	387	340.7	126	24	364.7
10	180	30	301	68.8	442	209.8	185	116	325.8
11	180	44	351	159.4	431	239.4	248	103	342.4
12	240	3.9	131	81	432	382	116	15	397
13	241	3.9	199	129	432	362	163	36	398
14	240	12.3	139	84.2	430	375.2	124	15	390.2
15	240	32.3	197	62	432	297	115	82	379
16	241	32.3	300	100.2	432	232.2	148	152	384.2
17	240	45.8	300	43.4	484.7	228.1	210	90	318.1
18	241	45.8	200	11.2	484.7	295.9	114	86	381.9
19	300	2	141	60.8	432	351.8	63	78	429.8
20	299	21	298	66.4	482.6	251	152	146	397
21	300	21	300	113.3	483.6	296.9	178.2	121.8	418.7
22	301	21	201	58	482.6	339.6	120	81	420.6
23	300	36	198	96.1	466.1	364.2	166	32	396.2
24	360	2	200	147	432	379	148	52	431
25	360	11	199	98.2	469	368.2	160	39	407.2
26	360	32	201	64.4	476.1	339.5	172	29	368.5
27	450	5	167	7.2	452	292.2	100	67	359.2
28	450	10	200	9	460	269	116	84	353

Appendix 5

Plots of rising head data

Field recovery data — semi-logged for Hvorslev anal

Date 16/4/'00

Piezometer 1 70mE 18mS

measured head 57cm

Ho 140cm

Time elapsed (sec)	Depth to water (cm)	(h)	Head ratio (h/ho)
0	197	140	1
60	173	116	0.828571429
120	160	103	0.735714286
220	158	101	0.721428571
300	152	95	0.678571429
1320	100.5	43.5	0.310714286

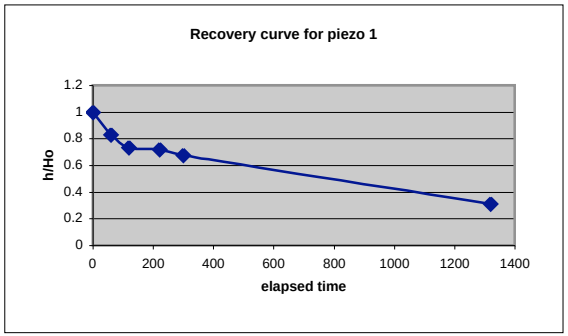

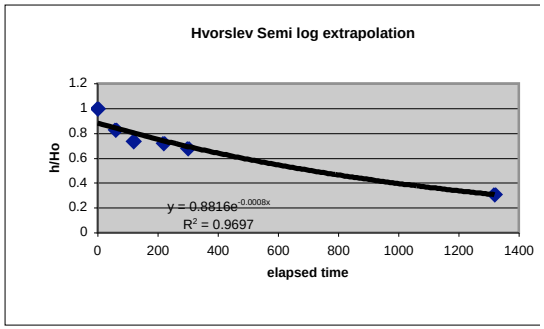

Piezometer 2 80mE 6.3mS

measured head 142 cm

Ho 38.5cm

Time elapsed (sec)	Depth to water (cm)	(h)	Head ratio (h/ho)
0	180.5	38.5	1
20	170	28	0.727272727
40	166	24	0.623376623
50	159	17	0.441558442
70	155	13	0.337662338
120	150	8	0.207792208
145	148	6	0.155844156
190	145	3	0.077922078
250	144	2	0.051948052
660	143.5	1.5	0.038961039

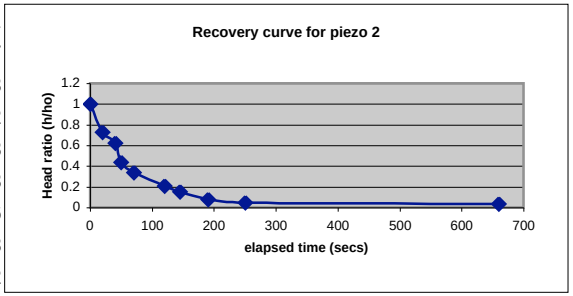

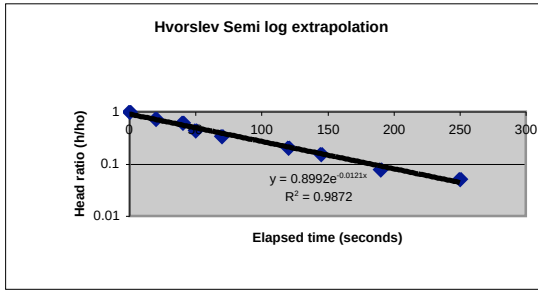

Piezometer 3 80mE 19.3mS

measured head 128cm

Ho 37cm

Time elapsed (sec)	Depth to water (cm)	(h)	Head ratio (h/ho)

Appendix 5

0	165	37	1
120	140	12	0.324324324
500	134	6	0.162162162
1050	129	1	0.027027027

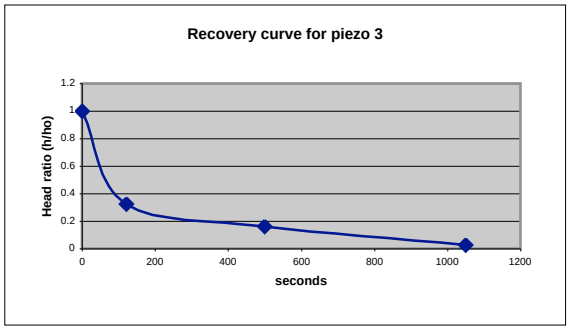

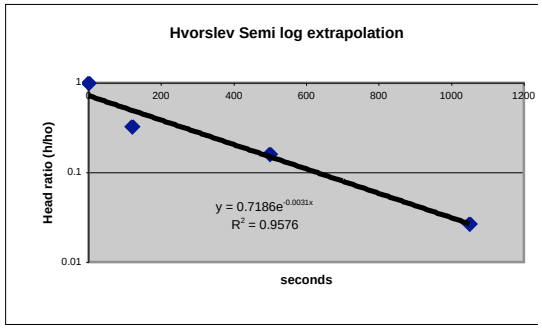

Piezometer 4	120mE	2mS	
measured head	120cm		
Ho	22cm		
Time elapsed (sec)	Depth to water (cm)	(h)	Head ratio (h/ho)
0	142	22	1
60	130	10	0.454545455
80	127	7	0.318181818
115	125	5	0.227272727
145	123	3	0.136363636
195	121.5	1.5	0.068181818
210	120.5	0.5	0.022727273

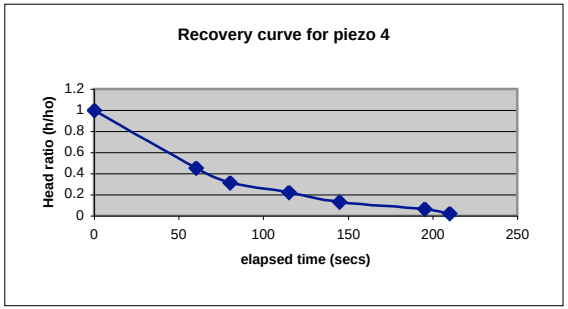

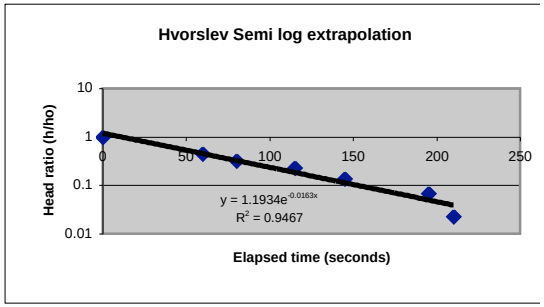

Piezometer 5	120mE	12mS	
measured head	128cm		
Ho	55cm		
Time elapsed (sec)	Depth to water (cm)	(h)	Head ratio (h/ho)
0	183	55	1
36	174.5	46.5	0.845454545
66	167	39	0.709090909
96	160	32	0.581818182
216	143.5	15.5	0.281818182
366	134.9	6.9	0.125454545
715	131	3	0.054545455
5256	130.5	2.5	0.045454545

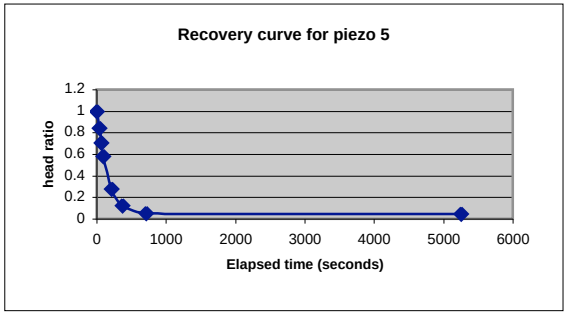

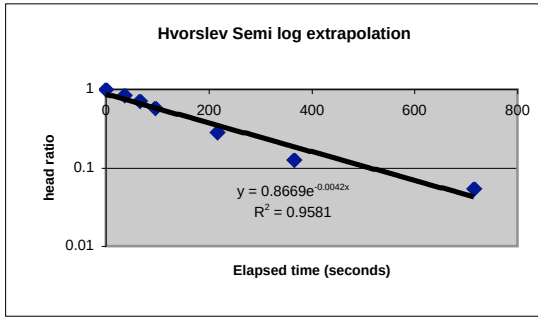

Appendix 5

lysis

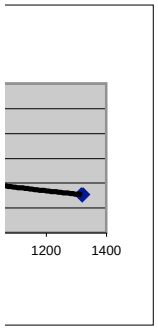

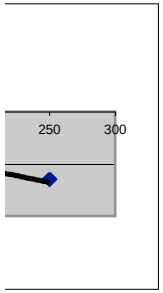

Appendix 5

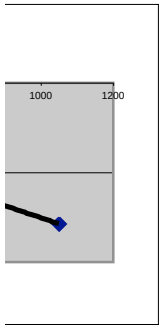

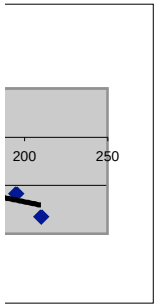

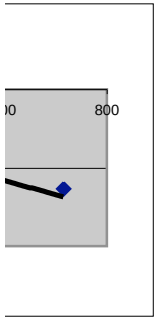

Piezometer 7 140mE 10mS

measured head 169.5cm

Ho 100cm

Time elapsed (sec)	Depth to water (cm)	h	Head ratio (h/ho)
0	279.5	100	1
48	269	90.5	0.905
72	255	85.5	0.855
198	235.2	65.7	0.657
348	225	55.5	0.555
648	219.5	50	0.5
948	218	48.5	0.485

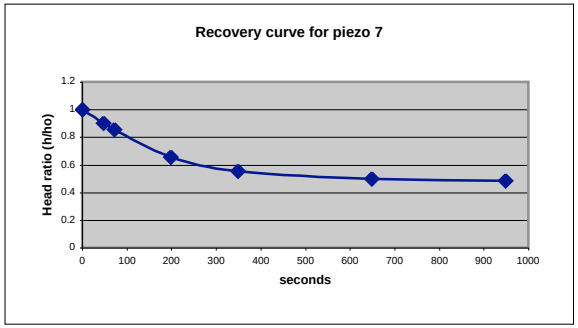

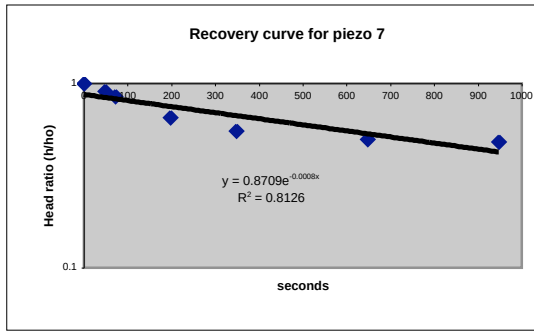

Piezometer 8 141mE 10mS

measured head 117.8cm

Ho 64.7cm

Time elapsed (sec)	Depth to water (cm)	(h)	Head ratio (h/ho)
0	182.5	64.7	1
50	173	55.2	0.85316847
78	170	52.2	0.806800618
384	169.5	51.7	0.799072643
720	169.5	51.7	0.799072643
4020	169	51.2	0.791344668

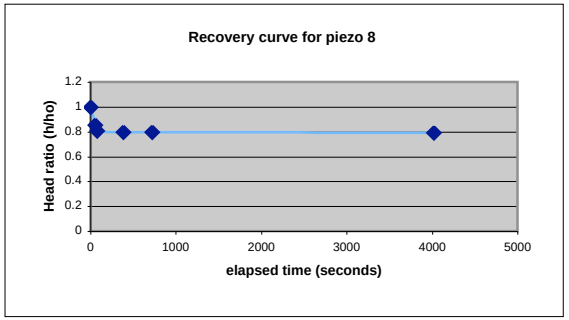

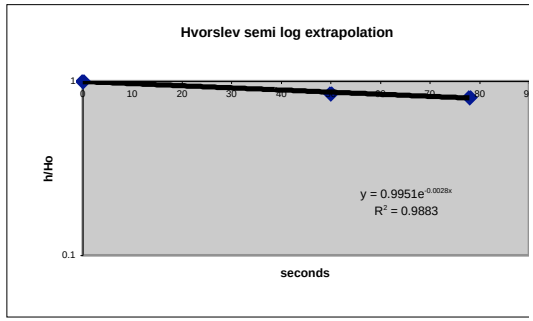

Piezometer 9

measured head 117.8cm

Ho 10.2cm

Time elapsed (sec)	Depth to water (cm)	(h)	Head ratio (h/ho)
0	128	10.2	1
33	122.5	4.7	0.460784314
63	120	2.2	0.215686275
123	118.5	0.7	0.068627451
333	118.5	0.7	0.068627451

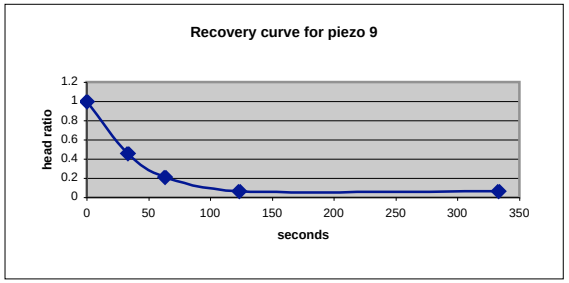

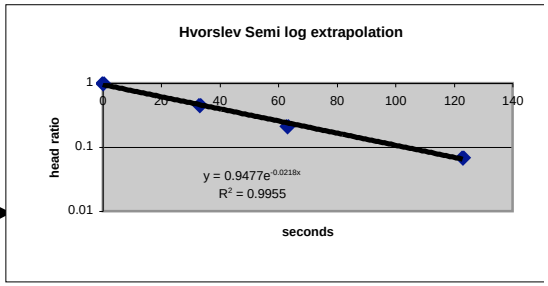

Piezometer 10	180mE	30mS	
measured head	163cm		
Ho	107cm		

Time elapsed (sec)	Depth to water (cm)	(h)	Head ratio (h/ho)
0	270	107	1
50	267	104	0.971962617
115	262.7	99.7	0.931775701
822	230	67	0.626168224
7176	171	8	0.074766355

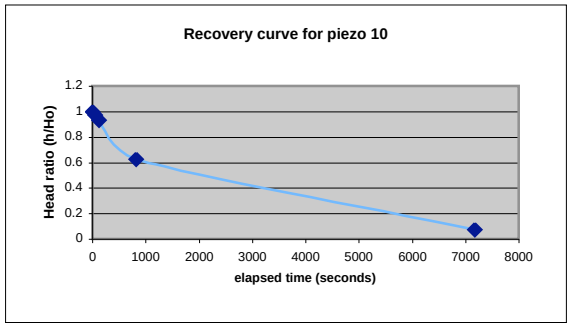

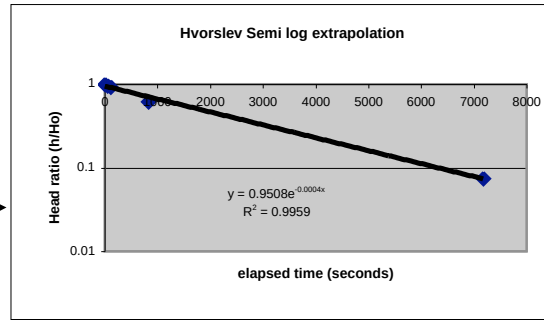

Piezometer 11	180mE	44mS	
measured head	227cm		
Ho	19cm		

Time elapsed (sec)	Depth to water (cm)	(h)	Head ratio (h/ho)
0	246	19	1
60	245.2	18.2	0.957894737
165	245	18.2	0.957894737
450	244	17.5	0.921052632
528	244	17.4	0.915789474
1236	243.5	16.6	0.873684211

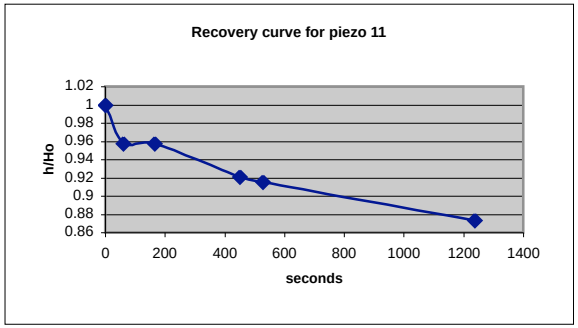

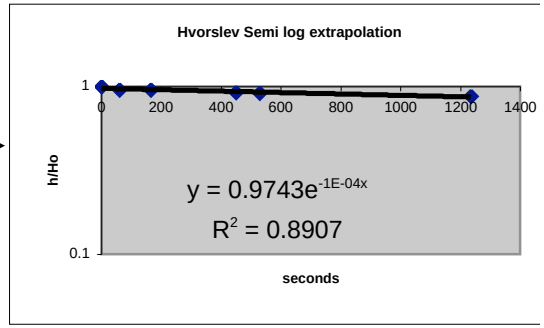

Piezometer 12	240mE	4mS	
measured head	99cm		
Ho	9cm		

Time elapsed (sec)	Depth to water (cm)	(h)	Head ratio (h/ho)
0	108	9	1
15	103	4	0.444444444
30	101.5	2.5	0.277777778
60	101.5	2	0.222222222
360	100.5	1.5	0.166666667

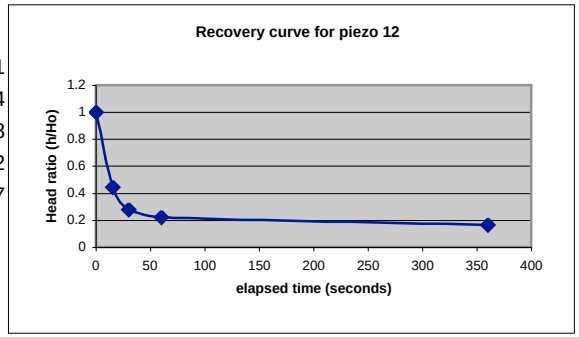

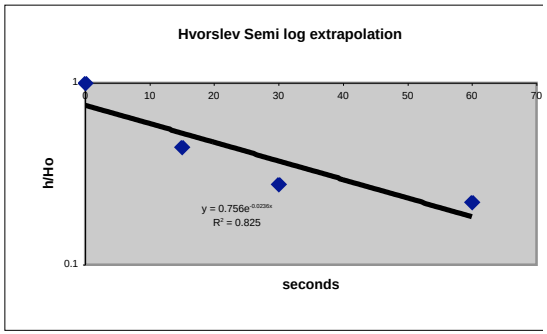

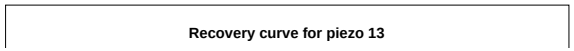

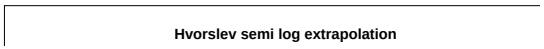

Piezometer 13	241mE	4mS	
measured head	147cm		
Ho	6cm		
Time elapsed (sec)	Depth to water (cm)	(h)	Head ratio (h/ho)
0	153	6	1
60	150	3	0.5
120	149	2	0.333333333
180	148.5	1.5	0.25

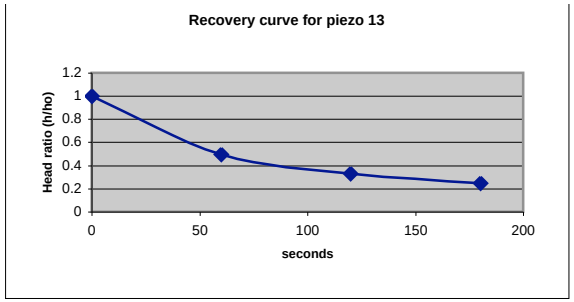

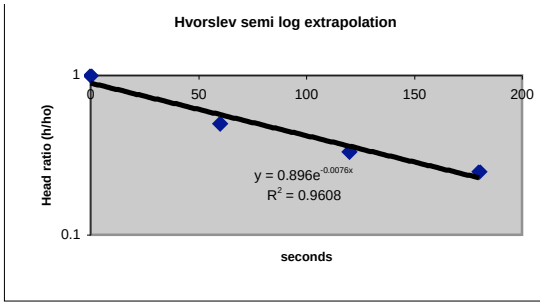

Piezometer 14	240mE	12.3mS	
measured head	109cm		
Ho	6cm		
time elapsed (sec)	Depth to water (cm)	(h)	Head ratio (h/ho)
0	115	6	1
20	111	2	0.333333333
65	109.3	0.3	0.05
110	109	0	0

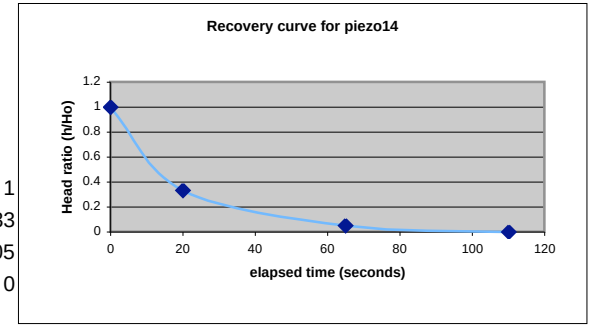

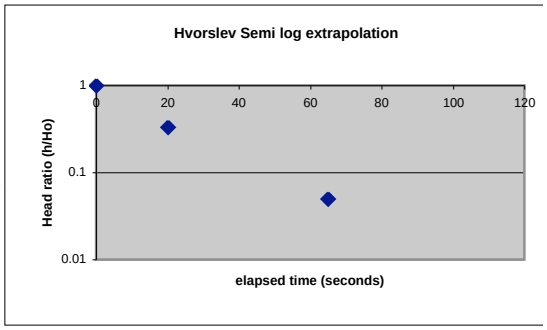

Piezometer 15	240mE	32.3mS	
measured head	115cm		

Piezometer 16	241mE	32.3mS	
measured head	150cm		
Ho	129cm		
time elapsed (sec)	Depth to water (cm)	(h)	Head ratio (h/ho)
0	279	129	1
40	278	128	0.992248062
81	277	127	0.984496124
240	276	126	0.976744186
378	274.5	124.5	0.965116279
4338	261.9	111.9	0.86744186

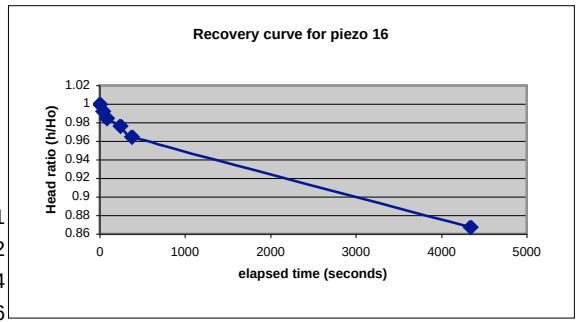

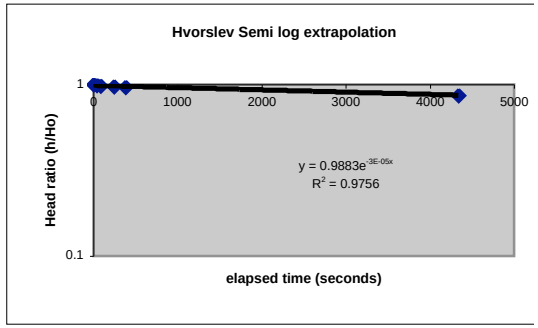

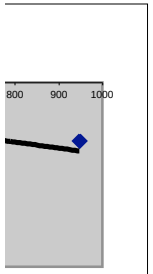
800
900
1000

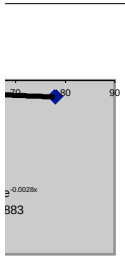
80
90
-0.0028x
883

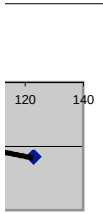
120
140

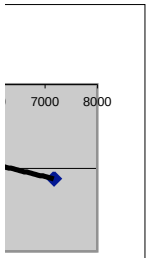
7000
8000

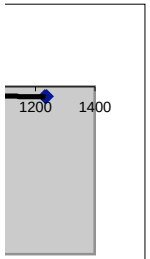
1200
1400

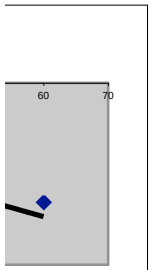
60
70

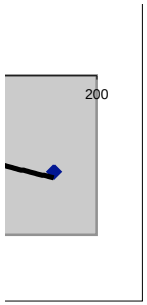
200

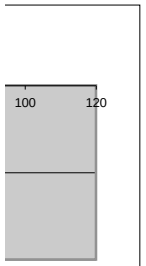
100
120

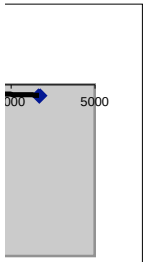
000
5000

Piezometer 17	240mE	45.8mS	
measured head	252cm		
Ho	38cm		

time elapsed (sec)	Depth to water (cm)	(h)	Head ratio (h/ho)
0	290	38	1
60	276	24	0.631578947
300	270	18	0.473684211
600	264	12	0.315789474
700	263	11	0.289473684

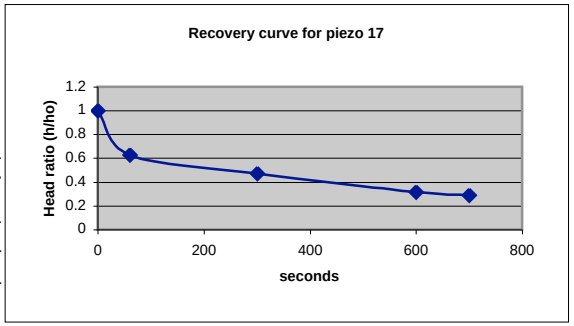

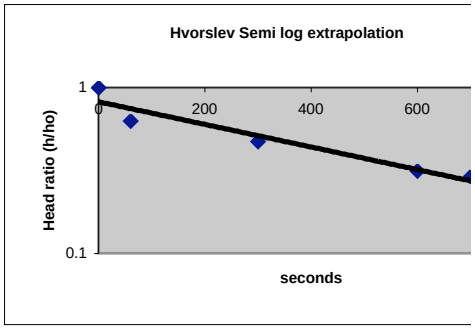

Piezometer 18	241mE	45.8mS	
measured head	136cm		
Ho	35.5cm		

time elapsed (sec)	Depth to water (cm)	(h)	Head ratio (h/ho)
0	171.5	35.5	1
210	163.5	27.5	0.774647887
3500	139.5	3.5	0.098591549
4680	138	2	0.056338028
6666	137	1	0.028169014
10740	136	0	0

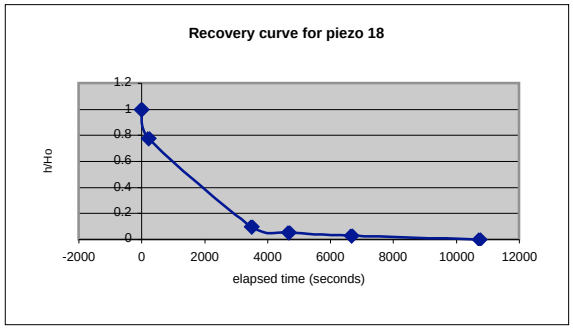

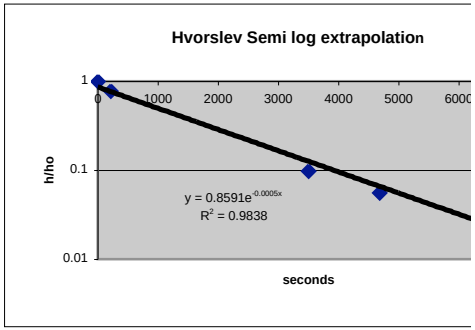

Piezometer 19	300mE	2mS	
measured head	59cm		
Ho	47cm		

time elapsed (sec)	Depth to water (cm)	(h)	Head ratio (h/ho)
0	106	47	1
30	92	33	0.70212766
40	85	26	0.553191489
60	78	19	0.404255319
90	70	11	0.234042553
120	66	7	0.14893617
150	63	4	0.085106383
180	62	3	0.063829787
240	60	1	0.021276596

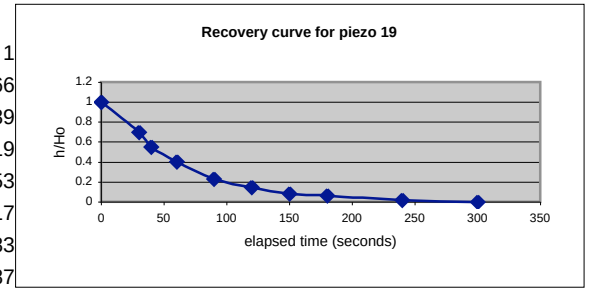

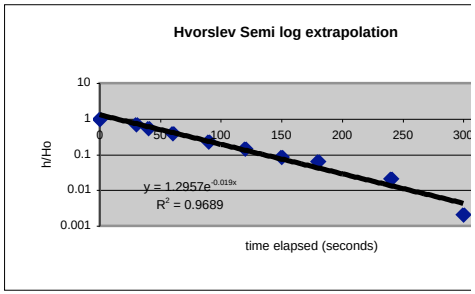

300	59.1	0.1	0.00212766

Piezometer 20 299mE 21mS
measured head 151cm
Ho 138.5cm

time elapsed (sec)	Depth to water (cm)	(h)	Head ratio (h/ho)
0	289.5	138.3	1
62	286	134.8	0.974692697
169	281	129.8	0.938539407
300	276.5	125.3	0.906001446
590	263	111.8	0.808387563
731	258	106.8	0.772234273
839	254.5	103.3	0.74692697
920	251.5	100.3	0.725234996
967	250	98.8	0.714389009
1033	247.2	96	0.694143167
1213	240.5	89.3	0.645697758
1609	229	77.8	0.562545192
1676	227	75.8	0.548083876
1849	223	71.8	0.519161244
5000	200	40	0.288808664
5929	187.5	36.3	0.262472885

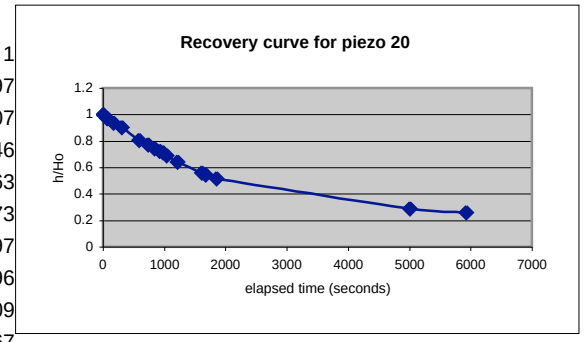

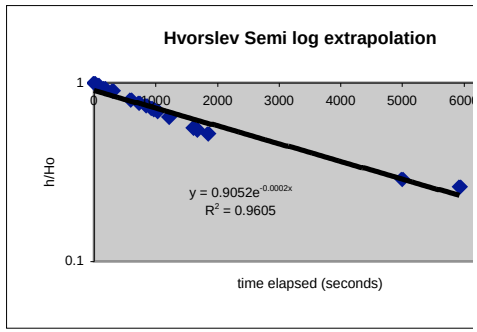

Piezometer 21 300mE 21mS
measured head 178.2cm
Ho 101.9cm

time elapsed (sec)	Depth to water (cm)	(h)	Head ratio (h/ho)
0	280.1	101.9	1
40	274	95.8	0.94013739
60	272	93.8	0.920510304
69	270.5	92.3	0.90578999
108	268	89.8	0.881256133
126	265	86.8	0.851815505
146	261	82.8	0.812561335
186	256.5	78.3	0.768400393
264	251.5	73.3	0.719332679
324	245.5	67.3	0.660451423

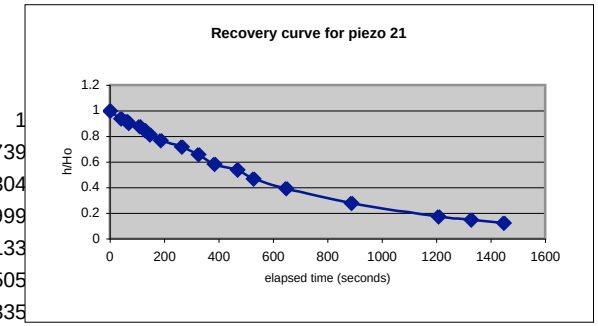

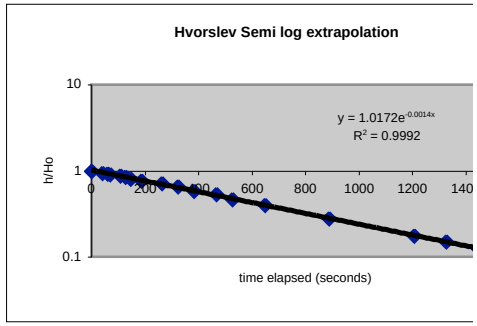

384		238	59.8	0.586849853
468		233	54.8	0.537782139
528		226	47.8	0.469087341
648		218.7	40.5	0.397448479
888		206.5	28.3	0.277723258
1206		196	17.8	0.17468106
1326		193.5	15.3	0.150147203
1446		191	12.8	0.125613346
Piezometer 22	301mE		21mS	
measured head		158	recovery test not performed	
Piezometer 23	300mE		36mS	
measured head	121.2cm			
Ho	60.3cm			
time elapsed (sec)	Depth to water (cm)		(h)	Head ratio (h/ho)
0		181.5	60.3	1
30		175	53.8	0.892205638
60		166	44.8	0.742951907
90		161	39.8	0.660033167
120		154.5	33.3	0.552238806
360		132	10.8	0.179104478
1020		121.7	0.5	0.008291874
2520		121.2	0	0

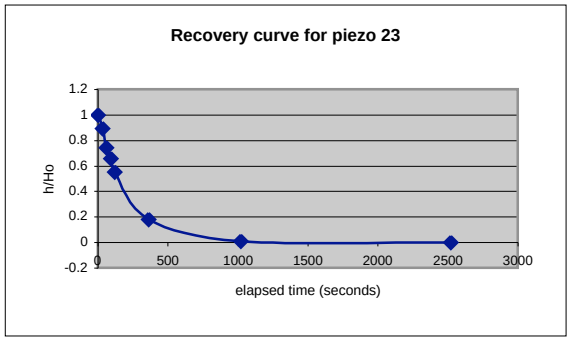

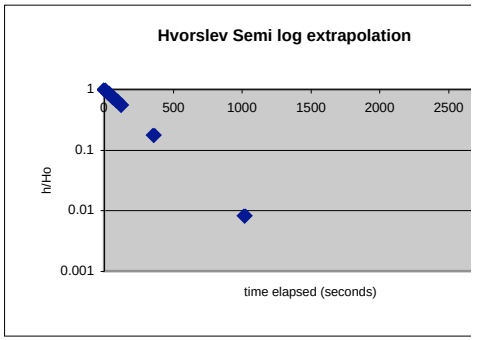

Piezometer 24	360mE		2mS	
measured head	141.3cm			
Ho	6.2cm			
time elapsed (sec)	Depth to water (cm)		(h)	Head ratio (h/ho)
0		147.5	6.2	1
120		142.8	1.5	0.241935484
189		141.7	0.4	0.064516129

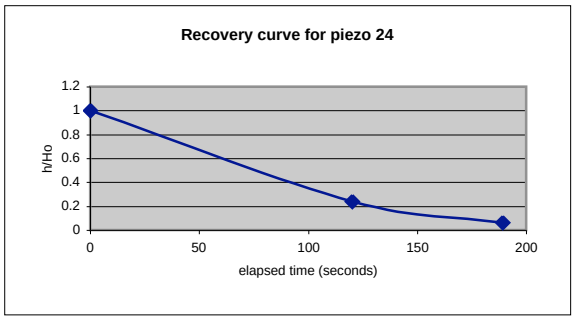

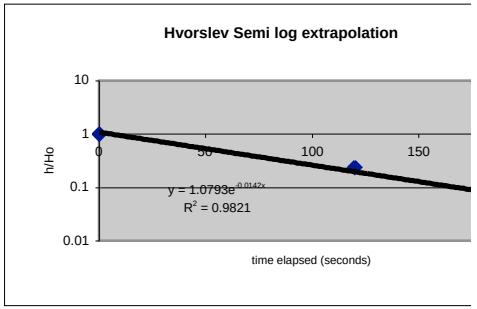

Piezometer 25	360mE	11mS	

measured head 148.2cm

Ho 1cm

time elapsed (sec)	Depth to water (cm)	(h)	Head ratio (h/ho)
0	149.2	1	1
60	148.6	0.4	0.4
120	148.5	0.3	0.3
270	148.2	0	0

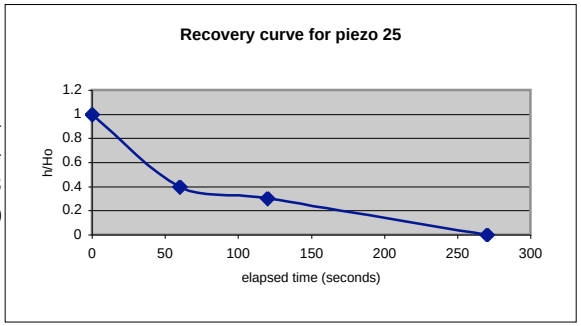

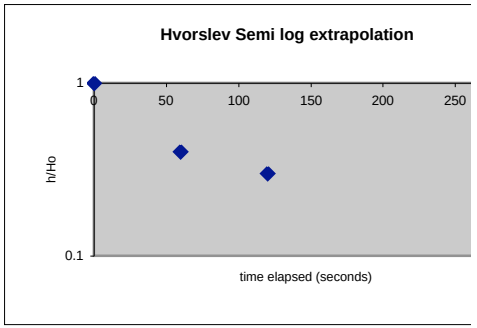

Piezometer 26 360mE 32mS

measured head 156cm

Ho 5.5cm

time elapsed (sec)	Depth to water (cm)	(h)	Head ratio (h/ho)
0	161.5	5.5	1
30	160.2	4.2	0.763636364
60	159.5	3.5	0.636363636
90	159	3	0.545454545
120	158.6	2.6	0.472727273
270	158.2	2.2	0.4
390	158	2	0.363636364
450	158	2	0.363636364
16560	156.5	0.5	0.090909091

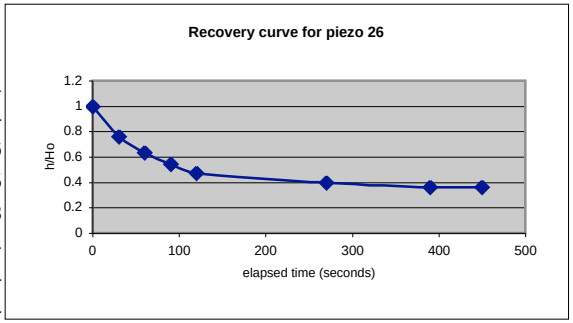

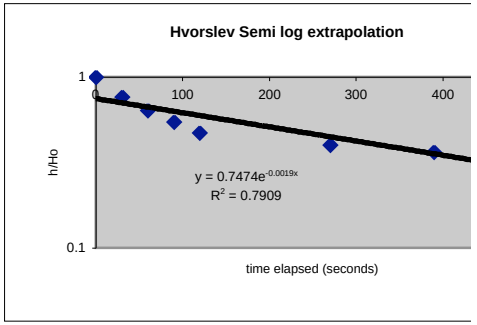

Piezometer 27 450mE 5mS

measured head 138cm

Ho 26.5cm

time elapsed (sec)	Depth to water (cm)	(h)	Head ratio (h/ho)
0	164.5	26.5	1
60	164.5	26.5	1
300	163.8	25.8	0.973584906
360	163.5	25.5	0.962264151
540	163.1	25.1	0.947169811
720	162.7	24.7	0.932075472
900	162.2	24.2	0.913207547
1200	161.8	23.8	0.898113208
1740	159.8	21.8	0.822641509
2820	157.5	19.5	0.735849057
4800	154	16	0.603773585
19600	151	13	0.490566038
25500	145.5	7.5	0.283018868
28000	144	6	0.226415094

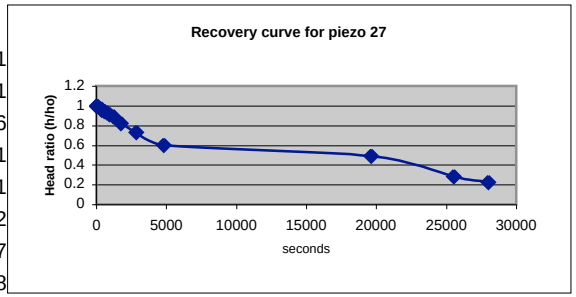

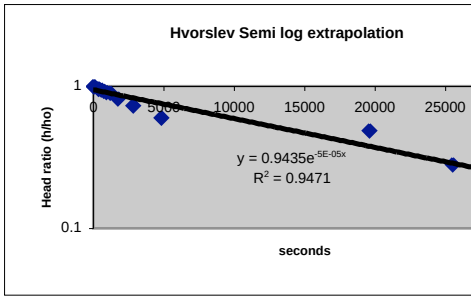

Piezometer 28 450mE 10mS
measured head 88cm
Ho 8.7cm

time elapsed (sec)	Depth to water (cm)	(h)	Head ratio (h/ho)
0	96.7	8.7	1
60	96.5	8.5	0.977011494
300	96	8	0.91954023
420	96	8	0.91954023
600	95.5	7.5	0.862068966
780	95.2	7.2	0.827586207
960	95	7	0.804597701
1260	94.7	6.7	0.770114943
1680	93.8	5.8	0.666666667
2700	92.8	4.8	0.551724138
50000	90	2	0.229885057
111840	89	1	0.114942529

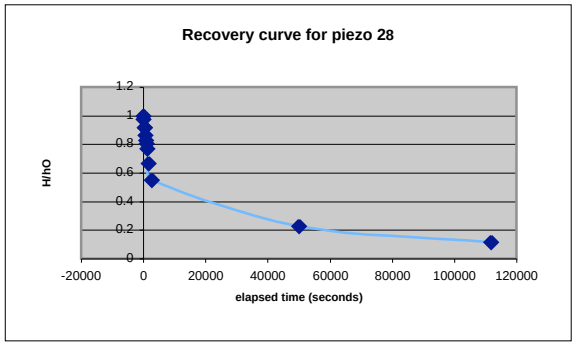

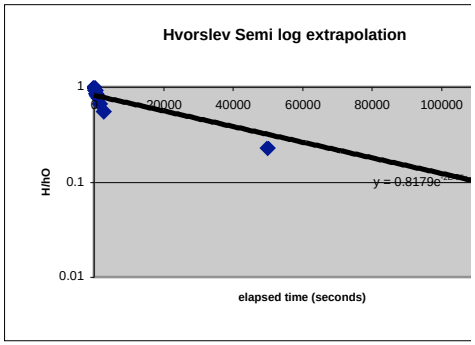

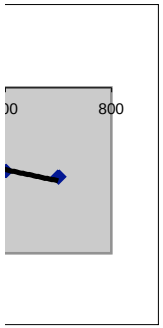
800

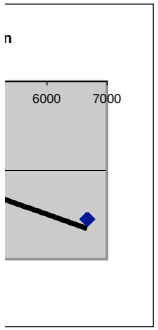
6000
7000

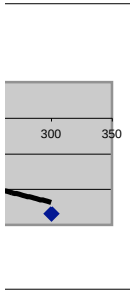
300
350

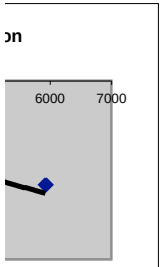
6000
7000

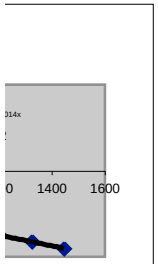
1400
1600

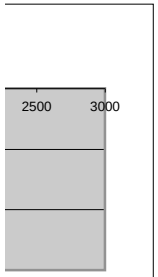
2500
3000

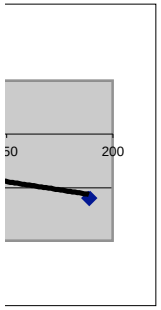
50
200

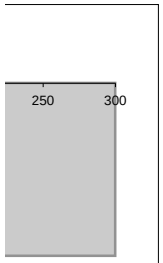
250
300

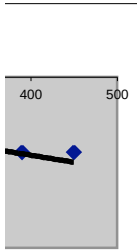
400
500

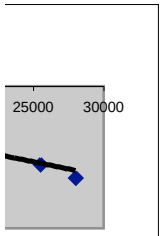
25000
30000

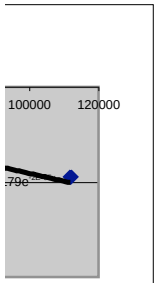
100000
120000

Recovery test for the 24/7/2000

Piezometer 1 70mE 18mS
measured head 64.5cm
Ho 92.5cm

Time elapsed (s)	Depth to water (cm)	h	Head ratio (h/ho)
0	157	92.5	1
60	156.5	64	0.691891892
120	155.3	62.8	0.678918919
270	153	60.5	0.654054054
400	150	57.5	0.621621622
800	130	37.5	0.405405405
1500	120	27.5	0.297297297
1900	110	17.5	0.189189189

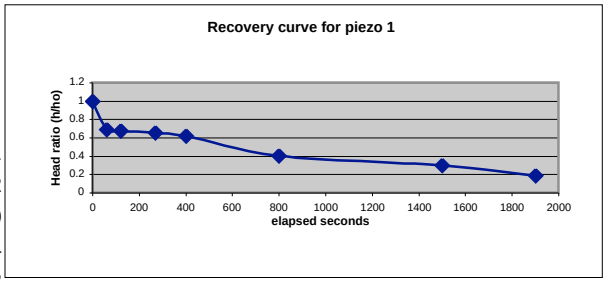

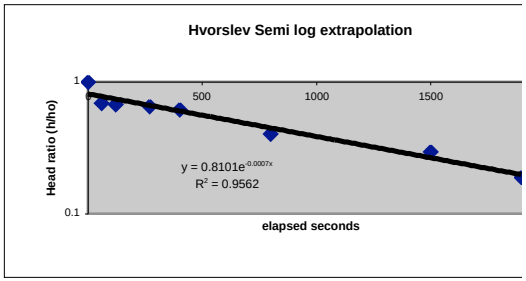

Piezometer 2 80mE 6.3mS
measured head 128cm
Ho 37cm

Time elapsed (s)	Depth to water (cm)	(h)	Head ratio (h/ho)
0	165	37	1
60	140	12	0.324324324
120	134	6	0.162162162
210	129	1	0.027027027
810	129	1	0.027027027

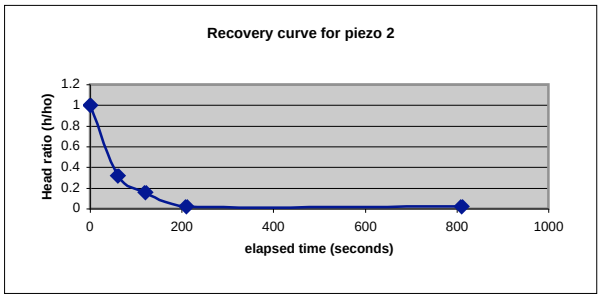

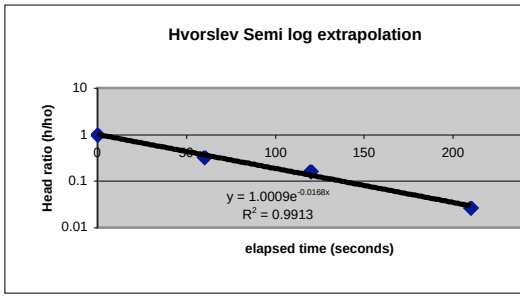

Piezometer 3 80mE 19.3mS
measured head 119cm
Ho 73cm

Time elapsed (sec)	Depth to water (cm)	(h)	Head ratio (h/ho)
0	192	73	1
50	182.5	63.5	0.869863014
120	171	52	0.712328767
180	164	45	0.616438356
230	160.9	41.9	0.573972603
2919	157.5	38.5	0.52739726

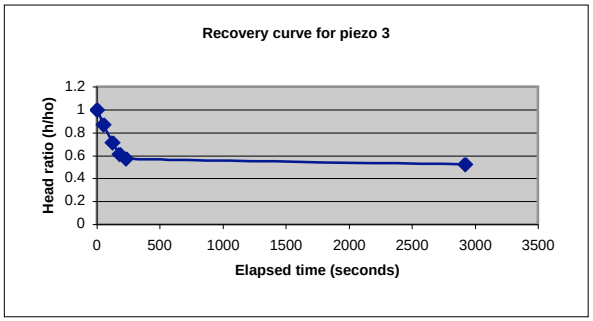

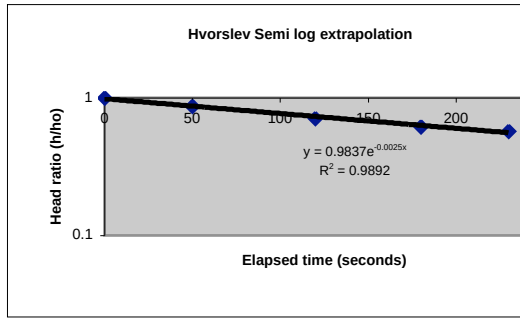

Piezometer 4
measured head 114cm

Ho	18.5cm		
Time elapsed (s)	Depth to water (cm)	h	Head ratio (h/ho)
0	132.5	18.5	1
60	120	6	0.324324324
120	116	2	0.108108108

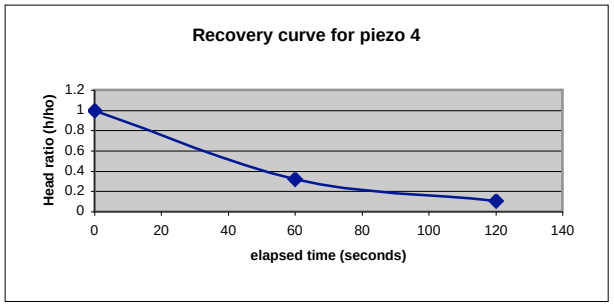

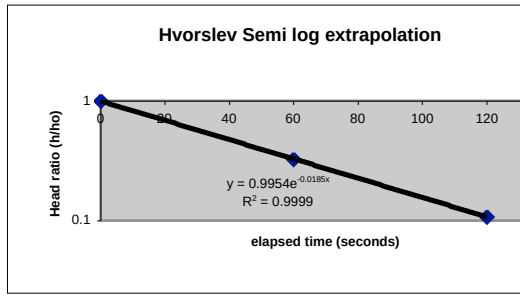

Piezometer 5	120mE	12mS	
measured head	123cm		
Ho	48cm		
Time elapsed (s)	Depth to water (cm)	h	Head ratio (h/ho)
0	171	48	1
90	150	27	0.5625
120	142	19	0.395833333
210	131	8	0.166666667
960	124	1	0.020833333

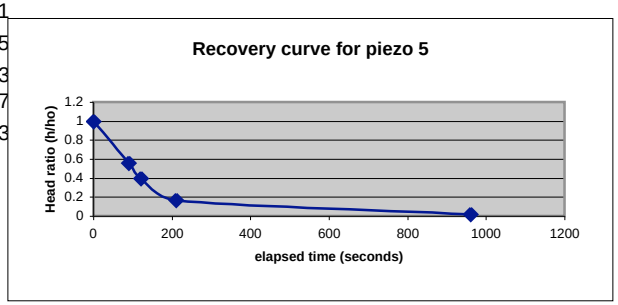

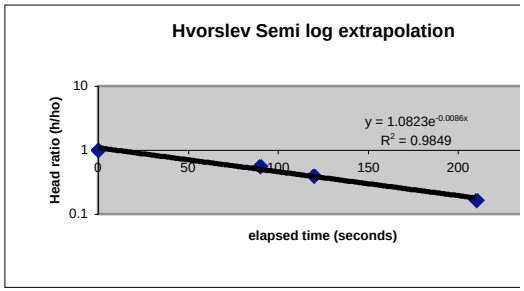

Piezometer 6	120mE	30.7mS	
measured head	134cm		
Ho	89cm		
Time elapsed (s)	Depth to water (cm)	h	Head ratio (h/ho)
0	223	89	1
30	200	66	0.741573034
60	190	56	0.629213483
800	172	38	0.426966292
2280	136	2	0.02247191

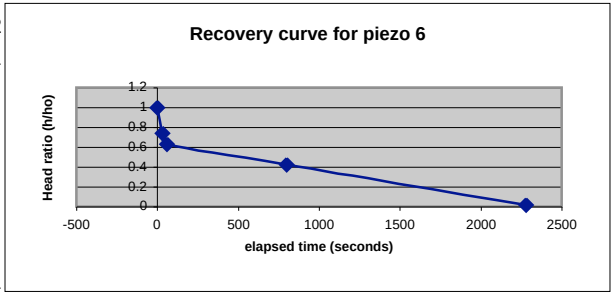

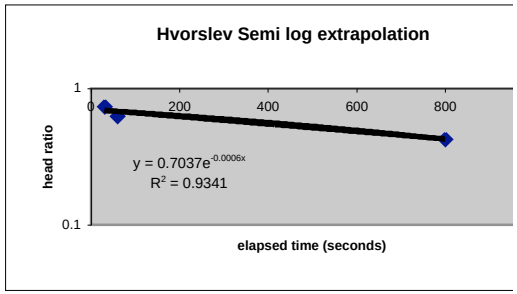

Piezometer 8	141mE	10mS	
measured head	109cm		
Ho	56cm		
Time elapsed (s)	Depth to water (cm)	h	Head ratio (h/ho)
0	165	56	1
30	148	39	0.696428571
90	138	29	0.517857143
150	131	22	0.392857143
390	124.5	15.5	0.276785714
510	115	10	0.178571429

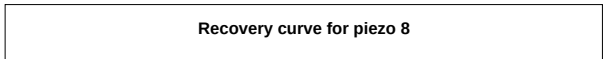

990	113	4	0.071428571
3000	110.5	1.5	0.026785714
4170	110.5	1.5	0.026785714

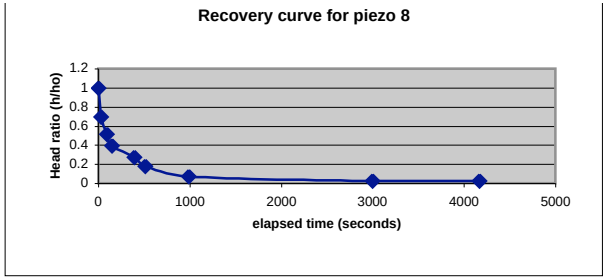

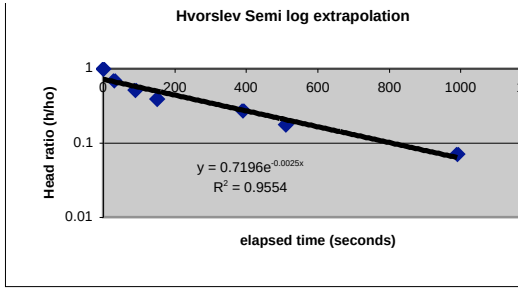

Piezometer 7

140mE	10mS
measured head	161cm
Ho	9cm

Time elasped (s)	Depth to water (cm)	(h)	Head ratio (h/ho)
0	170	9	1
42	162	1	0.111111111
63	161.5	0.5	0.055555556
200	161.5	0.5	0.055555556

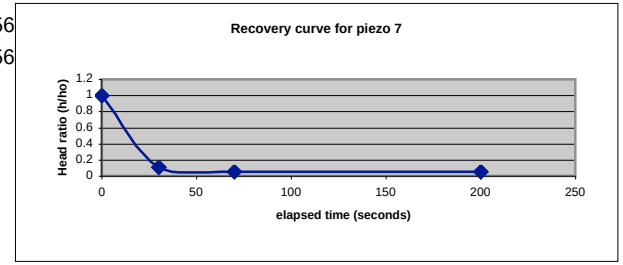

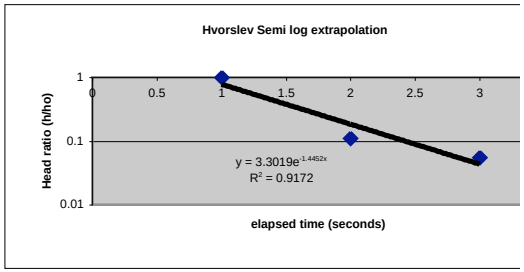

Piezometer 9	180mE	10mS	
n/a			
Piezometer 10	180mE	30mS	
measured head	144cm		
Ho	88.5cm		

Time elapsed (s)	Depth to water (cm)	h	Head ratio (h/ho)
0	232.5	88.5	1
60	238.5	94.5	1.06779661
120	224	80	0.903954802
810	206	62	0.700564972
900	202	58	0.655367232
1440	185.5	41.5	0.468926554
1740	178.5	34.5	0.389830508
2220	170	26	0.293785311
6960	145	1	0.011299435

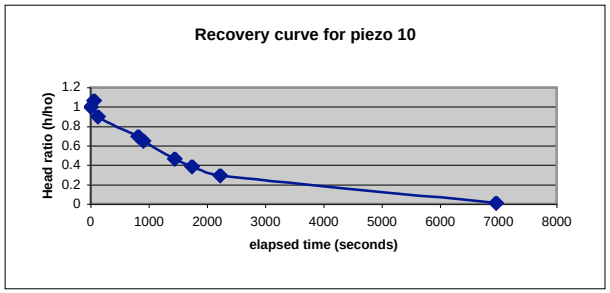

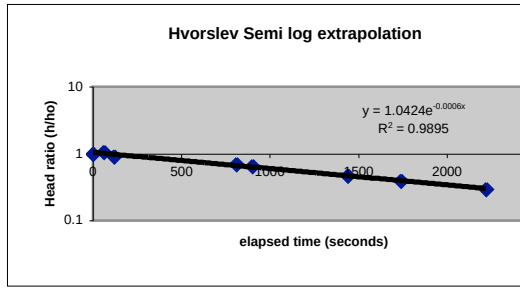

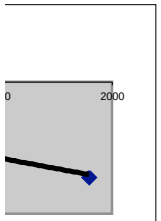
0
2000

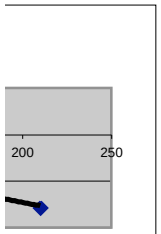
200
250

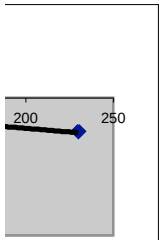
200
250

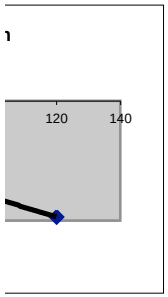
120
140

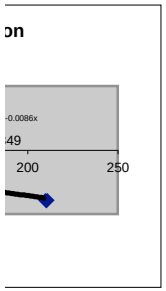
-0.0086x
49
200
250

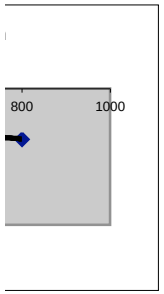
800
1000

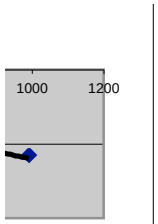
1000
1200

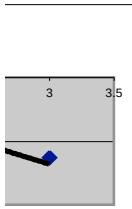
3
3.5

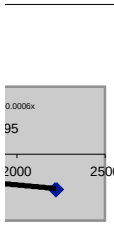
0.0006x
95
2000
2500

Piezometer 11 180mE 44mS

207cm

Ho 88cm

Time elapsed (s)	Depth to water (cm)	h	Head ratio (h/ho)
0	295	88	1
60	294	86	0.977272727
120	293.5	87.5	0.994318182
720	293.5	87.5	0.994318182
5268	289	82	0.931818182
10000	286	79	0.897727273
20000	282	75	0.852272727
32400	278	71	0.806818182

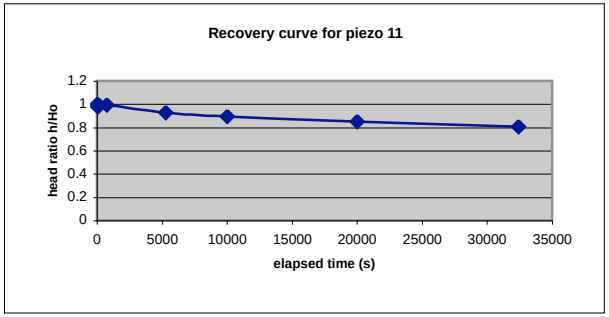

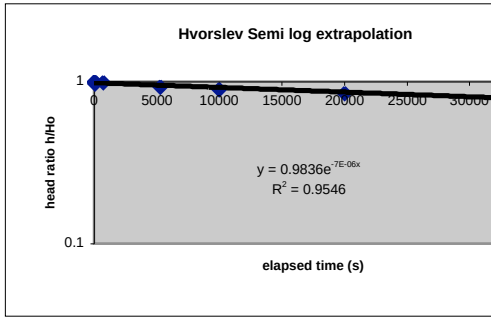

Piezometer 12 240mE 4mS

measured head 80cm

Ho 25cm

Time elapsed (s)	Depth to water (cm)	h	Head ratio (h/ho)
0	105	25	1
60	80	0	0

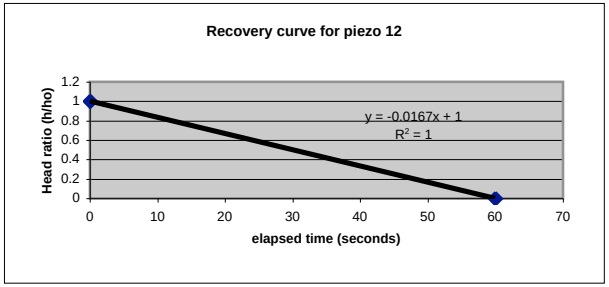

Piezometer 13 241mE 4mS

measured head 128cm

Ho 10cm

Time elapsed (s)	Depth to water (cm)	h	Head ratio (h/ho)
0	138	10	1
60	132	4	0.4
120	131.5	3.5	0.35
600	128	0	0

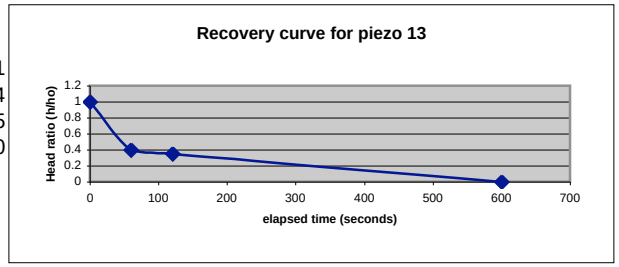

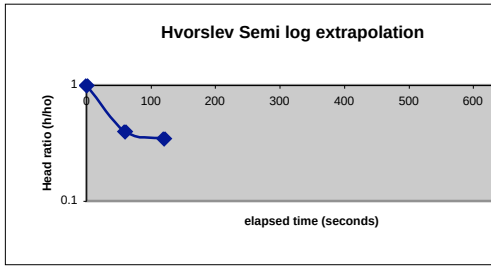

Piezometer 14 240mE 12.3mS

measured head 107cm

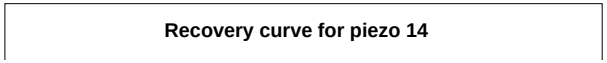

Ho	5cm		
Time elapsed (s)	Depth to water (cm)	h	Head ratio (h/ho)
0	112	5	1
30	108	1	0.2

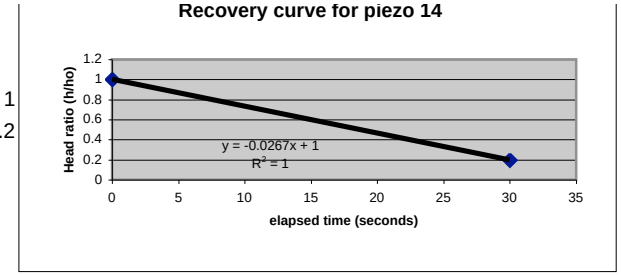

Piezometer 15	240mE	32.3mS	
measured head	86.5cm		
Ho	133.5cm		
Time elapsed (s)	Depth to water (cm)	(h)	Head ratio (h/ho)
0	220	133.5	1
120	216	129.5	0.970037453
180	216	129.5	0.970037453
240	213	126.5	0.947565543
780	203	116.5	0.872659176
1320	194.5	108	0.808988764
1770	188	101.5	0.760299625
2760	174.5	88	0.65917603
3120	170	83.5	0.625468165
3780	164	77.5	0.580524345
3960	162	75.5	0.565543071
4800	154	67.5	0.505617978
5010	152.5	66	0.494382022
7380	136	49.5	0.370786517
13500	111	24.5	0.183520599

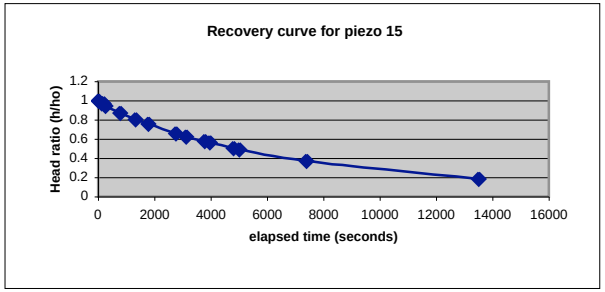

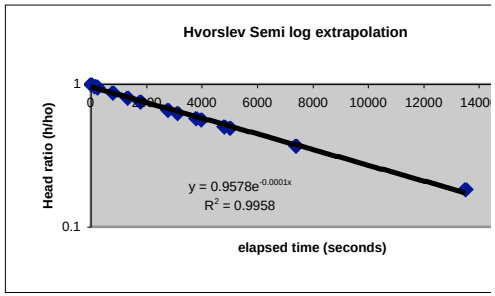

Piezometer 16	241mE	32.3mS
measured head	122cm	
full recovery (within 2 minutes).		

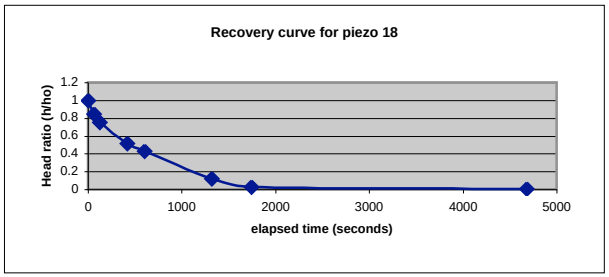

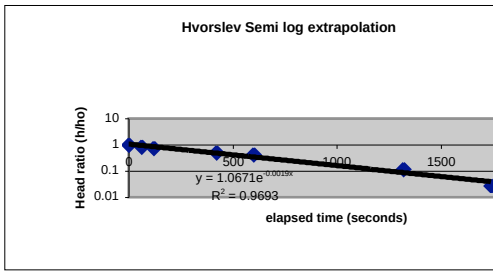

Piezometer 18	440mE	45.8mS
	114.5	
Ho	53.5cm	
Time elapsed (s)	Depth to water (cm)	h	Head ratio (h/ho)
0	168	53.5	1
60	160	45.5	0.85046729
120	155	40.5	0.757009346
420	142	27.5	0.514018692
600	137.5	23	0.429906542

1320	121	6.5	0.121495327
1740	116	1.5	0.028037383
4680	115	0.5	0.009345794

Piezometer 17 241mE 45.8mS
measured head 216cm
Ho 49.5

Time elapsed (s)	Depth to water (cm)	h	Head ratio (h/ho)
0	265.5	49.5	1
60	265.5	49.5	1
300	265.5	49.5	1
540	265.5	49.5	1
780	264.5	48.5	0.97979798
1740	262.5	46.5	0.939393939
2160	262	46	0.929292929
4920	252	36	0.727272727
11340	253	37	0.747474747

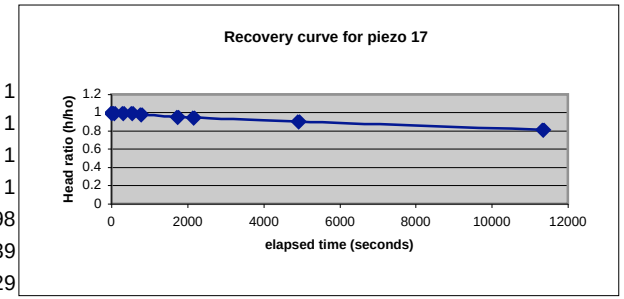

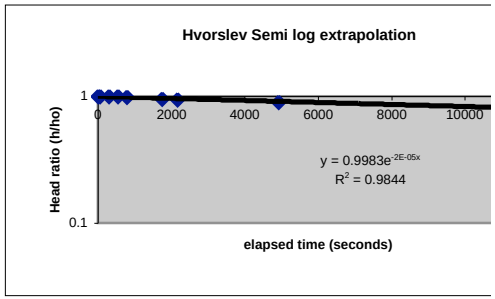

Piezometer 19 300mE 2mS
measured head 56cm
Ho

Time elapsed (s)	Depth to water (cm)	h	Head ratio (h/ho)
0	93	37	1
30	77	21	0.567567568
60	67	11	0.297297297
120	60	4	0.108108108

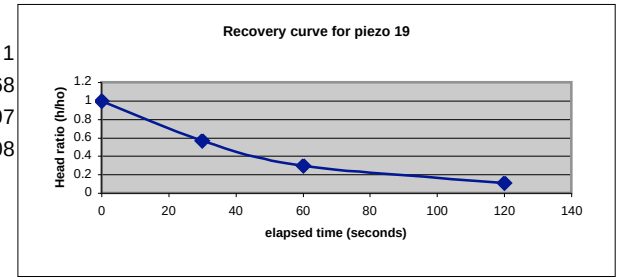

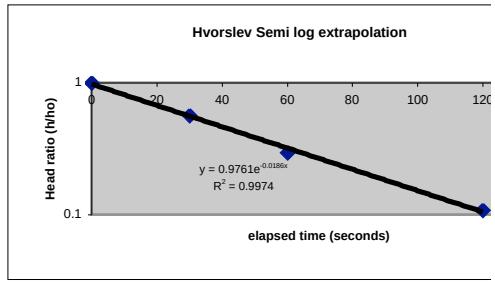

Piezometer 20 299mE 21mS
measured head 121cm
Ho 15cm

Time elapsed (s)	Depth to water (cm)	h	Head ratio (h/ho)
0	136	15	1
30	124	3	0.2
90	122	1	0.066666667
270	121.5	0.5	0.033333333

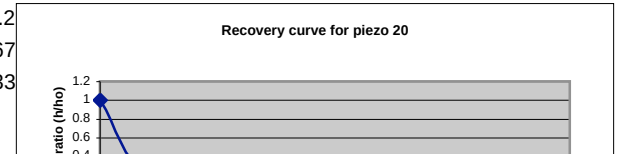

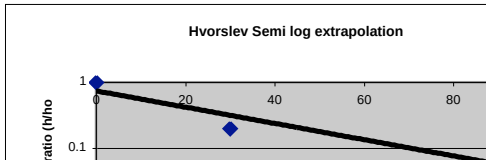

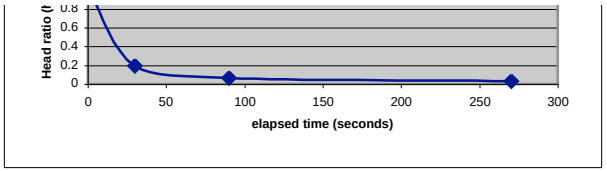

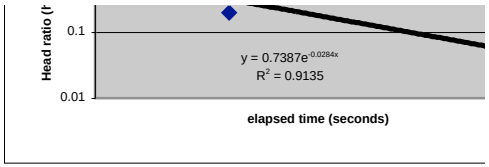

Piezometer 21	300mE	21mS	
measured head	168.2cm		
Ho	88.8cm		

Time elapsed (s)	Depth to water (cm)	h	Head ratio (h/ho)
0	257	88.8	1
60	254	85.8	1
90	252	83.8	0.976689977
95	251	82.8	0.932432432
100	249.5	81.3	0.915540541
115	248.5	80.3	0.904279279
120	244	75.8	0.853603604
200	238.5	70.3	0.791666667
400	229	60.8	0.684684685
500	221	52.8	0.594594595
600	214	45.8	0.515765766
700	209	40.8	0.459459459
1200	185	16.8	0.189189189
1800	174	5.8	0.065315315
2500	169	0.8	0.009090909

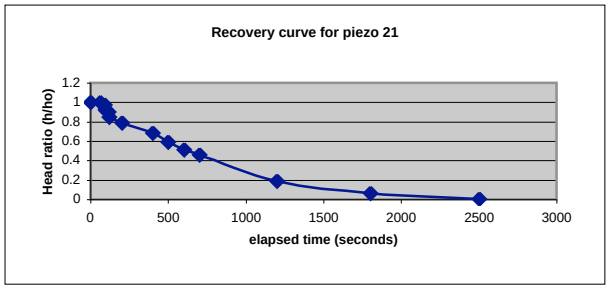

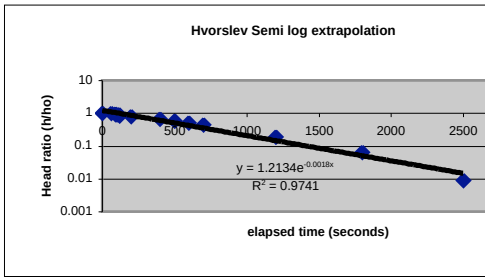

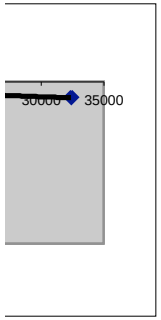
30000
35000

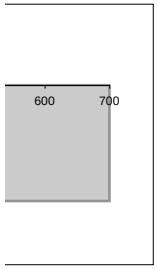
600
700

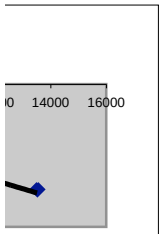
14000
16000

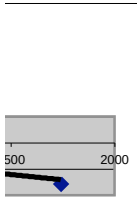
2000

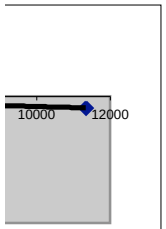
10000
12000

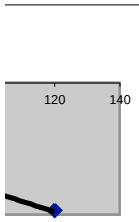
120
140

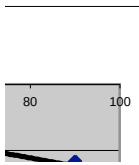
80
100

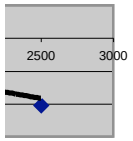
2500
3000

Appendix 6

Meteorological data

Year 2000 precipitation data at Strahn

These files contain climatological data taken from ADAM,
the Australian Commonwealth Bureau of Meteorology's climate archive.
The data has been extracted using a system called Eve.

Prepared by Climate and Consultancy Section in the Tasmania and Antarctica Regional Office of the Bureau of Meteorology on 2 October 2000
Contact us by phone on (03) 6221 2043, by fax on (03) 6221 2045, or by email on climate.tas@bom.gov.au

---

==========

Filename: Mal.280.1.csv
The file contains Monthly values of Total Monthly Precipitation (mm)
Fields within each record are delimited by commas.
Years run down the page and months run across. The last column
(the '13th month') contains an annual value for that year.
The data are for the following stations:
Number , Name , Latitude , Longitude ,Elevation, Opened on , Closed on , Locality
097000 , Cape Sorell , 42°11'59"S , 145°10'11"E , 19.3m , 1899-01-01 , Still open , Cape Sorell

Highlighted values are records from April, July, August

97000, 2000, Total Monthly Precipitation (mm),23, 84, 62.4, 78.6, 187.8, 105.6, 203, 63.4, 115.4,

Evaporation data for Queenstown (no data available for Strahn). Relative estimations of monthly evaporation were based on evaporation and corresponding precipitation data from Queenstown.

The data are for the following stations:
Number , Name , Latitude , Longitude ,Elevation, Opened on , Closed on , Locality
097034 , Queenstown (7XS) , 42°05'48"S , 145°32'41"E , 129.0m , 1964-01-01 , 1995-04-30 , Queenstown

==========

Stn_Num,Year,NameAndUnit,Jan,Feb,Mar,Apr,May,Jun,Jul,Aug,Sep,Oct,Nov,Dec,Ann
97034,1967,Total Monthly Evaporation (mm),114.7,,,45,,24,18.6,27.9,54,74.4,81,114.7,
97034,1968,Total Monthly Evaporation (mm),142.6,110.2,77.5,36,24.8,21,24.8,31,42,58.9,60,127.1,755.9
97034,1969,Total Monthly Evaporation (mm),117.8,109.2,65.1,45,34.1,24,,34.1,36,,96,74.4,
97034,1970,Total Monthly Evaporation (mm),,,,,,,,,,102,89.9,
97034,1971,Total Monthly Evaporation (mm),,128.8,96.1,42,,27,24.8,37.2,42,68.2,87,114.7,
97034,1972,Total Monthly Evaporation (mm),136.4,110.2,96.1,48,34.1,24,,46.5,42,74.4,105,108.5,
97034,1973,Total Monthly Evaporation (mm),114.7,109.2,80.6,42,,,24.8,43.4,48,83.7,99,124,
97034,1974,Total Monthly Evaporation (mm),139.5,120.4,89.9,54,31,36,40.3,40.3,,77.5,84,,
97034,1975,Total Monthly Evaporation (mm),,114.8,,,,24,9.3,9.3,,55.8,57,96.1,
97034,1976,Total Monthly Evaporation (mm),93,,,,,,,,49.6,96,,
97034,1977,Total Monthly Evaporation (mm),,89.6,77.5,39,,15,15.5,,33,65.1,54,74.4,
97034,1978,Total Monthly Evaporation (mm),89.9,86.8,68.2,33,27.9,18,18.6,31,48,55.8,72,58.9,608.1
97034,1979,Total Monthly Evaporation (mm),89.9,81.2,68.2,,31,18,24.8,31,33,68.2,81,80.6,
97034,1980,Total Monthly Evaporation (mm),89.9,66.7,46.5,42,27.9,18,21.7,37.2,45,62,69,111.6,637.5

97034,1981,Total Monthly Evaporation (mm),127.1,98,58.9,39,21.7,27,18.6,24.8,39,58.9,90,93,696
97034,1982,Total Monthly Evaporation (mm),108.5,84,58.9,27,24.8,15,12.4,31,45,49.6,63,93,612.2
97034,1983,Total Monthly Evaporation (mm),74.4,81.2,46.5,33,37.2,,18.6,34.1,57,55.8,87,99.2,
97034,Highest,Total Monthly Evaporation (mm),142.6,128.8,96.1,54,37.2,36,40.3,46.5,57,83.7,105,127.1,755.9
97034,Lowest,Total Monthly Evaporation (mm),74.4,66.7,46.5,27,21.7,15,9.3,9.3,33,49.6,54,58.9,608.1
97034,Mean,Total Monthly Evaporation (mm),110.6,99.3,71.5,40.4,29.4,22.4,21,32.8,43.4,63.9,81.4,97.3,661.9
97034,Median,Total Monthly Evaporation (mm),114.7,103.6,68.2,42,29.4,24,18.6,32.5,42,62,84,96.1,637.5
97034,Number of Obs,Total Monthly Evaporation (mm),13,14,13,13,10,13,13,14,13,15,17,15,5

Precipitation data for Queenstown

97034,1967,Total Monthly Precipitation
(mm),127.9,73.9,129.4,184.8,89.4,143.8,177.5,197.5,200.8,139.2,194.8,205,1864
97034,1968,Total Monthly Precipitation
(mm),75.9,181.6,118.9,251.4,436.9,347.2,250.4,357.3,286.4,369,403.3,114.9,3193.2
97034,1969,Total Monthly Precipitation
(mm),185.5,208.1,153.1,250.7,200.1,171,275.2,268.4,276.8,81.3,105.4,211.1,2386.7
97034,1970,Total Monthly Precipitation
(mm),76.5,72.7,91.4,265.9,247.7,122.2,510.1,430.3,279.6,237.8,65.9,184.1,2584.2
97034,1971,Total Monthly Precipitation
(mm),104.1,97,66.9,240,266.9,342.6,153.5,307.8,270,372.6,193.4,126.4,2541.2
97034,1972,Total Monthly Precipitation
(mm),94.2,89.9,146.8,219.6,140.1,161.5,466.1,217.3,293.4,116.2,96.7,162.8,2204.6
97034,1973,Total Monthly Precipitation
(mm),181.1,132.8,210.2,254.4,442.1,222.3,168.7,205.4,319.1,166.6,221.5,208.8,2733
97034,1974,Total Monthly Precipitation
(mm),98.5,125.4,78.9,162.2,51.4,222.5,288.8,275.8,344.7,136.8,110.3,327.6,2222.9
97034,1975,Total Monthly Precipitation
(mm),174.6,32,242.1,189.6,405.4,275.9,371.2,230.7,159.3,176,268.3,75.8,2600.9
97034,1976,Total Monthly Precipitation
(mm),130.7,43,138.2,214,323.1,235.9,227.8,253.3,98.9,143.5,136,359.5,2303.9
97034,1977,Total Monthly Precipitation
(mm),149.6,51.4,231.2,326.7,258.4,186.3,261.6,241,76.8,248,212.6,201.2,2444.8
97034,1978,Total Monthly Precipitation
(mm),82,131.2,63.2,201.7,182.8,60.2,348.6,300,136,210.2,238.2,162.6,2116.7
97034,1979,Total Monthly Precipitation
(mm),111.5,151.2,100,223.4,182,159.6,290,305.4,285.4,205,127.8,321.6,2462.9
97034,1980,Total Monthly Precipitation
(mm),158.8,123.6,200,244.4,230.8,182.6,267.2,368.6,553.8,217.8,133.8,37.8,2719.2
97034,1981,Total Monthly Precipitation
(mm),45,44.2,193.4,367.6,150,165,322.4,271.4,260.6,181.6,195.8,105.2,2302.2
97034,1982,Total Monthly Precipitation
(mm),112.4,88.8,177.6,157.4,397.2,156.2,116.4,156.4,252.2,203.8,195.8,111,2125.2
97034,1983,Total Monthly Precipitation
(mm),208.5,50.2,135.3,156.7,193.2,305.1,111.5,225,286,113.1,239.3,70.7,2094.6

Appendix 7

Resistivity principles

A current is injected directly into the ground with two current electrodes. The voltage, which is produced by the current, is measured between two other electrodes, referred to as potential electrodes. By dividing the voltage by the current the resistance is determined. Although resistivity will be constant for the same material, the geometry of the configuration must be considered. Hence, the formula becomes R= (x/A) where R is the resistance, is the resistivity which is the resistance of a cubed unit to current flowing between opposite faces, x is the distance the current must flow and A is the cross sectional area. The resistance is then converted to an apparent value by multiplying with a geometric factor, which is a function of the electrode geometry. This equates to V = I/ 2≠a for the electric potential at a distance (a) from a point electrode at the surface of a uniform half space (assumes homogeneous material) and I is the current. In a four electrode survey over homogenous ground a is (1/Pp-1/Np-1/Pn+1/Nn). Wenner arrays have equal distance electrode spacing e.g. Pp = a, Pn=2a, Np= 2a, Nn=a, hence, the formula reads =2≠aV/I. (figure A.4.1). A series of measurements taken at the one location with systematical increases in the spacing between the electrodes. As the separation increases so does the depth of investigation (figure A.4.2), (Telford *et al.*, 1998, Milsom, 1996).

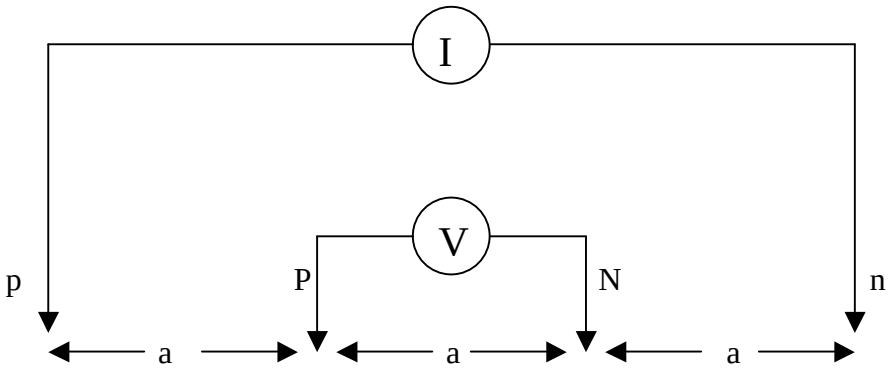

Figure A.4.1 Wenner array configuration

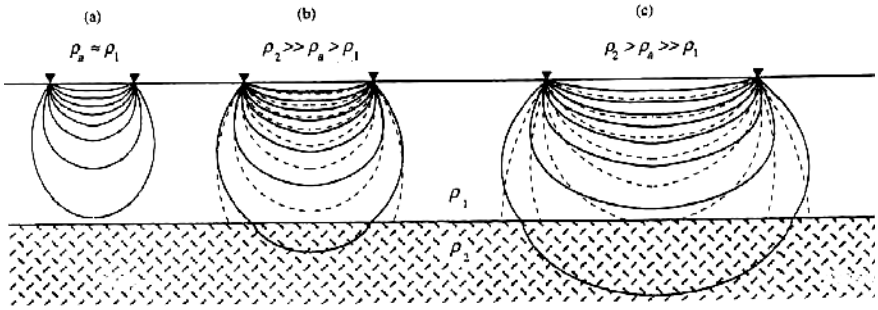

$P_2 > P_1$

current flow line – homogenous subsurface

current flow line – horizontal interface

Figure A.4.2. Depth of penetration increases with increased spacing.

Appendix 7.1

Resistivities of various rocks

Rock Type	Resistivity Range (ohm .m)
Gabbro	10^3 - 10^6
Wet dacite	2x 10^4
Hornfels	8 x 10^3 (wet) 6 x 10^7 (dry)
Tuffs	2 x 10^3 (wet) 10^5 (dry)
Quartzite	10 - 2 x 10^8
Clays	1 – 100
Schist	20 - 10^4
Sandstone	1 –6.4 x 10^8
Consolidated shale	20 – 2 x 10^3
Basalt	10 – 1.3 x 10^7
Lavas	10^2 - 5 x 10^4
Conglomerate	2 x 10^3 – 10^4
*Medium grained sandstone with 1% water	4.2 x 10^3
*Medium grained sandstone with 0.1% water	1.4 x 10^8
*Siltstone with 0.54 % water	1.5 x 10^4
*Siltstone with 0.38% water	5.6 x 10^8
*Coarse grained sandstone with 0.39% water	9.6 x 10^5
*Coarse grained sandstone with 0.18 water	10^8

A comparison of these figures indicates that a slight change in water percentage greatly affects the resistivity. Table adapted from Telford *et al.*, 1998).

Appendix 8

The Electromagnetic Principle

EM methods invlove the induction of low-frequency EM fields in the subsurface. A looped current-carring wire induces an artificial magnetic field that can be varied by alternating the current (frequency domain EM; FEM) or terminating the current (time domain EM; TEM). Both methods are based on the principle that the time-varying current is applied to a transmitter (Tx) that creates a magnetic field. The changes in magnetic field induce secondary (eddy) current in the subsurface conductors according to Faraday's law. Theses secondary currents produce their own secondary magnetic field dependent on operating freqency and terrain conductivity (figure A.4.3). In FEM, the current is typically sinusoidal with a given frequency. The Tx current is always on and therefore measurements are always made in the presence of a primary field. The secondary magnetic field is of interest as it is caused by currents passing through the conductor containing information about the geometry and conductivity of the target. The Rx records the total field and hence, to find the secondary field, the primary field must be subtracted from the total field. The secondary field has a different amplitude to the primary field and has components both in-phase and out-of-phase with the transmitted primary field (figure A.4.4). Transient systems (TEM) provide multiple frequency data by inducing a secondary current flow in a conductor by turning the current off at the transmitter. These secondary currents decay with time (resistive material decays faster) and as a primary magnetic field is not present the secondary magnetic induction (dB^s/dt) associated with the decaying currents is measured at the receiver coil (Telford *et al.*, 1998, Milsom, 1996).

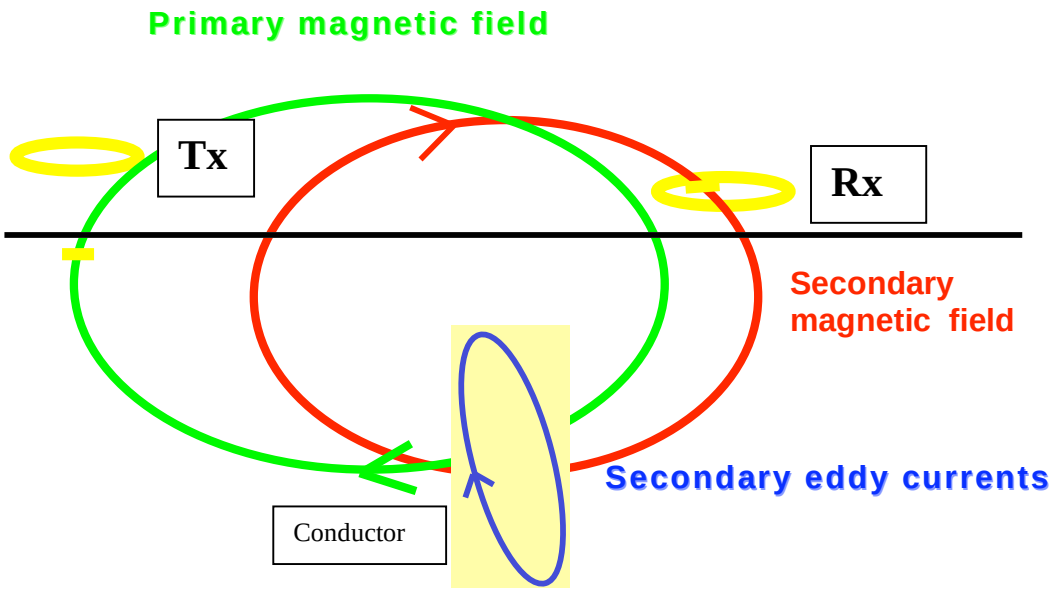

Figure A.4.3 The electromagnetic principle

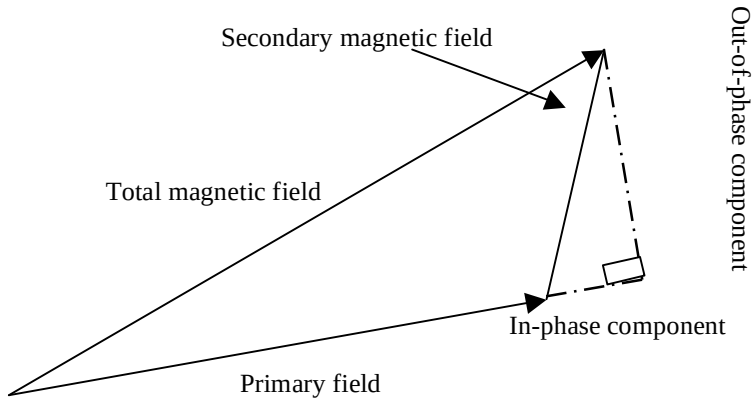

Figure A.4.4 Relationship between primary magnetic field and the two components of secondary field. The in-phase component is 180 degrees out of phase with the primary magnetic field and the quadrature response (in-phase) is 90 degrees out of phase with primary field. Ried, per.com.

Appendix 9

The following table illustrates the electrical conductivity of groundwater at different depths measured by a probe on the 24/7/2000. The deeper piezometers are highlighted. Electrical conductivity (EC) seems to increase with depth. However, by comparing the deep piezometers, no spatial distribution of EC is evident.

Piezometer	Easting	Southing	C	Depth (cm)
1	70	32	380	1.888
2	80	43.7	178	0.908
3	80	30.7	154	1.054
4	120	48	123	0.456
5	120	38	123.2	1.014
6	120	19.3	541	1.423
7	140	40	306	0.8
8	141	40	302	1.28
9	180	40	695	0.463
10	180	20	706	2.322
11	180	6	400	1.916
12	240	46.1	219	0.5
13	241	46.1	187.4	0.7
14	240	37.7	566	0.548
15	240	17.7	295	1.35
16	241	17.7	598	1.998
17	240	4.2	527	2.556
18	241	4.2	717	1.71
19	300	48	98	0.802
20	299	29	397	2.316
21	300	29	558	1.867
22	301	29	615	1.43
23	300	14	310	1.019
24	360	48	102	0.53
25	360	39	195.8	1.008
26	360	18	440	1.366
27	450	45	395	1.598
28	450	40	158	1.91
surface	240	40	563	

Appendix 10

Each of these diagrams shows a calculated Sligram apparant conductivity vs depth curve (dashed lines) over different theoretical layer earth models (solid lines). These diagrames illustrate that in the presence of a conductive or resistive layer, the apparent conductivity-depth curve tends to over-estimate the depth to the overburden /basement boundary (Reid and Fullagar, 1998). This method of Reid and Fullagar is approximate, hence pseudosection depths are not exact.

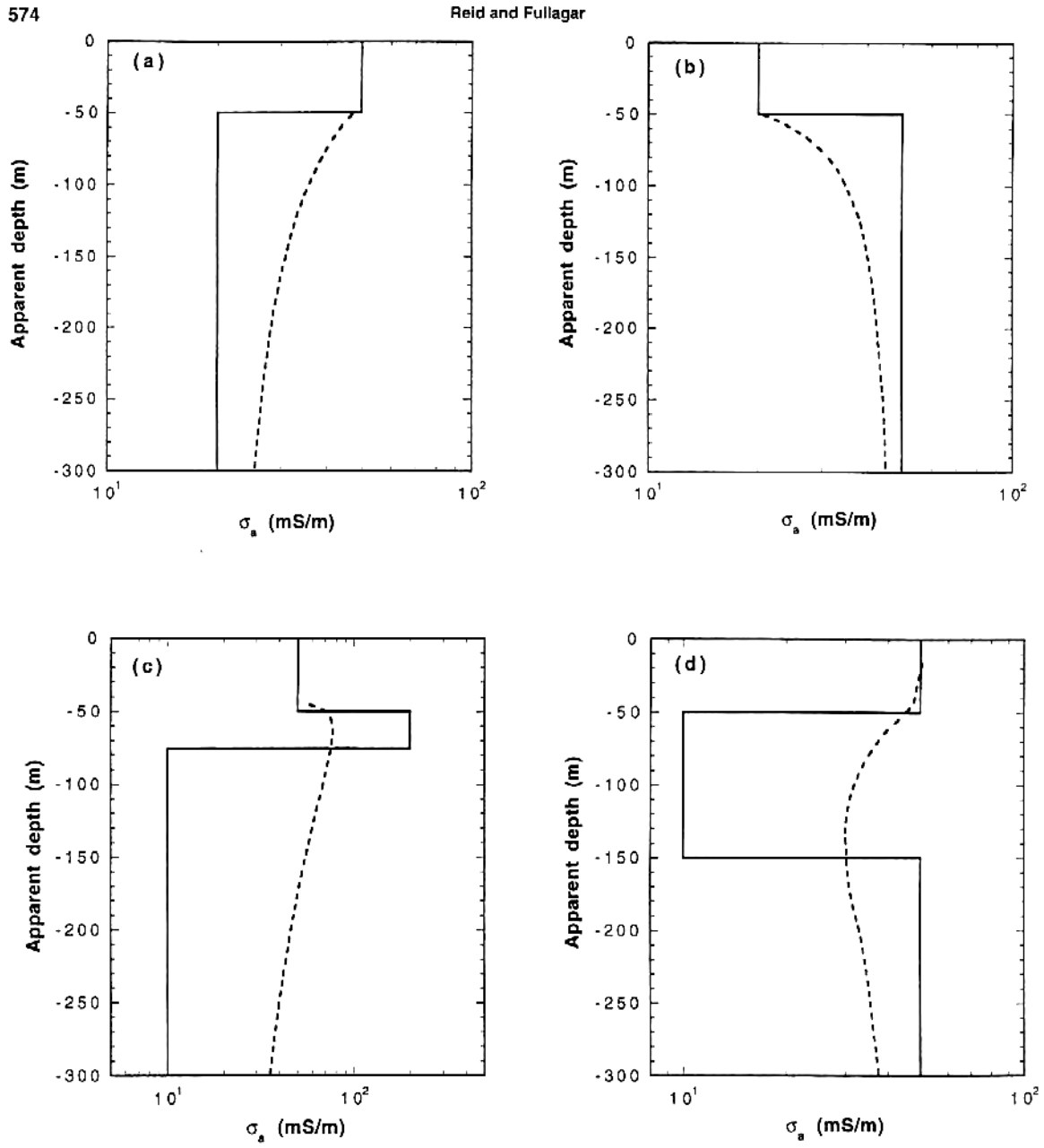

Appendix 11

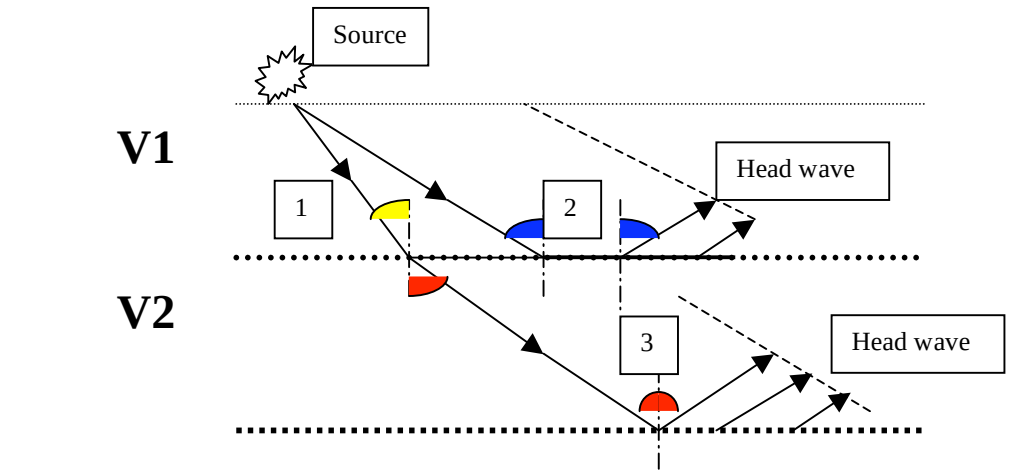

If V_2 is greater than V_1 refraction will be towards the interface (1), sin i= V_1/V_3. If sin $i_c = V_1/V_2$ the ray will be refracted parallel to the interface at velocity V_2 and some of the energy will return to the surface as a head wave which leaves the interface at the original angle of incidence (2). The head wave travel through the upper layer at V_1 but appears to move across the ground at V_2 velocity because of its inclination. Hence, it will take over the direct wave, despite the longer travel path. The third example is where sin r = V_2/V_3.

A seismic wave transmits acoustic energy by vibrations of rock particles. The sound waves are generated at a source and penetrate through the ground. When a seismic wave encounters an interface between two different velocity materials, a portion of the energy will be reflected and the remainder will be refracted at a different angle as it continues through the second material. Refraction is governed by Snell's Law, which relates the angle of incidence and refraction to the seismic velocities in the two materials; sin i /sin r = V_1/V_2.

The interfaces should be shallow, roughly planar and the dip should not exceed 15^o. The velocities must also increase at depth at each interface (acoustic energy travels faster in denser or elastic material). As a result the first arrivals at the surface will come from successively deeper interfaces as the distance from the shot point increases. Plotting of a known array of detectors (geophones) and the time for energy to reach them from the sounding event, yields an estimate of velocities along that path. A refraction in the plot represents an increase in velocity within the refractor. Since D (geometry of the vectors) and T are known, V is an

absolute. Thus, only the geometry of the layers needs to be interpreted. Milsom, 1996 Leman, 1997, Telford *et al.*, 1998)

Appendix 11.1

		Time(ms)			
Geophone	**Spacing**	**6mE**	**50mE**	**5mW**	**50mW**
1	0	22.5	73.5	105	95
2	5	33.5	75		85
3	10	40	81	52.5	81
4	15	49	88.5	48.5	80
5	20	52	93.5	46	76
6	25			41	71
7	30	52		32.5	65
8	35	53		27.5	60
9	40	64		27.5	56
10	45			19	51
11	50			17	46
12	55			8.5	45

First picked arrival times (ms)

Physical hydrogeological processes and factors influencing transport of contaminants from mine tailing impoundments.

Kate Polglase

Literature Review

School of Earth Sciences

University of Tasmania

July, 2000

Abstract

The direction and the rate of groundwater movement and the distribution of recharge and discharge areas are important aspects of groundwater flow systems in tailings impoundments and surrounding geological material. They are governed by factors such as the construction, management and placement of the impoundment, sedimentary and sorting of the tailings, surrounding rock types, local topography and climate. Several of these factors have characteristic hydraulic conductivities, which when combined with factors such as climate, rock type, topography or digenesis, will determine the potential flow regime. As these factors vary in different environments, the hydrogeology of tailing impoundments and the surrounding rock is site specific. However, because similarities can exist between sites, the knowledge gained from a particular study can be applied to other scenarios.

Chapter 1:Introduction

Contamination resulting from mine tailings is a serious threat to groundwater resources. Abundant literature is available on the processes and factors that control contamination transport. The aim of this literature review is to present an overview of parameters that influence groundwater contamination at mine tailings impoundments, and transport of contaminants from the site.

The hydrogeology of tailing impoundments is crucial as the watertable configuration will influence the quantity of acid mine drainage generated. The water table depth in a decommissioned tailings impoundment not only depends upon the physical properties of an impoundment, such as geometry, thickness, depositional mode, and tailings and dam permeability, but also on the rate of water table recharge (Robertson, 1994).

If there is no breach or leakage from the impoundment, then groundwater contamination is not an issue. However, even with well-constructed tailings impoundments and mitigation strategies, a portion of contaminated water is expected to reach the underlying material. Methods of minimising contamination transport are therefore the focus of most research activities, rather than unrealistic methods of attempting to eradicate the problem altogether.

The two principal methods of contamination dispersal away from an impoundment are surface water runoff and groundwater seepage through the base of the impoundment (Blowes et al., 1987). If overland flow is the main source of discharge, then it is assumed that the contamination at the surface will be leached out over a short period, and with time, water quality would improve. On this basis, subsurface flow is arguably the longer term environmental risk, and is thus the focus of this paper.

If there is leakage from an impoundment, then solute transport has to be monitored. For this reason, there needs to be an understanding of the physical factors that affect how rates and flow directions away from the site change. This includes the depositional environment, diagenesis, weathering, fracturing, topography and climatic effects.

Before the effect of each of these can be quantified and the tailings impoundment understood, an understanding of detailed features such as porosity and permeability is required, as these parameters control the groundwater paths and flow rates. In addition, the physical processes that affect contamination movement must be considered.

Chapter 2: Parameter controls on flow direction and velocity

2.1 Porosity

Porosity simply refers to a solid that contains pore space. It measures how much water a rock contains. Total porosity is the percentage of total pore space volume. Effective porosity refers to the interconnected pore space volume, which dictates the permeability of a rock (Domenico and Schwartz 1990). As Table 1.1 illustrates, a rock can have a high total porosity but a low Effective Porosity, the two may differ by as much as one order of magnitude (Domenico and Schwartz 1990). Effective porosity can be calculated using the following equation;

$$n_e = \frac{V_e}{V_t} \qquad (1)$$

Where n_e is effective porosity, V_e is total volume of interconnected pore space, and V_t is total volume of rock.

Porosity may either be generated by primary and/or secondary processes. In sediments, primary refers to interstitial porosity, which includes factors such as sorting, grain size, shape, arrangement and packing styles, whether the pebbles themselves are porous or if minerals have precipitated in the interstices (Domenico and Schwartz 1990). Secondary porosity occurs due to post depositional fracturing or dissolution (Domenico and Schwartz 1990). Consequently, the porosity of a rock depends on primary characteristics and diagenetic processes that have latter affected the rock.

Rock type	Porosity	Effective porosity
Fractured schist at Jabiluka.	2-10%	0.5 – 5%
Weathered rock at Jabiluka.	35%	Up to 10%
Sandstone	5-15%	0.5 –10%
Shale	1-10%	0.5- 5%
Limestone, dolomite	0-40%	0.1-5%
Anhydrite	0.5-5%	0.05-0.5%
Granite	0.1%	0.00005%

Table 1.1 Variations between total porosity and effective porosity for different material. Data from (Kaft & Dudgen,1999; Domenico et al, 1990).

1.2 Permeability

Permeability (length^2) is the intrinsic property of a porous rock that quantifies the effort required for fluid to pass through. This property is a function of pore spaces, grain boundaries of the bulk material, microcracks, as well as more widely spaced fractures. The importance of each factor depends upon the rock type. For example, in tailing impoundments, flow through pore spaces dominates, whereas for relatively non-porous igneous rocks, fluid generally passes through cracks, fractures and fissures (Oelkers, 1996). Permeability is not solely dependent upon porosity, but also increases with increasing particle size, particle size homogeneity and decreasing intergranular volume surface area (Oelkers, 1996).

Hydraulic conductivity (K), differs in the sense that it also considers the density and viscosity of the fluid, as the following equation illustrates (Robertson, 1994; Oelkers, 1996):

$$K = \frac{k\,g}{\quad}$$

Where K is hydraulic conductivity (m/s), is fluid viscosity, k is permeability, g is gravitational constant and is the fluid density.

The kinematic viscosity of the fluid (v) is the dynamic viscosity ( ), divided by the fluid density ( ) (Oelkers, 1996). Thus, the relationship between hydraulic conductivity and permeability can be simplified to; $K = \frac{kg}{v}$

As mine tailings impoundment research is only concerned with one type of near-isothermal flowing fluid, K values are preferred to permeability (Oelkers, 1996). In addition, the fluid properties may be affected by the composition and nature of the dissolved contaminants. For example, solutes containing acid and metals may have different fluid densities and viscosities in comparison to uncontaminated water. Flow in natural porous media is generally slow (Oelkers 1996) and can be measured by applying Darcy's Law:

$$q = -K\Delta h$$

where q is Darcy flux (specific discharge) and Δ h is the hydraulic gradient. Hence, for a given hydraulic gradient, the quantity of the fluid flow is directly proportional to its hydraulic conductivity (Oelkers).

or as we can now expand K:

$$q = \frac{-kg}{v}\ \Delta\ h$$

However, if the flow is rapid, it becomes turbulent with a non-linear function of hydraulic gradient. Oelkers (1996) suggested that the flow rate at which the flow begins to deviate from Darcy's law is when the Reynolds number for fluid flow (Re) exceeds 2200. Re is defined as:

$$\mathrm{Re} = \frac{2rq}{v}$$

where r is the radius of the grain in the porous media.

There are a number of methods and corresponding formulae available that determine permeability and hydraulic conductivity (Appendix A).

Chapter 3: Physical hydrogeology of mine tailings impoundment

Oxidation of sulphide minerals in the near surface can result from infiltration of air and surface water in the vadose zone where oxygen diffusion is rapid (Al and Blowes, 1996). As tailings are fine-grained, not only is the water content in the vadose zone likely to be high, but also the zone of tension saturation (capillary fringe) may extend several to tens of metres above the water table (Gillham, 1984; Appendix B). The extent of the capillary fringe is dependent upon the texture and structure of the material. For coarse sand, the zone of saturation may only be a few cm above the watertable (Blowes and Gillham, 1988). The subsequent oxidation of Fe^{2+} to Fe^{3+} ions, followed by hydrolysis, and the precipitation of Fe^{3+} as ferric hydroxides or ferric oxyhydroxides-sulphates, results in increased acidic waters. This in turn exacerbates mobility of metal ions and radionuclides to the infiltrating water (Al and Blowes, 1996). As saturation increases, the rate of diffusion of atmospheric oxygen through porous media can decrease by at least three orders of magnitude (Ritchie, 1994). Thus, it is desirable to maintain high water table levels in talings impoundments. Present methods of achieving this include a) construction of impermeable dams, b) use of impermeable liners and c) preference for disposal sites in which shallow water table depths can be easily maintained (such as lake basins; Robertson, 1994). A forth method is the addition of artificial recharge at high evaporation sites. The first two also act to inhibit solute migration away from the site.

3.1 What are mine tailings?

Mine tailings are the non-economic crushed mineral fraction that is separated during ore processing. Extraction techniques, such as gravitational settling, chemical leaching or surfactant-enhanced flotation, require the ore to be ground to silt and sand size particles. Large volumes are generated, because non-economic minerals can constitute more than 90% of all constituents in base metal and precious metal ores (Al and Blowes, 1999; Robertson, 1994).

3.2 Physical properties of impoundments

Tailings can have a wide range of grainsizes, and can be deposited using a variety of methods. Tailings from base-metal mines are commonly transported as thickened sediment-water slurry containing 20-40wt% of solids to an impoundment constructed close to the mill. Particles will settle out of the slurry when they are discharged to the impoundment, and gravitational settlings will most strongly affect the stratigraphy (Robertson 1994).

Hydraulic sorting results in two different but equally prevalent types of depositional environments. A subaerial beach extends from the spigotting (discharge) point for tens of metres. Accordingly, the sediments are characteristic of high-energy fluvial deposits (fine to medium sand) and thus have high K values. Deposition of the coarser sediment occurs along the banks and bed of the stream. This gradually increases elevation of the streambed until breaching resulting in new channel development (Robertson 1994). Finer grained silt tailings are retained in the slurry in the higher energy zone. Such sediment will only be deposited when the subaerial tailing stream discharges into pooled water, creating a lower energy environment (lacustrine deposit). As a result, such sediments are characterised by low hydraulic conductivities. When the spigotting point is periodically moved, the position of the beach and pond perimeters change, thus an impoundment shows sedimentary anisotropy and heterogeneity (Robertson 1994). Moving the spigotting point supplies fresh tailings to certain areas, which controls where oxidation is likely to occur after emplacement ceases (Sevick et al, 1998).

The majority of North American sites discharge low-density (10-20% wt solid) slurries from spigots located around perimeter contaminated dykes (Al and Blowes, 1999). Because of the position of the spigotting points, the deposit has a coarsening of grainsize towards to periphery (Robertson, 1994) and results in the formation of a shallow basin deposit surrounded by elevated contaminated banks. The height of the banks causes mill discharge water and surface precipitation to pond in the shallow basin centre of the impoundment. This water is either a) lost by evapo-transpiration, b) taken away for milling, or c) migrates as groundwater flow towards the perimeter of the impoundment (Al and Blowes, 1999). Copper Cliff, Ontario, (Canada) is an example of slurried tailings with large K ranges of more than 3 orders of magnitude (Robertson, 1994; Figure 3.1).

A more effective approach than Copper Cliff was adopted at Kidd Creek mine, Ontario. Slurry was discharged from the centre of the impoundment with a lower water content to produce thickened tailings (62 wt.% solid) which increases the viscosity. Central discharge results in the deposit being a cone shaped pile. This causes the centre to be a recharge area and the periphery being discharge areas (Barbour et al, 1993). Thus, elevated peripheral banks are not required and discharge of acidic waters outside the impoundment is minimised. Modelling results suggested that 90% of the total discharge occurs within the impoundment (Al and Blowes, 1999). Thickening inhibits hydraulic sorting and thus results in a more homogeneous deposit (Figure 3.1) and a thick tension saturated zone above the water table. Consequently, O_2 diffusion is reduced (Al and Blowes, 1996; Barbour et al., 1993).

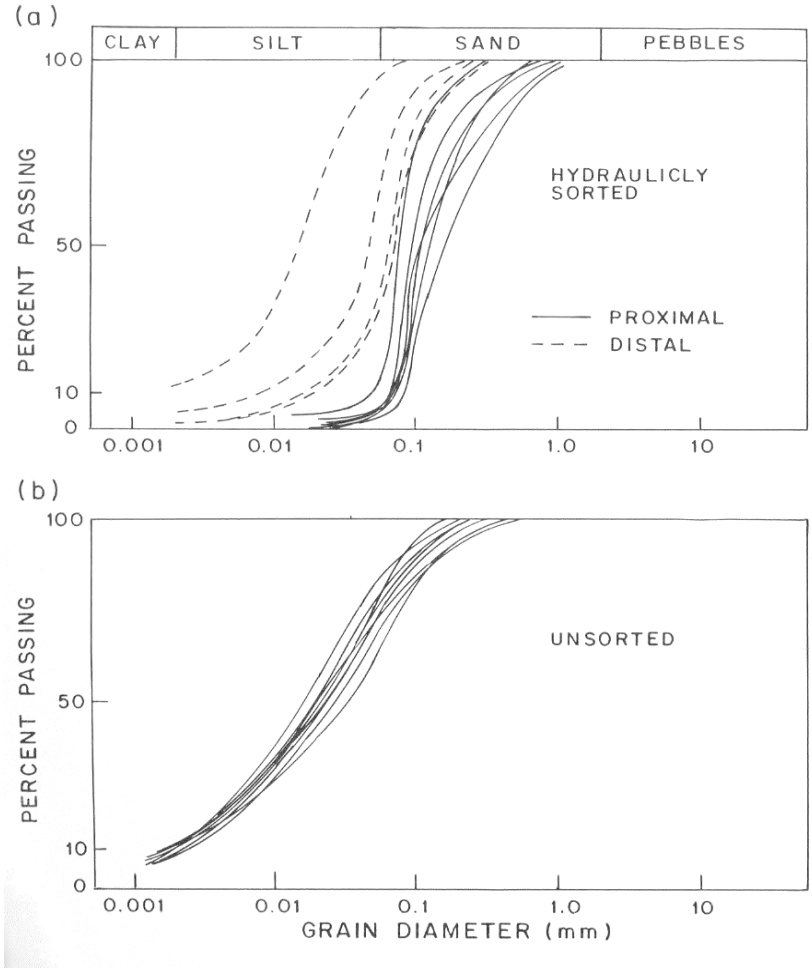

Figure 3.1 A comparison of grain size variability between two impoundments in Ontario. A) Slurried tailings from Cooper Cliff both proximal and distal to the spigotting. B) Thicken tailings from Kidd Creek. (Robinsky in Robertson, 1994).

Central discharging practices resulted in water table levels (with a depth of less than 2 metres) being maintained within 50 metres of the perimeter dam at a gold mine impoundment near Joutel, Quebec (Canada). In contrast, a uranium mill tailing impoundment near Elliott Lake, Ontario, chose to employ spigotting from the south perimeter of the dam. Accordingly, the water table depth is relatively high (less than 2 metres from the surface) in areas of the impoundment where finer grained tailings are present, but depths increase rapidly (up to 10 metres) approaching the low K dam area (Robertson 1994).

Whether impoundments are recharge or discharge areas is not only controlled by the impoundment geometry. During slurry discharge, the deposition of the tailings causes hydraulic loadings that result in downwards hydraulic gradients (Robertson, 1994). Where the

impoundments are placed is also important (in regard to the water table level in relation to the surrounding terrain). A 20–30 metre thick impoundment that is significantly elevated, may result in water levels that are up to 30 metres higher than in the surrounding terrain (Robertson, 1994), and is therefore acting as a potential recharge area. In reversed instances, vertically upward flow paths potentially exist where the water table elevation in the tailings is lower than in the surrounding terrain, and groundwater may migrate from the surrounding terrain into the tailings were aquicludes are absent. An example of such a scenario is when tailings are deposited in lake basins (Robertson, 1994).

It may not always be best practice to deposit tailings in subaqueous environments. Although uranium tailings were initially deposited under subaqueous conditions in a pit at Nabarlek, Queensland, research suggested that radon/radon daughter levels were not a problem in semi-dry operations. At this particular site, this method was more advantageous than subaqueous deposition as it offered a stable long-term storage option during decommissioning and rehabilitation. Hence, the tailings were dewatered and consolidated to allow the placement of geotextile and waste rock covers (Woods, 1989). However, the preferred option for uranium impoundments is to deposit neutralised tailings below the water table. After the pit is filled, a highly permeable envelope surrounds a mass of low K tailings. When regional groundwater levels return to their pre-dewatered condition, this envelope will direct the groundwater flow around the tailings, minimising hydraulic gradients across the impoundment, and therefore the release of contaminants by advection. In the long-term, mass loadings of contaminants released from the impoundment will be low because the tailings are submerged. This not only results in lower O_2 diffusion rates, but also causes molecular diffusion to remains the dominant contaminant transport mechanism which is slow (Donald et al, 1997).

Modelling the feasibility of upland tailing impoundments at Crandon (U.S.A.) also suggests that a dewatered tailings facility with a base liner, a leachate collective system and a dry low K cap can be designed to prevent most groundwater contamination. The leachete system and base liner are important in controlling percolation from the impoundment during dewatering periods. Once semi-dry, infiltration through the cap will control percolation (Sevick et al, 1998).

3.3 Anisotropy of tailing impoundments

Heterogeneity arises due to grainsize and compositional variations, and can cause K to be dependent upon the position within a geological formation. If K does not vary, the formation

is homogeneous. However, Freeze & Cherry (1979), suggest that no impoundment can be strictly homogeneous by true definition, and thus, defined homogeneity as maintaining a mean value of K. Heterogeneity can be expanded to directional K variations, termed anisotropic and isotropic if there is no directional variation (Freeze and Cherry, 1979). Tailing impoundments consist of horizontally stratified heterogenous material, with K values varying by several orders of magnitude over a few metres (Robertson 1994). Hence, determining bulk K is not always easy. Once bulk horizontal K is established, then it can be assumed that each individual layer is homogeneous and isotropic. The situation is then complicated by the fact that the layers themselves vary in K values, (Figure 3.2) so the impoundment acts as a single anisotropic homogeneous layer (Freeze and Cherry, 1979). Freeze and Witherspoon (1967) illustrate the flow regime of this scenario through the use of a two-dimensional flow net (Figure 3.3). Although the purpose of their study was to illustrate regional ground water flow, it can be applied to tailing impoundments where a simple water table configuration is likely (gentle constant watertable slope), such as a 1.5% slope average at Kidd Creek (Barbour et al, 1993). However, in rare situations where the impoundment has a hummocky terrain, as is the case at Copper Cliff impoundment (due to the vegetation cover and sloping terrain's; Coggans et al., 1991, then terrain effects have to be considered (section 4.3).

The bulk horizontal permeability (K_x) and bulk vertical permeability (K_z) can be calculated by the equations in Figure 3.2. By substituting arbitrary numbers for K values, Freeze and Cherry (1979) suggested that the K_x value is mainly controlled by the more permeable layers, whereas vertical K is predominantly influenced by less permeable layers such as clays. In tailing impoundments, the bulk vertical permeability is at least an order of magnitude lower than bulk horizontal permeability (Robertson 1994). Despite the variations of permeabilities within tailing impoundments, Kaft & Dudgen (1999) propose that the overall hydraulic conductivities range from 10^{-2} m/day to 10^{-3} m/day if the effects of overborne pressure are not included.

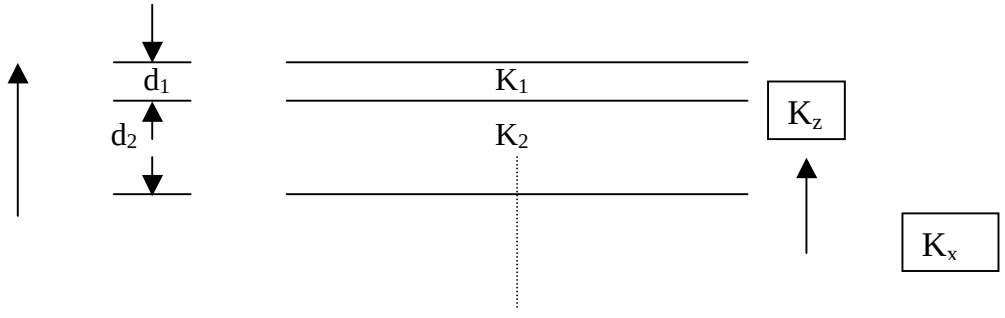

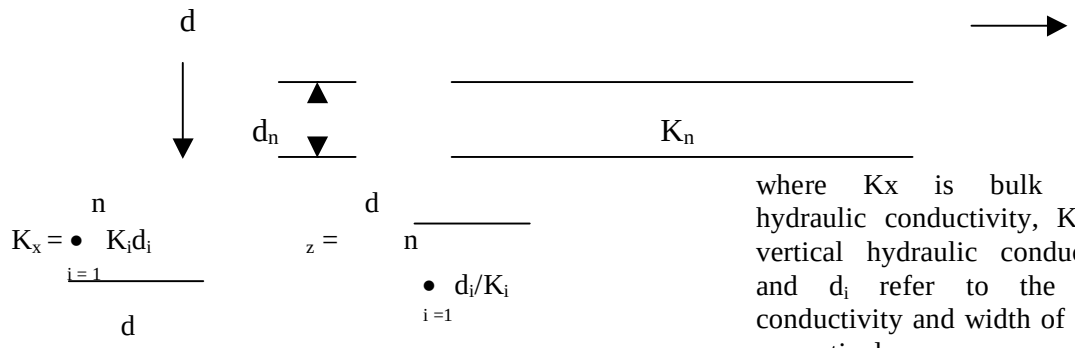

where Kx is bulk horizontal hydraulic conductivity, Kz is bulk vertical hydraulic conductivity, k_i and d_i refer to the hydraulic conductivity and width of each layer respectively.

Figure 3.2. Calculations of bulk vertical hydraulic conductivity (Kz) and bulk horizontal hydraulic conductivity (Kx) at a tailing impoundment.

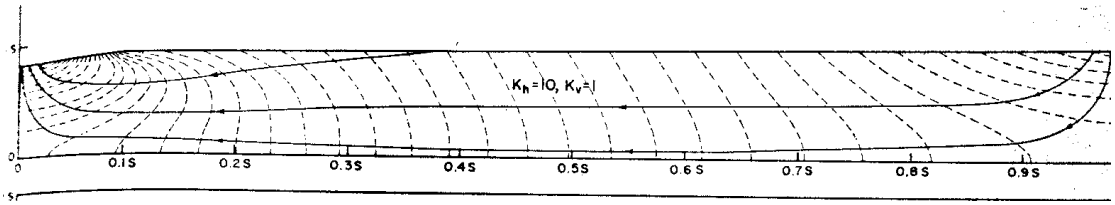

Figure 3.3 Flow regime where K_x is 10 times K_z.

3.4 Infiltration

The tailings flow system and the quantity of acid mine drainage generated are predominantly controlled by the rate of recharge on the tailings surface (Robertson 1994); precipitation, surface water runoff, and infiltration capacity control recharge.

In terms of infiltration into the subsurface, interflow and groundwater recharge are important (Appendix C). In regions of high precipitation, the intermediate zone, where interflow operates, may be absent, and moisture moves directly to groundwater recharge. Although water may first infiltrate readily, the rate will decrease with time (Domenico and Schwartz, 1990). When evapotranspiration equals precipitation, water infiltrates into soils, but will not proceed to groundwater recharge (Domenico and Schwartz, 1990). Hence, it is only when precipitation is greater than evapotranspiration that surface water will recharge ground water. Accordingly, temperature and dry windy climates must also be considered. Al and Blowes (1999) observed from hydraulic gradients at Kidd Creek, that it is possible that the water table level, the tailings moisture content and hence the unsaturated zone is dominantly controlling evaporation losses from the vadose zone. At Copper Cliff, the average annual infiltration rate through the tailings is 0.28m/a, which equates to approximately 30% of annual precipitation. The presence of vegetation had no effect on precipitation recharge to the water table.

However, there may be seasonal differences, with recharge in the summer months areas devoid of vegetation, whereas in the same months evapotranspiration reduces the flux of precipitation to the water table at the vegetated site (Coggans et al, 1991).

Surface runoff may be derived from springs (Ritchie 1994) or contaminated water from slagheaps (Taylor, 1998). Despite surface recharge being important, recharge to the water table can also come from other sources, such as fractures or lithological units beneath the tailings or slag heaps where upward flow occurs (Taylor, 1998).

Freeze (1983) suggests that if a water table does not rise in response to a high precipitation period (where precipitation is greater than evapotranspiration), then it is possible that an upper confining layer exists (aquitard). This leads to the formation of a saturated lens with unsaturated conditions above (Freeze and Cherry, 1979). Another possibility is that naturally formed cemented hardpans derived from sulphide oxidation, prevent infiltration, consequently resulting in perched water tables (Taylor 1998). The design of chemical caps and capillary barriers is based on this theory. Covering tailings piles with limestone forms a chemical cap, which operates during rainfall, because the lime reacts with the acidic tailings resulting in the precipitation of hardpans (Chermak, 1995). A capillary barrier involves a saturated fine-grained soil layer (low K) on top of a coarse-grained layer. The coarse layer drains to residual saturation where suction develops. This results in the coarse layer having a low K. Therefore, not being able to transmit much moisture downwards from the overlying fine layer and also prevents the fine layer from draining, which means the clay retains a high degree of saturation. It was determined that percolation increases with K saturation values greater than 1 x 10^{-7} cm/s (Woyshner and Yangful, 1995).

Despite it being desirable to maintain high water table levels in tailings impoundments, a downfall is that because of the high levels of tension saturation in the vadose zone (combined with evaporation at the surface), upward transport of solute from pore water is encouraged. In turn, an increase in contamination of overland flow results due to the increased contribution of tailings pore water to surface runoff (Al and Blowes 1999; Blowes and Gilham, 1988). Al and Blowes (1996) suggested that the maximum fraction of tailings pore water contributions to storm overland flow is 22-65%.

Chapter 4: Factors affecting groundwater flow away from tailing impoundments

All the principles mentioned in the previous chapters apply to factors that influence the flow paths and rates of groundwater as it migrates away from impoundments. The difference between groundwater migration through an impoundment to flow away from the site is the environment that the solute migrates through. Depending upon various combinations of the physical factors in an environment, the solute path, velocity and solute concentrations will be affected.

4.1 Climatic Effects

When dealing with solute transport away from an impoundment, it is important to consider the water table recharge to the area where the solute is travelling, as additional water will aid in diluting the contamination. An example of this is at Jabiluka, where high rainfall flushing events result in low concentrations of radionuclides in the groundwater compared to sites in other parts of Australia and the US (Kalf & Dungeon, 1999).

4.2 Soil and Rock Types

Soil coverage, and rock type, control whether the infiltrating solution will become part of the interflow or groundwater recharge component. If the soils are thin and the underlying rock is impervious, then the interflow component dominates. Correspondingly, if the soils are thick and the rock is more permeable, then downward migration dominates and soil moisture is more likely to recharges aquifers (Domenico and Schwartz, 1990).

Variations in permeability affect fluid movement within a tailing impoundment, which is also a factor influencing flow directions away from the site. However, in this environment, many more permeability combinations are possible, hence, numerous flow regimes are possible. Appendix D lists possible sedimentary environments and different rock types with their corresponding permeabilities and common the common scenarios are discussed here. In a two-layer scenario, where the underlying layer has a permeability 10 times that of the overlying beds, the lower aquifer allows essentially horizontal flow that is being recharged from above. As a result, the vertical component in the upper more confining units is enhanced compared to what it would be if the unit was homogeneous (Figure 4.1a and b). As the permeability ratio increases, the effects are exacerbated. Vertical upward or downward flow through the overlying layer becomes more evident and the horizontal gradient in the

underlying aquifer decreases. However, because of the increase in the number of flow-lines that enter the aquifer, the quantity of flow increases. This creates a larger discharge area (Figure 4.1 c). Freeze and Witherspoon (1967) suggested that the thickness of the basal aquifer has little effect on the nature of the flow pattern. However, the quantity of water flowing through the system would be greater in the case with the thinner upper lower K unit.

It is interesting to note that in the reverse geologic configuration (where the upper layer has a higher K value than the lower more impermeable layer), the flow pattern mirrors that of the homogeneous case (Figure 4.1 a). Again the quantity of flow would be different in each case. The same principles apply to cases where the aquifer is laterally discontinuous. Different flow regimes will result, dependent on the location of the aquifers. Figure 4.1 d shows one particular scenario where the presence of a discontinuous partial basal aquifer lens in the upstream part of a flat terrain results in the majority of the flow being discharged in the middle, and also into a second basin downstream.

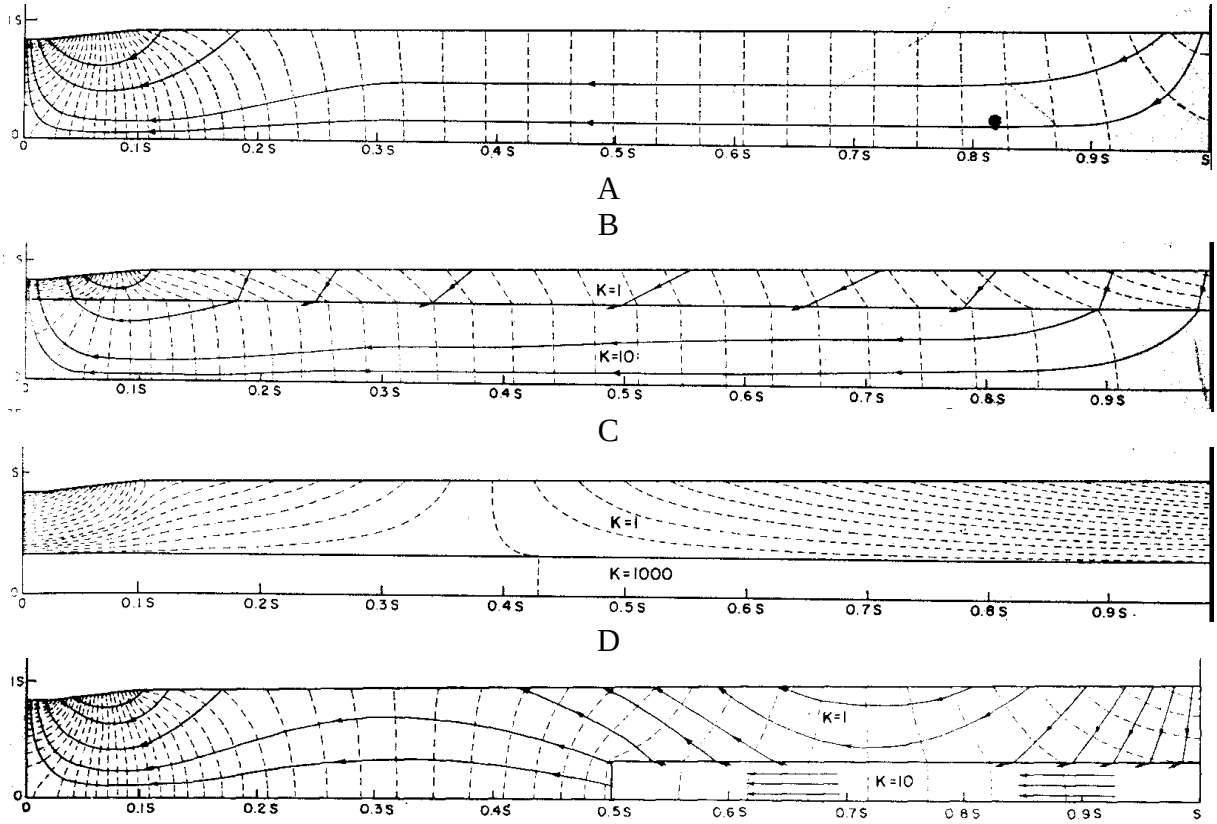

Figure 4.1. Four possible regional flow regimes showing the effect of permeability contrast in adjacent layers (B and C) and the effects of a high permeability lens in the upstream base of the region (D). (A) a simple water-table slope through homogenous medium.

4.3 Terrain effects

The effect of water table configurations on groundwater flow patterns also depends upon topography (Freeze and Witherspoon, 1967). When the topography mirrors a gentle constant regional slope over a homogeneous media, the flow is predominantly horizontal. When there is a major valley, the hinge line is mid-way up the steep valley. Although recharge occurs over the entire upland area, it is concentrated at the upstream end of the recharge area and at the break in slope above the steep valley flank. In contrasts, where a hummocky watertable configuration exists, numerous sub-basins result. Figure 4.2 a illustrates all three scenarios.

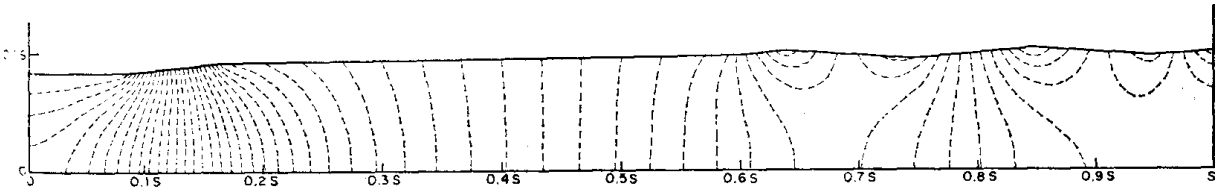

Figure 4.2(a). A hummocky water table in the upstream end of the region, an area of constant slope in the middle and major valley downstream (Freeze and Witherspoon, 1967).

When the watertable has a hummocky surface and a basal aquifer exists (Figure 4.2 b), the aquifer acts to intensify downward movement through the upper layer to pass through the lower unit and consequently restrict the sub basins-in the hummocky region.

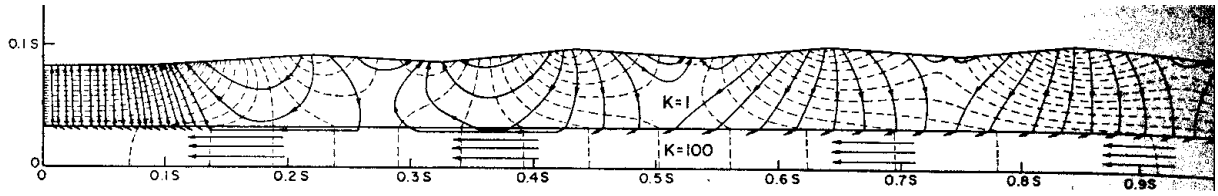

Figure 4.2(b) stratigraphic effects on groundwater flow when the water table has a hummocky surface (Freeze and Witherspoon, 1967).

4.4 Weathering

Weathering can contribute to secondary porosity, hence, resulting in a higher hydraulic conductivity. Although weathering can occur above and below the water table, it is generally slower in the saturated zone (Domenico and Schwartz, 1990). An example is when dissolution occurs along pathways of fluid movement such as pre-existing fracture zones in crystalline rocks. In such instances, the permeability can increase by between two and four orders of magnitude. Although this increase will generally only be noted within the first 20 metres of the surface, in tropical zones (where weathering is more extensive), the effects can extend to a

depth of 100 metres (Oelkers, 1996). Dissolution is also common in carbonate rocks where sinkholes and crevices can form (Domenico and Schwartz, 1990).

4.5 Diagenesis

When sediments are subjected to progressive burial, volcanic flow or any other mechanism that applies a pressure loading, the porosity of the sediment decreases with increasing depth due to compaction (Oelkers, 1996). Domenico and Schwartz (1990) elaborate on this principle by suggesting that the increase in pressure and temperature (as well as instigating chemical interaction between minerals and migrating pore water) changes the arrangement or shape of the grains. Diagenesis is extremely active in tailings piles, as mineral dissolution and precipitation is occurring constantly.

Whilst it is generally concluded that with an increase in pressure, K decreases, the same is not always true for increasing temperature. Some studies indicate that permeability increases with increasing temperature. This can be justified by the idea that at lower temperature, minerals can expand, leading to the closing of pore channels, and at higher temperatures, microcracks can develop due to thermal-elastic stresses (Oelkers, 1996).

4.6 Fractures and Faults

Effective Porosity can be applied to fractures. Hence, higher permeability results when the networks of fractures within a rock are joined. Studies of clays and shales on a basin-wide scale indicate that measurements of permeability increase by several orders of magnitude when the fracture network is considered (Oelkers, 1996). Al and Blowes (1994), suggest that fractures are the likely dominant flow path causing discharge of tailings pore water from the Kidd Creek impoundment to storm runoff. A similar situation exists at Rosebury, Tasmania, where leakage seams to channelise probably along fractures.

Fractured rock also behaves anisotropically due to directional variations in joints and spacing. Freeze and Cherry (1987) note that the bulk vertical hydraulic conductivity (Kz) is usually higher than the bulk horizontal hydraulic conductivity (Kx). Following this principle, an estimate of permeability for a set of fractures can be calculated depending upon the fracture orientation (Oelkers, 1996). For a set of parallel fractures orientated in the direction of interest: $k = \frac{ndf^3}{12\,L}$ where L = length of fracture, n = the number of fractures/cm and df is the fracture aperture.

For a set of randomly orientated fractures the formula becomes: $k = \underline{ndf^3}$

Permeability measurements are scale-dependent. On a large scale, there is often more structures with higher permeability, that is absent in small-scale systems, which dominate the permeability of the larger system (Oelkers, 1996).

Chapter 5: Contaminant transport mechanisms in groundwater systems

Physical, chemical and biological processes affect contamination movement in the subsurface (Frind and Molson, 1994). This chapter is only concerned with the physical processes, among which advection and dispersion are most important.

5.1 Advection

Advection transport potentially moves particles of the dissolved contaminant with the surrounding ground water (Figure 5.1; Kalf & Dungeon, 1999). Advection mass flux can be written as:

$F_x = nv_x C$ where F_x is the mass flux (M/L^2T), C is the solute concentration (M/L^3), n is Effective Porosity and v_x is ground water velocity in the x direction.

5.2 Hydrodynamic dispersion

Dissolved solutes (constituents including contaminants) have a tendency to spread out in three dimensions (Kalf & Dungeon, 1999). If advection alone were occurring, the contaminants would be restricted to a stream tube (Figure 5.1). This process is referred to as hydrodynamic dispersion (Kalf & Dungeon, 1999) and results from molecular diffusion and mechanical dispersion.

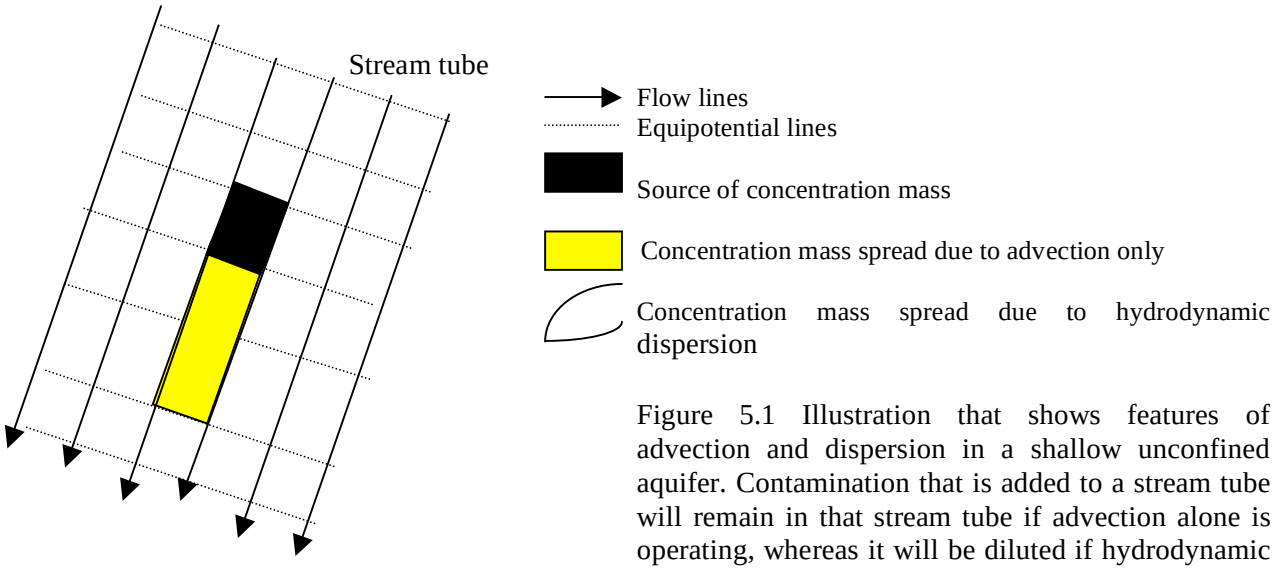

Figure 5.1 Illustration that shows features of advection and dispersion in a shallow unconfined aquifer. Contamination that is added to a stream tube will remain in that stream tube if advection alone is operating, whereas it will be diluted if hydrodynamic dispersion is applied.

Molecular diffusion describes the process when molecular or ionic constituents are transported under the influence of their kinetic activity in the direction of their concentration gradient (from high to low). This means that even when fluids are not moving at a significant rate, solutes can still move by diffusion and will only stop when there is no difference in concentrations. Fick's law can be used to calculate diffusion (Oelkers, 1996).

$$F_x = -D_a \frac{dC}{dx}$$

Where F_x is the mass Diffusional flux (M/L^2T), C is the concentration of the solute (M/L^3), dC/dx is the concentration gradient and D_a is the effective diffusion coefficient of the rock (L^2/T).

When applying this formula to porous media, the diffusion coefficient has to be adapted, as it is much smaller in porous media compared to water. The coefficient is not only a function of the concentration of each species in the solution, but also of the physical properties of the rock. The latter has an effect because aqueous diffusion occurs only through the pore spaces in the rock and the diffusional path may be much longer than the straightline distance in a direction of interest (Oelkers, 1994). Hence, considering the physical properties that affect the diffusion coefficient such as porosity, grain size, and distribution, we can adapt the equation to the following;

$$Fx = \frac{-Da}{e^2} \left(\frac{dC}{dx} \right)$$

Where Da is the effective diffusion coefficient of the aqueous species in pure solution, e is the effective tortuosity and is porosity of the rock.

The effective tortuosity incorporates all factors that alter the diffusional transport such as isolated pores, pore-throat constrictions, dead-end pore paths and grain surface effects. It represents the ratio of the mean path length of the dissolved species to the straightline distance of the overall path (Oelkers, 1996).

Diffusional transport is relatively slow at crustal temperatures, therefore, is a dominant transport mechanism in non or slowly advecting systems and to and from high permeability zones such as cracks and fissures (Oelkers, 1996). Table 5.1 lists the primary transport mode for different media.

Type of material	Dominant contamination transport processes
porous media	Advection- dispersion
low permeability material	Diffusion
Fractured rock	Advection and diffusion
Heterogenous porous media	Advection and diffusion

Table 5.1 Preferential transport processes for different rock types, adapted from text Fiend et al 1994

Mechanical dispersion is the result of variations existing in the groundwater velocity caused by local differences in permeability (Kalf & Dungeon, 1999). The process tends to diminish concentration gradients within the fluids flowing through the porous media. Consequently, depending on flow paths, the velocities of solutes will vary (Oelkers, 1996).

Permeability differences can occur at a range of scales from microscopic to macroscopic (Table 5.2). Oelkers (1996) suggests that on the microscopic scale, it is the friction between the mineral grains and the fluid that reduces the velocities along grain boundaries. Also, mixing or splitting of the flow streams can occur at pore space junctions. The severity of dispersion is consequently dependent on the spatial scale of the problem (Frind and Molson, 1994). Naturally, with increasing dispersivity there will be greater spreading and as a result lower concentrations with increasing distance from the source and visa versa (Kalf and Dungeon, 1999).

Dispersion coefficients are commonly treated as moving in two directions, one in the direction of the flow (D'_L) , the other perpendicular to the flow (D'_T). The same governing equation for determining molecular diffusion can also apply to mechanical dispersion (the mechanical dispersive flux equals the mechanical dispersion coefficient multiplied by the concentration gradients). Because of this, each coefficient can be summed together to create hydrodynamic dispersion coefficients as follows:

$D_L = L'_L + D$ and
$D_T = D'_T + D$

Where D'_L and D'_T refer to coefficient of longitude and transverse hydrodynamic dispersion and D is the diffusion coefficient of the solute species in pure solution.

1. pore geometry 2. dead-end pore space. 3. pore size distribution	1. Geological lenses 2. Permeability (non uniform, trends, directional) 3. Insulation to cross flow 4. Other irregularities in the material.	1. Reservoir geometry: such as faults, dipping strata and overall stratigraphic framework: channel fill and blanket 2.Hyperpermeability- orientated natural fracture system.

Table 5.2 Possible geological features that can contribute to nonidealities in porous medium. Adapted from Frind et al (1994).

A contaminant may be retarded, which decreases the velocity of the contamination relative to the groundwater flow rate. Retardation can result from processes such as adsorption, precipitation/dissolution other complex ion exchange reactions (Kalf & Dungeon, 1999), or decay due to radioactive processes (Domenico and Schwartz, 1990). As these are chemical or nuclear processes, they will not be addressed in this paper.

5.3 Nonlinear physical processes

Physical nonlinearity occurs when the density of contaminated water is notably higher than the density of the local groundwater. The concentration ratio dictates how much the denser fluid sinks and how much the lighter fluid will rise in the aquifer (Frind, 1994). The density of groundwater may vary slightly due to small variations in pressure or temperature or by the presence of dissolved trace elements (Herbert et al, 1988). In saline solutions when flow moves around repositories close to the sea, salt water may percolate into the surrounding rock. Alternatively, for buried waste in stable salt formations, nonlinearity can occur due to high concentration of the dissolved salt and also dispersion, which is dependent on velocity (Herbert et al, 1988).

Temperature variations also affect density. For example, sulphide-oxidation reactions generate heat that can be transferred to the underlying, cooler aquifer (Frind and Molson 1994) and circulating groundwaters can be driven by a local heat source such as heat given off from buried nuclear fuel waste (Yang, et al, 1998). Yang et al (1996) also suggest that fluid flow through fractures result in horizontal thermal gradients.

Chapter 6: Modelling

The purpose of numerical modelling is that it helps to understand the complex interactions between the physical, chemical and biological processes that can take place in groundwater systems. Hence, models can provide information needed to manage groundwater resources and reduce environmental contamination (Frind and Molson, 1994).

Modelling can be viewed as a procedural process, as there are several stages that need to be fulfilled in order to gain accurate interpretations (Appendix E). After identifying and defining the geological problem, the next step is to formulate a conceptual model of the tailings site. The purpose of a conceptual model is that it simplifies complex real life hydrogeological systems. This is done by incorporating the data and knowledge we have about a site and creating an idealistic system. Desired information includes the water table configuration and extent, properties of the hydrogeological units and processes that are relevant to the objectives. The latter is very important as the characterisation of the processes not only forms the basis of the conceptual model, but also dictates the transport modelling approach or solution techniques required. Hence, not only is the coupling and interaction between these processes important, but also the assumptions made that will include or exclude certain processes or interactions. Table 5.2 illustrates assumptions of dominant transport processes dependent on the rock type (Frind and Molson, 1994).

Once the physical processes are established and their corresponding equations are recognised, a physically based mathematical model can be developed (Frind and Molson, 1994). The appropriate equations for solute transport problems when the presence of the solute does not affect the density of the fluid are well recognised. For example, Darcy's law and the mass conservation equation are used to characterise the flow. However, if heat or the solute changes the density slightly, then the Boussinesq approximation can be used. When the density is strongly dependent on the concentration of the solute, the equation should be extended. Again the equation is adapted if the concentration varies significantly on the scale of the dispersitive length (Herbert et al, 1988). Also, the boundary conditions, initial conditions and the material properties need to be determined as well as the solution method that will be applied (Table 6.1; Frind and Molson, 1994).

The solution method then needs to be differentiated. There are numerous discretion possibilities that are dependent on the solution method chosen and type of mode. For example finite-element methods prefer triangles or tetrahedra and triangular prisms in 3D. In contrast,

finite-difference methods favour rectangular based cells (Frind and Molson, 1994). Kalf and Dungeon (1999) decided on a mesh with a quadrilateral and triangular element for their 2D finite element model. The quadrilateral shapes utilised secondary nodes 9th order integrations and the triangular shapes used 3rd order integrations. This discrimination was chosen as it results in a higher accuracy. To remove the no-flow edges of the model, infinite numbers were used which made the model think that the section extended to distance far beyond each of these edges.

Calibration is usually first applied to a model. This is used when an unknown parameter is estimated from the model by fitting a simulation to an observed response under controlled conditions (Kalf & Dungeon, 1999; Frind and Molson 1994). In most cases of mine tailings, data available is less than desirable (Kalf & Dungeon, 1999), hence calibration is a very important application. As dispersivity can only be measured directly with sophisticated and costly techniques, calibration is often used to estimate as this parameter (Frind and Molson, 1994). A disadvantage of calibration is that only one unknown parameter can be determined uniquely. One way to get around this is to acquire fits with different combinations of parameters, but then parameter selection will be non- unique (Frind and Molson, 1994).

Solution method	Advantages	Disadvantages
Analytical	✓ Provides an exact solution ✓ Computationally less demanding	Less realistic and less versatile Restricted to linear systems Properties must be uniform
Particle Tracking	✓ Commonly low computational demands ✓ No numerical dispersion ✓ Well suited for advection problems, pathlines, capture zones ✓ No matrix solution required	Sophisticated velocity interpolation required Local concentrations are difficult to define Complex processes difficult to include
Numerical Finite-difference method (FDM)	✓ Relatively simple compared to FEM ✓ May require less memory than FEM ✓ Versatile ✓ Coupled system can be solved	Computationally demanding Geometry must be simple Grid layout less flexible Susceptibility to numerical dispersion
Numerical Finite-element method (FEM)	✓ Geometry can be complex ✓ Realistic and versatile ✓ Coupled systems allowed ✓ Grid layouts very flexible	Computationally demanding Susceptible to numerical dispersion

Table 6.1 Possible solution methods, either analytical or numerical, and the advantage and disadvantages of each.

After the commencement of the procedures mentioned above, gaps in the available data can be identified and remedied and new data can then be incorporated into the model.

The sensitivity of a system with respect to the various parameters is the next application to be addressed. The purpose for applying this analysis is that it provides an insight about the behaviour of the system under various conditions and also information about the importance of the individual parameters and processes (Frind and Molson, 1994). Firstly, a base case is defined and then the parameters are changed within their respective ranges. Even if the actual parameter values are not know, their ranges should be known by experience hydrogeologists (Frind and Molson, 1994).

Through the use of modelling, the proposed Jabiluka project could be investigated. The proposal involved the solidification of tailings by adding concrete and storing underground in mine void and silos.

During the conceptual stage, Kalf & Dungeon (1999) made the assumption that because the fracture networks in the schist at the site are small in comparison to the fractures in the potentially contaminated region, the fractured rock can be represented as an equivalent porous medium on a regional scale. However, geological features such as major faults needed to be accounted for separately as flow conduits.

For the task of modelling the groundwater flow system at Jabiluka mine site, a two-dimensional SEEP/W finite numerical model was created based on data of the drainage pattern and aquifer properties. This particular model is based upon an internationally recognised groundwater flow model for steady-state saturated flow (Woyshner, 1995). For the Jabiluka project, the potentiometric surface could be justified to be at steady state, because the influence of seasonal variation on contaminant movement will cancel out below and above a mean potentiometric level. In addition, any change in flow velocity due to fluctuating water levels will lie within the range of velocities to be used in the analysis. To simulate steady state, constant heads at the elevation of the depicted potentiometric surface were set in the model. The model determined flow direction, head distribution and range of Darcy's velocities along a section parallel to the groundwater flow.

A project involving the rate of percolation through a soil cover first used the HELP model to predict the amount of annual infiltration. The data was then used as the soil surface boundary condition in the SEEP/W model. The HELP model simulated four hydraulic processes daily: runoff (hence infiltration), percolation, lateral drainage and evaporation (Woyshner, 1995).

The second aim of the Jabiluka project was to determine the leaching contamination concentrations from the tailings paste material (proposed tailings repositories). To do this, a three-dimensional numerical solute transport model (Modflow-surfact) was applied to a single representative 1m thick horizontal layer of flow through and around a repository (Kalf & Dungeon, 1999). Monte Carlo simulations were used to determine concentration profiles over a range of relevant variables such as time and distance. This was done by re-running the model using various model parameters selected randomly within a given range. Results using this type of simulation are an approximate representation of the results of all the possible combinations of the given parameters within each range (Kalf & Dungeon, 1999). The range of concentration vs distance curves derived from this simulation were extreme curves of very low probability. This means that even though the results indicate that significant concentrations of uranium and radium could occur in groundwater about 1 km from the mine and magnesium sulphate distances could be several of km, it is not likely. Predicted median relative curves of the same parameters hypothesised that even after 1000 years, U concentrations are negligible just 200 meters west of the source (Kalf & Dungeon, 1999).

An analytical contamination transport model was formulated to determine concentration due to advection, dispersion and retardation. It utilised range of velocities from the ground water flow model and source concentrations from the solute transport model. This model was then combined with Monte Carlo simulations to determine concentration profiles for numerous different parameter values within selection ranges (Kalf & Dungeon, 1999). The final conclusion was that if a permeability of 10^{-4}m/day of the set tailings paste were maintained, then leaching of contaminant by groundwater would have no adverse effect on Kakadu National Park.

Chapter 7: Summary

Important aspects of the groundwater flow system within a tailings impoundment and the surrounding geological material are the direction and the rate of groundwater movement and the distribution of recharge and discharge areas. Each of these parameters is controlled by a combination of factors, which for simplification purposes can be said to relate to hydraulic conductivity, and /or climate, and / or topography and /or diagenesis. Naturally, the hydrology between different tailing impoundment sites is going to vary, therefore, when determine the potential flow regime of an area, only the factors applying to the particular site need be considered.

Appendix A

Possible methods for calculating permeability and hydraulic conductivity

Method	Equation	Owner of equation
Grain size analysis	$K=C_1 d^2_{10}$	Hazen (1911)
	$k= (6.54 \times 10^{-4})d^2_{10}$	Harleman et al (1963)
	$k= 760d^2e^{-1.31}$	Krumbein and Monk (1943)
	$k= Cn^3/S^{*2}$	Kozeny (1927)
	$K=\frac{g}{(1-n)^2}\left[\frac{n^3}{180}\right]\left[d^2_m\right]$	Kozeny –Carmen Bear (1972)
Permeameter testing in laboratory	$K=\frac{QL}{Ah}$	**Darcy's Law**
Field measurements	$K=\frac{k_* g_*}{}$	Hubbert (1956)
Insitu piezometer testing and well testing better for K_x as influence by more permeable layers.	$K=\frac{r^2(L/R)}{2LT_o}$	
More direct method for estimating K_z is calculate Vz by using tracers such as tritium or sulphate and iz can be measured directly by installation of multiple piezometer nests .	$V_z=\frac{K_z I}{N}$	Darcy's equation
Field measurements for crystalline rocks.	$k=\frac{r^2 p}{ko} f^{1.5}$	(Bryce 1977)

Parameters

K= Hydraulic Conductivity
k = Permeability
C_1 = constant 100 to 150 for loose sand
d_{10} = effective grain size (with 10% particles finer)
d = geometric mean grain diameter
= log standard deviation of the size distribution
C_2 = dimensionless constant; 0.5 for circular, 0.562 for square and 0.597 for triangular pore openings
n= porosity
S^* = specific surface
g = gravitational constant
= fluid density
= fluid viscosity
d_m = any representative grain size.
Q= volumetric flow rate
L = length of sample
A =cross sectional area of sample
h=constant head
r= radius of piezometer
L =screen length of piezometer
R= radius of piezo tip
T_o= Hvorslev's basic time lag
iz vertical hydraulic gradient.
Vz (vertical flow velocity)
rp = average pore radius
ko = shape factor vary from 2 to3
f = formation factor

Adapted from Domenico, 1990; Freeze and Cherry, (1974); Robertson (1994); (Oelkers, 1996).

Appendix B

Ground water component as illustrated in Domenico and Schwartz, 1990

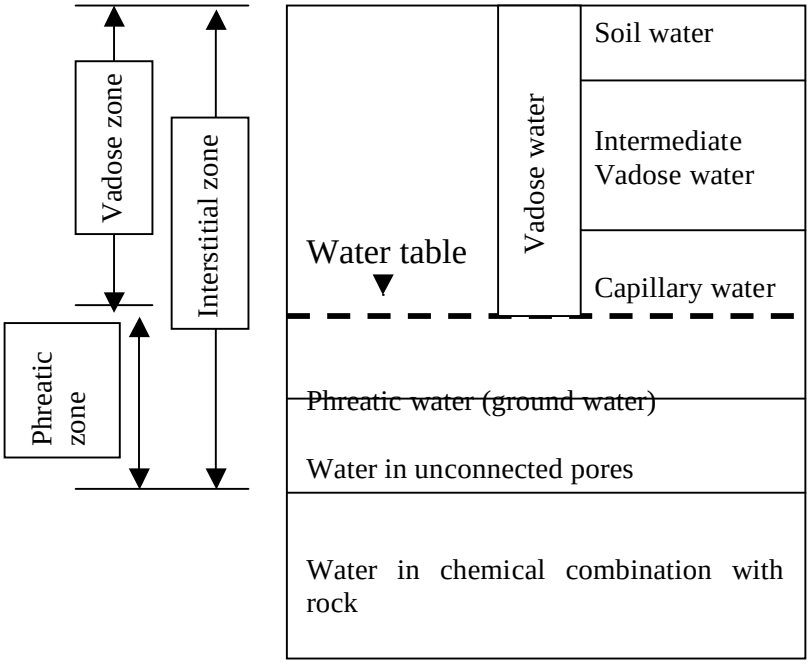

Note: The tension saturated zone lies immediately above the water table and is where the pores are dasaturated but the pressure head is less then the atmospheric pressure (Freeze and Cherry, 1979).

Appendix C

A flow system representing the hydrological cycle (Domenico and Schwartz, 1990).

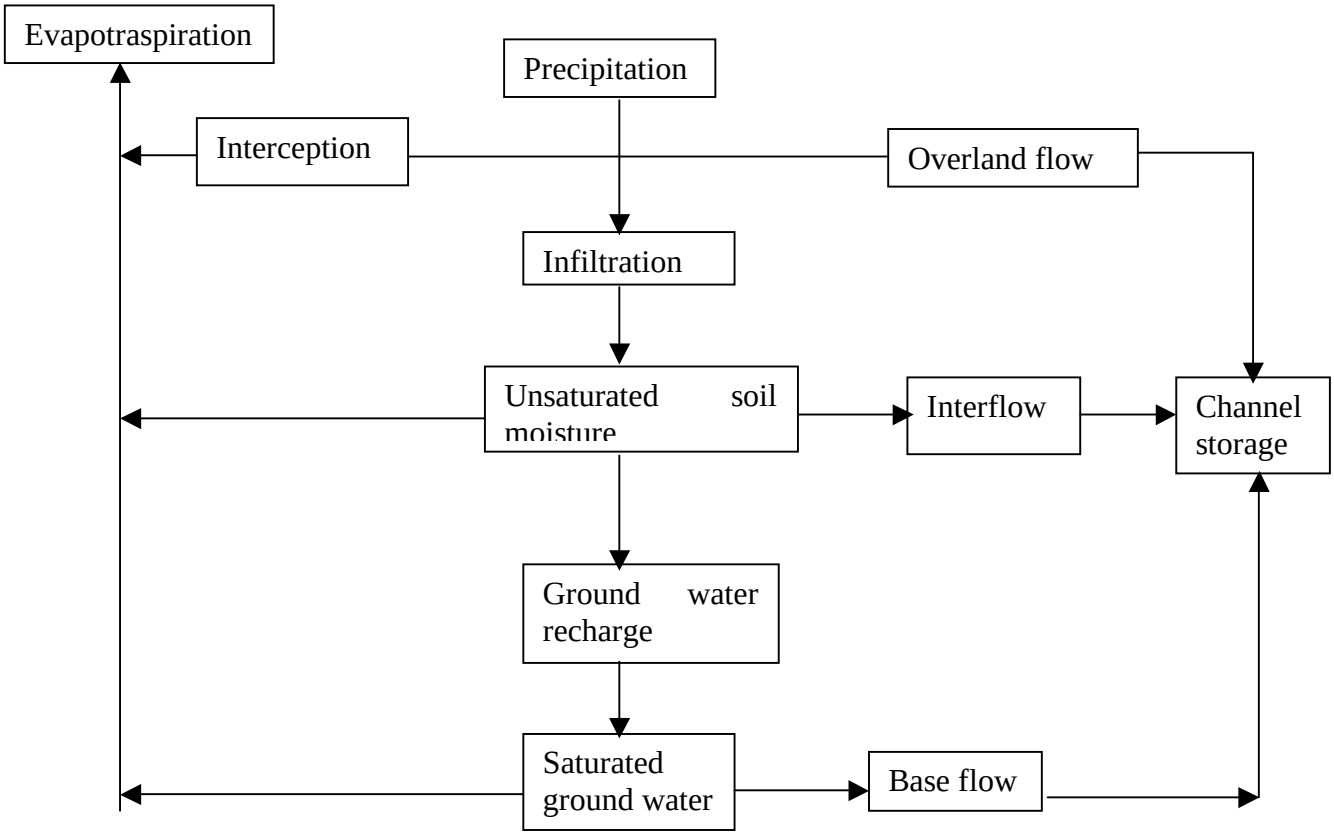

Note; Evapotraspiration is a temperature dependant quantity. Can be simply understood as a ratio of precipitation to potential evapotranspiration

Appendix E

A simplified flowchart of the modelling process put forward by Frind and Molson (1994).